INVESTIGATIONS ON ELECTRO-ACTIVE SHAPE MEMORY POLYMER NANOCOMPOSITES: POLYURETHANE – CARBON BLACK / CARBON NANOTUBE SYSTEMS

Thesis submitted for the degree of

Doctor of Philosophy

by

ARUN D I

Department of Aerospace Engineering

INDIAN INSTITUTE OF SPACE SCIENCE AND TECHNOLOGY
THIRUVANANTHAPURAM

SEPTEMBER 2019

If we knew what we were doing, it wouldn't be called Research

-Albert Einstein

Certificate

This is to certify that the thesis titled ***Investigations on Electro-Active Shape Memory Polymer nanocomposites: Polyurethane – Carbon Black / Carbon Nanotube systems*** submitted by Arun D I to the Indian Institute of Space science and Technology, Thiruvananthapuram, in partial fulfillment for the award of the degree of Doctor of Philosophy is a *bona fide record* of research work carried out by him under supervision of the undersigned. The contents of this thesis, in full or in parts, have not been submitted to any other Institution or University of award of any degree or diploma.

Dr. Chakravarthy P
Associate Professor
Department of Aerospace
IIST, Trivandrum

Dr. Santhosh B
Group Director – Carbon Carbon Development Group,
Composite Entity, VSSC, Trivandrum

Counter signature of HoD with seal

Declaration

I do hereby declare that the research work titled ***Investigations on Electro-Active Shape Memory Polymer nanocomposites: Polyurethane – Carbon Black / Carbon Nanotube systems*** submitted by me for the award of the degree of Doctor of Philosophy to the Indian Institute of Space science and Technology, did not form the subject matter of any other thesis submitted by me for any degree. This is an original work done by me and this thesis is entirely done at the Indian Institute of Space science and Technology with support from Vikram Sarabhai Space Centre, Trivandrum.

.

Arun D I

SC16D026

Thiruvananthapuram

September, 2019

Acknowledgements

Abstract

Materials those possess the ability to sense, process and respond to any external stimuli are termed as smart materials. Mimicking nature, human efforts towards smart systems have led to discovery of materials that are capable of sensing and responding to the environmental conditions. Such materials can be used in various applications such as medical, robotics, aerospace technologies, etc. The phenomenon exhibited by few smart materials to regain the original shape while exposing them to certain stimuli such as moisture, heat, light or chemicals etc., is termed as shape memory effect (SME) and such materials are called Shape Memory Materials (SMM). Polymeric shape memory materials with organic / inorganic nano scale fillers distributed homogeneously across the matrix, synthesized by physical blending or chemical polymerization methods are termed as Shape memory polymer nanocomposites (SMPC). The presence of nano fillers influences the mechanical, thermal and electrical property of such polymer nanocomposites. Material properties are also influenced by the synergistic combination of one or more kind of nanofillers in a polymer matrix.

To appreciate the current conduction phenomenon in polymer nanocomposites, correlation between experimental and theoretical model needs to be established. As the outcome of many of the models developed so far could not precisely match with the experimental results, a comprehensive model, which can predict percolation threshold and conductivity for specific fillers, is required to be worked on. Such a model can be used as a generalized prediction tool for any resin-filler system with their corresponding properties as input, and the same can avoid laborious experiments in the chosen system. This can take into account, the statistical and quantum tunneling approaches for current conduction in the polymer matrix filled with conducting nanofillers. Another grey area in the research of shape memory nanocomposite is about the synergy of multiple fillers in nanocomposites. Requirement of different orders of recovery speed and efficiency for specific applications demands the development of materials with variable sensitivity.

PU, being shape memory active and possessing tunable properties (based on careful selection of diisocyanates and polyols), was chosen as the matrix resin for synthesis of nanocomposites in current work. A two-stage pre-polymer route was followed for the PU synthesis, where the macroglycols were end capped with excess of diisocyanates, followed by chain extension of the diols. CB (Carbon Black, three-dimensional geometry) and MWCNT (Multi-Wall Carbon

Nano Tube, one-dimensional filler material) were used as filler materials with an aim to synthesize electrically conducting nanocomposites. The conduction phenomenon in these nanocomposites is either by contact between the fillers or by electron tunneling.

The synthesized PU has exhibited T_g of 85°C which is high compared to the reported values in published literature. The polymer resin and the CB filled nanocomposites were characterized for its chemical, electrical, thermal, mechanical and shape memory properties. The presence of 'aliphatic' diisocyanate (IPDI) and the CB in PU CB nanocomposite makes them stable against UV radiations thus making them an eligible candidate for space applications. The electrical, thermal and mechanical properties were observed to improve with increased carbon loading. The CB PU nanocomposite system has shown a percolation threshold of 6% by weight of resin experimentally which was simulated in the model considering the spherical particle dispersion in a Representative Cubical Volume Element (RCVE). For modeling the nanocomposite, a one micrometer size RCVE was considered and the filler particles were randomly placed in it. Varying the filler content, the process was repeated using Monte Carlo simulations to arrive at a converged percolation threshold. Beyond percolation threshold, the particles can have multiple networks thus increasing the conductivity of the material / system. Same approach was followed for CB and MWCNT as fillers whereas the model was tuned for the difference in parameters such as geometry, size, tunneling distance, contact possibility for each case. Visual C language platform was used for the development of the program and was optimised using multiple algorithms. On simulating the system, the first conductive network appeared at 6.2% weight fraction as per the model (statistically evaluated as the filler content corresponding to percolation probability of 50%).

A systematic modeling approach underlining the parameters specific to CNT-PU system was developed from the understanding of the CB-PU model. The RCVE filled with randomly oriented CNT with varying aspect ratio is simulated based on optimization algorithms. The percolation threshold in PU-CNT system based on the model and simulation arrives to 0.19% by weight of CNT. Compared to the CB model, the lower value of percolation threshold value is attributed to the high aspect ratio and geometry of the nanotubes. For evaluating the model, PU resin based nanocomposite was synthesized with MWCNT added in 0.1% - 10% by weight. The synthesized PU-MWCNT system was characterised for chemical, microstructural, thermal and mechanical properties and it was observed that the PU-MWCNT

nanocomposite was superior to PU-CB system in mechanical and electrical properties. The large aspect ratio of MWCNT contributed towards network formation at lower filler content and caused percolation experimentally at 0.21% by weight of MWCNT, which closely matches with the theoretical results. Thus, a reliable generalised structural model for understanding and predicting percolation in nanocomposite systems was developed and established the reliability.

A multi-filler system was also experimented to understand the synergy between the CB and MWCNT in PU to form nanocomposites. The combinations showed a trend of increasing conductivity with increased MWCNT content per CB weight fraction. The conductivities varied from the order of 10^{-12} to 10^{-5} S/m, with 5% CB – 0.15% MWCNT combination showing percolation threshold. The observed electrical conductivity was found higher than the individual filler contents in binary single filler systems.

The relationships between the various parameters (T_g, Voltage, time of exposure) that influence the shape memory effect were also studied for all three systems. This can be used as a reference for designers to select filler content based on the required time and power availability. The thermal and electrical stimulation of shape memory effect was evaluated for all the three developed systems, and the highest efficiency and fastest recovery for PU based shape memory systems reported so far were observed.

The knowledge from this exploration can help the researchers to look outside the conventional actuation systems employed to less complex and lighter systems from shape memory polymer nanocomposites. A comprehensive understanding of the conductivity phenomenon in such nanocomposites helps to deduce different combinations of the fillers and to arrive at the optimal composition theoretically prior to synthesis. The established models can predict the electrical percolation threshold of nanocomposite systems, which can help reduce the number of time taking experiments. The possibility of combining the advantages of individual nanofillers to create novel materials with superior properties can be opened to the scientific world by the synergistic approach.

Table of contents

List of Figures

and electrical actuation

List of Tables

Abbreviations, Acronyms & Notations

2D	2-dimensionsal
3D	3-dimensionsal
BD	Butane-diol
CB	Carbon black
CMCs	Ceramic Matrix Composites
CN	Co-ordination Number
CNF	Carbon Nano Fibre
CNT	Carbon Nano Tube
CTE	Coefficient of thermal expansion
DABCO	1,4-diazabicyclo[2.2.2]octane
DBTDL	Di-Butyl-Tin-di-laurate
DEM	Discrete Element Method
DMA	Dynamic Mechanical Analysis
DMCHA	Dimethylcyclohexylamine
DMEA	Dimethylethanolamine
DSC	Differential Scanning Calorimetry
EASMP	Electro Active Shape Memory Polymers
EASMPC	Electro-Active Shape Memory Polymer Composite
ESMP	Epoxy Shape Memory Polymer resin system
FRC	Fiber reinforced composites
FTIR	Fourier Transform Infra-red Spectroscopy
HDI	Hexamethylenediisocyanate
IPDI	Isophoronediisocyanate
ISRO	Indian Space ReasearchOrganisation
ISS	International Space Station
LASMP	Light Activated Shape Memory Polymer
MDI	Methylenediphenylmethanediisocyanate

MMCs	Metal Matrix Composites
MWCNT	Multi-Wall Carbon Nano Tube
NASA	National Aeronautics and Space Administration
PANI	Polyaniline
PBT	Polybutylene Terephthalate
PCL	Poly 3-caprolactone
PEEK	Polyether-ether ketone
PMA	Poly-methyl acrylate
PMC	Polymer Matrix Composite
PMMA	Polymetha methyl acrylate
PTMG / PTMEG	Poly-tetramethylene ether glycol
PTMO	Poly Tetra Methylene Oxide
PU	Polyurethane
QTC	Quantum tunneling composites
RCP	Random close packing
RCVE	Representative cubic volume element
RPSME	Reversible Plasticity Shape Memory Effect
SBS	Styrene–butadiene–styrene tri-block copolymer
SCF	Short Carbon Fiber
SEM	Scanning Electron Microscope
SMA	Shape Memory Alloy
SMASH	Shape Memory Assisted Self-Healing
SMC	Shape Memory Ceramics
SME	Shape Memory Effect
SMG	Shape Memory Gels
SMH	Shape Memory Hybrids
SMM	Shape Memory Materials
SMP	Shape Memory Polymers
SMPC	Shape memory polymer composites

SSEBS	SulfonatedpolyStyrene-b-[Ethylene / Butylene]-b-Styrene
SWCNT / SWNT	Single Walled Carbon NanoTube
TDI	Toluene diisocyanate
TEDA	Triethylenediamine
TEM	Tunneling electron microscope
T_g/ T_{trans}	Transition temperature
TGA	Thermal Gravimetric Analysis
TMP	Trymethylol propane
TPU	Thermoplastic polyurethanes
UV	Ultraviolet
XRD	X-ray Diffraction
eV	Electron volt
S/m	Seimens per meter
MPa	Mega Pascal
H	Hydrogen
(d)	Inter-particle distance
Φ	Filler volume fraction
ρ	Electrical resistivity
l	Length
A	Area
R	Resistance
I	Current
V	Voltage
σ	Conductivity
p	Filler content
p_c	Percolation threshold filler content
j	Critical exponent after percolation threshold
k	Critical exponent before percolation threshold

Q	Heat energy generated
t	Time
m	Mass
C	Specific heat
ΔT	Temperature change
R_f	Shape fixity efficiency
R_r	Shape recovery efficiency

Note: The symbols / notations that are not defined here are defined in the thesis wherever they appear first

CHAPTER.1
INTRODUCTION

Nature provides vivid depictions of smart systems that can be adopted for materials / structures / techniques in use for all fields of human advancement. Such materials / structures those possess capability to sense, process and respond to any external stimuli are termed as smart materials. Numerous applications in medical, mechanical, robotics, aerospace technologies, etc., have witnessed progress in development of smart materials. Mimicking nature, human efforts towards smart systems had led to discovery of materials that are capable of changing their properties by sensing and responding to the environmental conditions. Piezoelectric materials, quantum tunneling composites, magnetostrictive materials, light responsive materials, smart inorganic polymers, halochromic materials, chromogenic materials, photochromic materials, ferrofluids, photomechanical materials, dielectrics, thermoelectric materials and shape memory materials, etc., are the prominent terms associated with smart materials based on the definition.

Engineering / Scientific advancements in late 1960s directed smart materials research to synthesize actuators, vibration damping systems, microphones, sensors and other transducers, etc. This was based on three basic approaches like

   i.   Atomic or molecular level synthesis of new materials
   ii.   Conventional structures with embedded sensors or actuators
  iii.   Composite materials with properties superior to the individual components.

First approach favored a revolution in electronic industry, where doping of materials in atomic or molecular level introduced new material behaviors in existing systems which were demanded for many applications. Second approach introduced the capability of the systems to be maintained and to have a control over it. Third concept produced totally new materials with properties of its components imbibed in the final product.

1.1 Smart systems and materials

Smart materials are be those materials or combinations of which, that alter its behaviour physically or morphologically, by sensing and responding to specific environmental stimuli such as heat, magnetism, electricity, moisture etc.

The smart systems and materials in nature inspire the engineers and researchers for developing many stimuli responsive systems for various applications. Body colour camouflaging of chameleon, zebrafish and squid (refer Figure 1.1(a),(b), the touch-me-not plant which respond to the sense of touch (scientifically mimosa-pudica plant, refer Figure 1.2(a),(b)), are few examples of natural smart stimuli responsive systems.
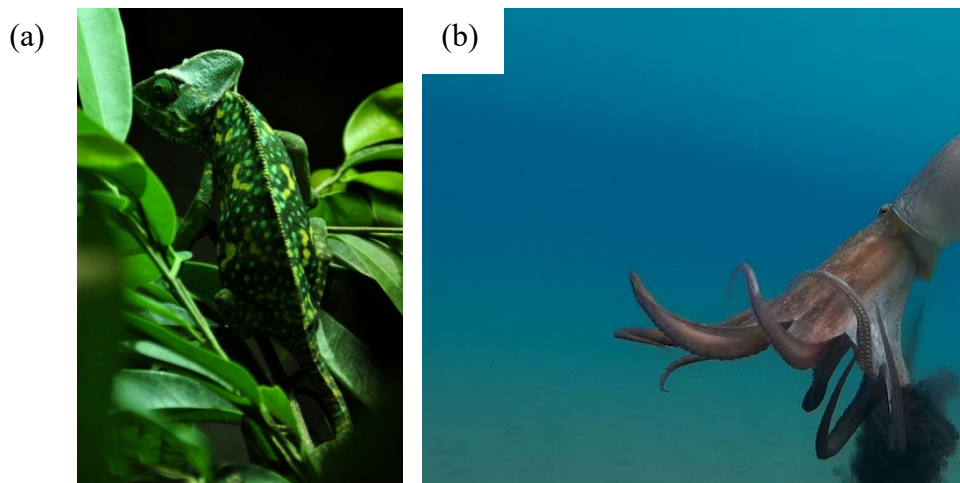
Figure 1.1 Smart systems of nature; (a) the outermost layer of the chameleon's skin is transparent, below which specialized cells called chromatophores that are filled with sacs of various coloring pigments are present which get released based on body temperature and mood; (b) The squid has color-changing cells with a central sac holding granules of pigment encapsulated with muscles, contraction of which sprays the pigment/ink granules

The most commonly found 'touch me not' plant also depicts smart stimuli responsive mechanism by closing the leaves in response to touch (refer Figure 1.2). Various chemicals such as potassium ions are released at certain regions of the plant body on stimulating (touch) externally. These are capable of initiating flow or diffusion of electrolyte either inward or outward of cells resulting in loss of cell pressure causing closing of leaves. On transmitting this stimuli to neighboring leaves, a series of closure of leaves can be observed (refer Figure

1.2(b)). This process occurs at the expense of energy gained through photosynthesis as a natural smart material concept against predators. The closed leaves gain back their original open-configuration on withdrawal of stimuli, in a short period, demonstrating the stimuli responsive nature of the plant as well as its shape memorizing ability.
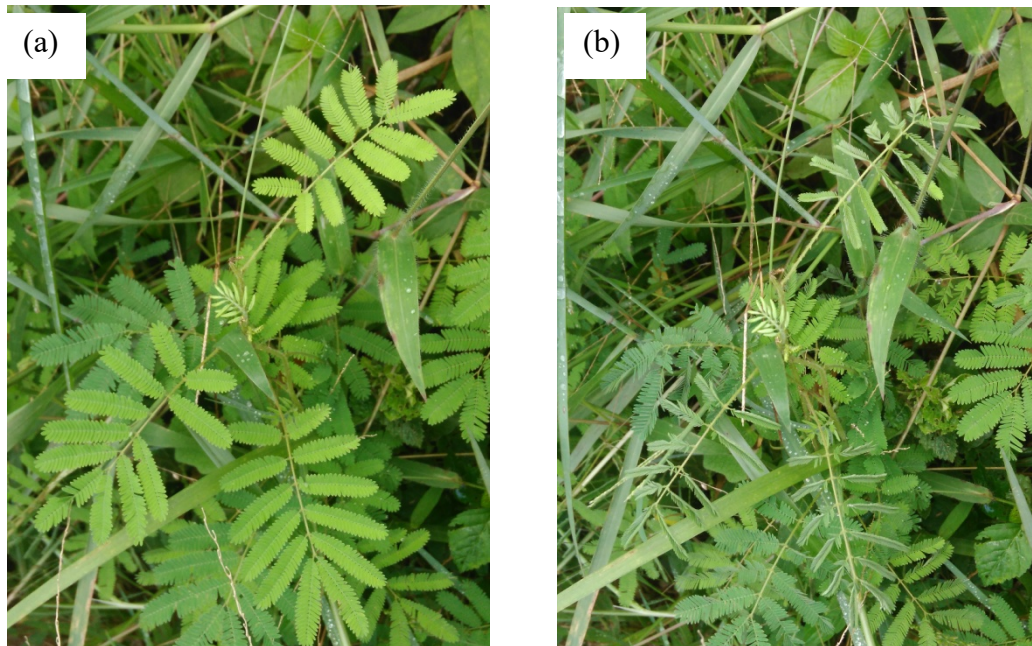
Figure 1.2 Nature's demonstration of stimuli response; (a) touch me not plant leaf in regular open configuration; (b) Leaves close in response to touch [image courtesy: DI et al., 2018]

Many such systems / material responses can be adopted in various daily use structures across different engineering fields. Spacecraft antennas are exposed to extreme temperature changes resulting in dimensional variations (due to expansion or contraction) and its attendant problems. It is inevitable that these materials should have very minimal variations in the dimensions / geometry for its best performance and the employment of smart materials for such applications becomes very pertinent. A smart antenna in such a situation shall sense the change in dimensions, judge the correction requirements and autonomously bring the structure to its design dimensions catering to the best performance. The conventional materials behave in an inert manner whereas; smart materials take over the situation intelligently to provide solutions that overcome the problem. Sensing, actuating and controlling capabilities can be intrinsically built into the

microstructure of such materials to make a judgment and react to the changes in ambient environment conditions. Changes in temperature, presence of electric / magnetic field, moisture, light, adsorbed gas molecules and pH values are the various stimuli that initiate the smart responses in the materials.

1.2   Stimuli responsive materials

Materials those respond to various stimuli are studied across past few decades and are in use in various engineering systems. This includes piezoelectric materials, quantum tunneling composites, electrostrictive / magnetostrictive materials, color changing materials, shape memory materials etc.

1.2.1 Piezoelectric materials

Appearance of an electrical potential across the sides of a crystal when it is subjected to an external mechanical stress is termed as piezoelectricity / piezoelectric effect. This was first understood from barium-titanate unit crystal, on which application of stress has caused a net dipole moment proportional to the external pressure resulting in the development of electrical potential. Sonar device used during world war-1 marked the first practical application of piezoelectricity.

1.2.2 Quantum tunneling composites

Quantum tunneling composites (QTC) are materials with the quantum particles / electrons passes a barrier that it cannot generally get through as per classical physics theories. If the potential energy barrier is higher than the energy of the particle, the barrier becomes impassible according to the 'classical theory of physics', whereas the quantum mechanics explains the possibility of the particle making it through, termed as Quantum tunneling. A polymer – metal composite material containing a non-conducting elastomeric binder can be used as a pressure sensor and this is based on the principle of quantum tunneling effect. National Aeronautics and Space Administration (NASA) is studying the possibility of using QTC for touch sensation in the Robonaut project for future space missions.

1.2.3 Electrostrictive / Magnetostrictive materials

The dielectric materials display a shape change with respect to the direction of the field, on exposure to an external electric field. It is attributed to the accumulation of displacements of positive and negative ions in the crystal lattice while the electric field is applied which lead to an introduction of a strain corresponding to the field vector. Insulating materials with more than one type of atom are found to shows electrostrictive behaviour. Magnetostriction is an analogous property of ferromagnetic materials that results in the change of shape or dimensions due to influence of an external magnetic field. These are being studied for applications in fuel injection, noise / vibration cancellation experiments, sensing and actuations in biomedical field and in aerospace.

1.2.4 Shape memory materials

Materials those change the shape towards a specific stimulus memorizing the original shape from a trained temporary shape are termed as Shape Memory Materials (SMM). The discovery of Nickel – Titanium Shape Memory Alloy (SMA) by Buehler and team in 1962 (US Naval Ordinance Laboratory) has initiated the use of shape memory property of materials for different applications.
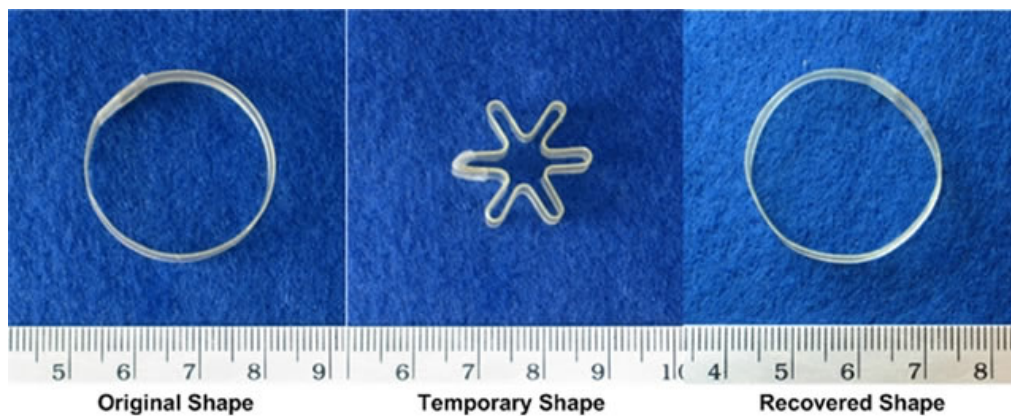
Figure 1.3 SME of a polymeric material (PMMA) under thermal stimuli.

Figure 1.3 depicts the shape memory stages of a polymeric sheet from polymetha methyl acrylate (PMMA) which recovers its original shape on application of heat. Here, a memorized original shape (circular configuration) is regained while

subjecting the material to external heating [Merlin J et al., 2008; Humbeeck, Van Jan., 1999].

The flow chart in Figure 1.4 summarizes the domain of smart materials journeying from intelligent responsive materials to the shape memory categories based on various stimuli. The materials showing shape memory effect can be classified as Shape Memory Alloys (SMA), Polymers (SMP), Hybrids (SMH), Ceramics (SMC) and Gels (SMG). Inclusion of filler materials for property enhancement to any of the above SMM can result in composite materials generally termed as Shape Memory composites.
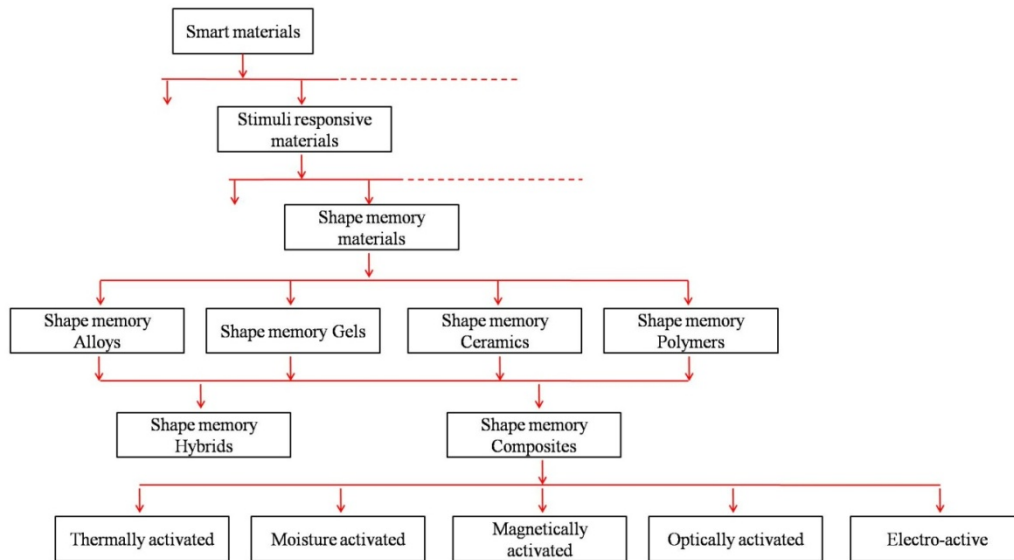
Figure 1.4 Shape memory material domains

Studies in the field of SMM are rapidly advancing as they find applications in Micro-Electro mechanical devices to replace complex mechanisms and aerospace deployment systems, bio-medical surgical needs etc.

The phenomenon of regaining the original shape of a material by subjecting them to suitable stimuli like moisture, heat, light or chemicals, is termed as shape memory effect (SME). It is named after the change inducing stimuli such as hydro-active electro-active, thermally activated, magnetically activated shape memory etc. These distinctive behaviors make them useful in various engineering

and scientific applications, including textile, deployable structures, shape morphing, cardiovascular surgery, and many other fields.

1.3 Shape memory polymers and composites

Shape memory polymers (SMPs) are polymeric materials that are capable of regaining the original shape from a temporary deformed shape, when triggered by an external stimulus. Unlike other SMM, the shape change of SMPs can be initiated by large number of stimuli specific to application, such as temperature change, electric or magnetic field, light source, presence of chemical or moisture etc. Compared to SMAs and other SMMs, SMP possess many advantages which shift the research interests to SMPs. To mention a few, the SMP can exhibit large elastic deformations up to 800%, they are available at lower cost, possess lower density, can have tunable actuation temperatures, easy to synthesize / process, has potential biocompatibility and biodegradability properties. The polymer morphology attributes to the shape memory behavior in polymers, which are explained in detail in the following chapter. Driven by the demand from applications, the studies towards the enhancement of properties have opened horizons of introducing of filler materials in polymeric matrices to form composites. The macro and micro properties of such shape memory polymer composites are studied across decades and current focus is on polymeric resin matrices with nano-sized filler materials [DI et al., 2018].

1.3.1 Nanocomposites of shape memory materials

Polymeric shape memory materials with organic / inorganic fillers of nano scale (between 10 and 100 nm in at least one dimension), distributed homogeneously across the matrix and are synthesized by physical blending or chemical polymerization methods are termed as Shape memory polymer nanocomposites (SMPC). Thermoplastics, thermosets and elastomers are used to make polymer nano composites with a wide range of nano reinforcements with different shapes have been used in making polymer nanocomposites. The mechanical, thermal, and electrical property enhancement of the polymeric materials is the main objective

of nano composites. Due to the introduction of nanometer size fillers, there is an obvious increase in the interfacial area that can be observed. The larger surface area results in enhanced bonding of matrix to high strength filler materials (nanotubes and nanofibers) improving the mechanical properties. The presence of conductive fillers can enhance the electrical / thermal conductivity of the matrix and improvement in shape memory ability are the advantages of polymer nanocomposites. Material properties are enhanced by the synergistic combination of one or more kind of nanofillers and polymer matrix from application point of view.

The polymer matrix chemistry, degree of curing of the composite, polymer chain mobility, degree of crystallinity etc., influences the properties of polymer nanocomposites. These nano-fillers used are specific to few of the properties intended for the final application, and this includes carbon black (CB), carbon nanotubes (CNT), carbon nanofibers (CNF), graphenes, SiC, Ni, Fe_3O_4, clay, etc.

Applications of SMPC includes but not limited to heat shrinkable polymer tubing, films, safety tags, self-deploying chair, surgical tools and products, cardiovascular stents, orthopedics, endoscopic surgery, orthodontics, kidney dialysis, photodynamic light therapy, aneurysm therapy or neuro-prosthetics, drug delivery system, smart surgical sutures, and laser-activated SMP microactuator to remove a clot in a blood vessel, artificial muscles research, sutures in cryo-surgery, remotely deployable clinical devices implanted in the human body, textiles, automobile actuators and self-healing systems etc.

As addressed earlier, the conventional pyro-techniques, which can even cause operational failure of spacecrafts (as history testifies), are being replaced with such intelligent systems. Thus the larger structures can be accommodated inside the confined heat-shield space, during launch and can be deployed on orbit. This supplements maximum use of the launch space inside a payload fairing with light weight shape memory polymer materials. This helps for optimal use of payload space and can positively affect launch cost per rockets.

1.4 Motivation for the work

The International Space Station (ISS) is an experimental space platform in low Earth orbit since 1998. It consists of pressurized habitable modules, solar arrays, radiators, docking ports, experiment bays and robotic arms which spread across 72.8m x 108.5 m area (Figure 1.5(a)). It is estimated that the cost of building ISS is about 150 billion dollar which took 36 space shuttle flights of 1.4 billion dollar each for carrying the materials to space. Hence the launch cost amounts to 33% of total cost of installation of the platform. The solar arrays with its truss assembly accounts for approximately 30% of the ISS by weight (ISS weighs to 419.7 tones). The solar arrays are rigid elements carried to space in different flights and assembled.

Giving it an out of the box thought, if the solar arrays were printed on a flexible substrate, the number of launch could have been lesser than what actually NASA had to execute to deliver them to ISS. This could have been possible when a flexible light weight cloth like substrate is folded (collapsed / stoved) as one single payload in shuttle, which on reaching the destination can be deployed to the complete size (illustrated in Figure 1.5(b)). Space being inert to any force, the cloth can remain without any rumble, serving the purpose of a rigid substrate. Considering the cost of launch, 30% of the total weight could have been accommodated in a single payload causing a straight reduction of nearly 30% cost.

The concept of flexible solar array substrate was studied in India by a team of engineers headed by Dr. A P J Abdul Kalam, scientist and former president of India. Dr. Kalam and his composites structures engineers' team, in late 1980s, have formulated an activity profile for the decade 1990-2000. This activity profile (refer Figure 1.6) for the composite materials and structures for space fairing and exploration consisted of many innovative concepts which were aimed at enhancing the science and technology.
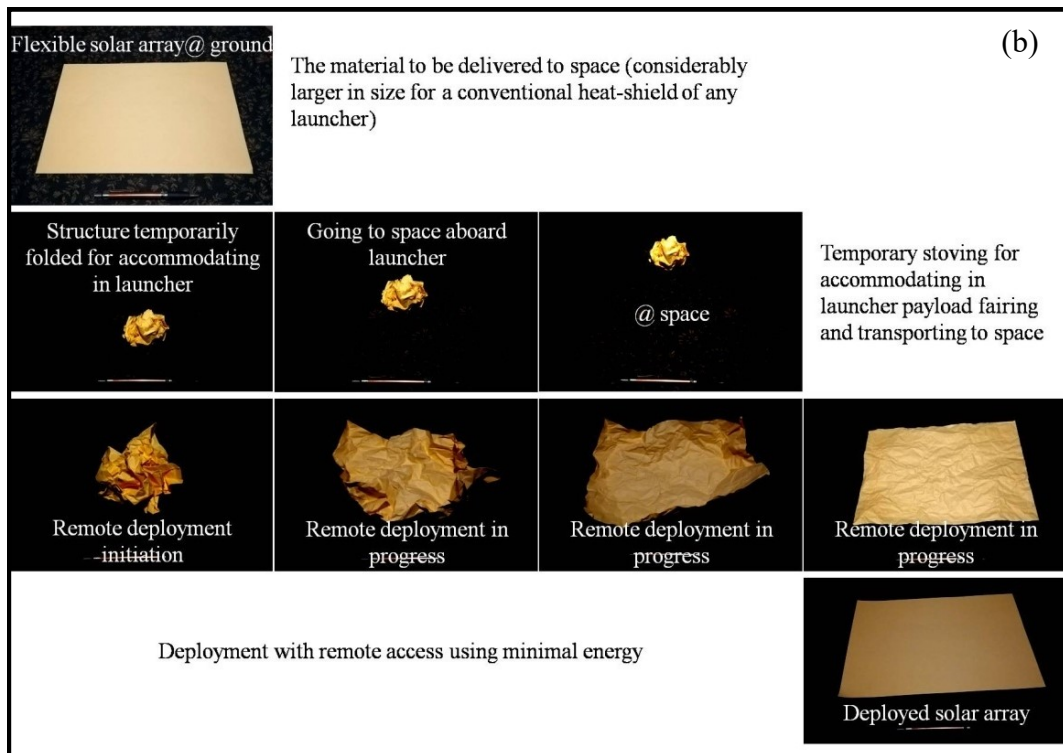
Figure 1.5 (a) International space station with the solar arrays stretched as power source; (b) Flexible solar substrate concept as an alternative system for future explorations.

Most of the concepts mentioned in the presentation were realized in the following years except the 'Flexible solar substrate' (highlighted in Figure 1.6).

ACTIVITY PROFILE 1990-2000: COMPOSITE MATERIALS / REINFORCED PLASTIC DIVISION, ISRO -COURTESY : Shri. ENAMUTHU, Retd. DD, CMSE VSSC

Figure 1.6 Activity profile for year 1990 to 2000, ISRO (A-current products, B-products for future missions, C-demand of materials, D-technology demands, E-facility augmentation)

A material that is flexible as cloth, with printable surface, which can tolerate the space conditions and deployable to the required configuration would serve the purpose for realizing such a platform for solar panels. The studies about shape memory materials become one of the viable options for such a material development.

This becomes a motivation for this thesis work for which the inspiration accounts from the smart stimuli responsive materials / structures seen in nature as discussed earlier. A thorough literature review is done in this line regarding the shape memory materials, the mechanisms, the activation technique and the problem

identification to achieve the goal of realizing such a material, and presented in the following chapter.

1.5 Organization of the thesis

This thesis describes the research on electro-active shape memory polymer nano-composites. It focuses on the effects of matrix morphology, content and type of carbon fillers, and the composite properties which has got direct influence on shape memory behaviour of polymer nanocomposites. The structure of the thesis is presented in the following chapters.

Chapter.1 introduced smart materials with stimuli responsive capabilities which include shape memory materials and presents shape memory polymers and nanocomposites.

Chapter.2 explains the basic principles involved in the activation of shape memory polymers and their nano-composites and gives the systematic description on the existing works on shape memory materials published in the line of this research work and identifies the luster of the fresh researches which forms the basis of this work. This chapter ends with the research problem definition of this thesis.

Chapter.3 presents the scope, objectives and methodology of this investigation.

Chapter.4 describes the materials and methods used for the synthesis of the polyurethane resin and the various characterization techniques employed to understand the behavior of the synthesized polymer composite.

Chapter.5 is divided into three parts of which part one explains the effect of carbon black reinforcement in the polymer resin, interpreting the microscopic, thermal, mechanical and electrical property analysis results. The electrical conductivity imparted due to the inclusion of carbon black nano fillers is modeled and the results are compared with the experimental values. It describes the electro-active shape memory behavior evaluation of CB-PU nano-composites.

The second part explains the carbon nanotube reinforced PU matrix nanocomposites with details regarding the evaluation of its various properties and adds to understand the electrical conductivity process by modeling the composite. This chapter explores the shape memory effect of CNT-PU nanocomposite and the same is demonstrated by passage of electricity.

Third part of the chapter contains the study of synergy between two filler materials: carbon black and carbon nanotube in polyurethane matrix. A comparison study of the experimental results of CB-PU, CNT-PU and combination of fillers are investigated and presented in this chapter.

Chapter.6 summarizes the conclusions drawn from this research and offers recommendations for future scope of the work.

CHAPTER.2

LITERATURE REVIEW

The evolution of civilizations on earth is primarily marked by the advancement of materials in use for specific periods. The demand for better materials for technological and cultural progression has put the foundation stone for the field of materials science. Understanding of newer materials with preferred capabilities, specific to applications helped to coin the term 'smart materials'. Smart materials are those engineered materials which can impart a change physically or chemically, by sensing and responding to specific environmental stimulus and are capable of regaining the original configuration on withdrawal / modification of the stimuli.

The basic inspiration for development of many stimuli responsive systems in use, are derived from nature. Engineers have attempted to mimic and develop materials & methods that would artificially respond to prevailing environmental conditions. A zebra-fish or squid or a chameleon changing its body color to match with the surroundings, the touch-me-not plant (mimosa-pudica) responding to the sense of touch, are few examples from nature.

Smart materials find numerous applications in the field of medical, mechanical, robotics, architecture, and space technologies. The basic principle of realization of such materials are primarily based on three approaches viz atomic / molecular level modification of conventional materials, conventional structures with embedded sensors / actuators, composite materials with properties superior to the individual components.

2.1 Shape memory effect in Polymers

Polymeric materials that are capable of memorizing a permanent shape that can be recovered from an assumed temporary shape under appropriate conditions are termed as Shape Memory Polymers (SMP). SMP stand out among other SMM in the aspect of enhanced usable strain adding to the versatility of forming composites [Merlin et al., 2008; Quan et al., 2015].

The polymer structure, morphology and stimuli altogether are responsible for the SME with proper shape training techniques. Published literature suggests from experimental data that SMPs are extensible up to 800% and possess properties like tunable elastic modulus, tunable response time / transition temperature, and low mass density etc [Jinsong et al., 2008; Huang et al., 2013].

Shape memory behavior of a polymeric material is explained in Figure 2.1, where the material is trained for a particular shape by heating above its transition temperature (T_g / T_{trans}) and subsequently deforming to a temporary shape. Cooling the material retaining the stress of deformation will fix the shape as it reaches the room temperature from its T_g. Once shape is fixed by this process, the externally applied stress can be removed, and the fixed temporary shape is retained by the material. Further, increasing the temperature to T_g shall cause the material to recover the original remembered shape, thus completing one thermomechanical SME cycle [Mather T et al., 2009].

It can be observed from Figure 2.1, that the plot starts from point (iv), where the temperature of the material is raised to approximately 80°C (T_g of the chosen polymeric material). The rising portion along the stress axis (stress increases from 0 MPa to 700 MPa - specific to selected polymer) denotes the shape training process from point (iv) to (i), which acquires its temporary shape at point (i). The material is then cooled below its T_g denoted by the line (i) – (ii), when the stress is retained.
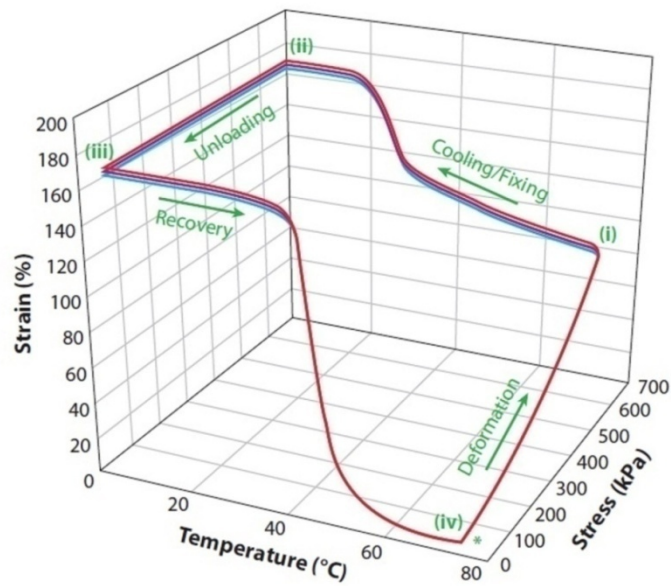
Figure 2.1 Thermomechanical cycle for a typical shape memory polymer (SMP)

On reaching point (ii), the temporary shape is fixed and the stress / external loading can be removed (return along the stress axis through (ii) – (iii) line. This is considered as the operating temperature of the polymer (strained to approx. 170% in this particular case). The material is heated again to its transition temperature (near 80°C) denoted via the line (iii) to (iv), when it is required to gain back its original shape.

2.1.1 Mechanism of shape memory in polymeric materials.

Mechanism of shape shifting and recovery in SMP is achieved through polymeric segmental phase transition initiated by a transition temperature. Two phases of which one allowing for shape fixity (termed as hard segment / net points / frozen portion of polymer) and the other allowing for reversibility or recovery (termed as soft segments in polymer) inside polymers are attributed for the shape memory behavior. Shape memory occurs due to the phase change from rigid to flexible soft phase while the temperature of the material changes across T_g.

It can be observed from the Figure 2.2 that the hard phase acts as anchor points which allow the free deformation of the soft phase at a temperature above T_g. When the material is cooled to room temperature, the shape is retained due to the

soft segment repositioning. For regaining of original shape, the material may be heated again to a temperature above Tg, which causes the hard segments to pull back the soft phase from strained condition.

Original shape	Trained temporary shape	Recovered original shape
Polymeric hard segments (red dots) and soft segments (black worms) at room temperature or temperature $<$ T_g	Heating above T_g allows free movement of soft segments anchored at hard segments / net points. Deformation by external force causes stretching of soft phase with respect to hard phase. Cooling the material with the external force retains the shape	On heating again above T_g, the hard segments pull back the softened phase causing shape recovery

Figure 2.2 Shape memory effect depicted with respect to hard and soft segments

Thus shape memory effect is an efficient way of energy storage in the form of temporary shape (strained condition), as the initial heating and shape training causes storage of strain energy and the recovery of shape results in energy dissipation [Lan et al., 2008].
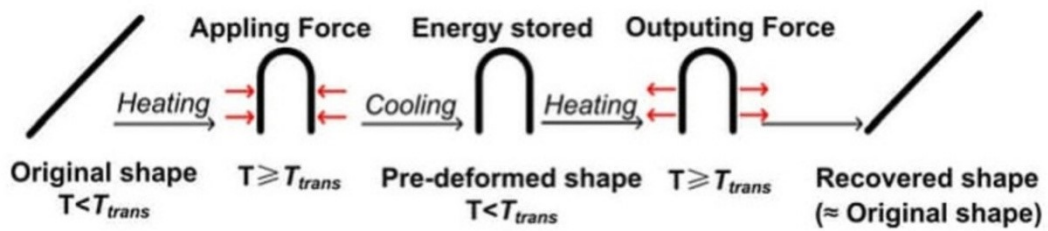
Figure 2.3 Schematic of shape-memory effect during a typical thermo-mechanical cycle

Figure 2.2, showed the morphological depiction of shape memory effect where as the Figure 2.3 gives a physical understanding of the SME. The original shape of the material at T $<$ T_{trans} is shown as a straight line which by heating (T $>$ T_{trans}) and application of external force is deformed to 'U' shape. Straining on

deformation of the material is described as 'energy stored' in the Figure 2.3 (material at $T < T_{trans}$, on cooling after deformation). For regaining the straight line configuration, again temperature is increased above T_g and the original shape is recovered.

Achieving the temporary shape or shape fixity can be referred as a meta-stable form of the material which stores the strain energy. Heating the material above the threshold temperature (shape transition temperature, T_g / T_{trans}) will make the material to regain its original shape by giving away the stored potential energy [Mohd Jani et al., 2014; Liu et al., 2009; Ramdas et al., 2015; Behl and Lendlein, 2007; Hartl and Lagoudas, 2007].

The ability of the reversible segments (refer Figure 2.2) in a polymeric material to retain the temporary shape is termed as shape fixity (R_f), whereas the ability of the materials to recover its original shape is termed as recovery efficiency (R_r). R_f and R_r are calculated specific to a particular SMP from equations (2.1) and (2.2) respectively.

$$R_f\,(N) = (\varepsilon_p(N) \,/\, \varepsilon_m) \qquad\qquad\qquad (2.1)$$

$$R_r(N) = ((\varepsilon_m - \varepsilon_p(N)) \,/\, ((\varepsilon_m - \varepsilon_p(N\text{-}1)) \qquad\qquad\qquad (2.2)$$

where N is the cycle number, ε_m is the maximum strain imposed on the material, and $\varepsilon_p(N)$ and $\varepsilon_p(N\text{-}1)$ are the strains of the sample in two successive cycles in the stress-free state before yield stress is applied. [Lan et al., 2008].

The studies of Lendlein and Kelch, 2012 revealed that the polymer chains assume a completely random distribution within the matrix during the amorphous state. This results in strongly coiled conformation for an amorphous linear polymer chain which is a state of maximum entropy. This relationship (coiled chain conformations and entropy) are explained in the context of cross linking (section 2.6.1) using the theory of Boltzmann's entropy formula. During the transition from the glassy state to an elastic state, an increase in the rotations around segment bonds are observed allowing the polymer chains to assume equivalent conformations. Hence the Entropy elasticity releases the polymeric chains from

strained configuration (temporary shape) to a less complex configuration (original shape), which is the basic principle of shape memory realization [Liu et al., 2009].

Lan et al., 2008; Merlin et al., 2012 have reported three basic working for SMPs which are as detailed below:

1. Molecular polymeric chains are considered as reversible phase and the connecting nodes of macro- molecule segments attributed to physical or chemical cross-links are regarded as the permanent phase. This consideration is termed as 'dual-state' mechanism.

2. One of the components is able to switch stiffness depending on stimuli and the other is regarded as elastic. This consideration is defined as 'dual-component' mechanism.

3. On heating up to deformation temperature (glass transition temperature in this case), the hard portion may serve as the elastic component to store elastic energy, while the softened portion may act as transition segment, thus depicting a 'partial-transition' mechanism.

2.2 Glass transition temperature

The phase change is achieved by training the polymeric material at temperature 15 °C to 30 °C above a specified defined as glass transition temperature (T_g) or transition temperature (T_{trans}). For temperatures above T_g, the polymeric chain alignment deforms, dislocating the nodal points. This softens the material and allows accommodating any temporary shape with new chain interactions. On training to temporary shape, the polymer is cooled below transition temperature to retain the shape. For regaining the original shape, the temperature is increased beyond T_{trans}. Hence the evolved definition of transition temperature becomes the temperature beyond which the polymer gets softened for shape training due to the entropy elasticity [Behl et al., 2007]. A vital requirement in the SMP to exhibit SME is the chain mobility that depends on the viscosity of the chosen monomers.
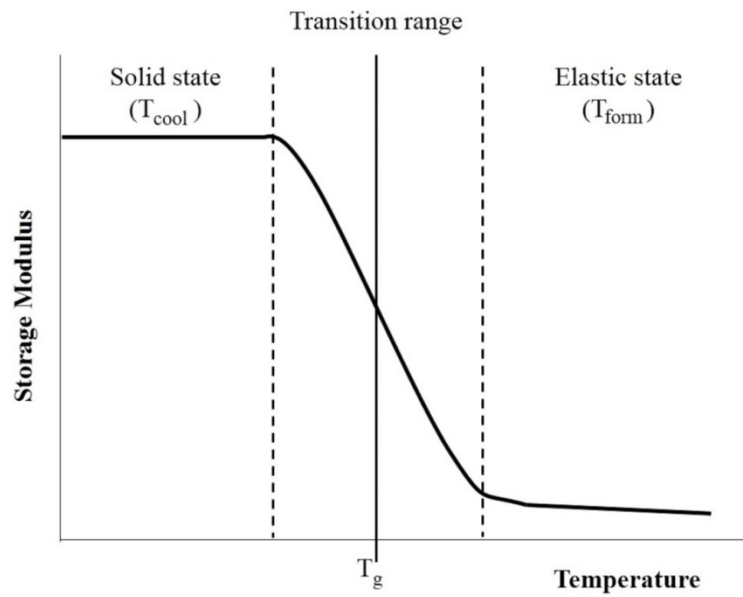
Figure 2.4 Transformation of a polymer elastic modulus across the glass transition

Figure 2.4 depicts the storage modulus reduction across the temperature range as indicated, where the material gets softens from its glassy solid phase. Arun et al., 2018, have explained the transition of the polymeric material across a range of temperature from its glassy state to elastic state. It is a range of temperature over which the glassy phase properties depreciates, and the midpoint of the range is generally accepted as the T_g value of a material. Xu and Song, 2011 reports that T_g is a function of molecular mobility of polymer chains in the SMP and a wider transition temperature range has been reported as a harmful impact on the property of shape memory as if affects the recovery / fixity efficiencies. The transition temperature is a function of synthesis conditions, curing time, cross-linking and the monomer viscosity.

2.3 Response Stimuli

Shape memory polymers respond to different stimuli such as moisture, chemical, magnetic field, heat, electric current etc. Most studied among the various stimuli is direct heating (application of heat via heating element / heater. Driven by demand from applications, heating to T_g by various means were studied such as resistance heating by passage of electric current, induction and magnetic heating,

laser light sources etc [Lan et al., 2008; Humbeeck Van Jan, 1999; Quan and Hai, 2015; Mohd Jani et al., 2014].

Those materials in which shape recovery is triggered by the exposure to light which causes heating of the system are termed as Light Activated Shape Memory Polymer (LASMP). Reversible photo-dimerization of cinnamic acid derivates are the most prominent example of LASMP. Photo sensitive portion in SMP acts as molecular switches and causes shape recovery. This is achieved by incorporating reversible photo-reactive molecular switches which respond to light of specific wave-number / frequency light [Ramdas et al., 2015].
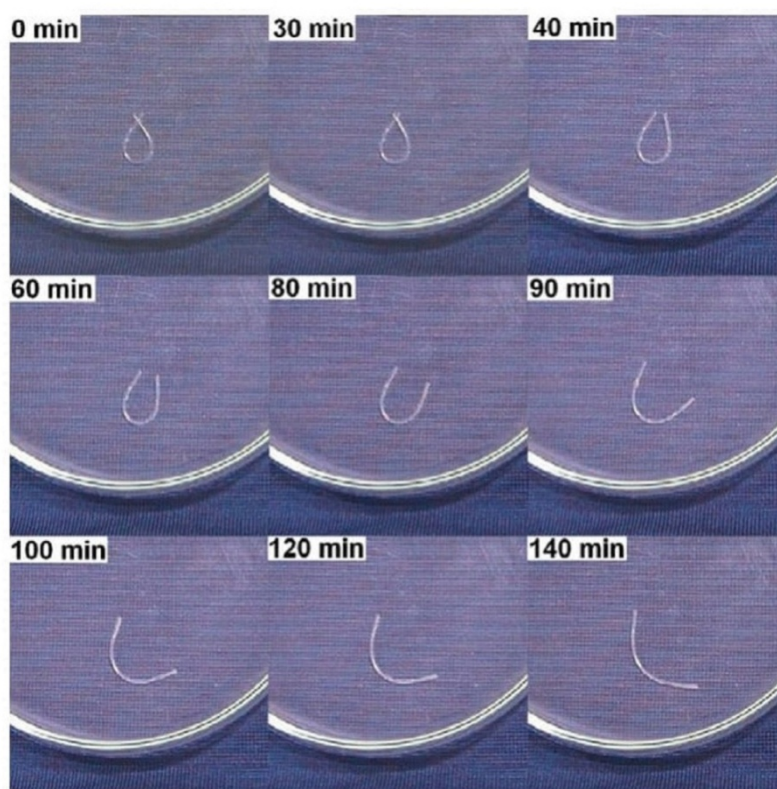
Figure 2.5 Water-driven actuation stages of shape memory polyurethane.

High intensity focused ultrasonic sound was also studied as a trigger for SME in polyurethane polymers. The temperature within the polymer rises to T_g when the ultrasonic sound is passed and this results in shape recovery.

Bio-clinical application prefers chemo-responsive SMPs due to its effectiveness inside sensitive system like human body. Moisture responsive polymeric SMM works with a unique approach of lowering the T_g of the polymer to the ambient water temperature and thus SME is initiated [Quan and Hai, 2015; Merlin J et al., 2008]. Such an experiment from the study of Jinsong Leng et al., 2011, is depicted in the Figure 2.5.

A polyurethane wire, in the form of a closed loop as original shape, with low T_g is introduced in water (0 minute as per Figure 2.5). The water particles slowly start diffusing in it reducing its T_g value, thereby the loop is untied slowly through 40, 60, 80, 100, 120 and 140 minutes achieving its original shape. The solvent / water molecules diffuse into the polymer imparting flexibility and softness to the system and thereby causing flexibility of polymer chains leading to shape recovery.

Stimulation using electrical potential is one of the most studied areas as it facilitates remote controllability of SMP that is significant in aerospace applications.

Polymers which are mostly non-conducting are made conductive by adding conducting filler materials and the passage of electricity heat the material to its transition temperature. Thus heating of the bulk of polymer causes the rearrangement of the hard and soft domains inside the polymer facilitating shape memory.

Another triggering mechanism is magnetism which causes non-contact mode for actuation in SMP, achieved by inductive resistance heating in alternating magnetic fields. It is achieved by incorporating magnetic nanoparticles fillers [Taha et al., 2015]. R.Mohr *et al.* 2006, have used frequency, f = 258 kHz; magnetization, H=30 kAm^{-1} for verifying the concept and has reported the use as smart implants or surgical instruments to facilitate fine adjustments in a noncontact mode.

Infrared light stimulation results in heating causing indirect thermally induced SME in polymers supplemented with conducting fillers results in joule / resistive heating initiating SME [Taha et al., 2015, Ramdas et al., 2015].

2.4 Thermoset and Thermoplastic SMPs

Thermoset and thermoplastic are the two types of polymers based on the cross-linking of the carbon chains. These polymers differ in their shape memory ability due to the chemical and physical cross-linking in microstructure. Thermoset polymers are reported to possess higher T_g than thermoplastic polymers attributed to the strong chemical cross-links. They show better mechanical properties and find applications in many severe environmental conditions. By controlling the cross-link densities which regulates the rigidity of the polymer chains, the T_g and mechanical properties can be tuned for specific applications [Ma et al., 2015; Zang et al., 2009].

Strong chain to chain interactions cause chain entanglements or local crystalline domains and these serve as the physical cross-linking in thermoplastic SMPs. Physical cross-linked are flexibile, mouldable, and possess high shape deformation range compared to thermoset polymers.

The T_g of any polymeric system is observed to be influenced by modulus which in turn is a function of cross link density [Arun et al., 2018].

2.4.1 Cross-linking

Chemically cross-linked SMPs generally exhibit better strain fixing ratios and strain recovery ratios, faster strain recovery rates, larger shape recovery stress, and most importantly lower strain-to-failure values [Leng et al., 2009]. Such a combination of properties of thermoset SMPs may arise from their higher cross-linking density and the ability of the chemical cross-links to withstand tensile stress. Physical cross-links are found to give large strain and chemical cross-links give high stress recovery. Many challenging applications require high failure strain and good mechanical stability [Xu and Song, 2011]. Thus a trade-off

between the physical and chemical cross-linking is on demand for advanced polymer applications such as shape memory.

2.4.2 Storage modulus and loss modulus

Storage modulus and loss modulus are the terms associated with the viscoelastic materials depicting the stored energy (elastic behavior) and the energy dissipation as heat (viscous behavior). The potential elasticity of the materials results in high storage modulus in polymeric materials that is referred as glassy state. The micro-Brownian movement (micro particles excited at higher energy level) results in a low storage modulus referring to rubbery state. The glass transition temperature T_g is the demarcating region for this phase change, which provides heat energy for exciting micro-level particles [Yang et al., 2014; Gross Korey Edward, 2008; Lan et al., 2011; Xiao et al., 2016].

The complex dynamic modulus of a polymeric material with shape memory property describes the dynamic mechanical properties and is defined as follows;

$$E^* = E' + i\,E'' \tag{2.3}$$

where E' is the storage modulus and E'' is the loss modulus.

The viscoelastic properties of SMP are derived from dynamic mechanical analysis (DMA) in which a cyclic force / stress is applied to a material and the strain is recorded. The stress and strain are in phase and for purely elastic material, whereas a 90° phase lag exists between stress and strain in viscous material. SMPs, are viscoelastic materials and hence the stress and strain characteristics can be expressed as follows.

$$\text{Stress, } \sigma = \sigma_o \, \text{Sin}(\omega t + \delta) \tag{2.4}$$

$$\text{Strain, } \varepsilon = \varepsilon_o \text{Sin}\,(\omega t) \tag{2.5}$$

Here, ω represents the frequency of strain, 't' is time, δ is the phase lag that exists between stress and strain.

Storage Modulus, can be expressed as a function of cosine of the stress strain relationship and loss modulus as function of sine of the phase angle that exists between stress and strain measurements.

$$E' = (\sigma_o / \varepsilon_o) \times Cos\ \delta \qquad\qquad (2.6)$$

$$E'' = (\sigma_o / \varepsilon_o) \times Sin\ \delta \qquad\qquad (2.7)$$

The phase separation can be the arc tangent of ratio between loss modulus and storage modulus.

$$i.e.,\ \delta = tan^{-1}\ (E''/E') \qquad\qquad (2.8)$$

For small deformations, it is reported storage modulus is approximately equal to the Young's modulus.

Boltzmann's entropy formula gives the thermodynamic explanation of shape memory effect in polymers which relates the entropy of the system to the probability of a coiled conformation (randomly distributed long polymer chains that are coiled inside the matrix representing an amorphous state). The degree of freedom of the chains is a function of the cross-linking as inter / intra chain interactions are influenced by cross-links (physical / chemical).

Entropy (S) is articulated as a function of the probability of a coiled conformation (W) in the formula, given by

$$S = k\ ln\ W \qquad\qquad (2.9)$$

where k represents the Boltzmann's constant.

Entropy is hence a measure of the possible microstates in thermodynamic equilibrium with the macroscopic properties accounted by Boltzmann's constant [Liu et al., 2009; Xiao et al., 2016].

The rotations around segment bonds get unrestrained, while a polymer is in the transition from the glassy state to a rubber-elastic state by thermal activation. On supplying energy externally, the polymer chains become free to get un-entangled

and new confirmations are formed, which may or may not contribute to densify the microstructure. The parameter 'W' depends on the degree of freedom of chains induced by the chaotic energy level inside the matrix from the heat energy supplied. At this particular point, application of an external force (tensile / compressive) can cause straining of the chains which are anchored at cross-linked points. If the applied stress exceeds a critical limit, the cross-link breaks and the chains undergo permanent de-coiling / slipping resulting in value of 'W' (in above equation) tending to zero causing entropy to become unreal [Arun et al., 2018].

The critical value of straining is influenced by the type of cross-linking as in the case with covalent bonds (chemical cross-links) and hydrogen bonds (physical cross-links). Removal of the supplied energy acts on the chain movements resulting in fixing a new conformation with strained cross-link points. This is the process involved in the shape training of an SMP by external thermal stimuli producing new configuration, both internally and externally [Sunitha et al., 2013].

2.5 Morphology

Polymer chains in an SMP network are responsible for the temperature-dependent deformation and recovery resulting in shape change in response to various stimuli. H Zang et al., 2009 have studied the morphological features of SMP blend of styrene–butadiene–styrene tri-block copolymer (SBS) and poly 3-caprolactone (PCL) for understanding the molecular mechanism in SMP. For the same, a combination of SBS and PCL acting as elastomeric and crystalline domains respectively were studied varying the content between 0 and 100. The Microscopic imagery of the individual combinations was observed as depicted in the Figure 2.6.

Primarily, it can be observed that the elastomeric as well as crystalline segments contribute towards shape fixing and recovery.   Figure 2.6 through series 'a' to 'd' shows the gradual increase in elastomeric PCL   content and corresponding decrease in switching segment SBS. It can be seen that the shape fixity of series 'a' and 'c' are reported less efficient, while the series 'b' and 'd' have shown better efficiency. This infers that SBS (switching domain) being major phase is

not advisable for better shape fixation. The recovery efficiency for series 'c' and 'd' are reported poor compared to that of series with dominant elastomeric domain (PCL as major component).
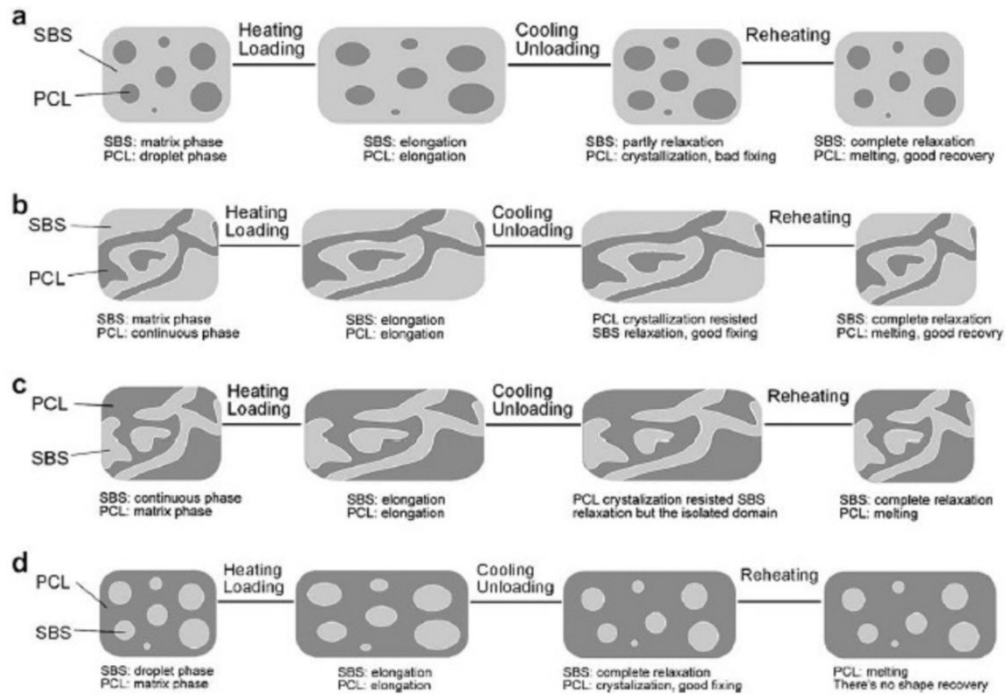
Figure 2.6 Four combinations of styrene–butadiene–styrene tri-block copolymer (SBS) as switching segment and poly(3-caprolactone) (PCL) as elastomeric segment, for complete shape memory cycle observed at each stage in atomic force microscope.

An intersection of better shape fixation and recovery points towards the combination with elastic segment as major phase and switching segment as minor phase, i.e., series 'b'.

Hence a general mechanism for polymer blend SMP can be derived based on above morphological study. In case of block copolymers like Polyurethane, the two immiscible components of the blend separately contributed to shape memory effect. The temporary shape fixation in an SMP depends on reversible bonds between the immiscible components, while the recovery is derived from the switching segments [Zang et al., 2009; Luo and Mather, 2010].

2.5.1 Self-healing property of SMP

The property by which a material that can repair a mechanical damage by itself though rearrangement of the micro / macro-structural parameters is termed as self healing behavior of the material. SMPs are among the most studied self healing materials where the melting of elastic phase in macrolevel and thereby diffusion of polymeric chains in micro scale can heal the damage when triggered by a suitable stimuli. Many methods are developed to harness the self healing ability of the polymeric materials, such as embedding healing agents, introduction of reversible interactions etc. The major challenge for this is the requirement of presence of the healing component close to damaged area for achieving healing. The concept of bulk Shape Memory Assisted Self-Healing (SMASH) system introduces the healing packages distributed uniformly in the matrix to widen the healing coverage. Since self-healing of cracks and damages of structures would significantly extend the lifetime and utility of such smart structures, self-healing of structural damage is a remarkable significance for the researchers [Liu et al., 2009; Xu and Li, 2010; Luo and Mather, 2013; Ratna and Karger-Kocsis, 2008; Leng et al., 2011].

In a self healing system, the process of occurrence can be explained in few steps.

On sensing damage by the monitoring system, the location is identified by co-ordinates and magnitude of damage is estimated. The smart sensing and actuation signals the controlling system and then the heating of concerned location will induce shape recovery of SMPs to original designed shape and thus heal the damage locally. A term Reversible Plasticity Shape Memory Effect (RP SME) is introduced in the course of research in the field of shape memory self healing concept and it allows plastic deformation of a specific area in the system to fill the gaps and rectify the damages. This system approach works in polymer composites where the multiple components take up the functions of sensing, controlling and healing [Hu et al., 2012].

2.6 Shape memory polymer composites

Polymers with intrinsic shape memory property when used as matrices for synthesis of composite materials results in shape memory polymer composites (SMPCs). Filler reinforcements are dispersed / aligned in the matrix and the entire system is cured to fabricate composite materials [Liu et al., 2014].

Composites are classified broadly into two categories namely particle and fiber reinforced. Due to the obvious advantage of strength in desired direction and predictable load transfer mechanisms, fiber reinforced composites (FRC) gained significance among composite materials. FRC are broadly classified based on the matrix constituents, as Polymer Matrix Composites (PMCs), Metal Matrix Composites (MMCs) and Ceramic Matrix Composites (CMCs).

Due to the easiness in fabrication, characterization and ready availability of polymer matrices, they are preffered over other matrix materials for composite synthesis. Polyurethane, polyester, Vinyl ester, epoxy, phenolic, polyimide, polyamide, polypropylene, poly-ether-ether-ketone are few to name as matrix materials used in FRC. Carbon, aramid, glass, cellulose etc., are the commonly used fibers for composite fabrication.

Looking to aerospace applications, most of the launch vehicles and satellites in use today are made of composite materials due to the weight advantages of composite materials over metal parts. Mechanisms or actuators made of mechanically movable parts are contributions to the complexities and weight of such structures. Use of shape memory polymers in actuations can potentially replace many complex mechanisms. Combining one or more materials with shape memory behavior for specific applications can make a Shape Memory Polymer Composite (SMPC). Either of these components need not be an SMM, with minimum of one of the ingredients can be to enhance the mechanical or chemical properties to serve the application. With the complete understanding of behavior of shape memory polymer composites as an alternative material combination / part for an existing 'mechanism' shall add to the endeavor to find launch

advantages in rocketry and spacecrafts [Liu et al., 2008; Lan et al., 2011; Bergman, 2014].

The currently popular and reliable mechanisms used for configuration change / deployment / detachment of structures in rocketry and orbiting spacecrafts are by means of mechanical hinges or stored energy devices (pyro-systems) and motor driven tools. The disadvantages for such traditional devices are multifarious complex mechanisms, sensitive assembly process, large volume / weight and undesired effects such as shocks during deployment which are least admissible for spacecrafts. SMPCs become a replacement of such mechanism that can overcome the bottlenecks mentioned [Liu et al., 2008].

2.6.1 Nanocomposites

SMP with nanomaterials introduced as reinforcements are referred as Nanocomposites. It is noteworthy that the polymer matrix is found highly affected by nanosized reinforcements where the dimension, dispersion state and interaction of the reinforcements play significant roles. An important attribute of the shape memory polymer nanocomposites as pointed out in many literatures is the trade-off between recoverable deformation and the external force that causes the deformation [Balasubramanian, 2013].

It is a recent development to use nanosized carbon fillers to very small amount (3.3 weight percentage Multi Walled Carbon NanoTubes MWCNTs), into polyurethane SMPs to form SMPC with increased recovery stress to the order of four times. Polyurethane SMPs reinforced with combinations of CNTs and CB showed increased shape fixity with almost 100% shape recovery, whereas polyurethane SMPs reinforced with CB alone showed only 30% recovery. The anisotropic CNTs interactions with the crystallizing polyurethane switching segments results in such accurate shape recovery. This reveals that CNT is superior to CB as reinforcement for SMPC while considering the shape recovery [Leng et al., 2008; Xiong, 2005; Zhang et al., 2009].

Due to large value of thermal conductivities (near 3000 W m^{-1} K^{-1}) of CNT, it can be good candidate for heat conduction inside an SMPC that can be thermally activated by suitable stimuli. Molecular dynamics of aligned CNT polymer nanocomposites Multi-Wall Carbon Nano Tube (MWCNT) / Single Walled Carbon NanoTube (SWCNT)) predicts better thermal properties which are already been in use in a variety of applications including electronics thermal management [Amy M et al., 2014]. Out-of-plane and inter-laminar properties of advanced composite structures were found to be enhanced by use of these materials.

2.7 Electro-Active SMPC

The current focus of SMPC research is oriented to improve the recovery stresses (depends of modulus), recovery speed (primarily understood as due to poor thermal conductivities) and the inertness to electromagnetic stimuli (due to the electrical insulation of most polymeric materials). To overcome these limitations, fillers are added that can improve the rubbery moduli, thermal and electrical conductivities.

It is known that thermally activated actuators can offer large strains on expense of large amount of energy and eventually the response is slow. Magnetically driven shape memory devices requires heavy and intricate mechanisms to trigger the SME in the material, It demands the material to be made magnetic by either introducing fillers or coating, and the efficiency on study was found lesser efficient compared with electrostrictive (electric field-driven) shape memory devices, Electrictro-activate SMPs are observed to show faster response, compact in size, and solves most of the drawbacks experienced by other stimuli responsive shape memory materials [Tajeddini and Muliana, 2016].

Thermo-responsive SMPC uses the heat energy to achieve the material temperature above T_g for phase transformation and hence a good amount of energy is used for raising the temperature of the bulk. In case of electro active actuation, the conductive part alone is heated by resistive heating / joule heating and hence Electro Active Shape Memory Polymers (EASMP) proves to be more efficient and faster compared to thermo-responsive SMPs. When the polymer

composite exhibits its shape memory property due to application of electric current / field, it is termed as Electro-Active Shape Memory Polymer Composite (EA SMPC). Electro active shape memory effect typically depends on the amount of induced Joule heating and it can only occur when the temperature is above T_g for a polymer. The induced Joule heating is inversely proportional to the resistance of the materials and directly proportional to the applied voltage. It is observed that faster electro-active response can be associated with the improvement of thermal and electrical conductivity of the composites. The electrical conductivity of such polymers depends on the uniform heating of the volume of the material which can be achieved by dispersion of fillers in the continuous phase. Thermal conductivity and T_g are observed to show strong dependence on the weight fraction of filler materials in the shape memory polymers. Inclusion of conductive polymers or conducting filler materials can improve the electrical / thermal conductivity of the bulk and thereby enhance electrical actuation [Meng and Li, 2013; Jiang et al., 2014; Leng et al., 2011; Varga and Tröster, 2014].

A polymer can either be synthesized intrinsically to be electrically conducting using monomers with good electrical properties or by doping conductive fillers (Carbon Nano Tube (CNT), Carbon Nano Fibre (CNF), graphite, graphene and metallic particles) into the insulating polymer matrix.

2.7.1 Intrinsically conductive polymers

Polymeric materials those conduct electricity by its nature (conductive polymers) are called intrinsically conductive polymers. For being electrically conductivitive, a polymer has to mimic a natural conductor like metals, by letting the electrons to move freely inside them. This is chemically possible inside an organic material by the conjugate nature of the bond between carbon atoms as the possibility of polarization can result in electron movement. In conjugation, the bonds between the carbon atoms are alternately single and double. Every carbon-carbon linkage bond contains a localized "sigma" (σ) bond or strong covalent bond and a weaker localized "pi" (π) bond or double bond. This leads to shifting of electrons by

breaking weaker bonds resulting in release of electron in presence of suitable medium. One of the simplest forms of conjugated polymer is Polyacetylene, which is formed by polymerization of acetylene. Figure 2.7 depicts the general chemical structure of few polymers (conjugate bond polymers) that are intrinsically electrically conducting (polyacetylene, polyphenylene vinylene, polypyrole (X = NH), polythiophene (X = S), polyaniline (X = NH/N) and polyphenylene sulphide (X = S)).
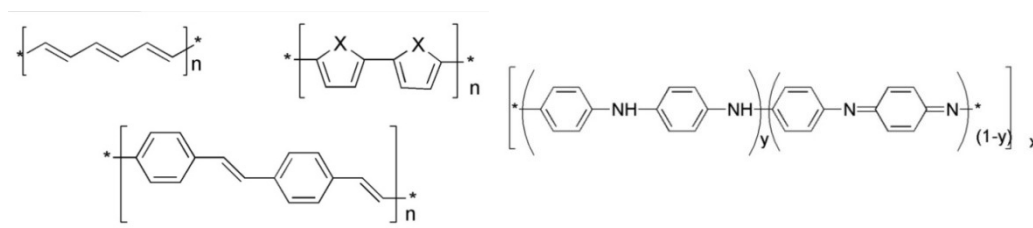
Figure.2.7 Intrinsically conductive polymeric structure

The component monomers having conjugated chemical bonds (as in **Figure 2.7**), under certain conditions (doping leading to protonation), ensure the electron conductivity of the polymer. For example, Considering Polyaniline (PANI) in emeraldine oxidation state, is treated with acids, the protons primarily interact with the imine atoms of nitrogen (protonation process) and this result in formation of polycations. This causes localization of positive charges on adjacent nitrogen atoms and it increases the total energy of the system. This positive charge accumulation pushes the electron density causing unpairing of lone electron pair of nitrogen atoms thus increasing the material conductivity [Wu et al., 2013].

2.7.2 Conductive filler materials for facilitating electro-activity

Conductive fibers or powder shall enhance the electron transfer proprty in the bulk matrix of the polymer and thus facilitate electrical conduction. Preparation of conductive polymer composites by mixing various kinds of conductive fillers such as Short Carbon Fibers (SCFs), carbon black, metallic (Ni powder) powders, CNT are being studied by material scientists across the world [Wu et al., 2000; Bilotti et al., 2013]. Studies reports that the variation in the T_g of the epoxies due to the presence of the filler materials as content of filler beyond the critical requirement

becomes the dominant phase and shall regulate the property of the composite. Hence the weight / volume percentage of filler material is significant in case of a doped conductive SMPC. Optimal filler content reduces the resistance to molecular mobility due to reduced viscosity of the matrix and thus the transition happens over a short range of temperature. A narrow glass transition helps in efficient recovery and stable phases across the T_g.

Carbon as reinforcement fillers in various forms in the SMPC will positively influence the properties like modulus, conductivity, T_g, etc. An electrically percolating network was found to be provided by the nano sized fiber morphology that results in high electrical conductivity, enhanced heat transfer and better recovery stress. Carbon fibers, particles, nanotube and graphene are probed mostly by the material scientists to understand the conductivity phenomenon, and for electrical triggering of the shape memory behavior.

2.7.2.1 Carbon Nano Fibers (CNF)

Carbon nanofibers are short carbon fibers that are known for their potential thermal, electrical, frequency shielding, and mechanical property enhancements to the composites. It is thereby known that, filler material not only influences the electrical properties, but also the mechanical and thermal properties of a polymer. CNF are observed to have got better properties than normal carbon fiber in use due to the nano scale advantage which provides better surface area, continuous internal network of fibers, better strength and modulus. Shape recovery for EASMP with CNF can be accomplished by applying an external electric current through leads connected to the material [Chen et a., 2013; Lu et al., 2014].

SMP nanocomposites having excellent high-speed electrical actuation capabilities have been developed by many material scientists by incorporating electrospun continuous non-woven CNF into an epoxy-based SMP matrix [Zhang et al., 2015]. Non-woven nanofibers commonly have the characteristics of a large surface area and high porosity. Electrospinning is one of the effectual techniques for synthesizing non-woven continuous polymer nanofibers of diameters range varying from several micrometers down to a few nanometers. These fibers hold properties

similar to the fibers produced using both electro-spraying and conventional solution dry spinning [Lee et al., 2016].

Studies with Epoxy Shape Memory Polymer resin system (ESMP) as matrix with CNF as reinforcement have shown reduced SME with increased CNF content. As learnt, it is because of high interfacial friction between ESMP macromolecular segment (matrix) and the fillers. This emphasizes the need of optimizing the nanofiber content for specific properties [Deng et al., 2016]. Thus, it can be inferred that filler content is a tradeoff between interfacial bond strength between matrix and reinforcement, and electrical property [Davies et al., 2007]. It is noted that unlike Ni powder, incorporation of CNF showed little effect on transition temperature. ESMP CNF composite showed that the recovery speed is influenced by the narrow glass transition of epoxy and an increased thermal conductivity due to the incorporation of CNFs.

Changing the triggering voltage also influence the speed of shape recovery (Figure 2.8), as demonstrated through an experiment on ESMP-CNF composite that the recovery time less than 2 seconds is achievable by application of increased triggering voltage.
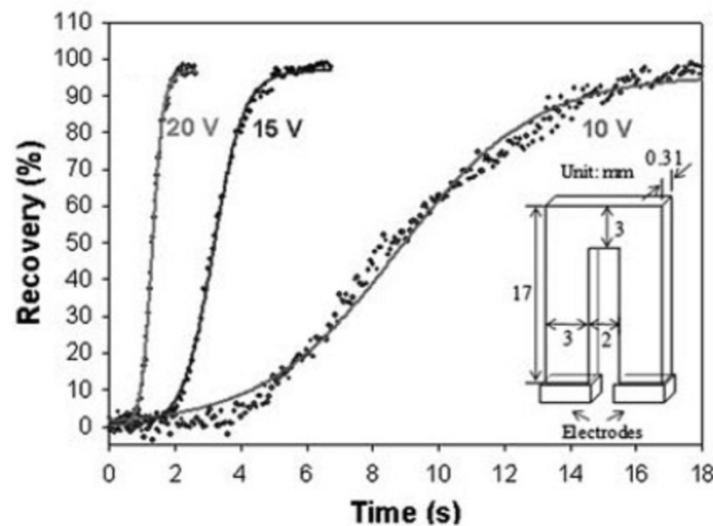
Figure 2.8 Recovery time vs. recovery efficiency for voltages 10V, 15V and 20V for electrically activated shape recovery of epoxy/CNF nanocomposites [Luo et al., 2010]

The comparison of recovery speed for various applied voltage can be seen in Figure 2.8, which clearly shows that increasing the voltage lowers the recovery time. This is an indication of the overall energy supplied to the system as potential difference, which converts to the heat energy due to resistance heating inside the bulk of the system causing shape recovery.

2.7.2.2 Carbon Nanopaper

Planar-conductivity was intended while shifting the attention parallel to the studies in nanoparticles, fibers and nanotubes. Studies on composites with multiple layers of the nanopaper incorporated have shown improved electrical properties and fast actuation with less triggering voltage. The major approach towards synthesis of carbon nanopaper are from 'Graphene' or single-layer carbon foil and the other route is by stacking of CNT / CNF films together known as 'buckypaper'. It is reported that vacuum assisted resin transfer moulding is used to synthesize nanopapers from CNT / CNF layers. Buckypaper is observed to possess one tenth the weight of steel but has strength around 500 times when its sheets are stacked / aligned to form a composite [Lu et al., 2014; Lu et al., 2010; Meng and Li, 2013; Pilate, 2016].

The mechanical properties and performance of the polymer composites are enhanced by the interfacial bonding of matrix and multi layered nanopaper. Agglomeration of the planar conductive carbon fillers is a major challenge in synthesizing the conductive composites for various applications. It is observed that non agglomerated randomly distributed nanopaper effects uniform conduction and thereby uniform heating for shape memory activation [Ratna and Karger-Kocsis, 2008].

2.7.2.3 Carbon Black (CB)

Carbon Black represents spherical particles with size in the range of 10nm to 500nm, which typically contains 95% pure carbon. Addition of CB as reinforcement filler reports to show improvement in the resilience, tear strength, conductivity and other physical properties of the polymer matrix composites.

Figure 2.9 depicts the tunneling electron micrograph of dispersed carbon nanospheres in resin magnified to 400nm.
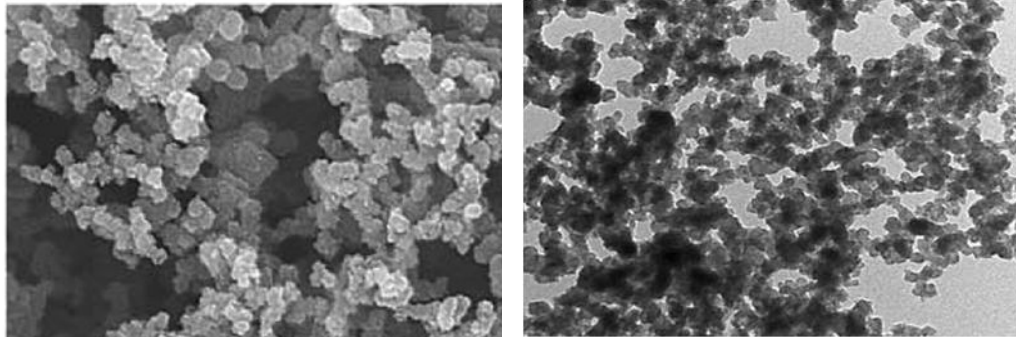
Figure 2.9 Carbon black nanoparticles as observed in tunneling electron microscope (TEM) (400nm magnification)

Literatures report an increase in its resistance with an increase in temperature (Positive Thermal Coefficient / PTC) on addition of 5% carbon black, while addition of short carbon fiber (SCF) along with CB as combination in styrene based resin decreases its resistance with an increase in its temperature (Negative Thermal Coefficient / NTC). Thus, the SMPC with CB-SCF reinforcements acts as a thermistor which regulates the resistance based on filler content. This is a significant observation as it can be understood that a combination of CB and SCF could increase the volume conductivity and provide better SMP property by enhancing the Joule heating by conduction. The positive thermal coefficient effect for conducting polymer composites depends remarkably on the properties of polymer matrices and conducting fillers [Ma et al., 2015; Macutkevic et al., 2013; Leng et al., 2008; Balberg, 2002; Lan et al., 2008; Meng and Li, 2013].

Electrical resistivity was found extremely high in CB content less than 2% but a sharp transition occurs between 2% to 6% (reported as percolation threshold range). Thus, keeping CB content as 5%, the other filler content is varied to understand the synergy of reinforcements in a particular matrix. Another observation about this composite is that the combination of CB and SCF has decreased the T_g value, as SCF content increased from 0 to 2% for 5% constant CB content. An important inference from this study to be noted is about the inherent fibrillar form of SCF / CNF. These are having higher tendency to form a

three-dimensional network in the composites, ensuring better electrical response than CB as filler. Fibrils are slight thread like projections from the sides of SCF making it an imperfect surface material (undulated surface). These undulations and projections are advantageous as connecting links to the adjacent SCF entity making a network possible in three dimensions (inter-fiber linkages). Hence it was observed that individually, as the amount of SCF filler content increased, the electrical conductivity of the SMPC also increased with lesser recovery time as reported, which is attributed to the fibrillar form as explained above [Leng et al., 2008].

A higher weight percentage of CB in Polyurethane SMPs showed better strain fixity, but further CB addition decreased the shape recovery ratio and shape recovery speed while T_g remained unaffected. As the CB content increased above 10%, the crystallinity was found decreasing and it affects the ability of the deformed sample to retain its shape after the removal of load. This reduces the shape fixity ratio and thus the recovery ratio also [Lan et al., 2008].

Effects of CB nanoparticles in two-way reversible shape memory cycles in cross-linked polyethylene showed improved shape memory behavior. The development of a stable physical cross-linking structure preserves the elastic energy in the recovery process in a CB reinforced polymer matrix [Ma et al., 2015].

Figure 2.10 (a), (b), (c) shows the shape memory effect of random dispersed fiber composite matrix with three different combinations of CB and Ni particles. The particles are interconnected internally forming conductive networks resulting in electrical conductivity of the composites as explained earlier. The continuity of well dispersed reinforcements in anisotropy improves the overall electrical conductivity of the matrix. The original shape is recovered within 120 seconds in 10 volume percentage of CB and 0.5 volume percentages of chained Ni particles. The performances are found improving as the network of nickel getting arranged / chained to form continuous network [Leng et al., 2011].
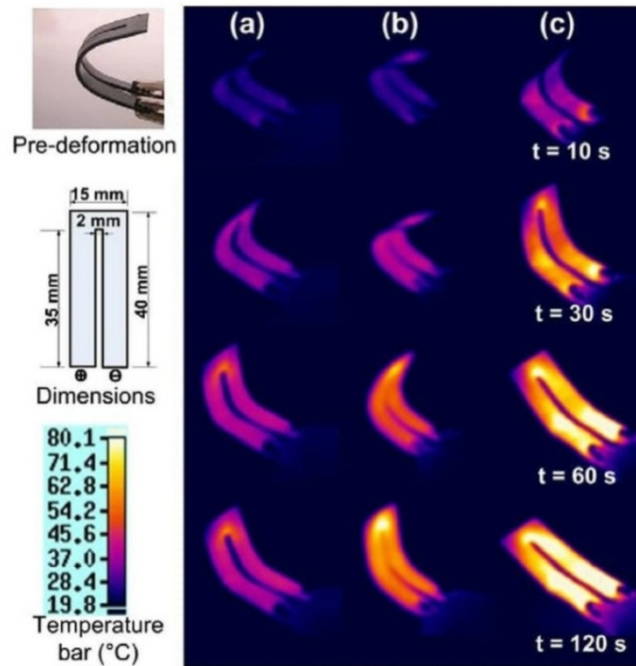
Figure 2.10 Temperature distribution via IR observation of three combinations of Ni and CB ((a) 10 vol.% of CB alone, while undergoing shape recovery;(b) 10 vol.% of CB, 0.5 vol.% of randomly distributed Ni; (c) 10 vol.% of CB, 0.5 vol.% of chained Ni) The dimensions of sample and the temperature variations are shown at side. [Arun et al., 2018]

The studies to improve the properties of composites supplementing smart materials lead to search for better alternative filler for EASMP materials which led to researches on nanotubes.

2.7.2.4 Carbon Nano Tubes (CNT)

Tubular carbon structures with diameters approximately 5 to 10 nm having large aspect ratio were observed for the first time by Dr. Sumio Iijima. The advantages of conductivity of carbon, the aspect ratio, formidable strength etc., form the base of adopting these tubular structures referred as nanotubes for various applications. Generally, Multi-Wall Carbon Nano Tubes (MWCNTs) and single walled carbon nanotubes(SWNTs) are produced by three techniques: arc-discharge, laser-ablation, and catalytic growth. CNT has reported to possess an average value of Young's modulus as 1800 GPa, which is much higher than conventional carbon fibers (680 GPa) used as reinforcements. The MWCNTs synthesized by Chemical vapour deposition method shows thermal conductivity of 4 to 300 K in

temperatures varying from room temperature to elevated temperature conditions. The specific strength of CNT is found to be extremely high compared with the traditional fibers and are very good conductors of heat and electricity. CNT are stacks of one up to ten & hundreds of concentric shells of carbons separated by approximately 0.34 nm. This is analogous to honeycomb arrangement of the carbon atoms in the graphite sheets with very high Young's modulus and tensile strength, making them preferable for composite materials with improved mechanical properties [Popov, 2004; Kordµs et al., 2006, Friedrich and Breuer, 2015].

Nanotubes are rolled graphite sheets as hollow cylinders in molecular level with classification as single-walled (0.5–2 nm diameter) and those with multiple concentric cylinders as multiple-walled (2–50 nm diameter). Efficiently aligned CNT can replace continuous carbon fibres which can be woven and stacked to realize fabrics exhibiting extremely high strength and integrity for engineering applications. The nanotubes of about 10 nm in diameter are found to have an interfacial area with matrices which is almost 1,000 times greater than that of 10-micrometre fibres of the same volume.

A significant concern in case of CNT expressed in literature regarding its use as reinforcement for enhancing electrical property is the challenge of preserving the highly electronically active surface of CNTs (not covered by a surfactant), and to make sure that the CNT does not break under shear exceeding a certain threshold, due to its extremely high aspect ratio. Due to the effect on electrical conductivity, an established trade-off between surfactant coating and electrical response is required. Another major drawback of CNT reported as reinforcement material is the difficulty of their homogeneous integration (dispersion) into a matrix because of their pronounced agglomeration tendency. Functionalisation / surface modifications are reported as the solution for the mentioned issues and this technique has improved the interfacial properties of the SMP CNT system, for which many researchers have used nitric acid and sulfuric acid surface treatments of nanotubes. On mixing surface modified CNT into polyurethane SMP and when activated by applying electrical voltage, it is shows that the surface modification

to an optimized content increases the matrix-reinforcement bondage and improves electrical properties. Figure 2.11 depicts the dispersion of surface modified CNT in Sulfonated poly (Styrene-b-[Ethylene / Butylene]-b-Styrene) (SSEBS) matrix, as observed through TEM. The composite SSEBS-CNT has been tested for SME and it showed better results compared to non-modified CNT in same matrix [Lu et al., 2013; Wang et al., 2009; Ahir et al., 2008].

Electrical properties of nanotubes in composite systems suggests that electrical conductivity of surface-modified MWCNT composite was found lower than that of the composites filled with untreated MWCNT for same filler content. This is attributed to the increased defects in the lattice structure of carbon–carbon bonds in nanotube surface owing to the acid treatment / modification. Thus, even though strength and interfacial bonding is favoured by surface treatment, negative effect on electrical behavior reduces shape memory response of the composites. Hence, it is established that the shape-memory effect depends on the filler content and degree of surface-modification of the MWCNTs [Du et al., 2015; Wu et al., 2007].

Figure 2.11 Multi Walled Carbon Nanotubes 20-30nm as observed in TEM (100nm)

The major challenge to address is the dispersion of CNTs in polymer matrix which affects the uniformity in the electrical properties of composites. Studies have proven that the CNT is one of the most effective fillers for making SMPs electrically conductive. Degree of surface-modification of the fillers (in case of

41

CNT), mode of synthesis and the matrix properties are identified as the research areas those need to be attended in CNT polymer nanocomposites.

Out of the many methods of nanocomposite synthesis, in-situ polymerized structures shows better distribution of the fillers / CNTs compared to direct mixing. Electrical conductivity is found to have enhanced 100 folds for chained / aligned CNT compared to randomly distributed fibers in the polymer matrix. The alignment of the nanotubes provides a more effective path for electron transfer along the length (alignment direction) of the composite. Quantification of the electrical property is required as the material choice becomes significant for space grade materials. Measure of resistance against, filler contents, applied voltage and the matrix properties evaluation can be the key to categorizing the nanocomposites. Distribution of fillers plays a major role in forming the percolation network in the matrix and this can be observed through microscopic verifications. Other than filler content and dispersion, the monomer content also influences the properties of the final polymeric product. This has been verified from the results obtained in case of a composite matrix made of poly(propylene carbonate) (PPC) and Poly(lactic acid) (PLA) as monomeric units and MWCNT as reinforcements [Qi et al., 2016].

It was observed that the sequence of blending affects the dispersion of CNT, as the viscosity changes every moment of polymerization [Zhang et al., 2009]. Change in viscosity of matrix affects the reinforcement fiber dispersion which plays vital role in electrical properties SMP matrix [Yan et al., 2009].

Carbon Nano Fibers, Carbon Nano Paper, Carbon Black and Carbon Nano Tube have showed enhancement in the electrical and thermal conductivity, heat transfer inside the matrix, mechanical properties and improvement in specific strength compared to other dense fillers. As learnt from the literature, dispersion of the fillers in case of particle / fiber reinforced SMPs is the main challenge to be solved without affecting the other required property of the material, and the actuation mechanism of this SMPC needs to be discussed for an optimal electric power supply for the system [Lorenz et al., 2009; Jiang et al., 2014; Jung et al., 2010].

2.8 Resin system for polymer nanocomposite matrix

Polymer resin matrix combined with fibrous reinforcement dispersed phase is termed as Polymer Matrix Composite (PMC), and when the dispersed filler is in nanoscale, it becomes nanocomposite. The matrix bonds the fillers (particles, whiskers, fibers, or fabrics) and transfer loads between them. The properties of the matrices primarily decide the resistance of the PMC towards the degradative effects of surroundings that eventually protects the reinforcements from external factors. The load transfer between the matrix and the reinforcement occurs at the interface region in a PMC. The extent of interaction of reinforcement and matrix is designed specific to the application, thus the properties of the PMC varies based on the matrix, reinforcement, and the interface between them. Based on the chemistry of the polymer resin, the matrices are categorized as thermosets and thermoplastics. Generally thermoset resins possess low viscosity, high crosslink networks of polymer chains, tend to have high dimensional stability, high-temperature resistance, and good resistance to solvents. Once cured, solid thermoset resins cannot be converted back to their original liquid form. Common thermosets / thermoset resins are thermosetting resins include polyesters, vinylesters, epoxies, bismaleimides, polyamides and polyurethane [Davies et al., 2007; Sen at l., 2015; Li et al., 2013].

Thermoplastic resins (known as engineering plastics), are not cross-linked and, so, can be melted, formed, re-melted and re-formed. It consists of long discrete molecular chains, which changes its phase with increased temperature to a temporary state (an amorphous, semicrystalline, or crystalline solid). The degree of crystallinity has a strong influence on the final matrix properties. Few of the common thermoplastic matrixes includes polyesters, polyurethane, poly - etherimide, polyamide imide, polyphenylene sulfide, polyether-ether ketone (PEEK) etc. Thermoplastics are more resistant to cracking and impact damage, flexible eventhough they are inferior to thermosets in high-temperature strength and transition temperature. Thermoplastic elastomers possess high viscoelasticity, amorphous with immiscible hard and soft phase, which leads to a phase separated structure [Zapletalova et al., 2006].

Thermoplastic polyurethanes (TPU) are elastomeric thermoplastic materials which possess rubber-like properties upon solidification / curing. This contains polymeric hard segment regions, which acts as anchor points, while soft segments melts to assume temporary shapes when subjected to temperature changes beyond T_g. A balance between the soft and hard segment is required to maintain the optimal shape memory properties. An increase of soft segment phase causes deterioration of the recovery properties of the polymer. With higher hard phase content, the polymer hardness and the glass transition temperature increases as per published data [Zapletalova et al., 2006].

Polyurethane is the reaction product of a macroglycol, a diisocyanate, and a short chain diol or diamine. Many formulations of polyurethane are studied to optimize various properties. Huang W M, 2012 explored the shape memory effect in polyurethane polymer and its composites, the thermomechanical responses, electrical conductivity enhancements by various filler materials, percolation concentration, magnetically triggered shape memory effect and shape memory nanocomposites formed by carbon additives.

Yang B, 2007 studied regarding the shape memory behavior of polyurethane polymer resin based SMP where the effects on various properties due to moisture were explored.

Hence, being a polymeric material with well established chemistry and predictability in behaviours, polyurethane is a good candidate for shape memory composite matrix.

2.9 Actuation mechanism

Direct heating process, Microwave heating and Inductive heating process are the methods by which electric potential is applied to the materials as per researchers on this field [Park et al., 2014; Fabré et al., 2012; Wu et al., 2007]. Direct electrical heating is achieved by contact between the surface of the composite and the electrical source through a lead. Microwave heating is a non-contact mode of heating which is achieved by the interaction between molecules and an

electromagnetic field with a frequency range of 0.3 to 300GHz. It is reported as one of the fastest ways to increase the temperature of the material where volumetric heating can be ensured. The filler content plays a vital role in this method of heating as the energy of the microwave is absorbed directly by the fillers. Formation of hotspots / local burns on the material due to concentration / overlap of wave energy is the disadvantage of microwave heating [Yu et al., 2014]. The principle of induction heating is by passing an alternating current through a magnet, an eddy current is created in the material and thereby resulting in heating of the bulk is achieved. Material conductivity can enhance the heating rate when this method is employed. Material thickness is the limiting factor for this method, as thicker materials may get heated up non-uniformly due to uneven distribution of eddy current heating. In induction heating, power requirement bares direct ratio with the required heat [Van Humbeeck, 1999]. The reach of the heating extend is limited by the thickness of the material, which is limiting its applications

Space structures can operate by remote access, where electrical signals can cause actuation. In exposed condition, in space, the unexpected surge of electric charge can trigger the SME prematurely. This requires the SMPs to be suited for a specific specific electric current / field intensity which are different from the operating conditions. This imposes another condition of necessity of higher T_g for extending the application of SMPs in higher operating temperatures [Datashvili et al., 2005; Ge et al., 2016; Xiao et al., 2015].

The experimental methods give specific inputs for developing generalized theory for reproduction of results and validation of similar systems. This generalization is achieved by making theoretical models which help to understand the theory behind the results that can be used for improvisation of results by studies or to predict results of similar system [Colpo et al., 2007]. Following session introduces the modeling techniques that can serve to understand the theory and simulate the experimental conditions in computer programs.

2.10 Modeling techniques to evaluate the mechanisms

Electrical conductivity of mixtures of conductive and insulating materials is influenced by primarily by the content of the conductive filler materials. It is observed that the conductivity of composites increases at a certain concentration of the filler material which is termed as percolation concentration. A number of factors influence the conductivity of the composites such as the filler dispersion, shape, size, its interaction with the matrix, the processing technique. Different models (that statistical, geometric or thermodynamic) were proposed to understand the mechanism and prediction of the conductivity and percolation concentration. The following session explains the different models and the mechanism for evaluation / prediction of electrical conductivity.

2.10.1 Statistical percolation models

Zallen, 1983 and Kirkpatrick, 1973 through their works, have introduced electrical percolations in binary mixes. Electrical conductivity is one among the many fields of engineering which the classical percolation theory deals with (other fields are flow of liquid in a porous medium, spread of disease in a population, communication or resistor networks, conductor insulator composite materials, composite superconductor metal materials, discontinuous metal films, Stochastic star formation in spiral galaxies, quarks in nuclear matter etc.

They dealt with the points and bonds that form clusters and continuous path for electrical current passage, resulting in percolation. Kirkpatrick's power law relationship of percolation has based the classical percolation theory which describes electrical behaviour of nanocomposite before and after percolation threshold [Rodwick et al., 2007]. The conductivity before (σ') and after (σ) percolation threshold follows relationships as

$$\sigma' = \sigma_0 (p_c - p)^k \qquad\qquad (2.10)$$

$$\sigma = \sigma_0 (p - p_c)^j \qquad\qquad (2.11)$$

where *k* and *j* are the critical exponents and with reported values close to 0.7 and 2.0 respectively for 3D networks, σ_o is the filler conductivity, p is the filler content and p_c is the percolation threshold both of which are arrived by experimental results. The values of the critical exponents are affected by the degree of filler dispersion in the matrix, methods of synthesis, geometry of fillers, orientation, aspect ratio, conduction mechanism, possible interactions between different phases of composite and dimensionality of the conductive network [Oskouyi Amirhossein et al.,2014; Yenny et al., 2008; Xinxin and Mo, 2009; Mdarhri et al., 2012; Huang et al., 2012; Aczel, 2012; Sattar et al., 2015; Sun et al., 2012; Lan et al., 2008].

The parameters *k* and *j* are explained as indicative of of tunnelling resistance distribution by the studies of Zhang et al., 2009. Hence the larger values represents a broader distribution of interparticle distance in the matrix which inturn reflects larger tunnelling resistance.

Studies of Balberg, 2002 reports that the critical exponent *j* can have values greater than 2.0 when the conducting fillers are separated by resistive connections with a distribution of resistivities. The value of *j* below 2.0 suggests that the polymer interface thicknesses is narrow and conduction occurs by contact of fillers and a higher value represents wider distribution of interparticle distance resulting in combination of tunneling and contact conduction.

Gurland, 1966; Aharoni, 1972 and Janzen, 1975 have worked out the medium number of contacts of adjacent particles in a system to form network. As per their works, the conductive network formation is possible when the number of contacts of adjacent particles takes the value of 2. Classical percolation theory formed the basis of this approach which derived the volume percolation concentration (V_c) as,

$$V_c = \frac{1}{(1+0.67\,z\,\rho\,\varepsilon)} \qquad (2.12)$$

where *z* represents the coordination number in a specific lattice, ρ the density of the filler and ε the specific pore volume of the filler materials.

Scarsbrick's model [Scarsbrick, 1973] depends on four factors such as filler conductivity σ_c, filler volume fraction V_f, probability of formation of a network p_n, the surface fraction of the conductive phase at the sample electrode boundary C^2. Based on the third and fourth factors, the following equations were arrived for percolation probability and mixture conductivity corresponding to the percolation concentration.

$$p_n = V_f 1/ V_f{}^{2/3} \qquad\qquad (2.13)$$

And the mixture conductivity was given as,

$$\sigma = \sigma_c\, p_n\, C^2 \qquad\qquad (2.14)$$

The drawback of this particular model is that the assumptions account only for the conductivity behavior above the percolation point and hence predicting the percolation concentration is not possible.

Bueche, 1972 based his model on Flory - stockmayer theory of polymer gelation (Paul Flory (1941) and Walter Stockmayer (1944) suggested the probabilistic approach of gelation nodes in polymeric systems) in conductivity of binary mixtures. An equation based on resistivity was derived accounting the maximum number of contacts made by particles.

$$\frac{\rho}{\rho_m} = \frac{\rho_f}{(1 - V_f \rho_f + V_f \omega_g \rho_m} \qquad\qquad (2.15)$$

where ρ is the resistivity of the mixture, ρ_m the resistivity of the insulating material, ρ_f the resistivity of the conductive material, V_f the volume fraction of the conductive phase in the mixture, ω_g the fraction of the conductive phase being incorporated in an infinite cluster; its value is determined by the sub-factors f (the maximum number of contacts a particle can make with its neighbours) and α (the probability for the appearance of a contact between neighboring particle).

2.10.2 Thermodynamic percolation models

The serious disagreements that exist between statistical percolation model predictions and the experimental percolation concentration values resulted in attempts towards development of thermodynamic model researches. Percolation phenomenon is considered as a phase separation phenomenon in this modeling method.

Sumita et al., 1982, 1986, 1991 developed a model that is based on the principles of chemical thermodynamics in which the overall interracial free energies in the mixtures are considered. The network formation is assumed to occur at a particular mixture-independent of the overall interracial free energy, g* (the concept is borrowed from the theory of the glass transition in polymers). It can be inferred that percolation threshold is inversely dependant on the specific interracial free energy, which explains the lower percolation threshold value corresponding to a greater value of specific free energy. However, viscosity of the polymer melt and the diameter of the particles are also considered significant for deciding upon the percolation concentration. An equation was derived based on the above concept as follows,

$$\frac{1-V_c}{V_c} = \frac{3}{g^*R}\left\{\left[\gamma_c + \gamma_p - 2(\gamma_p\gamma_c)^{\frac{1}{2}}\right] \times \left(1 - e^{\frac{ct}{\eta}}\right) + K_0 e^{\frac{-ct}{\eta}}\right\} \qquad (2.16)$$

where V_c represents the percolation threshold, γ_c represents the surface tension of the CB particles, γ_p is the surface tension of the polymer, g^* is the universal interfacial free energy, K_0 is the interracial free energy at the start of mixing process, c is a constant to account for the speed of evolution of the universal interracial free energy, t represents the time of mixing the two components, η is the viscosity of the polymer resin during the mixing process and R is diameter of the individual CB particles.

Even though similar to the one proposed by Sumita et al., 1991 in many ways, the model of Wessling et al., 1989 which is called as the dynamic boundary model, is unique in two aspects. In this modeling approach, the percolation process is considered to be based on non-equilibrium thermodynamics, and few assumptions

limit the non-confirmities with experimental results. This assumes that the filler particles (CB is considered) as spherical in shape, covered fully with polymeric resin while the content is below percolation threshold. The non-homogenous distribution of the particles is considered, the strong interaction between the filler particles and the polymer matrix are also accounted in this model. The adsorption kinetics, the minimum tunneling distance and the agglomeration phenomenon found in the nanocomposites forms the basis of formation of three dimensional networks for electron passage.

The percolation equation, resulting from the considerations of Wessling et al. calculates volume percolation concentration as,

$$V_c = \frac{0.64(1-c)\emptyset_0}{\emptyset_c}\left[\frac{x}{\left(\gamma_c^{\frac{1}{2}}+\gamma_p^{\frac{1}{2}}\right)^2} + y\right] \qquad (2.17)$$

where V_c is the percolation threshold, γ_c is the surface tension of filler, γ_p represents the surface tension of the polymer, *(1-c)* is the amorphous part (by volume) of the polymer resin matrix (at room temperature), *x* is a parameter that is dependent on the molecular weight of the polymer, *y* is a which defines the non-equilibrium basis of the theory. ϕ, ϕ_0 represents the factor to recognize the adsorption layers on filler reinforcement.

This model prediction was reported to have shown closest confirmation with the experimental results.

2.10.3 Geometrical percolation models

Geometrical models do not take into account the fluid properties of the resin matrix and the percolation phenomenon is considered for dry-premixed components with conductive and insulating powders which are subsequently sintered. It is assumed that during the sintering process the insulating dominant phase particles are deformed into cubic particles and the conductive fillers are ordered in a regular manner on the surfaces of the super-particles (dominant phase).

With these considerations, Slupkowski, 1984 presented a model which resulted in the equation

$$\sigma = 2\pi\sigma f \frac{d([x]+P)}{Dln\left\{1+\frac{1}{([x]+1)\alpha}\right\}} \tag{2.18}$$

where σ is the conductivity of the mixture, σ_f the conductive phase conductivity, D the diameter of the insulating powder particles, d the diameter of the conductive particles, P represent the probability for the formation of a three dimensional network of conductive particles. It is reported that Slupkowski's equation accounts for the variation of the percolation threshold when the ratio of the particle diameters changes, which gave closer to actual results.

Rajagopal and Satyam, 1978 derived a model for wax/graphite system which considers wax particles as cubic grains of size D, and the graphite particle possessing diameter d. Bhattacharya and Chaklader, 1982 optimized the model equations proposed by Malliaris and Turner, 1971. The volume considerations of this model derives the characteristic of the onset of the network formation V_A and V_B given by,

$$V_B = \frac{2.99d/D}{1+2.99d/D} \tag{2.19}$$

$$V_A = 0.5V_B \tag{2.20}$$

V_A represents the volume concentration as characteristic of the onset of the network formation; V_B is the characteristic volume concentration of the end of the drastic increase of the conductivity.

These equations gave closely resembling values with the experimental percolation concentration.

2.10.4 Structure-oriented percolation models

The homogeneity of the conductive phase distribution in the matrix is taken into account in the structural oriented models. Yoshida et al. 1990 have substituted the actual materials with micro level spherical structures homogeneously dispersed in

the matrix phase. The modeled conductivity compared with the conductive volume fraction of the experimental values were found to exhibit a close correlation. The electrical conductivity in binary composites are studied by Nielsen, 1974; McCullough, 1985 and Ondracek, 1991 subsequently and proposed individual models considering the general class of transport properties like the electrical / thermal conductivities, the dielectric / magnetic properties and the permeability properties. In addition to this, the consideration of aspect ratio of the filler particle extends the research domain to particle shapes other than spherical.

Apart from the above models, combinations of statistical, geometric and structural percolation models are also attempted, which are shaped based on the assumptions considered in each case. Electrical percolation studies based on continuum mechanics and Monte Carlo simulation are examples of such combined approaches where multiple considerations are brought together. Monte Carlo simulation methods have been extensively used for the computational analysis of identifying percolation threshold, probability of formation of the percolation networks and also the effects of varying different parameters. Zhao *et al., 2011* used Monte Carlo simulations to study the electrical properties of MWCNT/epoxy resin composites. This is followed by simulation through simple 2D models to study the effects of nanotube volume fraction, degree of waviness and degree of anisotropy as well of the aspect ratio in relation to the percolation threshold behaviour, with further approaches of incorporating quantum effects such as inter-tube tunnelling, which was carried out via tight binding simulations. Natsuki *et al., 2005* investigated percolation behaviour with respect to orientation as well as the aspect ratio of the fillers with the help of 2-dimensionsal (2D) modeling of the randomly dispersed fillers. Studies by Behnam *et al., 2007* state the orientation dependence of the CNTs and specifies that certain orientation of the CNT fillers would correspond to maximum conduction. Many such 2D considerations also provides similar conclusion on dependence of the percolation and conduction on the aspect ratio, waviness, possibilities of agglomerates, tendency to curl and dispersion of the CNTs throughout the matrix. Review by Bauhofer *et al., 2009* provides a comprehensive overview of experimental results based on electrical percolation of CNTs in polymer composites which are published in different

articles. The work also provides details about effects on minimum percolation threshold and maximum conductivity due to different production methods or dispersion methods. Zhao *et al., 2011* have reported numerical studies using 2D sticks results of which matched with their experimental conductivity value.

The work by Qian *et al.*, 2018 involves using discrete element method (DEM) to solve random close packing (RCP) of different cylindrical particles under optimal vibration conditions and corresponding characteristics such as packing density, coordination number (CN), radial distribution function, particle orientation, orientation randomness and also the forces involved. The modeling has been carried out using elemental-spheres model, where each cylinder is considered to be made up of elemental spheres and forces between them are manipulated to arrange them in a spatial distribution. Overlapping is eliminated by considering the occurrence of overlaps between each of the elemental spheres within a cylinder to every other elemental sphere of other cylinders to be packed. Another similar work by Tangri*et al*., involves using discrete elemental method to solve packing of cylinders, in specific Hertz-Mindlin contact method of DEM is used (Incorporating Hertz-Mindlin contact model, normal force-displacement relationship is achieved by using Hertz theory and tangential force-displacement relationship is achieved by using Mindlin theory). In their DEM approach, dynamics of the particles and their trajectories are tracked by integral equations of Newton's laws of motion. Gravitational force and particle-particle interactions were taken into consideration. For each particle, both rotational and translational dynamics were tracked with the help of integral equations. Cylinders were constructed using glued-sphere technique. Detailed studies on effect of container diameter, filler height, effect of deposition intensity, effect of fixed versus variable drop height, effect of centre-fill versus whole cross-section fill, effect of co-efficient of restitution and effect of co-efficient of friction, effect of particle representation, vibration frequency, vibration amplitude and container size were also studied. Hence, the method of DEM seems to be a good solution for the problem of packing of spheres and cylinders. In case of carbon nanotubes, further studies on percolation and conduction is needed where DEM approach is viable but considered a complicated in many studies.

The above discussed models represent the prominent and popular modeling attempts among many works published to understand and predict the percolation behavior of polymer composites, which are essential for electro-active shape memory actuation. Irrespective of the models, the following parameters are found significant while predicting the percolation concentration.

- the size and the geometry of the conductive fillers
- the quantity and distribution of conductive particles in insulating matrices
- interactions between the conductive and insulating components
- composite preparation methods
- viscosity of polymer resin matrix while mixing / preparing
- wettability of particles
- aspect ratio of particles
- mixing / dispersion process

A thorough understanding of the electrical conductivity mechanism can help to predict the shape memory behavior and its mechanism, as the energy flow inside the system gives clear indication of the phase changes initiated by it.

2.11 Problem definition

A journey through the published literatures discussing shape memory effect, parameters, stimuli, morphological features, nanocomposite fillers, resin system and the modeling techniques has helped to identify the gap in research field to be bridged.

Following are the concepts those require further appreciation and attempts to understand via experimental and theoretical studies.

- Matrix material properties

- Nano-filler dispersion

- Geometry of filler materials

- Experimental understanding of percolation behavior in nanocomposite with fillers having different geometrical parameters

- Realistic model for predicting electrical percolation of nanocomposite with multiple filler geometry

- Shape memory parameter study and evaluation

- Relationship between material properties and shape memory effect

- Design of shape memory material for specific applications

- Synergy study of multi-filler system in nanocomposites

There are many studies with individual attempts to understand the above concepts, both theoretically and experimentally. A comprehensive understanding of a single system by experimentally and modeling approach is required to establish the shape memory effect and the associated parameters.

CHAPTER.3

SCOPE AND OBJECTIVES

The research on shape memory began since the discovery of shape memory Nickel titanium alloy by Arne Olander, in 1932. Since then a lot of work has gone into it which brought out many advancements in the material science of shape memory materials deriving them as alloys, polymers, gels, polymers, hybrids and composites. Thermal actuation is the widely studied shape memory triggering mechanism, while other methods are also explored for specific operations. For remote actuation of shape memory materials, electrically triggered shape memory materials are best suited as per the published data.

3.1 Scope of work

The existing literature suggests the use of thermoset cross-linked polymer resin for operating conditions which demands high transition temperature where as thermoplastic polymers are preferred for applications that require higher usable strain,. Polyurethane shape memory effect is studied for thermal as well as electrical actuations and many results have been derived with T_g ranging in the order of 40°C to 60°C. This work identifies it as a gap to be bridged for having SMPC with better T_g as well as good elongation property.

It is observed from the above studies that shape memory effect can be observed through electrical actuation i.e., raising the temperature of material volume through resistive heating. The primary understanding of current conduction in a heterogeneous mixture of conducting and insulating materials are either by contact of conductive filler or by tunneling. Lack of an optimized model is identified as another area to be researched on, and hence a comprehensive model based on structural orientation percolation accounting for statistical and tunneling approaches is presented for carbon nanofiller reinforced polymer matrix.

Another grey area in the research of shape memory nanocomposite is about multifiller materials in the matrix and the synergy. A combination of zero-dimensional and one dimensional filler material is used for synthesis of PU SMP nanocomposite and the properties are evaluated considering the synergism that exists between different geometry materials.

Recovery time has been a concern for robotic applications as less recovery time is advisable, while space deployment of stowed structures can afford for a slow recovery to prevent shock or damage to the sensitive instruments on sudden deployment. Thus, a variable order of recovery speed based on application demands development of materials with different shape change speed based on stimuli and component characteristics of composites in SMPC. This work attempts to develop a set of shape memory materials those actuates faster and with better efficiency for high precise and quick response systems.

3.2 Objectives

The objectives of the thesis are as listed,

- Synthesize polyurethane resin for having higher transition temperature
- Synthesis of electrically conductive polyurethane shape memory composite using carbon black spherical particles as reinforcement fillers and modeling its percolation behaviour
- Synthesis of multi-walled carbon nanotube based electrically conductive polyurethane shape memory composite and modeling its percolation behaviour
- Synergy study of Carbon black and carbon nanotube fillers in PU resin and the shape memory evaluation.
- Demonstration and comparison of shape memory effect in PU nanocomposites with different filler

The work flow of the thesis is explained via the following flowchart (Figure 3.1)
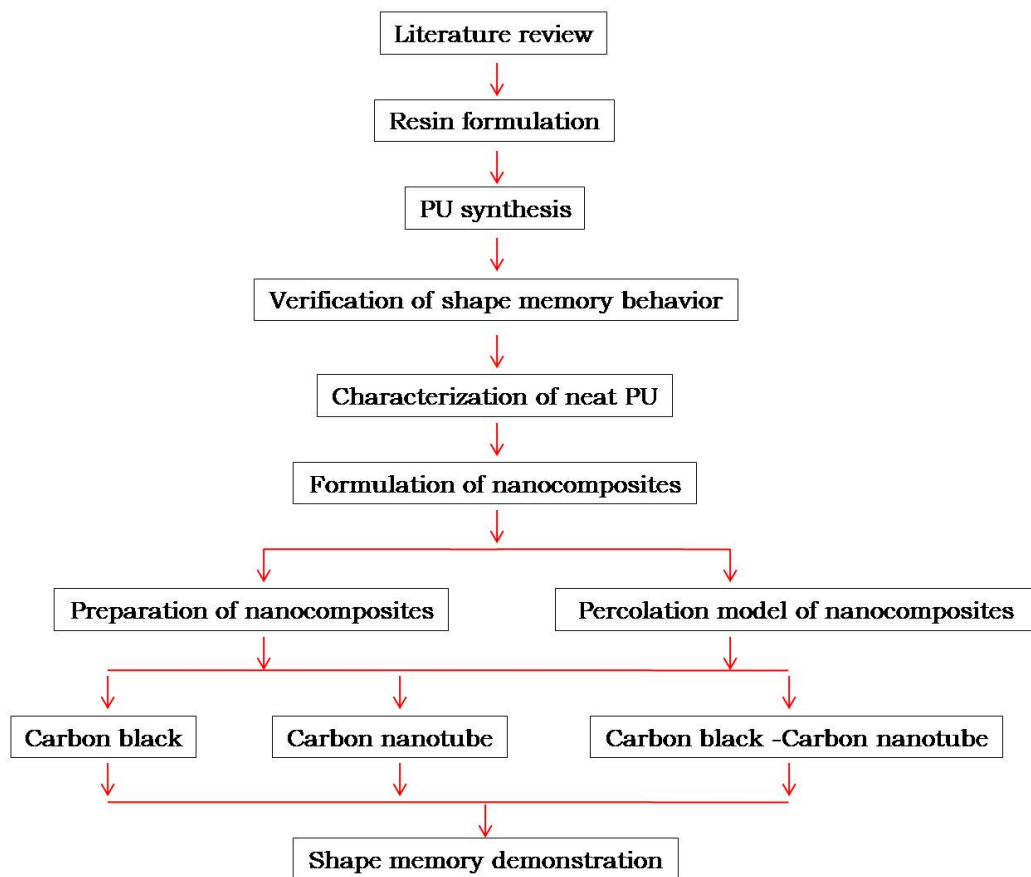
Figure 3.1 Work flow of the thesis

The work consists of two parts of which one is experiment and other is modeling of electrical behavior of the nanocomposites. Parallel approach of both the parts helps to evaluate the results and prove the electrical actuation possibility of shape memory polymer composites.

CHAPTER.4

MATERIALS AND METHODS

Polyurethane (PU) based shape memory materials (SMM) are widely studied due to their predictable wide range of properties, low cost and proven shape memory ability [Huang et al., 2012]. Polyurethane shape memory behaviour is dependent on the hard and soft phases of which the soft segments are generally polyether/polyester chains and the elastic hard segments are the urethane bridges [Meng and Li, 2013, Yong et al., 2012] Due to improved stability against moisture and the possibility of tailoring Tg values for various applications, PU-SMM synthesized from polyether polyols are gaining significance in the smart material world.

The origin of the PU industry is attributed to the invention of the diisocyanate polyaddition technique in 1937, with PU produced through the polymerization of diisocyanate and polyester diol [Akindoyo John O et al., 2016]. The versatility of PU and its suitability to replace other scarce materials led to the demand in several applications. The continuous research in synthesizing methods, various combinations of isocyanates and polyols have contributed for the widened popularity and applications of PU polymeric materials. Currently, PU is of interest to many in the scientific community because of its versatility. The application domain spreads across biomedical, infrastructure & construction, automotive, aerospace, textiles etc., owing to its combination of properties like elongation, hardness, strength, modulus and the ability to demonstrate shape memory effect.

The reaction between an isocyanate and polyol molecule in the presence of a catalyst give rise to PU resin, where the isocyanate and polyol molecules should necessarily contain respectively more than one isocyanate group (-R–(NCO)) and hydroxyl group (-R–(OH)). The property of PU depends on the amount and type of the hard and soft segments attributed to polyols and isocyanates respectively. Apart from the basic ingredients, presence of chain extenders and cross-linking agents influence the final product morphology. Soft and elastic PU polymers are

produced from flexible long polyol segments, whereas rigid, tough PU polymers are produced from higher amount of cross-linking of the carbon chains. Elastomeric PU are obtained through long chains with minimum cross-linking, whereas hard PU polymers results from shorter chains with higher cross-linking. The combination of long chains with average optimized cross-linking produces PU foams by release of volatiles that results in foaming.

For PU synthesis, polyols with two or more –OH groups are used, like polyether polyols and polyester polyols. Polyols are used as mixtures of similar molecules but with different molecular weights having different number of –OH groups. Larger molecular weight (around thousand to ten thousand) polyols results in formation of flexible PU and the lesser molecular weight polyols (a few hundred units) form rigid PU, thus forming a criteria of selection of polyol based on application.

The isocyanates react with the hydroxyl-group-containing compound to form urethane linkages and are accelerated with increased temperature. Isocyanates exists as aromatic (for example toluene diisocyanate (TDI) and diphenylmethane diisocyanate (MDI)) and aliphatic (for example isophorone diisocyanate (IPDI) and hexamethylene diisocyanate (HDI)) with the aromatic being more reactive than aliphatic isocyanates. The modifications and vividness in the properties of the raw materials and the synthesis routes adopted determines the final properties of the product.

4.1 Materials in use

The polyols can be broadly categorized into polyether polyols and polyester polyols. Polyether polyols are synthesized by reaction of an epoxide with active hydrogen-containing compound or by the ring-opening polymerization of epoxy monomers. Polyester polyols are obtained from the polycondensation of hydroxyl compounds and multifunctional carboxylic acids.

Polyether based poly-tetramethylene ether glycol (PTMG / PTMEG / PTMO), obtained from polymerization of tetrahydrofuran is used in current

work for synthesis of PU resin. The PTMG (CAS no. 25190-06-1) is a white waxy solid that melts to colourless ordourless liquid at temperature between 20 °C and 30 °C and was sourced from Sigma-Aldrich. As learnt from the existing literature that the molecular weight of the polyol determines the elasticity and flexibility of the final PU and since shape memory materials requires elasticity and flexibility to assume / recover shape, **PTMG with molecular weight 2000g/mol was used for this work. The waxy solid was heated to 70 °C and maintained for 4 hours under vacuum. PTMG being hygroscopic, was stored in dry nitrogen sealed bottled or air tight bottles to prevent adverse reactions with moisture.**

The second component of PU, the isocyanates are categorized as di-functional / hetero-functional based on the number of isocyanate groups present in the basic structure. Depending on whether the basic structure is made of straight carbon chains or ring of carbon, they are further classified as aromatic or aliphatic isocyanates. The most commonly used ones are methylene diphenyl diisocyanate (MDI) and toluene diisocyanate (TDI) because of the availability and reactivity compared to other isocyanates. Other groups of isocyanates includes aliphatic and cycloaliphatic isocyanates, which are having ability to remain stable against ultraviolet (UV) range of electromagnetic spectrum. 1-isocyanato-3-isocyanatomethyl-3,5,5-trimethyl-cyclohexane (isophorone diisocyanate, IPDI) 4,40-diisocyanato dicyclohexylmethane, (hydrogenated MDI or H12MDI) and 1,6-hexamethylene diisocyanate (HDI) are the commonly used isocyanates in various industrial applications.

Considering the reactivity of aromatic diisocyanates and the UV protection provided by aliphatic diisocyanates, a combination of TDI (174.16 g/mol; CAS No.26471-62-5; sourced from Bayer material science) and IPDI (222.3g/mol; CAS No.4098-71-9; sourced from Evonik Industries) was used in current work to form the hard segments in the polyurethane polymer resin.

As reviewed from the published literature (section 2.6, chapter.2), the optimal crosslinking adds the properties of thermoset polymers retaining the basic character of thermoplastic polymers. **Considering this, a crosslinking agent**

Trymethylol propane (TMP; 134.2g/mol, sourced from Lanxess industries, CAS No.77-99-6) was used in current work to induce cross-linking. This is a colourless solid which is chemically known as 2-(hydroxymethyl)-2-ethylpropane-1,3-diol and is widely used as building block segments in the polymer industry. The long carbon chains are linked laterally by TMP to stiffen the bulk of the polymer. This result in a polymer with superior thermal and mechanical property compared to non-crosslinked polymers.

For ensuring the chain continuity and extension 1,4-Butane-diol (BD; 90.12g/mol, Loba chemie, CAS no.110-63-4) was introduced in to the system as chain extenders. This provides the extra –OH functional group to react with the –NCO terminated urethane linkages of polyurethane prepolymers and extends the carbon chains. The longer carbon chains add to the shape memory ability of the polymer as the usable elastic strain increases with the long continuous chains inside the PU.

For ensuring the complete reaction and to impart enhanced reactivity, catalysts are used in PU synthesis which can be categorized as metal complexes or amine compounds. Amine catalysts consist of tertiary amine groups, for which dimethylcyclohexylamine (DMCHA), dimethylethanolamine (DMEA), 1,4-diazabicyclo[2,2,2]octane (DABCO) and triethylenediamine (TEDA) are few examples. The metal complexes are derived from compounds of bismuth, lead, zinc, mercury etc, for example Dibutyltin dilaurate (DBTDL), Dibutyltin oxide, Monobutyltin trichloride etc. **For the current work, an organometallic catalyst -dibutyltin dilaurate (95%, sourced from Sigma Aldrich) was added at an amount of 0.013g per 100g of resin**.

To control the viscosity while synthesizing the resin and during the composite preparation, a suitable solvent is required to be introduced. **A combination of poly-methyl acrylate (PMA; 99% pure, Alfa Aesar), Xylene (97%, Qualigens), Toluene (99%, Fisher scientific) and Methyl isobutyl-ketone (MIBK; 99%, SRL) were used to prepare PU solvent.**

For introducing electrical conductivity to the polymer resin, many options were discussed in the literature survey in chapter.2, out of which Carbon black and carbon nanotube are used in this current work as filler reinforcements.

Super conductive Carbon black, (99%, apparent density of 0.23g/cc – procured from Alfa Aesar) was used pristine as filler material in the preparation of the PU-CB nanocomposite.

Carboxylic acid functionalized Multi-Walled Carbon Nano Tube (MWCNT; CAS no. 308068-56-6; bulk density: 0.04-0.05 g/mL) with aspect ratio ranging between 100 to 200, sourced from Chemapol industries and was used in this work for developing electrically conductive PU-MWCNT polymeric nanocomposite material.

4.2 PU Resin synthesis

The resin preparation involves multiple stages which includes the preparation of PU solvent which is a volatile entity to maintain the consistency of the monomer mix during the polymerization. The volatile nature, polymer dissolving ability and the presence of basic elements (carbon, oxygen and hydrogen) makes the combination (PMA, xylene, toluene and MIBK) suitable for solvent.

4.2.1 Solvent preparation

PMA, xylene, toluene and MIBK were taken in a cleaned glass bottle in weight ratio 2:1.5:1:1 and were mixed thoroughly. The solvent is colourless with strong pungent smell and was kept undisturbed in room temperature for preparation of PU resin.

4.2.2 Resin synthesis

A two-stage prepolymer route was followed where the macroglycols were end capped with excess of diisocyanates which is followed by chain extension of the diols giving PU.
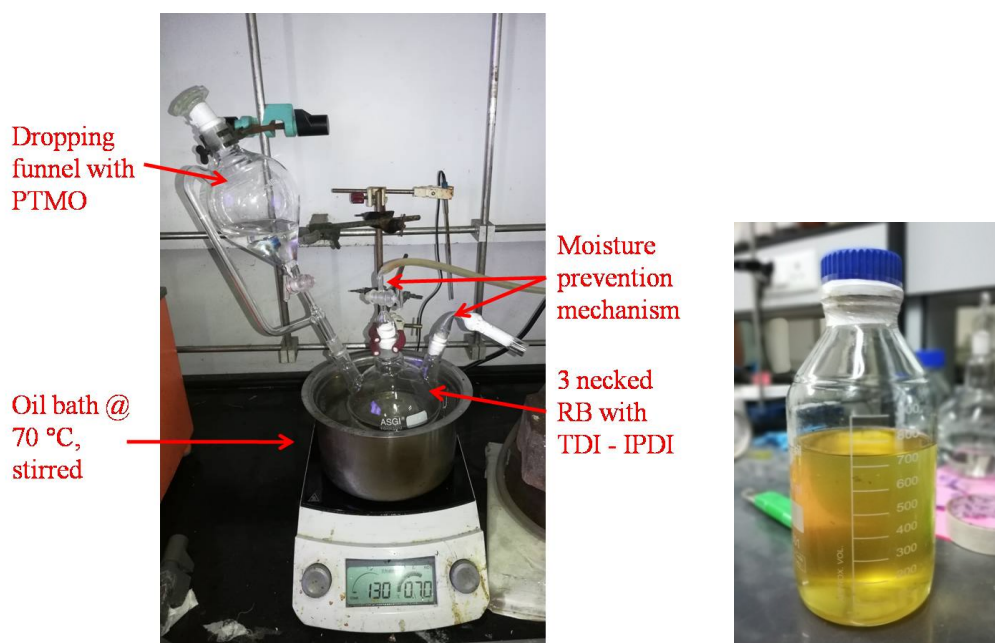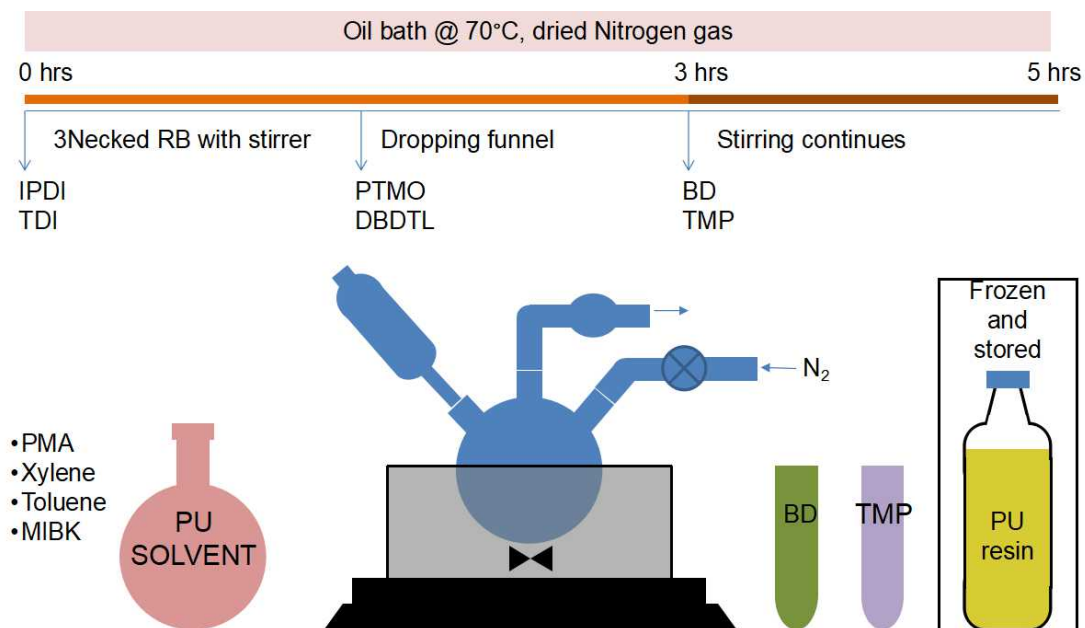
Figure 4.1 Resin synthesis; (a) Sequential procedure of resin synthesis illustrated; (b) Resin synthesis arrangements; (c) Prepared PU resin in airtight container

The set-up for the resin synthesis includes an oil bath maintained at 70 °C with constant stirring, nitrogen dry air supply for removing moisture, weighing balance / measuring device to quantify the chemicals in use. The following procedure explains preparation of 150g of PU resin (refer Figure 4.1).

- 5.8 g of TDI and 21.1 g of IPDI were measured and taken in a three-necked round-bottom (RB) flask. For continuous stirring, a magnetic stirrer bead was introduced and the assembly was kept in oil bath over a hot plate to maintain 70 °C temperature. approximately 20 ml solvent was added to maintain consistency.

- 40 g PTMO with 40 ml solvent approximately was taken in a dropping funnel, well shaken and was emptied drop-wise at one of the mouth of the RB flask (refer Figure 4.3(a) & (b). 0.01 g of DBDTL in 5 ml solvent was added to the mixture. Dry nitrogen gas was allowed to pass through the system by connecting it to the RB flask. A guard tube with Calcium silicate was also introduced to prevent moisture ingress.

- The PTMO gets emptied completely to TDI - IPDI mix in 30 to 40 minutes and was continuously stirred in the RB flask. The stirring continued for another 3 hours with solvent added whenever required, maintaining the consistency of the mix.

- 1.34 g of TMP and 3.6 g of BD were added and mixing was continued for another 2 hours, with necessary solvent.

Continuous stirring with TMP and BD for 2 hours resulted in a pale yellow colour PU resin, which was then removed from the oil bath. The prepared resin was cooled to room temperature and was stored in freezer for subsequent composite preparation (Figure 4.3(c)).

A 55/45 ratio between the soft and hard phase was maintained for the preparation of the PU resin for the current work. This is because many literatures reported that increased hard phase (Isocyanate group) content reduces the required elastic property for the polymer. The basic chemical formulation is as explained in Figure 4.2, where the ingredients combine to form PU chain linkages.
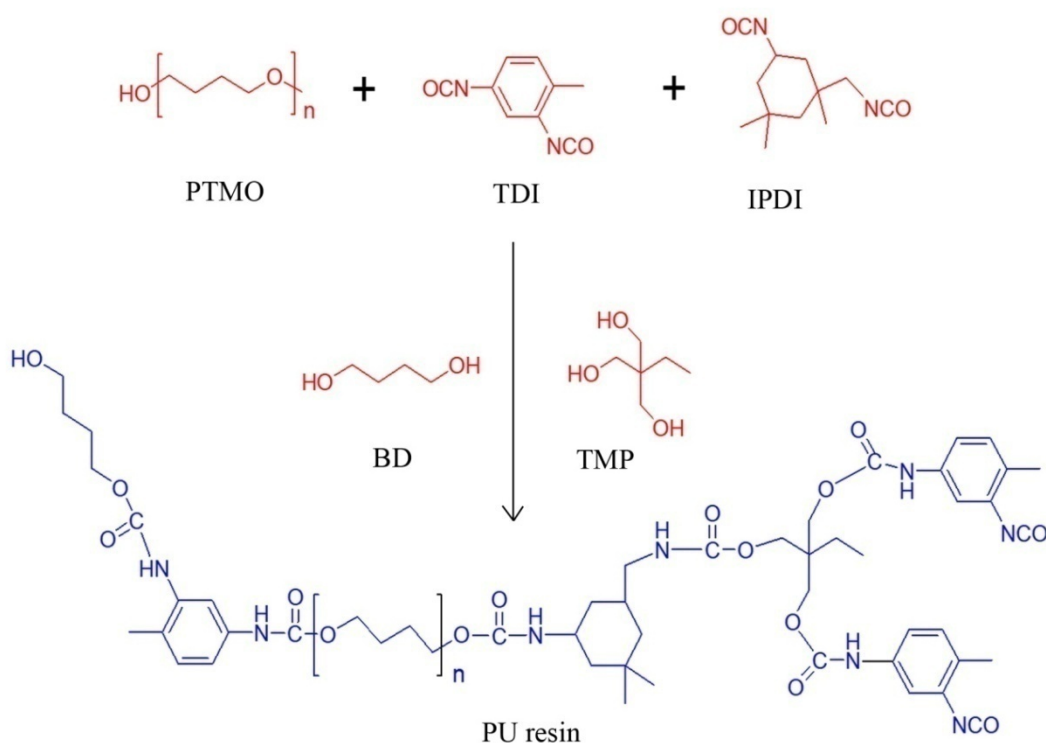
Figure 4.2 Resin syntheses from PTMO, TDI, and IPDI with addition of BD and TMP added for chain enhancements; (DBDTL not shown here)

The -NCO group interacts with the –OH forming urethane linkages on either sides of PTMO with the –OH of BD and TMP enhances the chain length as well as intra-chain linkages. The cross-link density decides the closeness to the properties of the polymer either to thermoplastic or to thermoset resins. The long chain elastomeric polyurethane elastomers are industrially important materials that find applications in footwear industries, household items, surfboards, goggles and ski-boots. Being lighter to metals and with high stress recovery properties, it can withstand several environmental loads. For enhancing mechanical, thermal and electrical properties, which are desirable for various applications, nanocomposites based on carbon fillers are prepared from the PU resin.

4.3 Carbon composite preparation

As understood from literature review (secition 2.8, chapter.2), the materials' characteristics are improved by the incorporation of nanoparticles or

nanomaterials. Nanomaterials such as carbon nanofibres (CNFs), carbon nanotubes (CNTs), carbon black nanoparticles (CB) and nanoclays, are attracting significant interest as important fillers into polyurethane elastomers. The enhanced properties are based on the suitability of these nanofillers with uniform nano-scale dispersion and thereby improving the anisotropic properties of PU materials. It is to be noted that the influence of nano-reinforcements on the properties of PU and its composites depends on several factors, such as particle size, shape, morphology and degree of dispersion.

For studying the influence of nanofillers on the composite of PU, CB and MWCNT were used in current work in varying combinations by weight fraction of the resin.

4.3.1 CB nanocomposite

CB was mixed mechanically in percentages 0%, 2%, 3%, 7%, 10%, 20%, 25%, 30% and 40% by weight of solid content of the prepared resin for composite preparation.

Figure 4.3(a) Carbon black mixed with resin and solvent ready for mechanical roll milling for getting uniform dispersion; (b) Room temperature casting of the composite in flat moulds

Carbon black in desired quantity was measured in polypropylene bottles (250 ml capacity) with measured weight of PU resin (with necessary solvent to maintain

viscosity of resin) and was mechanically milled for 24 hours to ensure uniform dispersion of the filler in the resin (Figure 4.3 depicts the PU-CB blend ready for milling). Mechanical roll milling machine was used for the mixing of carbon black in PU resin for synthesis of PU-CB nanocomposites. After mixing, the same was transferred to the moulds as thin layers so that the solvent evaporation from each layer is facilitated (refer Figure 4.3(b). After solution casting, the PU-CB nanocomposites was cured for a minimum of 240 hours at room temperature followed by 10 hours of oven curing at 150 °C.

4.3.2 MWCNT nanocomposite

For preparing MWCNT-PU nanocomposites, the MWCNT was weighed and added in percentages 0.1%, 0.3%, 0.5%, 1.0%, 1.5%, 2.0%, 2.5%, 4.0%, 7.0%, 10.0%, 15.0%, 20.0% by weight of solid content in the resin. This mixture (mixture of resin, solvent, MWCNT) was subjected to ultrasonication for 15 to 20 minutes for uniform dispersion of the nanotube in the resin matrix. **SONICS Vibra-cell ultrasonicator (750 Watt Ultrasonic Processors –VC 750) with 13 mm probe was used for ensuring dispersion of MWCNT in the resin.** The particle dispersed resin is then cast as thin layers. It was cured for 240 hours at room temperature followed by 10 hours of oven curing at 150°C (same curing cycle followed as in PU-CB system as the same solvent was used).

4.3.3 CB-MWCNT nanocomposite

A combination of the CB and MWCNT were also used for the nanocomposite preparation, where the weight percentages as shown in Table.4.1 are added to resin and subjected to ultrasonication (for 15 to 20 minutes) for filler dispersion.

Table 4.1 CB-MWCNT combinations

Combination No.	CB content (wt%)	MWCNT content (wt%)
1	1.0	0.05%, 0.10%, 0.15%, 0.20%, 0.25%
2	3.0	0.05%, 0.10%, 0.15%, 0.20%, 0.25%
3	5.0	0.05%, 0.10%, 0.15%, 0.20%, 0.25%,

This mixture is solution cast and the same curing procedure of above two systems is followed for getting nanocomposite with multiple fillers in PU resin.

4.4 Characterization techniques

The materials that are studied and experimented for scientific objectives need to have defined properties and predictable behaviors. Characterization of each material involved and the synthesized products help to establish the properties and thereby facilitate choosing the most suitable one for applications and further researches. The chemicals / monomers for polymerization can be used pristine (known properties from manufacturers) or after probing into the properties by various methods. Various methods are available for product level analysis and characterization in case of polymers and their composites. This includes chemical / spectroscopic analysis, microscopic studies, mechanical property studies, electrical and thermal properties evaluation. Product specific characterization can include shape memory evaluation in case of SMP or SMPCs. The shape memory characterization is introduced in many literatures in terms of efficiency of shape fixation, recovery and cyclic tests.

Fourier Transform Infra-red Spectroscopy (FTIR) relies on the fact that the most molecules absorb light in the infra-red region of the electromagnetic spectrum. This absorption corresponds specifically to the bonds present in the molecule.

The frequency range is measured as wave numbers typically over the range 4000 – 600 cm-1. FTIR identifies chemical bonds in a molecule by producing an infrared absorption spectrum. **In current work, FTIR spectra of the composite with various Carbon loading were recorded on Thermofisher-Nocole-iS-50 FTIR in ATR mode for wave number range between 4000 and 550 cm−1 with a resolution of 4cm−1. A sample of size 5 x 5 mm weighing approximately 1.0 g is sliced from the cured nanocomposite sheet for the FTIR analysis. Attenuated total reflection method was employed for obtaining the spectrogram.**

Many chemical species absorb light in either the visible or ultra violet region of the electromagnetic spectrum. This absorption is caused by the changing electron energy levels in the molecule and is therefore characteristic of the molecular structure. The technique is particularly useful for performing rapid quantitative concentration measurements of organic species in solution. For obtaining the **solid-state UV spectra of the neat PU and PU-Carbon composite, a flat sample of approximately 10.0 mm size with 2.0 mm thickness was sliced from the cured sheet. The UV spectra for the samples were obtained using Perkin Elmer Lamda-950 instrument, for a combination of transmittance and absorbance mode for 250 to 800cm-1. The instrument gave the absorbance / transmittance of the radiations which was plotted against the frequency and analyzed. Samples weighing 5.0 g was used for obtaining the IR spectrogram of CB and CNT.**

Raman spectroscopy, based on Raman Effect is a scattering technique. The inelastic scattering of incident radiation and its interaction with vibrating molecules are the basis of this technique. The scattered light generated when the sample is illuminated with a monochromatic laser beam to interact with its molecules is used to construct a Raman spectrum [Gurvinder Singh, 2016]. **The Raman spectra of the composite was recorded on WITec alpha 300R Confocal Raman Microscope in 5 accumulations, with a laser source with wavelength 532nm. Thin samples (1.0 mm thick) of the nanocomposite were sliced into geometries of maximum size of 10.0 mm x 10.0 mm for obtaining**

the Raman spectra. Raman spectrogram for reinforcements like CB and MWCNT were obtained using samples weighing 5.0 g.

X-ray diffractogram of the samples were recorded on a Bruker-D8-discover X ray diffractometer operating with a copper anode (40kV, 40mA) which uses Cu-Kα radiations (1.5419Å wavelength), recorded by a solid-state detector Lynx-Eye from an angle range between 10°and 90° at a scan rate of 0.02° in 0.5 seconds. Samples of size not exceeding 5.0mm are sliced and taken without any contamination for obtaining the XRD. The principle of this technique depends on the irradiated of the sample with X-rays and capturing the emmisions. If an X-ray photon is absorbed by the sample of sufficient energy then an electron is emitted via the photoelectric effect resulting in an electron hole in the atom. An inner shell electron will then fall back to fill this 'hole' resulting in the release of electromagnetic energy with a frequency characteristic of the element present.

Scanning electron microscope (SEM) produces images of a sample by scanning the surface with a focused beam of electrons that interacts with atoms producing various signals that contain information about the surface topography and composition of the sample. For conventional imaging in the SEM, specimens must be electrically conductive, at least at the surface, and electrically grounded to prevent the accumulation of electrostatic charge**. The sample cut at room temperature with sterilized tools to prevent contamination and was coated (sputtered) with a thin layer (maximum 10 micron) of gold for making it conductive for avoiding charging of the specimen while irradiated with electrons. The specimen was then mounted on to the specimen stub and vacuum was applied before electron beaming on to the sample. Scanning electron micrographs of the representative samples of prepared SMPC and pure PU were taken using Carl-zeiss zigma HD FESEM with an accelerating voltage of 30kV. For obtaining finer details of the fractured surface, micrographs were taken with different magnification (20000x, 30000x, 80000x) at different locations of the specimen.**

Differential Scanning Calorimetry (DSC) is a technique in which the difference in the amount of heat required to increase the temperature of a sample and reference (material with known thermal events) are measured as a function of temperature. **100 mg of sample was sliced from the cured nanocomposite and a reference material with known thermal events was taken in the crucible of the calorimeter. Both these crucibles were maintained at nearly the same temperature throughout the experiment and the thermal events of sample was compared with that of reference. A normal temperature range from 30 °C to 600 °C was used for the DSC analysis. The glass transition temperature of the sample is arrived as the temperature corresponding to the slope change of the differential curve.**

Thermal Gravimetric Analysis (TGA) uses stoichiometry and heat ratios to determine percentage of mass of the sample. **Test was carried out by increasing the temperature of a sample (approx. 100 mg weight) gradually whilst plotting weight loss against temperature. DSC Q-20 and SDT Q-600 were used for obtaining the DSC, specific heat and TGA of the PU-Carbon composites.**

Because of their elasticity and varying composition, mechanical properties of polymers are hard to be defined. But the physical and mechanical testing of polymers is a vital part of the product development in research and application point of view. **The tensile modulus, strain to fracture (elongation) and strength of the synthesized PU composites were measured using Microtest EM2/50/FR Universal testing machine, as per ASTM-D3039. Samples were sliced to micro-dumbel shape (40 mm long, with gripping edges and average thickness of 1.5 mm - minimum 3 nos) and were loaded at the rate of 2 mm/minute. Load cell and linear scale was used to measure the instantaneous load and displacement. During the tension test, the load and displacement was continuously recorded using the data acquisition system. Using the raw data, the stress strain curves were also plotted. The breaking load, elongation, tensile strength and the modulus for the sample were obtained from the test.**

Addition of carbon filler particles have obvious effect on the electrical conductivity of the final composite, which can be quantified by means of ohms law. **Sample was sliced to strips of known size (varies for each case) and a known voltage was passed through them and the current was recorded. The current and voltage for each instance gave the resistance as per Ohm's law and the resistivity of the material with known cross section and length was found. Inverse of the resistivity values was read as conductivity of the material.**
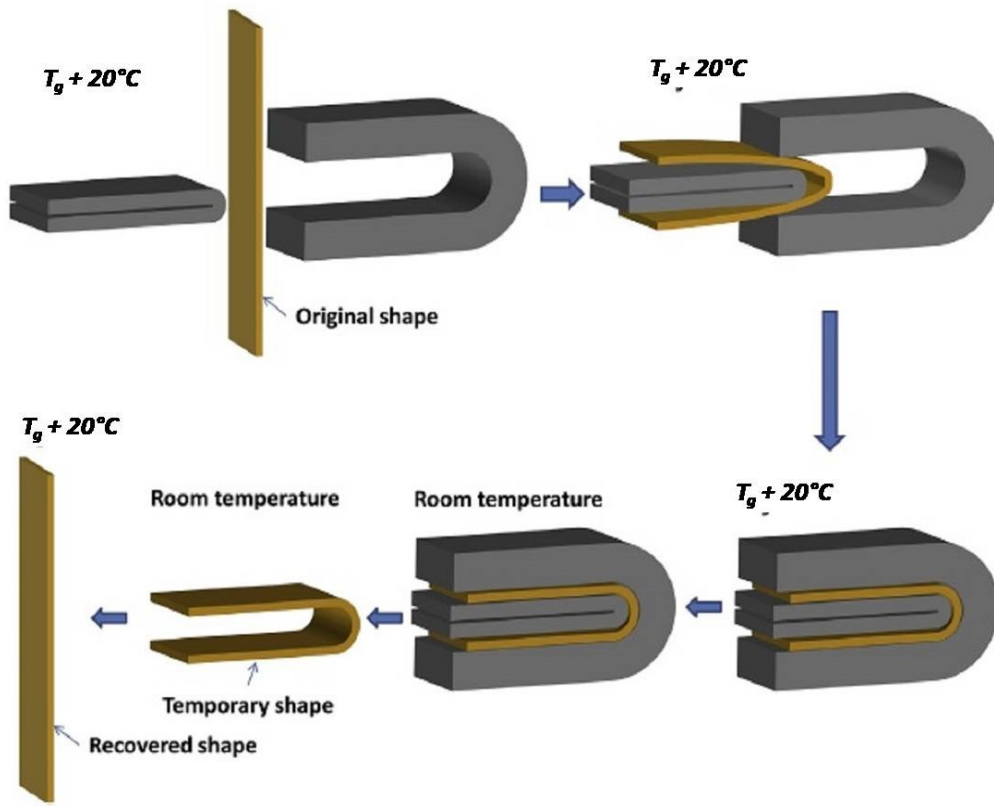
Figure 4.4 Cyclic thermo-mechanical test / fold deploy test

Shape memory of the prepared SMPC was tested using the well accepted fold-deploy test (as depicted in Figure 4.4), where the composite sample was bent to U-shape, constrained and heated to temperature, Tg +20°C for temporary shape fixing [DI et al., 2018]. The system was then cooled below Tg to evaluate the shape fixity (R_f in % by measuring the angle of recovery). The sample was heated to Tg +20°C again, and at this temperature to initiate shape recovery (recovery ratio, R_r in %). The heating was carried out by two different methods: external

heater and by passage of electricity (known voltage for respective heating time) and the experiment was repeated for multiple independent cycles.

The shape fixity and recovery ratios for the fold-deploy cycles were found using the following relations:

$$R_f = \theta_f / \theta_m \qquad (4.1)$$

$$R_r = 1 - (\theta_m - \theta_e)/\theta_m \qquad (4.2)$$

where, θ_f denotes the unload-strain, θ_m is maximum strain applied and θ_e is the permanent strain.

Bend deploy test used in this work followed isothermal dynamic testing method.

The time of recovery and the angle of fixity / recovery are the measured parameters from which the shape memory is evaluated. Standard stop-watch was used for measuring the time of recovery and a graduated protractor (0° to 180°) was used for the angle measurements.

Constant stress recovery test (where the stress do not vary with time) is found to give most informative results and it can be either dynamic or isothermal for evaluating cyclic behavior.

4.5 Modeling tools and inputs

For enhancing conductivity of the polymeric matrix and to enable them to respond against electrical stimuli, carbon based filler materials such as carbon black (CB) and multiwalled carbon nanotubes were used. Conduction phenomenon occurs in nanocomposites due to these conductive fillers having contact with each other or by the method of quantum tunnelling of electrons across a tunnelling barrier distance [Simmons, 1963; Jang and Yin, 2016, Razavi et al., 2017]. Attributed to the formation of a continuous network of conductive fillers within the insulating polymer matrix, conductivity of polymer nanocomposites exhibits percolation threshold. [Keith et al., 2016]. During filler loading below the percolation threshold, conductivity between the particles occurs by means of hopping and

tunnelling mechanisms. Studies by Piasecki 2003, Song 2016 and Kremer et al., 1988 explains interfacial polarisation effect, quantum tunnelling and inter-particle interaction as reasons for conduction in nanocomposites depending on the filler content.

In current work, the power law relationship of percolation based on the classical percolation theory of Kirkpatrick, 1973 was used to describe the behaviour of electrical conductivity of a nanocomposite above and below percolation threshold. The conductivity above (σ') and below (σ) percolation threshold follows as represented

$$\sigma' = \sigma_0(p_c - p)^k \qquad\qquad\qquad (4.3)$$

$$\sigma = \sigma_0(p - p_c)^j \qquad\qquad\qquad (4.4)$$

where k and j are the critical exponents and with reported values close to 0.7 and 2.0 respectively for 3D networks, σ_0 is the filler conductivity, p is the filler content and p_c is the percolation threshold for both of which are obtained experimentally. Based on the literature survey, it is understood that the values of these two critical parameters are affected by various factors like degree of dispersion of filler, methods of fabrication, geometry of conductive fillers, orientation, aspect ratio, and composition of system, type of conduction mechanism, possible interactions between different phases of composite and dimensionality of the conductive network.

Various modeling attempts (as discussed in section 2.12, chapter.2) have provided different approaches to the conductivity phenomenon in polymer nanocomposites. This obviously has helped to narrow the gap between actual experimental outcomes and theoretical predictions.

4.5.1 CB-PU model

In order to understand the conduction mechanism in PU-CB composite, a pseudo random model was developed by dispersing spherical CB particles in varying volume fractions in PU matrix. The statistical evaluation of model was be

achieved by multiple simulation of the system for various volume fractions and distribution. As per literature, Monte Carlo methods are considered as effective way for predicting the electrical conductivity of nanocomposite systems [Aczel, 2012]. Evaluating the complete system may turn out to be expensive in case of Monte Carlo simulation and hence a representative cubic volume element (RCVE) of 1 μm dimension was considered for modeling and corresponding simulations. Carbon black spherical nanoparticles resulting in an isotropic system assuming uniform dispersion of particles in the matrix was considered for the model. Visual 'C' based algorithm was developed for the RCVE in which spherical CB particles are dispersed. The possibility of interconnected network formation was studied for increasing volume fraction of the CB in PU matrix. Figure 4.5(a) depicts the network formation by tunneling / contact of CB spherical particles. The probability of percolation was evaluated in an ensemble of 100 simulation runs for a fixed minimum tunneling distance between the particles. A probability of 0.5 was fixed as the criterion for percolation to occur and the corresponding volume fraction was identified as percolation threshold. Few material specific parameters such as potential barrier height for tunneling, tunneling distance (which is the minimum distance between particles for conduction to occur), density of particle and dimension of CB particles were required for construction of the model.
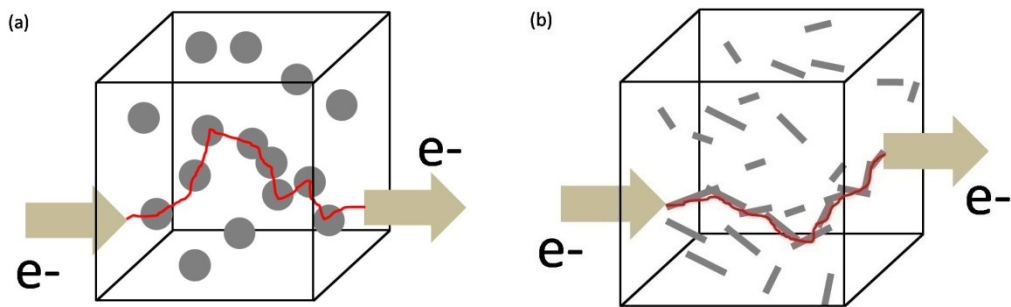
Figure 4.5 Representative volume element considered for modeling the specimen with carbon fillers (a) Carbon black; (b) Carbon nanotube. The red worm indicates the electron path (3D network formation at percolation threshold).

Spherical particles were considered efficient in terms of geometry, orientation and aspect ratio leading to a simplified system as this avoided the orientation issues as in nanotubes. Simmons, 1963 had derived the formula for electron tunneling

76

between similar electrodes (CB in this case) separated by a thin insulating matrix layer and the tunneling resistivity between two carbon particles is expressed as

$$\rho = \frac{h^2}{e^2\sqrt{2m\lambda}} \exp\left(\frac{4\pi d}{h}\sqrt{2m\lambda}\right) \qquad (4.5)$$

$$\text{conductivity}, \sigma = \frac{1}{\rho} \qquad (4.6)$$

where d is inter-particle distance, h is plank's constant, λ is the potential barrier height for tunneling, m and e are mass and unit charge of an electron. From the above expression, it is clear that λ and d influences the conductivity of particle filled nanocomposites. Johnson et al., 2011 reported that no robust method exists for measurement of barrier heights in bulk solids or polymer matrices. In current work, λ value was assumed as 1 eV for PU resin matrix material, (based on values of similar polymeric matrices from studies of Johnson et al., 2011).

For each setting of volume fraction (V_f), the algorithm was sequentially run 100 times and the number of conducting instances was obtained to determine the probability of percolation of particles in the composite.

4.5.2 MWCNT-PU model

Similar to the considerations in carbon black model, an RCVE of 1.0 x 1.0 x 1.0 micrometer cube was considered for the particle distribution and simulation of the system. Volume fraction of the carbon nanotubes in the matrix was taken to be twice as that of its weight fraction, as per general assumptions made in the working of MWCNTs nanocomposites. Number of cylinders to be packed was estimated with the help of volume fraction of MWCNTs, which can be easily correlated with experimental weight percentage predetermined. Filling up of CNTs throughout the system with maximum possible chirality and uniform distribution throughout the considered space was taken up as the primary priority. Cases of overlapping and possible extension of the cylinders outside the considered region was considered subsequently and optimised to maximum possible extent to make this computational study as close to realistic experimental approach.

Initial placement of the CNTs was achieved by random generation of two endpoints of the axis of the cylinders with no constraints for axis length. Then considering the orientations of these axes as parent axes, subsequent final initial placement was done by specifying height and diameter for each cylinder over the parent orientations. Heights of cylinders were taken to be in the range of 180 to 600 units, diameter in the range of 3 to 5 units and aspect ratio in the range of 90 to 120. These calculations were made as per the quantitative study over the experimentally available carbon nanotubes (CNTs). The verification of aspect ratio was done by comparing conduction results of both experiment and computational data. The cylinders were then sorted as per inter-particle distance as found in the previous section (d) for the possible tunnelling current to pass through. This was achieved by rearranging the two end points of the axes, such that first end has co-ordinates closer to centre than the second axes. Further the distances of the first end of the axes from cylinders to the centre was used to rearrange numbering of the cylinders in ascending order. This approach of placing cylinders may lead to some cases of overlaps and some projections of cylinders outside the representative volume element. These cylinders that either overlaps with other cylinders or those which lies out of the confined space were considered as invalid placements. The invalid placements within RCVE was identified using an algorithm for further optimisation steps, where optimising their position relative to all other perfectly / imperfectly placed cylinders was taken up as objective and solved to possible extent. These computational steps were inspired from the actual functionalization of MWCNT for preventing agglomeration and constant stirring (ultrasonication in MWCNT nanocomposites) which were given paramount importance during synthesis of nanocomposites. Analogous to these preventive measurements, our computational method aims to de-cluster any possible bundling by trying to optimise the packing of MWCNTs without overlaps and trying to fit them inside the RCVE. The improper placement (either overlaps or out of cube) was detected by employing mathematical approach of shortest distance between two straight lines. Carbon nanotubes being nanomaterials with high aspect ratio were first estimated to be infinite space lines and the shortest distance between every two possible pair of cylinders within the

space was calculated. The shortest distance between the cylinders was calculated by finding Euclidian distance (assuming the perpendicular distance between cylinders under consideration). Cases of overlapping were identified by comparing the obtained distance between the axes to that of minimum possible distance between axes of two cylinders in non-overlapping configuration i.e. the just touching case, which is numerically equivalent to the sum of radii of the two considered cylinders. The cases of cylinders being out of the RCVE, during the initial placements were identified by validating all 6 co-ordinates of the axes to be lying within the RCVE. Co-ordinates of every cylinder placed along with their dimensions were stored, out of which cylinders which were improperly placed were flagged. Optimisation of entire space was carried out for each occurrence of an improperly placed cylinder with the help of nonlinear optimization.

Two surfaces of the cube were considered as the probing surface and mathematical approach was made to mark touching pairs out of all available pairs in the system and feed into the optimisation studio algorithm as a linear optimisation problem, with required constraints and objective function. Hence, prediction of whether a successful network could be formed by the MWCNTs over the RCVE with specified volume fraction and optimised placement was verified. Wolfram Mathematica was used to plot the CNTs for better visualisation. The percolated network formed by interconnected nanotubes / tunnelling between the inter-particle distance is shown in Figure 4.5 (b).

A combination of statistical percolation, geometric, structural orientation modeling approach based on fillers visualised as discretised elements was attempted in this work for understanding the percolation behaviour of polymer nanocomposites. Monte Carlo simulation method was used for optimisation of the results and the results were evaluated using experimental values.

CHAPTER.5

RESULTS AND DISCUSSIONS

The demand for remote actuation and getting away with external heaters (as used for thermally activated shape memory) have led to the development of electro-active SMP composites with different filler reinforcements (carbon nanotubes, carbon black, graphene, carbon nanofibers, fullerenes or metal fillers like nickel powder) [Meng et al., 2013; Sun et al., 2012; Sattar et al., 2015; Jin Ho et al., 2015; Kim et al., 1996; Zhang et al., 2009; Arun et al., 2018]. This chapter details the various results obtained for the three different systems (CB PU, MWCNT PU and combination of CB & MWCNT fillers in PU) both experimentally and by a computer generated program for understanding and predicting the percolation behavior of CB & MWCNT nanocomposite systems. A synergy study between CB & MWCNT in varying combinations (ternary nanocomposite systems) were also studied and compared with individual nanocomposite systems (binary systems).

I. Experimental and modeling studies on Carbon black - PU SMP nanocomposite

The process of electric current conduction occurs in nanocomposites due to the conductive reinforcement fillers touching each other or by the method of quantum tunnelling of electrons across a barrier distance. It is learnt form the review of literatures that a large number of factors affcet the phenomenon of conduction such as filler distribution in matrix, shape, size, aspect ratio, filler conductivity and matrix interaction, nature of polymer matrix, wetability, particle size distribution, orientation, surface energy and processing techniques [Arun et al., 2018]. All these factors are accounted in formulating the experiment as well as modeling of the system. The geometry of spherical CB particles was found simpler over nanotubes and nanofibers while evaluating the above factors and hence CB is chosen as filler material for this initial part of the study.

The conduction at lower CB loading occurs by means of hopping and tunnelling mechanisms. Piasecki 2003, Song 2016 and Kremer et al., 1988 explained interfacial polarisation effect, quantum tunnelling and inter-particle interaction as reasons for conduction in nanocomposites depending on the filler content. On applying an external voltage to the material with lower filler contents can cause an accumulation of charges at the interface between filler and matrix. This can cause polarisation of the dielectric matrix material leading to a possibility of charge transfer if the available filler particles are aligned in a random distribution. With increase of filler content, the conduction process changes to quantum tunnelling, subject to the particle closeness within the maximum allowable tunnelling barrier. For higher filler loadings, electron transfer occurs due to particle interaction and network formation [Jang and Yin, 2016]. Being with rare chance of conduction, interfacial polarisation is not considered as a possibility of conduction in many scientific articles.

A defined transition from an insulator to a conductor can be observed with increasing CB loading upon connecting to a specific electrical source. This was possible through formation of 3D networks which forms electron pathways for

electric current. During low filler volume fraction, lesser number of networks are formed which increases with CB loading. Beyond percolation threshold, the conductivity increases exponentially due to formation of multiple networks that allows more electron paths. The initiation of formation of a continuous conductive network spreading across the polymer matrix occurs at the percolation threshold and thus the conductivity of the composite increases in several orders of magnitude around this critical value. Hence it can be understood that percolation threshold corresponds to the lowest filler concentration to form continuous conductive path in the matrix [Belashi, 2011].

Feng and Jiang, 2013 and Zhang et al., 2009 observed that the inter-particle distance (*d*) of a dispersed spherical particle system is proportional to $\varphi^{-1/3}$, where φ is the filler volume fraction.

i.e. $d \ \alpha \ \varphi^{-1/3}$ (5.1)

If the overall filler content is too low to have direct contact among each other, the particles remain with a small separation distance. On application of a potential difference, electrons tend to jump across the inter-particle distance (termed as the quantum tunneling barrier) causing conduction. The quantum tunneling barrier depends on the properties of the matrix, inter-particle distance, and the voltage applied at the junction [Belashi, 2011; Soto et al., 2015; Balberg, 2002; Wu et al., 2000; Seidel and Lagoudas, 2009]. For a low applied voltage, electrons merely behave like particles and they bounce back on hitting the tunneling barrier. However, when applied voltage increases, more electrons hit the barrier leading to penetration of the barrier causing conduction based on quantum mechanical consideration [Radzuan et al., 2017]. As the volume fraction of the particles in the matrix increases, the inter-particle distance reduces leading to large number of conductive networks [Merzouki et al., 2012; Keith et al., 2006; Feng and Jiang, 2013; Piasecki, 2003; Hu et al., 2007]. Hence it can be understood that a combination of both electron hopping at nanosclae and conductive network formation at microscale contributes towards electrical conductivity.

The PU resin synthesized as explained in chapter 4, was mixed with CB fillers to prepare the nanocomposite. The process of blending was by means of mechanical milling as explained earlier, which provided a uniform dispersion of filler materials in the matrix volume. The distribution of filler materials plays a vital role in the current conduction as well as uniform heating of the system that affect the shape memory behaviour. As mentioned in chapter.4, the carbon black spherical particles were mixed as 3%, 7%, 10%, 20%, 25%, 30% and 40% by weight percentages of the resin. Samples of size 100 mm x 100 mm / 50 mm with thickness of 2 mm to 3 mm were prepared. Complete curing of the nanocomposite resulted in thin flexible sheets (black in colour). as shown in Figure 5.1.

Figure 5.1 PU CB nanocomposite, after curing, 2 to 3 mm thin sheets of size 100 mm x 50 mm were obtained after 240 hours of air curing and 10 hours of oven curing (150°C).

5.1 Characterization results

The material was characterized for its chemical and microstructure and the thermal, mechanical and electrical properties were also evaluated as explained in chapter.4. The results and discussions of the characterization, modeling of percolation behavior of the system in computer programming and the validation of the same with experimental data, shape memory demonstration are discussed subsequently.

5.1.1 Chemistry, Hydrogen bonding and Microstructure

Understanding of the microstructure and chemistry of SMPC is inevitable and is made possible by various characterization techniques. The FTIR spectra of control specimen (0%CB) and for varying weight % of CB in PU resin are shown in Figure 5.2.
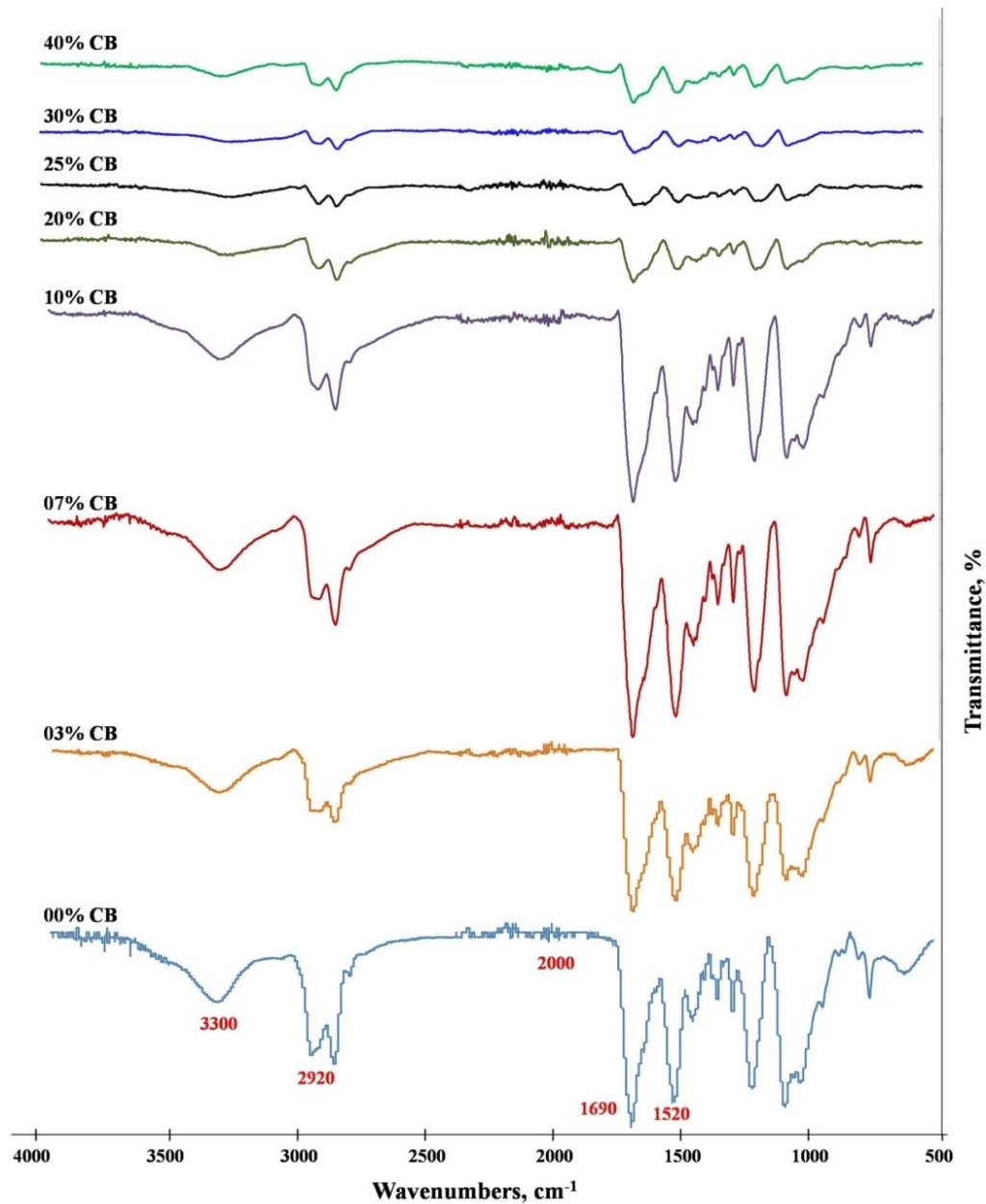
Figure 5.2 FTIR plots for CB PU combinations with 3% to 40% filler content

As the carbon content increases, the intensity of transmittance was found reducing, which can be interpreted as due to the absorption of the radiations by these carbon particles resulting in dissipation of the energy as heat. From the FTIR spectrograms, typical polyurethane linkages can be observed for all the carbon loading samples within the functional and fingerprint regions. All of the spectrogram shows similar patterns in peaking at the frequencies specific to the presence of urethane bonds.

Presence of N-H- bonds (primary and secondary amines) is evident from the stretch absorptions between 3200 and 3500cm^{-1}. Peaks around 2850 to 2950cm^{-1} indicate the C-H stretching linkages. The N-H bending, C=O and aromatic C=C stretching are observed at peak region 1600 to 1700 cm^{-1}. The peak absorptions between 1000 and 1520 cm^{-1} denote the C-H bending and C-N stretching which is typical to PU.

Apart from the assurance of PU formation through the observed peaks, the chemistry of shape memory can also be understood from the FTIR plots. The distinction of hard and soft domains depends on types of the polyol and diisocyanate used, ratio of polyol to diisocyanate, hydrogen (H) bond formation, crystallization of the segments, extent of solubility of the segments and entropy and free energy changes of the matrix [Gunes, 2009; Garrettet al., 2000].
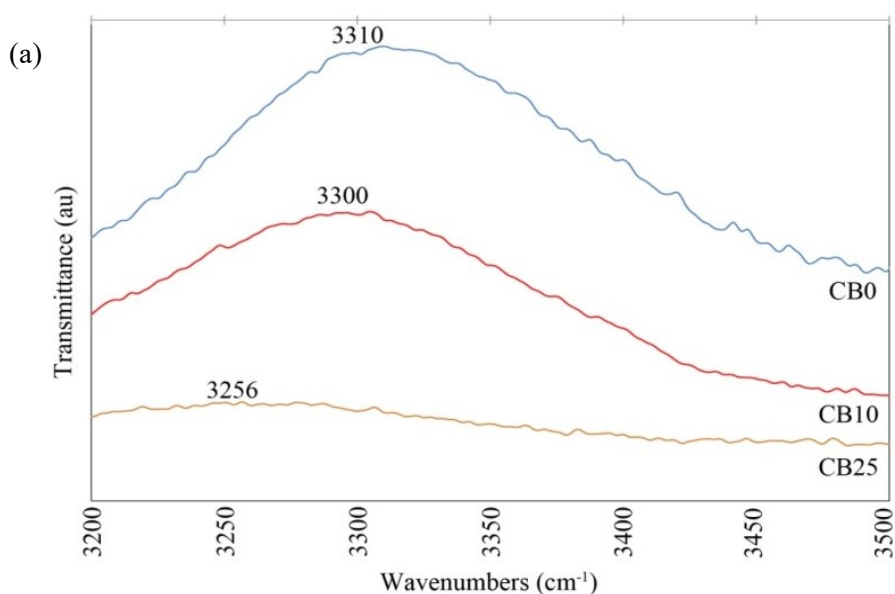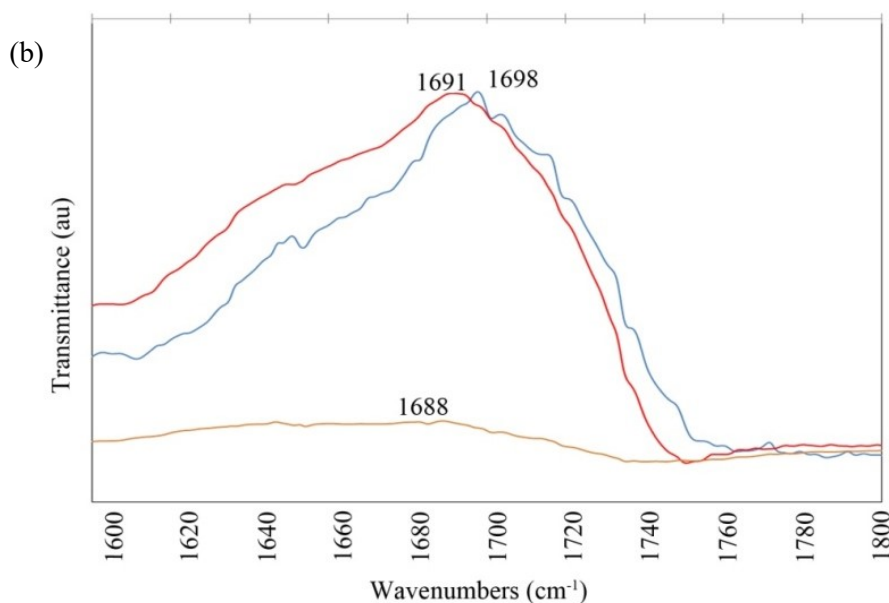
Figure 5.3 IR spectrogram for understanding the H bond (a) spectra in N–H; (b) C=O region of spectrum for CB0, CB10 and CB25 as representative combinations.

The mutual affinity of hard segments and the molecular arrangements allows formation of stress free H-bonds (hydrogen bonds) which can be read from FTIR spectra of the system, as depicted in Figure 5.3. 25%, 10% weight and pure PU were considered for understanding the hydrogen bond formation.

The H-bond formations within the resin are to be interpreted from the N-H- and C=O stretching regions [Pangon et al., 2014]. Two regions in FTIR spectra were mainly considered; N-H region of spectra between 3200-3500 cm^{-1} and C=O region between 1600-1800cm^{-1}. The N-H region can be further divided into four bands, where the N-H peak fits in. These are free N-H (3500-3460 cm^{-1}), disordered (3460-3350 cm^{-1}) and ordered H-bonded N-H (3350-3307 cm^{-1}) and the N-H linked to the ether oxygen of PTMO (3310-3200 cm^{-1}) i.e., N-H…O. From Figure 5.3(a), it can be observed that the N-H peak for CB content up to 25%, the absorption peak remains within the N-H…O region which confirms the hydrogen bonding with PTMO oxygen atoms. This confirms the H-bond linking which provides the elastomeric behavior to the polymer and underlines the role of hard segment to recover original shape. An obvious drift from 3310 to 3256 cm^{-1}

can be found while the CB content changes from 0% to 25% which can be due to the dispersed carbon nano-particle between chains causing a possibility to form ordered N-H hydrogen bonds.

The Figure 5.3(b) depicts the hydrogen bonding in C=O region of spectra, where three bands exist such as free C=O band (1750-1700 cm^{-1}), disordered (1650-1700 cm^{-1}) and ordered hydrogen bonding (1600-1650 cm^{-1}). All the three sample peaks were found near 1690 cm^{-1} which indicates disordered H-bonded C=O that can be due to combination of an aromatic and aliphatic isocyanate in the system (TDI and IPDI).

The UV spectrogram (plot of absorbance against wavelength) has not shown any specific peaks in the ultraviolet region of the spectrum for neat resin as well as composite specimens (refer Figure 5.4). This can be due to two major reasons, one of which is the presence of 'aliphatic' diisocyanate (IPDI). It is established via studies that saturated cyclic and aliphatic polyisocyanates are more stable to ultraviolet radiation and the polyurethanes prepared out of such aliphatic components are stable against UV radiations [Robert and William, 1983].
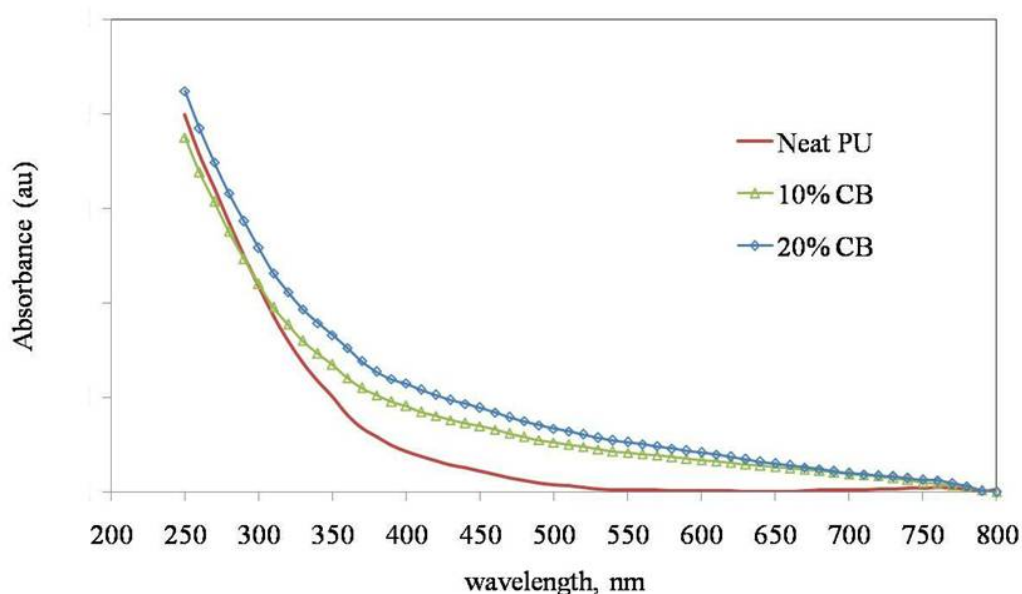
Figure 5.4 Ultraviolet spectrogram for varying CB combination

Second reason is specific to the composites that points towards the presence of CB, which is proven as a UV stabiliser for polymeric materials [George W, 2015]. The CB particles are reported to absorb the UV radiations and dissipate the same as heat energy, thus protecting the resin from degradation due to UV rays.
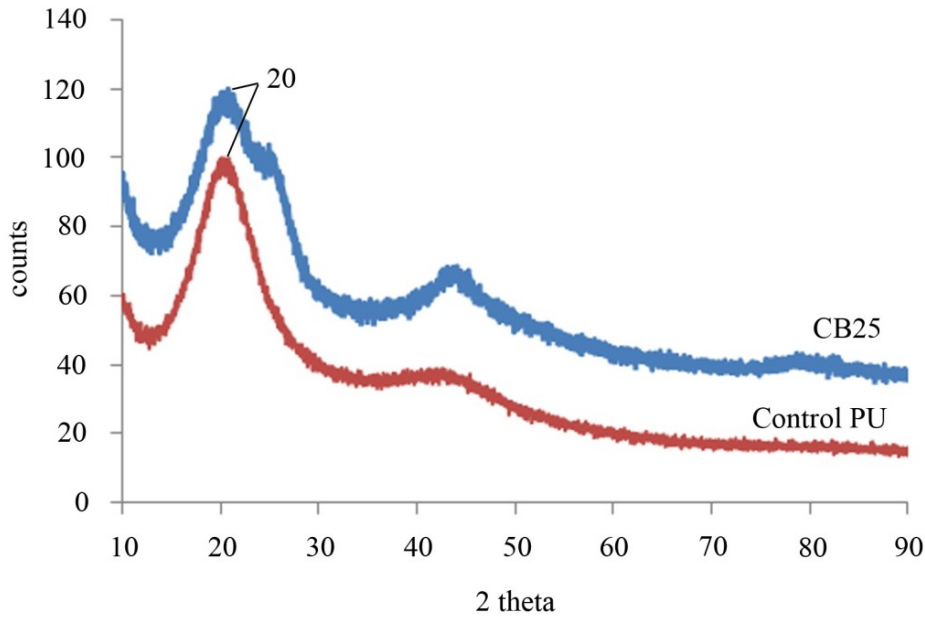
Figure 5.5 X-ray spectrogram for varying CB combination

The profile of XRD for CB PU nanocomposite synthesised showed similar trend for different weight % of CB between 3% and 40%. The normalised XRD spectrograms plotted for representative 25% CB PU composite and pure PU specimen (control PU) are shown in Figure 5.5.

It can be observed that the XRD (X-ray Diffraction) patterns of the nanocomposites were found identical due to the basic amorphous nature of the polymer composite. As depicted in Figure 5.5, a pronounced peak is observed peak at the 2θ value of 20° and a minor peak at 45° both of which are attributed to the amorphous nature of the PU. The same trend is observed for CB loading from 2% to 40% (due to which only representative sample with 25% weight fraction is depicted), which clearly shows the non contribution of CB towards the peaks of XRD spectrum.

(a)

| 1 µm | EHT = 4.00 kV | Signal A = SE2 | Date :8 Feb 2018 | ZEISS |
| | WD = 6.1 mm | Mag = 20.00 K X | | |

(b)

| 1 µm | EHT = 6.00 kV | Signal A = InLens | Date :21 May 2018 | ZEISS |
| | WD = 7.7 mm | Mag = 20.00 K X | | |
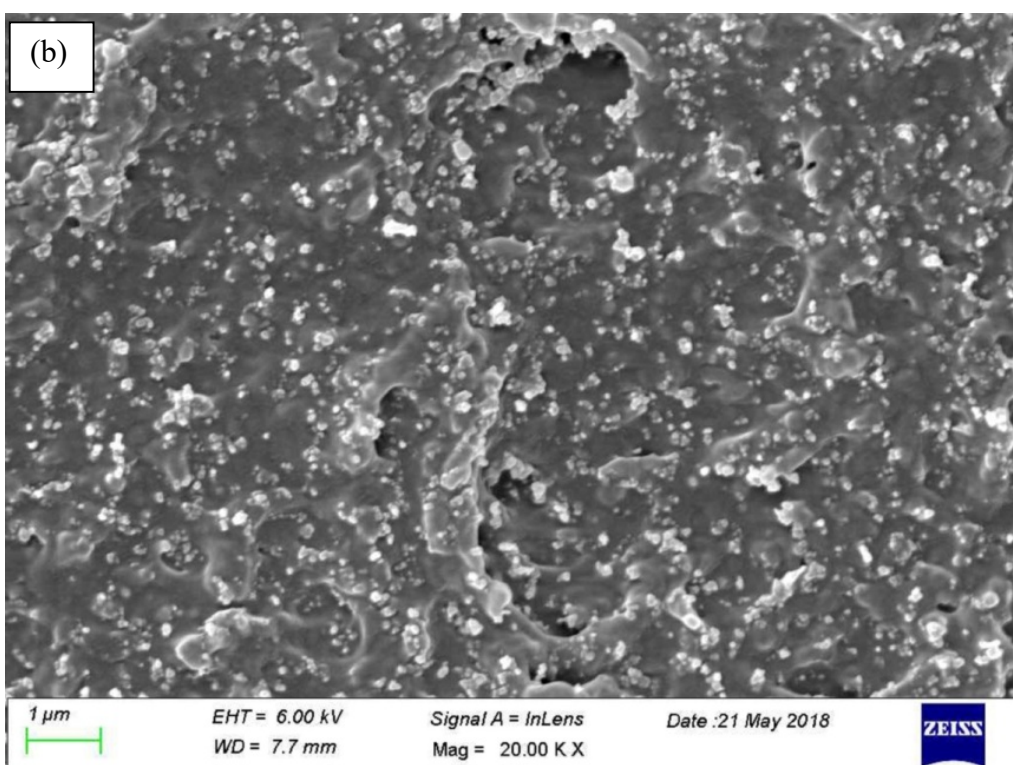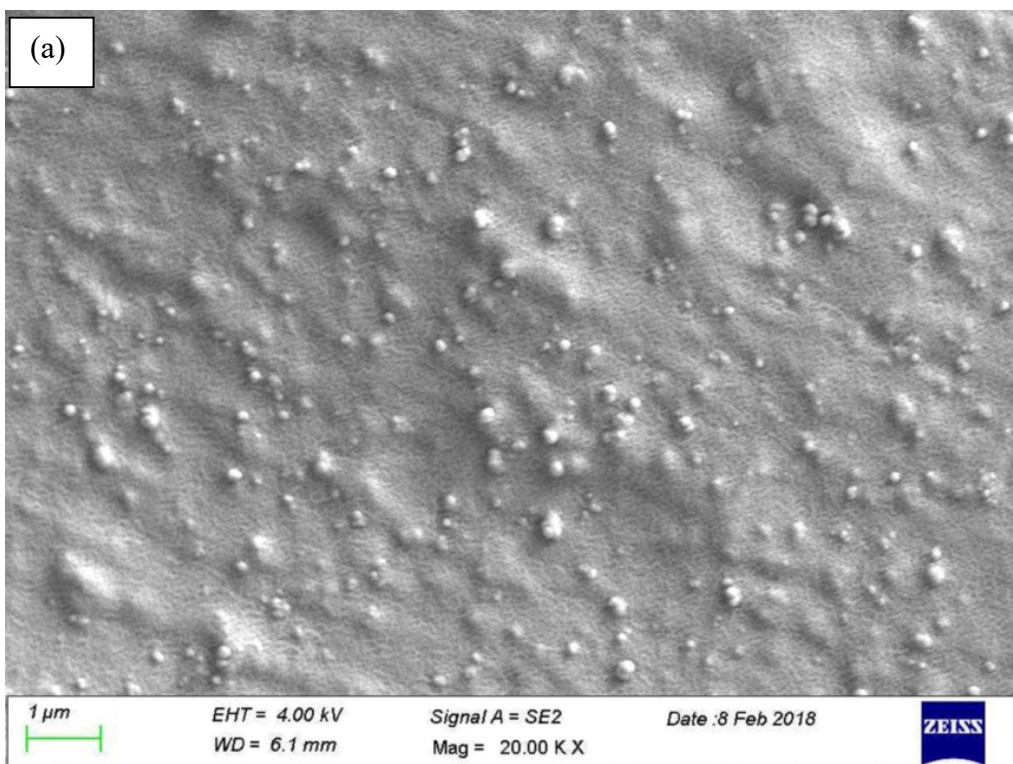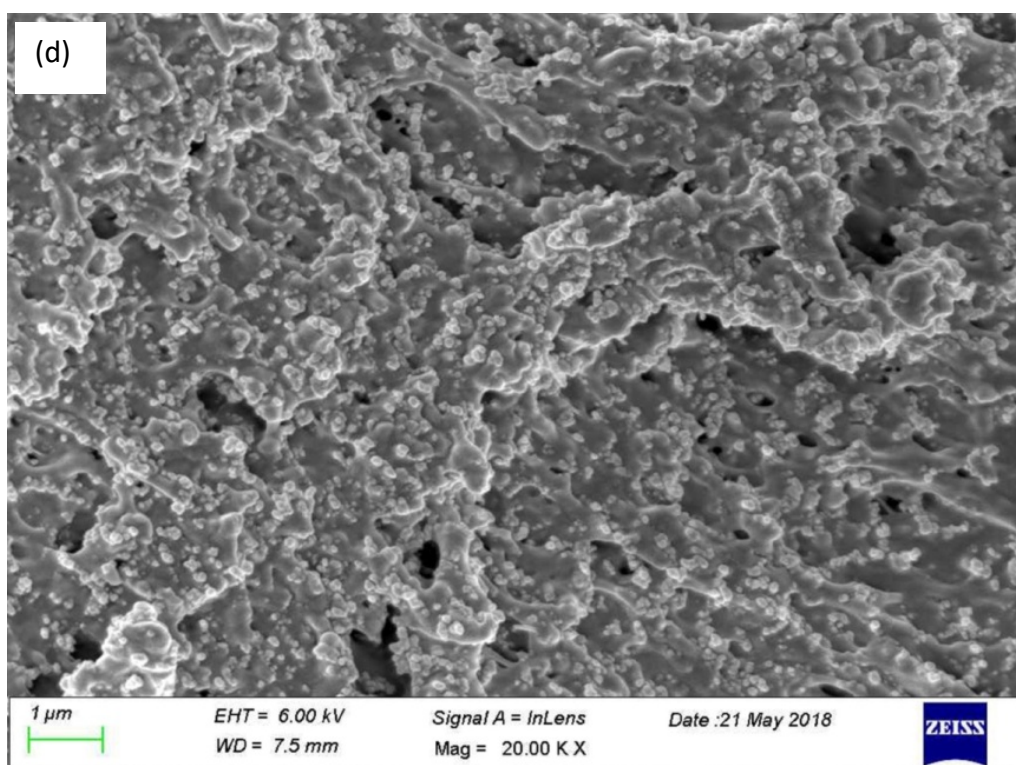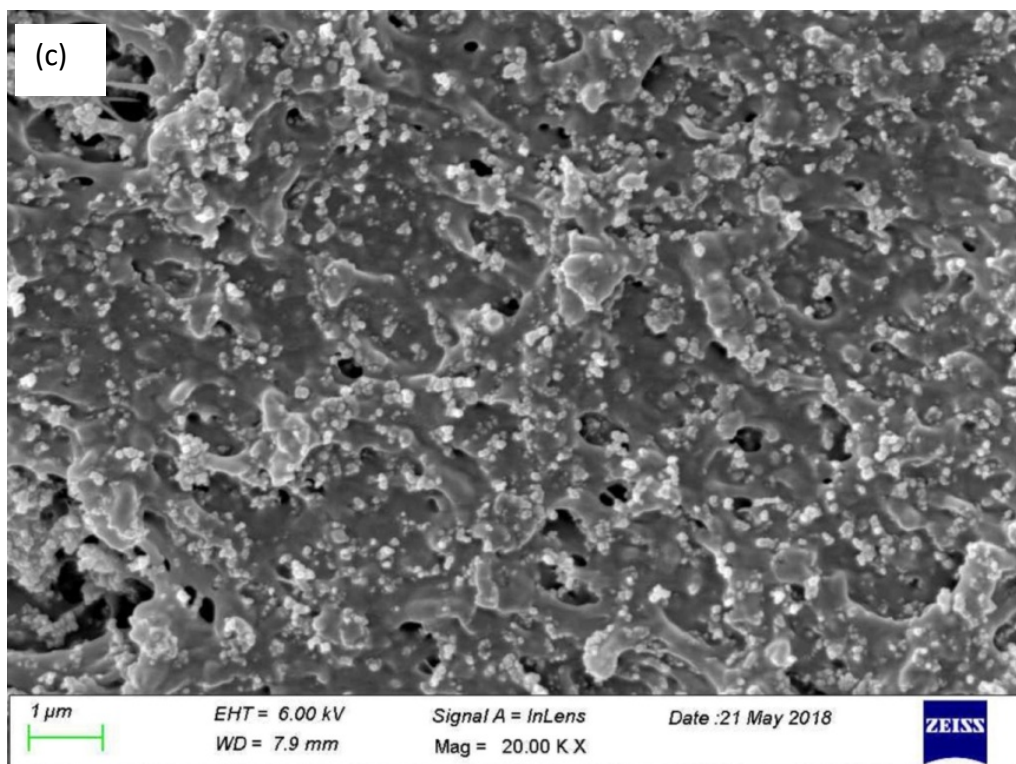
Figure 5.6 Scanning electron micrograph for CB combination (a) 3%; (b) 5%; (c) 7% and (d) 10% in PU matrix

The CB filler was dispersed in PU matrix by means of mechanical milling process and the actual dispersion can be observable from a microstructure image. SEM micrographs (as shown in Figure 5.6 (a)-(d)) of various weight fraction (*3%, 5%, 7% and 10%)* of CB in PU revealed the particle sizes in matrix and the dispersion trend. An average particle size (diameter) of 168 nm was observed from SEM images of various volume fractions. This is the average of the diameters measured at various locations from SEM images.

It is evident from the spectrograph that the population density of the CB particles increased with increase in content of fillers. The CB particles were also observed to be uniformly dispersed in the matrix and the inter-particle distance was found to reduce as the carbon loading increased. The same has been verified with sample images taken in longitudinal as well as transverse fracture planes of the nanocomposite prepared. This inference concurs with the studies of Merzouki et al., 2012 and Rodwick et al., 2007. The images showed well dispersed carbon particles system which is a good indication that 24 hours mechanical mixing is effective for proper distribution of the CB reinforcements in the resin matrix.

5.1.2 Mechanical and thermal properties

The Figure 5.7(a) depicts the stress-strain plot for carbon content varying from 0% to 25%. It can be observed that the elastic modulus (stiffness) of the composite increased with increase in carbon loading (slope of the curve becomes steeper with increasing carbon loading). As reported by Lawrence and Robert, 1944, it is obvious that the addition of CB particles having large surface to volume ratio increases the surface energy, which results in better interfacial adhesion in the particulate-filled composite matrix resulting better strength (Figure 5.7(b). An increase in slope of the stress strain plot indicates a rising modulus value corresponding to increase in CB content Figure 5.7(c).

(a)

(b)

(c)

(d)
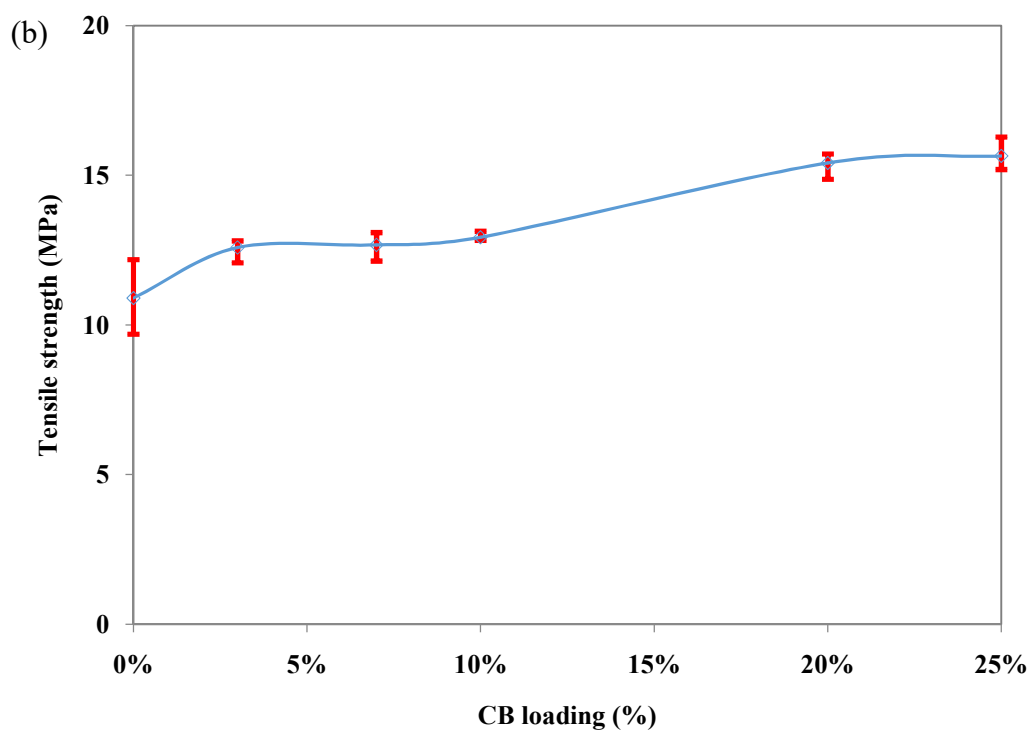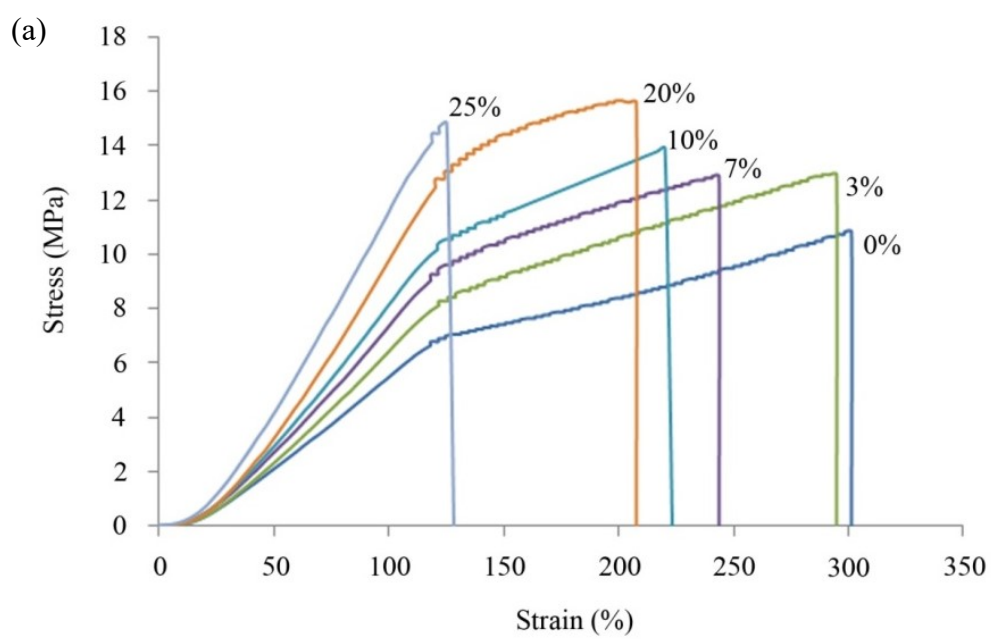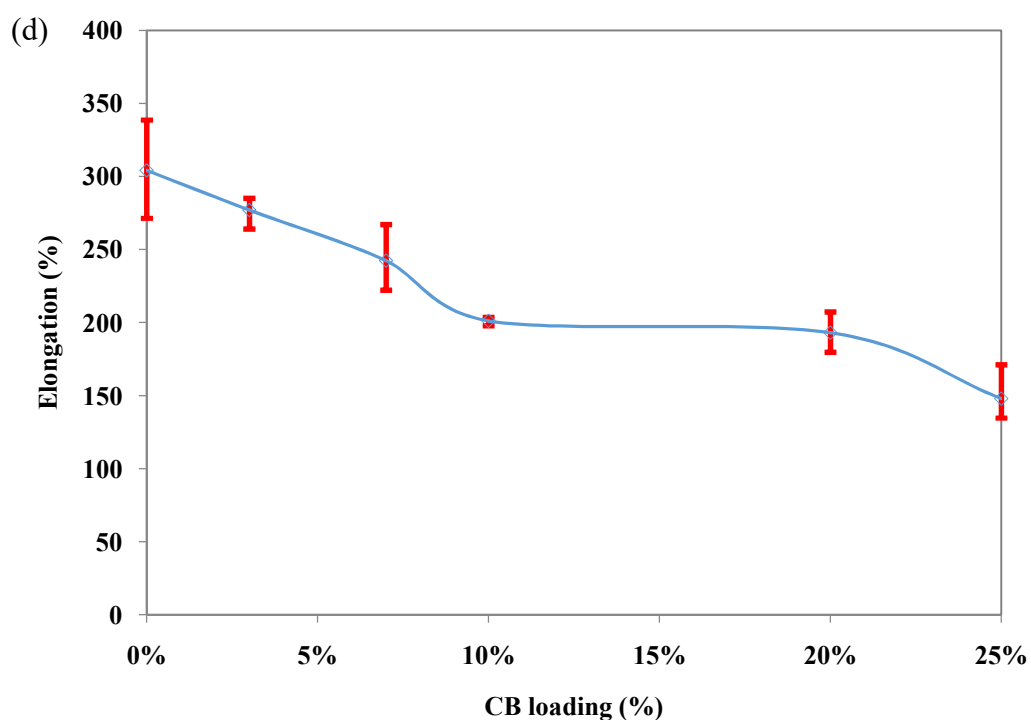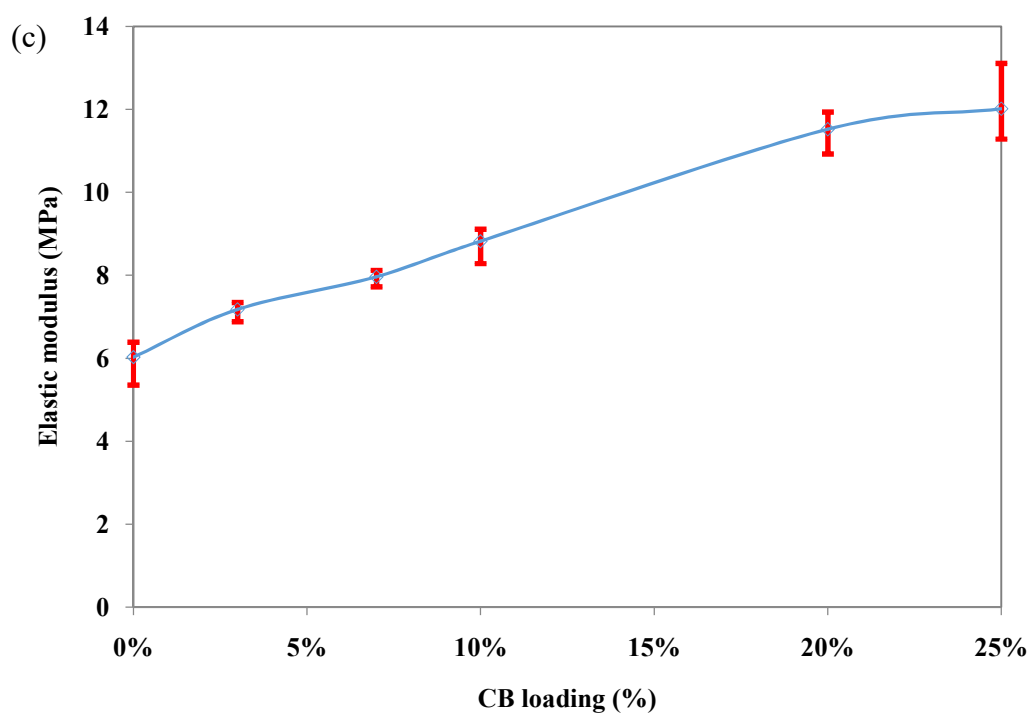
Figure 5.7 Mechanical property evaluation of CB-PU nanocomposites; (a) Stress–strain plot; (b)Tensile strength against varying CB loading; (c)Elastic modulus of the nanocomposites; (d) Elongation of the material for varying loading of carbon black

The reason for increase in the modulus value can be further substantiated by the

molecular level interactions in which the fillers offer resistance to the free movement of chain stretching and thereby increasing rigidity of system. The reason for the reduction in elongation is from the increased rigidity (Figure 5.7(d)). The strain to failure (Figure 5.7(a)) followed a decreasing trend with increase of CB loading in the matrix. Application of load beyond a threshold value results in loss of interfacial adhesion, causing de-wetting of the fillers in the matrix. This leads to void formation and ultimately leading to failure of material under tension. Larger the filler content, the probability of de-wetting of the particles from the matrix increases (as matrix to reinforcement ratio decreases) and thereby resulting in brittle failure. It was observed that CB loading beyond 25% resulted in increased brittleness of the composite and cracks were observed during curing and thereby no mechanical testing was carried out for samples beyond 25%CB. The cracking may be due to the large difference in coefficient of thermal expansion (CTE) between the matrix and the reinforcement phases. A residual tensile stress is thus set up in the matrix leading to nucleation of cracks during the process of curing. On the other hand, beyond 25%CB loading, the composite formation was affected by crazing of the matrix while curing. This is attributed to the increased interfacial energy beyond the optimal value of 25% filler content causing de-wetting the particles from the matrix.

The resistance offered by the CB particles in the matrix towards chain movement affects the load carrying ability. The stretchability of the material gets affected by the increased carbon content as the inherent elastomeric behavior of matrix is lowered beyond an optimal content (25%). The values of modulus and elongation observed above on each CB loading were found higher than the values reported for respective CB loading by Huang et al., 2012. This may be attributed to different reasons like the blending method adopted, special combination of low molecular weight polyols [Ahmad et al., 2012] (PTMO-2000) and proper dispersion of filler in matrix. The presence of CB also add to increase the shore hardness of the PU nanocomposite from 37D (0%CB) to 44D (25%CB) which may be due to the influence of reinforcement imparting rigidity to matrix.
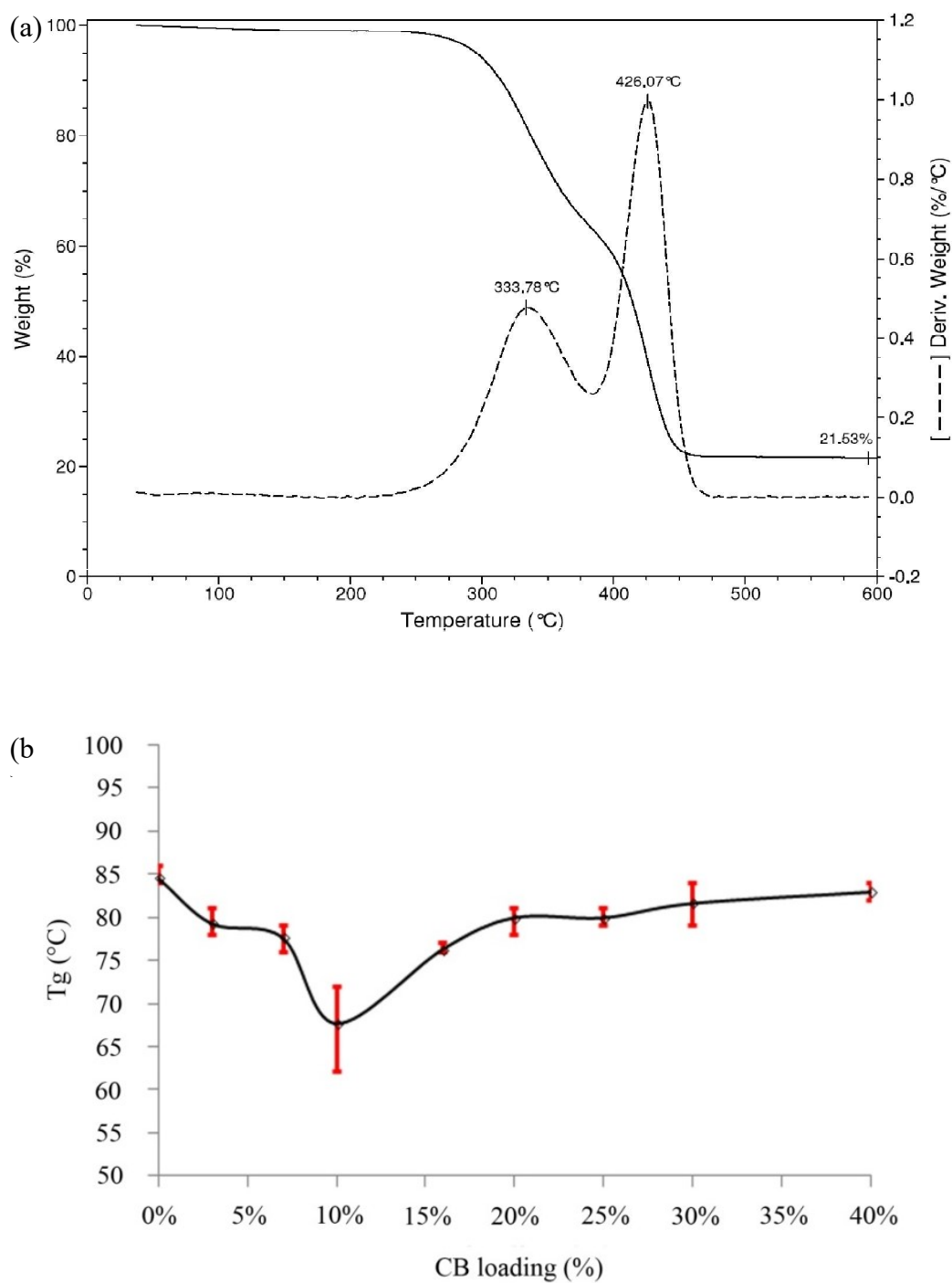
Figure 5.8 (a) TGA plot for 25% CB in PU; (b) T_g variation with carbon loading.

The results of TGA (Figure 5.8(a)) showed that the material is relatively stable up to temperatures above 300°C and the addition of CB was found to have little effect on stability of the system. The same trend was shown in TGA curves of all the CB loadings.

Determination of T_g of SMPC is significant in ascertaining the temperature at which SMP behaviour initiates. Higher T_g polymer is recommended for applications where the operating temperatures are higher as in aerospace/defence sectors. A high T_g value of 85°C was observed for the control resin, compared to the reported T_g values in literature [Sattar et al., 2015; JinHo et al., 2015; Kim et al., 1996; Gu et al., 2013; Su et al., 2014; Bin and Min, 2005; Yang et al., 2005; Huang, 2010; Huang et al., 2012; Ahmad et al., 2012]. This is attributed to the aggregation of hard segments via hydrogen bonding and the cross-linking of the matrix. Increased rigidity of hard domains in molecular scale was found enhanced by presence of carbon particles which helps to achieve higher transition temperature for the SMPC. The variation of T_g value for various CB loading are shown in the Figure 5.8(b). it is observed that the T_g values followed a decreasing trend up to 10% which can be due to gradual increase in thermal conductivity and thus heat absorption by CB particles. Then the T_g increased beyond 10% as the increased particle content affected chain mobility and thus adds to the hard domain rigidity. Hence it can be interpreted that beyond 10% CB content, the rigidity of composite matrix governs the transition and thus the temperature to achieve transition increased resulting in higher T_g.

5.1.3 Electrical conductivity

As reviewed from literatures [Akos et al., 2012; Xiaomei et al., 2011], that one dimensional and two-dimensional fillers like CNT and nano-papers caused continuous networks to enhance electrical conductivity due to high aspect ratio, while zero-dimensional fillers like carbon nano particles / CB induce conductivity by convective electron transfer (electron hopping) by tunneling effect.

The electrical resistivity ($\boldsymbol{\rho}$) of the material with known dimensions (length l and area A) was obtained from resistance R measured by passing known current I and applying known potential difference V.

Resistance, $R = \dfrac{V}{I}$ (5.2)

Resistivity, $\rho = \dfrac{RA}{l}$ (5.3)

Conductivity, $\sigma = \dfrac{1}{\rho}$ (5.4)

The experimental conductivity measure against volume fraction of CB in PU is presented in Table 5.1.

Table 5.1: Electrical conductivity measured against weight fraction of carbon black filler

Weight fraction of CB	Measured Conductivity, S/cm
0%	2.03×10^{-11}
3%	9.40×10^{-11}
5%	1.30×10^{-09}
7%	1.47×10^{-04}
10%	9.09×10^{-04}

A sigmoidal distribution (increased slope beyond 5% weight fraction) of measured value shows a steep increase in conductivity between 5% and 7% and hence confirms transition of material to a conductor.

The PU-CB nanocomposite synthesized was found to transform from an insulator to an extrinsically conductive material as the carbon loading increased beyond 5% weight fraction of CB in matrix (refer Figure.5.9(a)). A percolation threshold of 6% CB loading can be observed, which concurs with the results reported in literature for PU CB systems [Merzouki and Haddaoui, 2012; Huang et al., 2012].

(a)

(b)

200 nm   EHT = 6.00 kV   Signal A = InLens   Date :21 May 2018   ZEISS
          WD = 11.3 mm   Mag = 75.00 K X
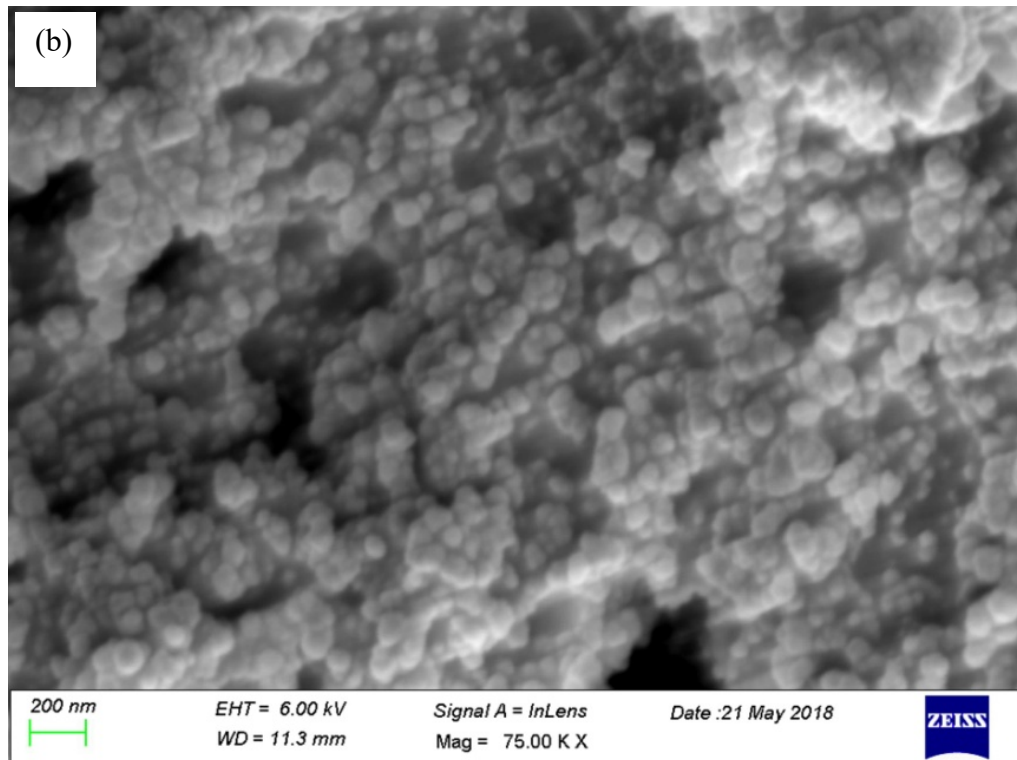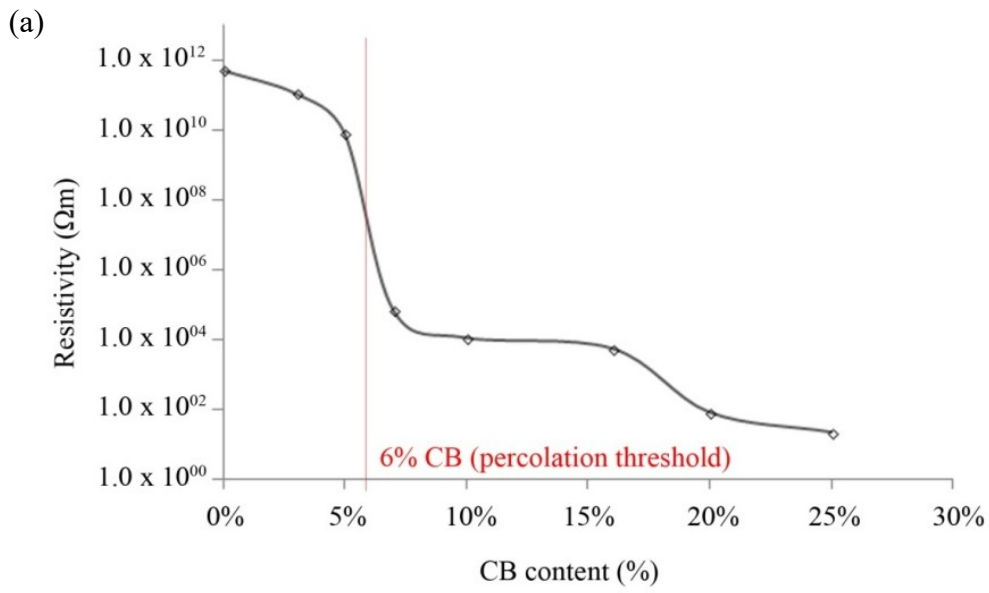
Figure 5.9 (a) Variation of electrical resistance of PU-CB composite with carbon loading, (b) closer particles as observed in SEM for 25%CB loading in PU resulting in network formation.

The obtained value of 6% was found matching with the reported values from studies of Huang WM et al., 2012. SEM analysis revealed (Figure 5.9(b)) that an increase in CB loading resulted in closer distribution of the particles in the

matrix which caused contact of particles or reduces inter-particle distance. The electron conductivity in such systems was explained as quantum tunneling at nanoscale and conductive network formation at microscale [Jinsong et al., 2008; Kirkpatrick, 1973].

5.1.4 Classical percolation theory

The critical exponents 'k' and 'j' from Kirkpatrick's classical percolation theory were evaluated from the plot in Figure 5.10.
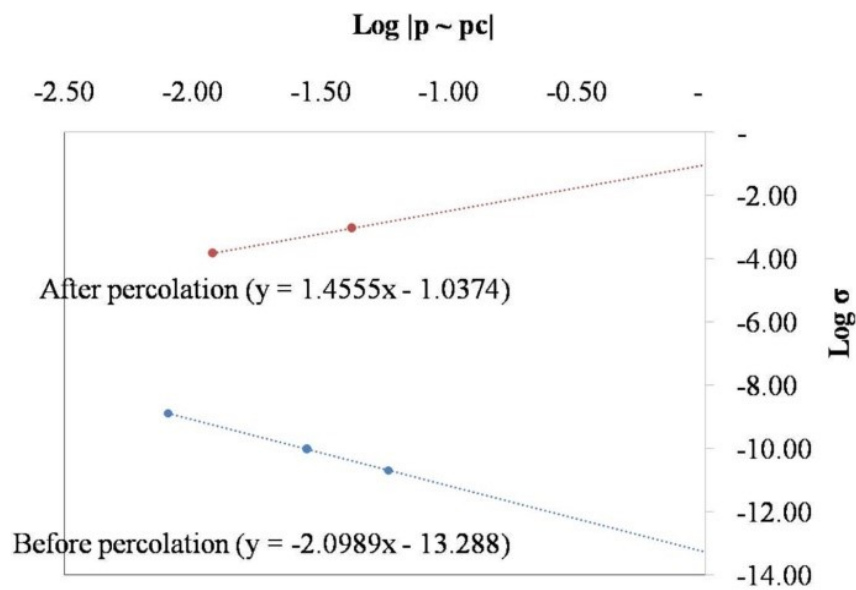
Figure 5.10 Plots of log σ vs. log (p ~ pc) based on classical percolation theory for the nanocomposite

A logarithmic plot of conductivity against difference in filler content with percolation threshold value gives the values of the critical components. Knowing the filler content and corresponding conductivity of the matrix thus allows finding the values of the critical exponents from the slope of the lines connecting the points. From Figure 5.10, 'j' value and 'k' value obtained were 1.456 and 2.099 respectively. It is observed that when j value is below 2.0, the conduction occurs by particles touching each other forming networks. Current experimental value of 'k', obtained from the plot is found higher compared to published literature data [Mdarhri et al., 2012], which may be explained as the

99

conduction below percolation is purely due to tunneling as the critical exponents are established as indication of inter-particle distance. As understood from the literature that k and j are indicates tunnelling resistance distribution, a larger values represents separated particles which eliminates the chance of contact conductivity.

5.1.5 Relationship of time and T_g

An empirical relationship between, time and temperature for various voltages has been established in PU-CB composite with representative specimen having 25% CB (as depicted in Figure 5.11).
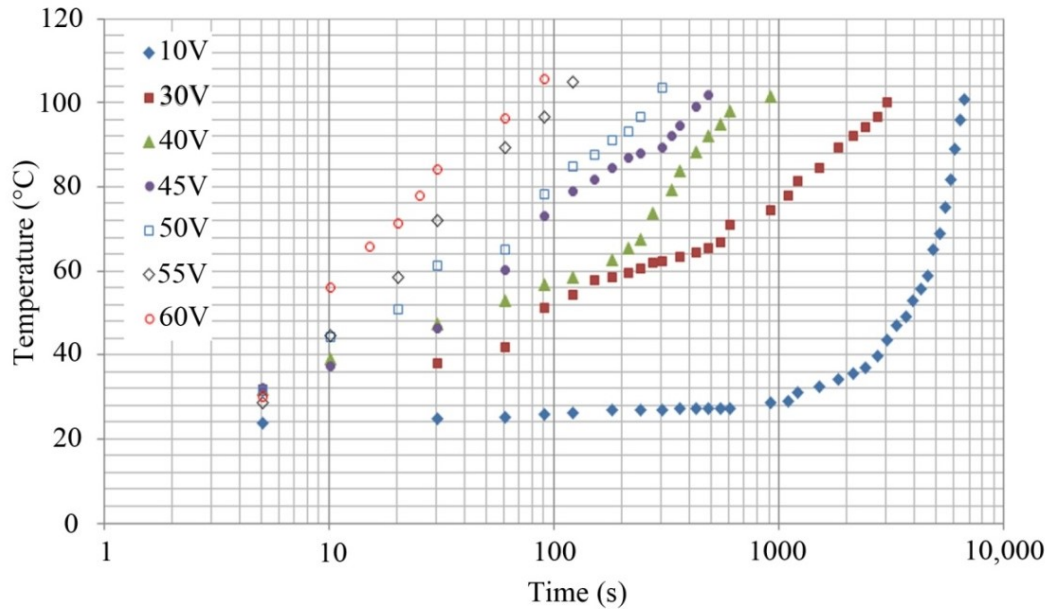
Figure 5.11 Variation in time to achieve transition with change in applied voltage (in 25% CB).

Figure 5.11 shows that the relationship between time and temperature is transforming from parabolic to linear as the voltage advances to 60V. This can be explained as due to the increased energy (as potential difference / voltage) for the phenomenon of tunneling of electrons between conducting carbon particles through the insulating. The rate of increase of temperature in the system depends on the number of parallel electron path generated due to tunneling, which is found exponentially proportional to the applied voltage [Kirkpatrick, 1973]. Time to

achieve T_g +20°C, thus reduces from 5000seconds (for 10V) to 26seconds (for 60 V) due to increased number of parallel paths formed.

5.2 Monte Carlo simulation results of pseudocode validation

A generalized model for nanocomposites can be helpful to predict the percolation concentration; thereby the trials of experimenting with varied contents can be reduced to a smaller band. A structural orientation geometrical model for the above synthesized system was prepared from the parameters understood (dimensions of the fillers, conductivity, tunneling barrier height, tunneling distance etc.) from the synthesized nanocomposite system for the CB PU system. As explained in chapter 4, a visual C base was used for the generation of the pseudo-random code. For converging results, multiple runs of the simulation model were required which was obtained by following the Monte Carlo methods.
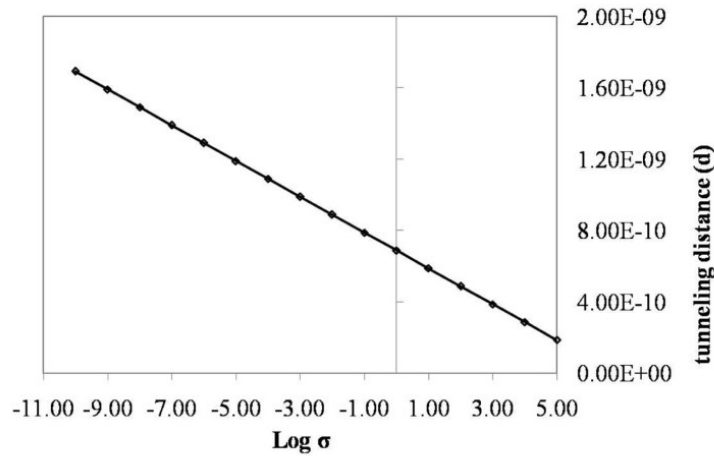
Figure 5.12 Conductivity (log) of nanocomposite plotted against tunneling distance (based on Simmon's equation as discussed in section 4.6.1)

Since inter-particle distance, d is proportional to $log\ \sigma$, the plot of $Log\ \sigma$ (measured conductivity) against varying d as shown in Figure 5.12. This clearly indicates the contribution of inter-particle distance in conductivity [Simmons, 1963].The inter-particle distance for spherical conducting particles in

polyurethane matrix (λ value assumed as 1 eV) varies between 1.69 nm to 0.186 nm while conductivity varies from 10^{-10} S/m to 10^5S/m. From experimental results, it is known that percolation occurs near conductivity value of 10^{-6} S/m (conductivity corresponding to percolation threshold of 6%). From Figure 5.12, d value corresponding to conductivity of 10^{-6} S/m is approximately 1.2 nm. This distance is used as a criterion for verifying whether the conductive network is formed or not. For $d \leq 1.2$ nm, the existence of an electron path is confirmed.

5.3 Percolation threshold

The probability of percolation was calculated from the ratio of successfully percolated microstructures over the number of simulations performed per volume fractions. Figure 5.13(a) depicts the typical distribution of particles in a random simulation run for a volume fraction. This shows the RCVE of $1\mu m^3$ with particles of diamter 168 nm distributed uniformly, with the distance from xy-plane towards z-direction. Figure 5.13(b) is a typical network path formed based on the criteria satisfying the tunneling condition (inter-particle distance $\leq$ minimum tunneling distance calculated). The indicative colour of the particles changes from blue to red as the distance changes from starting to end terminal. This is a representative network path among many networks formed which improves conductivity of the nanocomposite. Figure 5.13(c) shows the probability of percolation for volume fraction from 1% to 10%, for 100 Monte Carlo simulations of the model. It can be observed that the sigmoidal shaped plot follows closely against the experimental values in profile.

(a)

(b)
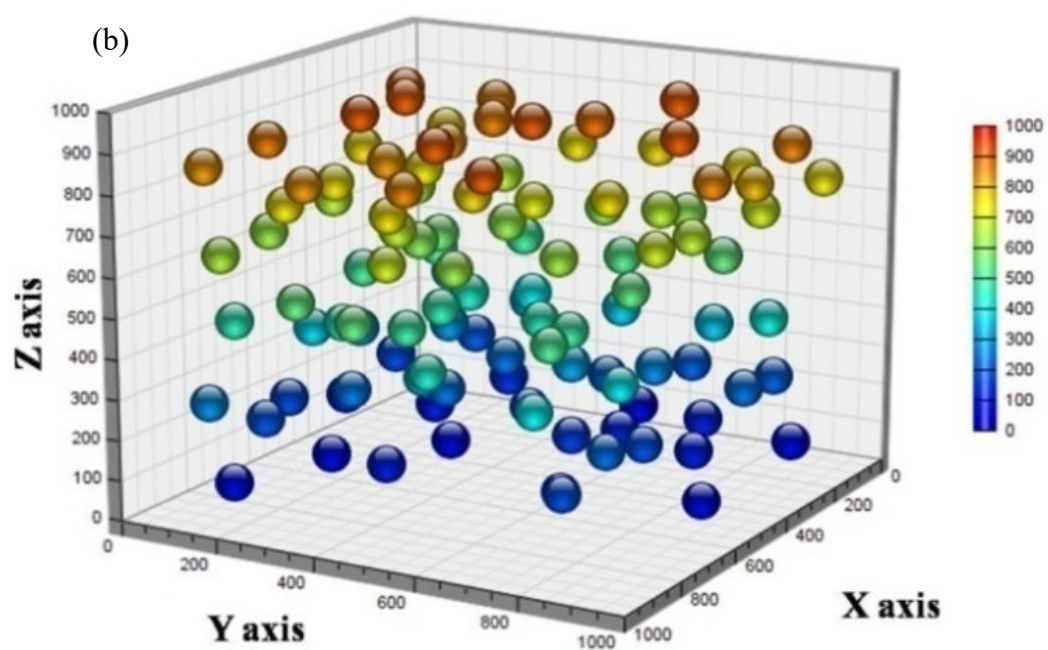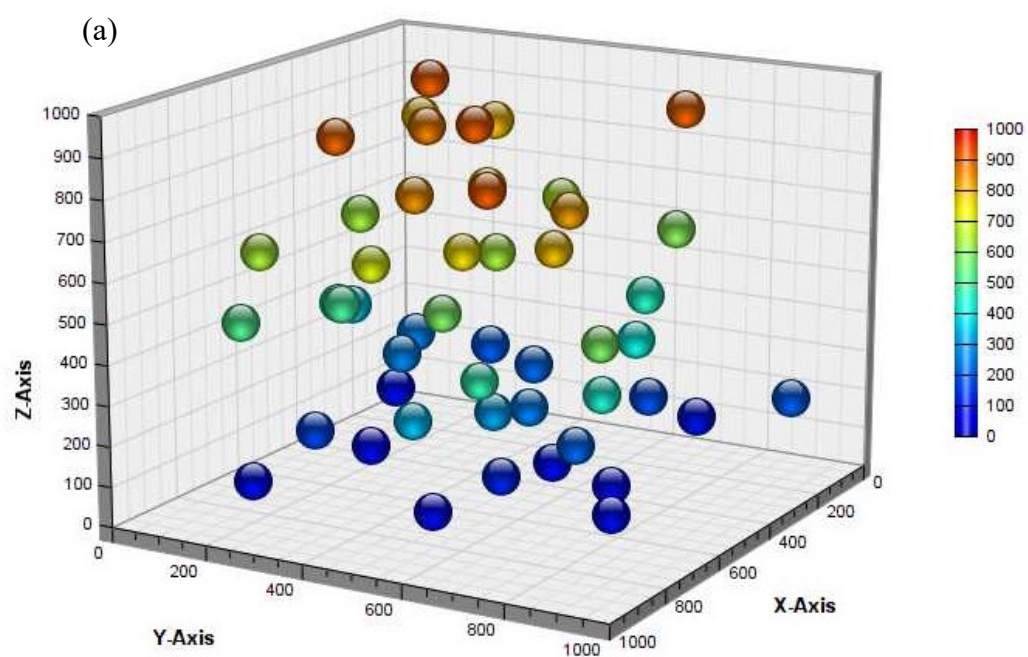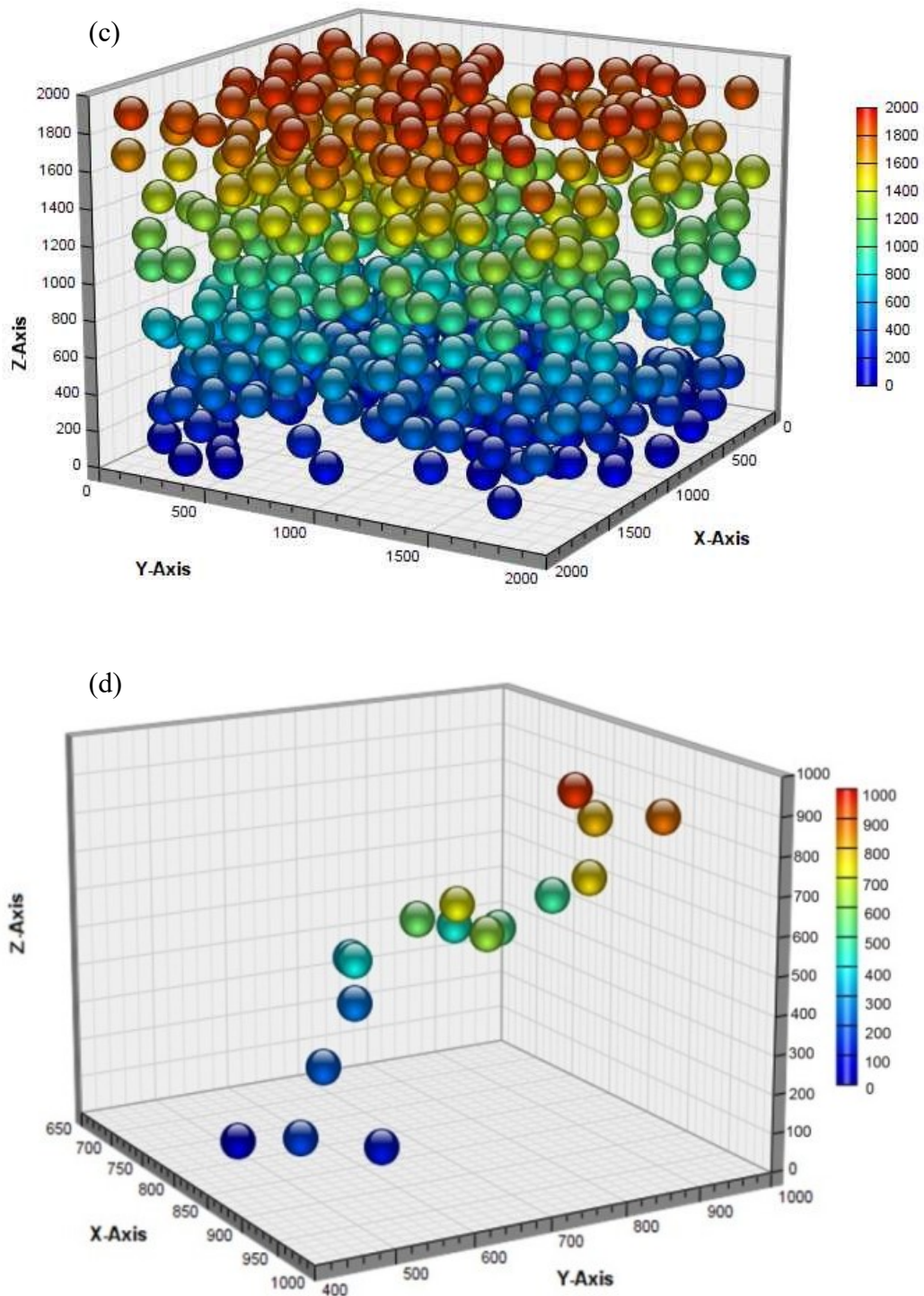
Figure 5.13 Particle distribution in the matrix (RCVE) as simulated using model;(a) RCVE before percolation threshold with wide separated particles; (b) Particle distribution at percolation concentration (6% wt fraction); (c) RCVE after percolation threshold with multiple network paths; (d)Typical network formed by particles satisfying tunneling criteria.

The sudden rise of the conductivity across 5% to 7% weight of CB indicates the transformation of the material from insulator to conductor. Hence 6% (middle of 5% and 7%) is considered to be the percolation concentration / threshold for the system, as obtained from the experiment.

The Figure 5.13(a) depicts the carbon loading in nanocomposite below the percolation concentration where there exists no networks for electron passage and the material remains as an insulator. Figure 5.13(b) depicts the minimum CB content at which the network appears to form by either contact of particles or separated by tunneling distance. The Figure 5.13(c) shows the CB loading above the percolation concentration where the material has already become a conductor with multiple 3D networks for electrical conduction. Figure 5.13(d) shows a typical network for electron passage formed by either touching of particles or particles separated by the tunneling distance.
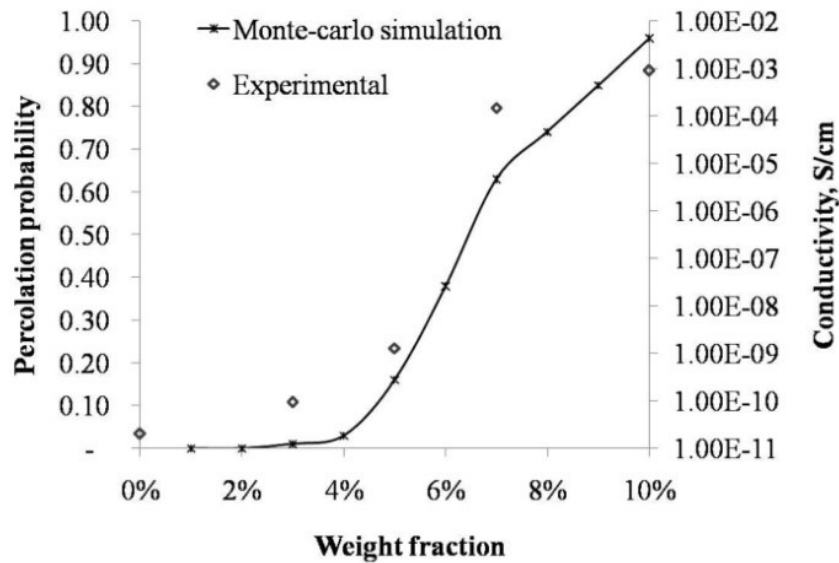
Figure 5.14 Plot of experimental and simulation model conductivity values

Referring to Figure 5.14, the weight % of CB against probability of 0.5 is read on the weight fraction axis to get the percolation threshold as per the model. Thus, a percolation threshold of 6.2% is obtained from the Monte Carlo simulation of the model against 6% from the experimental results. The closeness of percolation

threshold values validates the algorithm and the model for electrical conductivity in case of PU-CB system.

The number of networks increased with increasing volume fraction and multiple networks contributes for conduction. The model found out the number of spherical CB particles involved in network formation, but finding the total number of networks is expensive as it requires verification of 'n-factorial' possibilities for 'n' number of spheres involved in network. Being uniformly distributed and the conductivity probability increased with volume fraction, multiple 3D pathways can be formed resulting increased conduction.

A factor called co-ordination number was introduced in the model, which indicated the average number of particles around one CB particle to form a continuous path (Figure 5.15 gives the complete picture of co-ordination number).

2 particle in contact; Co-ordination no. = 2 (minimum criteria for percolation)

1 particle in contact; Co-ordination no. = 1 (insulator)

3 particle in contact; Co-ordination no. = 3 (conductor)
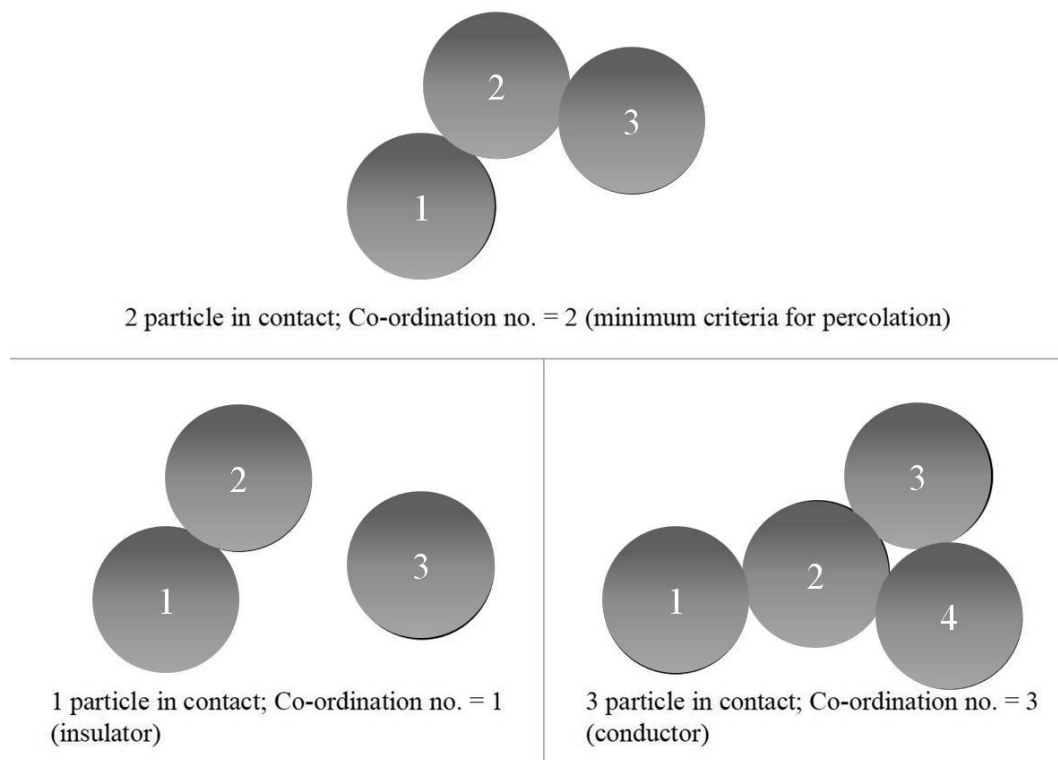
Figure 5.15 Illustration of co-ordination number, a parameter introduced to evaluate network formation in modeling

Co-ordination number below 2 indicates the material to be insulator as no continuity exists in the part networks formed in the system; where as a co-

ordination number above 2 shows the contact of more than one particle which assures a continuity of network. The average value of this indicator confirms the percolation probability in the current model. Table 5.2 shows the average co-ordination number obtained per CB content from 1% to 10% in the RCVE of the model.

Table 5.2 Co-ordination number (average number of particle in contact) corresponding to carbon loading in PU resin

Weight fraction of CB in PU	Co-ordination number
1%	0.05
2%	0.90
3%	1.42
4%	1.57
5%	1.69
6%	2.11
7%	2.23
8%	2.44
9%	2.78
10%	2.96

The value averages above 2.6 (up to 10% CB) in volume fraction beyond percolation, which clearly shows the possibility of more than one path as at a junction. The minimum particles required for one network continuity are 2 (one at fore and one at aft end of a particle), and any number above justifies formation of branching from a path.

5.4 Shape memory effect

Among the synthesized SMPC, 25%CB content showed optimal mechanical and electrical properties and hence it was chosen for demonstrating shape memory effect (SME). Figure 5.16 (a) shows the samples (A) and (B) for SME demonstration with thermal and electrical activation respectively. Dimension of sample (A) measures to 60 mm x 10 mm x 2 mm and sample (B) is of size 74 mm x 24 mm x 2 mm.

5.4.1 Thermally-activated SME

Sample (A) was trained to a 'U' shape after heating to T_g +20°C which was then cooled to room temperature and shape fixity was measured in angle. On heating again to T_g, the sample recovered to original shape, which demonstrated its response to thermal stimuli (Figure 5.16(b)).

(a)
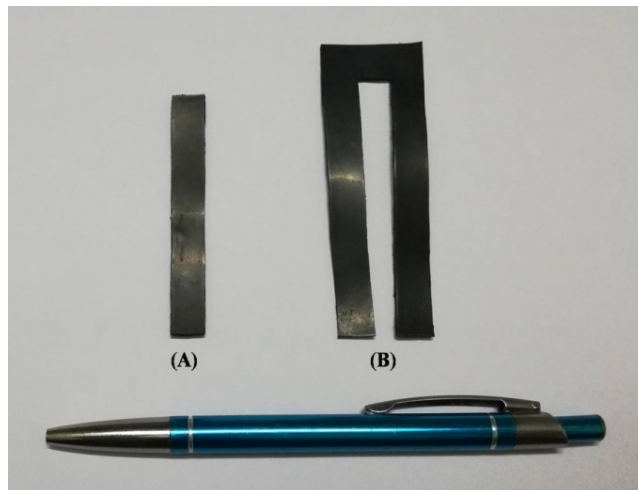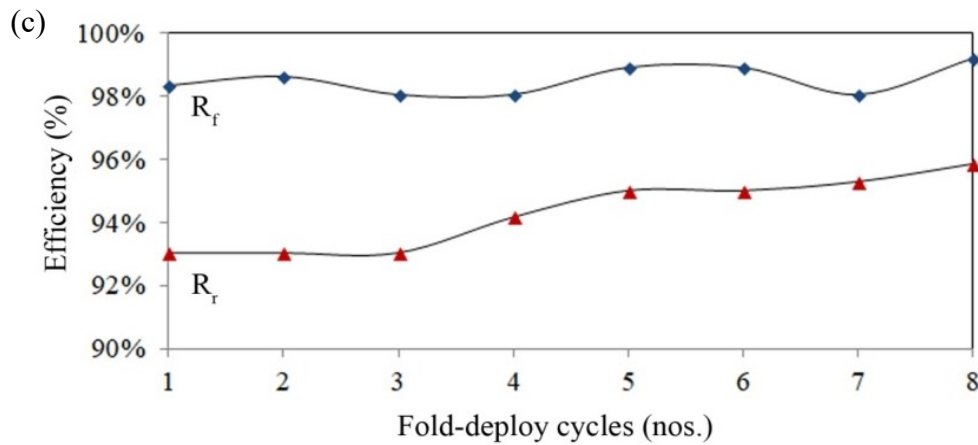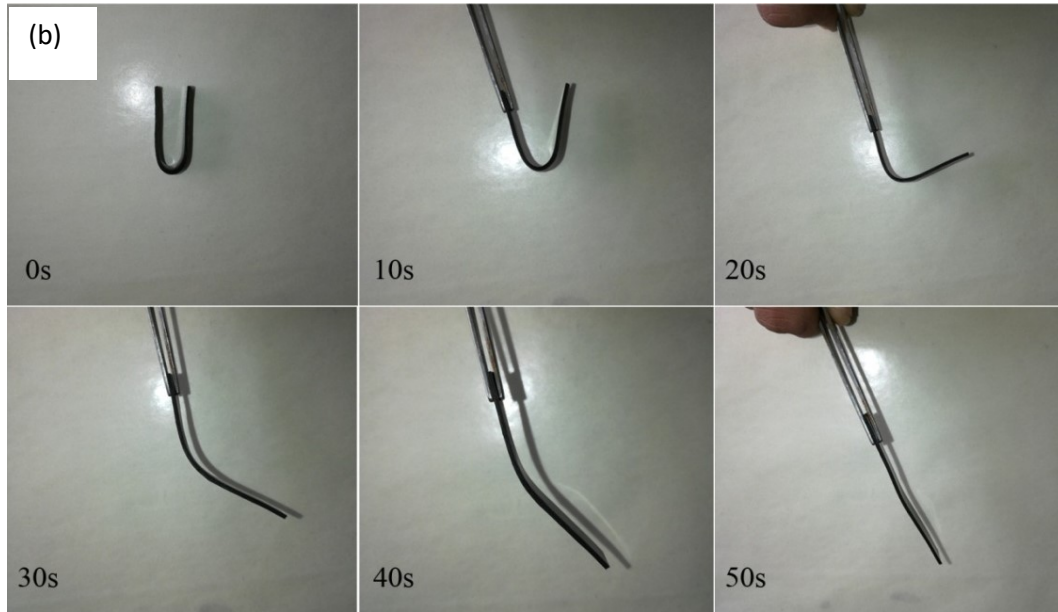
Figure 5.16 Thermally activated shape memory effect (on 25% CB); (a) 25%CB for thermal-active and electro-active shape memory demonstration using sample (A) & (B) respectively; (b) thermal stimulated SME demonstration; (c) Shape fixation and recovery efficiency for 8-cycles of the bent-deploy test

5.4.1.1 Shape fixity and recovery efficiency of thermal-actuation

The angle of fixity / recovery for each cycle are measured and converted to a ratio between the measured angle and the fixed / recovered angle, to get the efficiency. This is plotted in Figure 5.16(c). The overall duration of shape recovery in this case was up to 50s for an average recovery efficiency of 94%, which showed an increasing trend from 93% to 95%. The average shape fixity arrives to 98% for

the 8 nos cycles.

The reason for the duration of 50 seconds is attributed to the time delay in transferring the heat from the material surface to the interior for shape memory action to get initiated.

5.4.2 Electro-active SME

Conductivity of nanocomposite is understood to be the result of inter-particle interaction either by filler to filler contact or by electron hopping across the tunneling resistance on application of a potential difference.

The 3D parallel conductive paths established by the filler material allowed electron movement which volumetrically heated the specimen. Sample (B) (Figure.5.16(a)) was trained for a temporary shape by heating up to T_g +20°C after constraining it to folded shape. On cooling the specimen to room temperature, the shape fixity efficiency was measured. A known voltage is applied to initiate joule heating for shape recovery when the shape memory was triggered (refer Figure.5.17(a)). The sample is connected in series with a power supply source providing 60V potential with an ammeter in the circuit and a volt meter in parallel to the sample. An infrared non contact thermometer was used to verify the temperature at the sample while the circuit was turned on. The material started recovering when the temperature reached beyond its T_g.   The sample with 25% carbon loading, while subjected to 60V DC power supply, recovered near 100% to its original shape within a time duration of 26 seconds by reaching a temperature of 104 °C (T_g +20 °C) (refer Figure.5.17(b)).
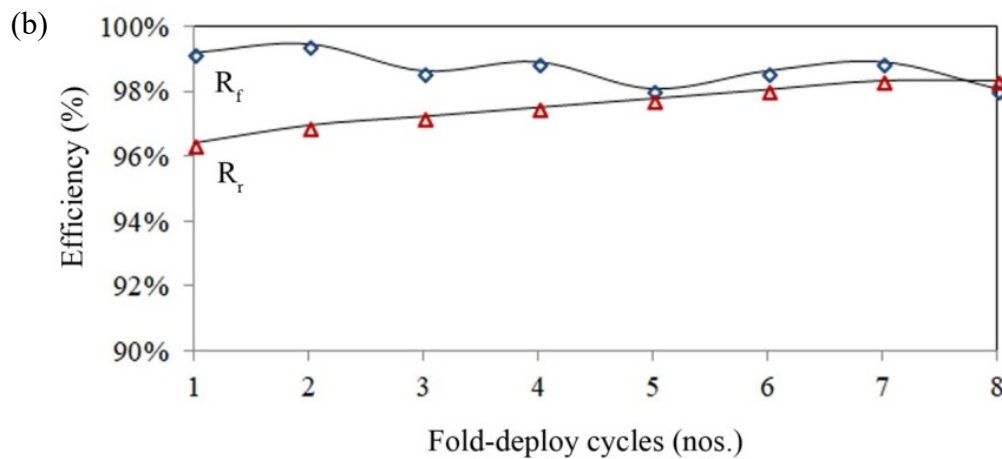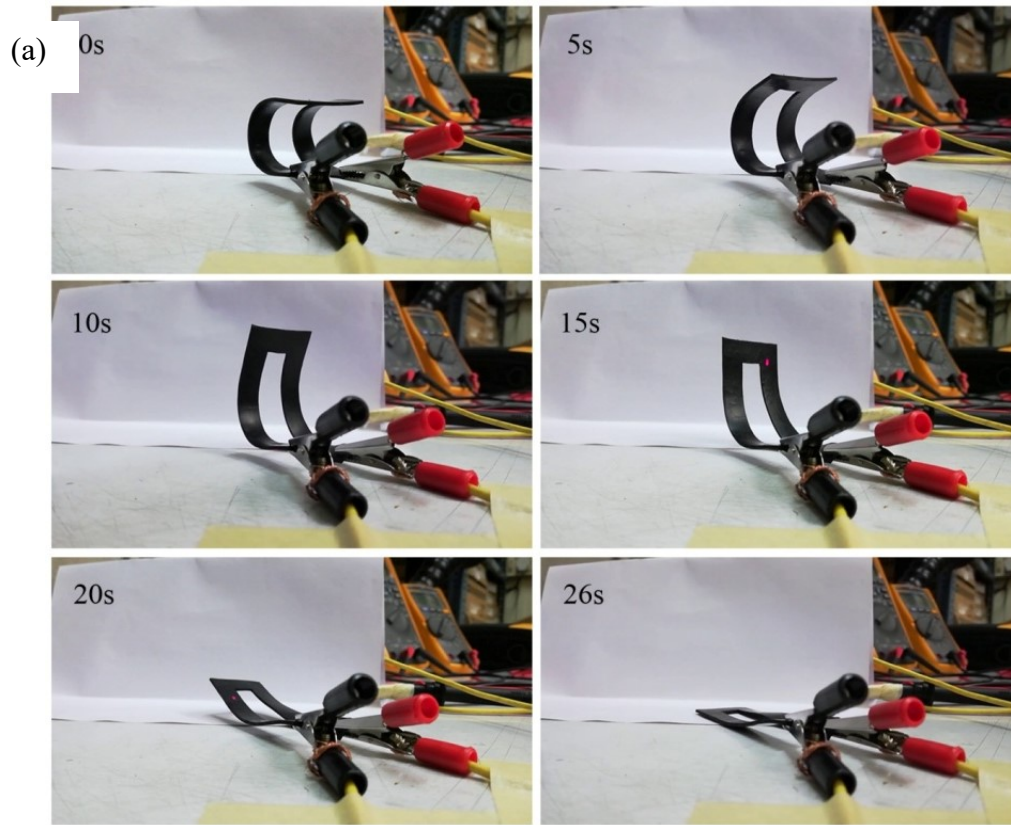
Figure 5.17 Electro-activate shape memory effect (on 25% CB); (a) electrically stimulated SME demonstration; (b) Shape fixation and recovery efficiency for 8-cycles of the bent-deploy test

The shape fixity and recovery has shown similar trend as that of thermally active SMP, with shape fixity showing consistently 98.5% efficiency and shape recovery showing increasing trend from 96.3% to 98.2%

5.4.2.1 Shape fixity and recovery efficiency of electro-actuation

The fixation and recovery exhibited definite pattern in either case (thermal and electrical stimuli).

(a)

(b)
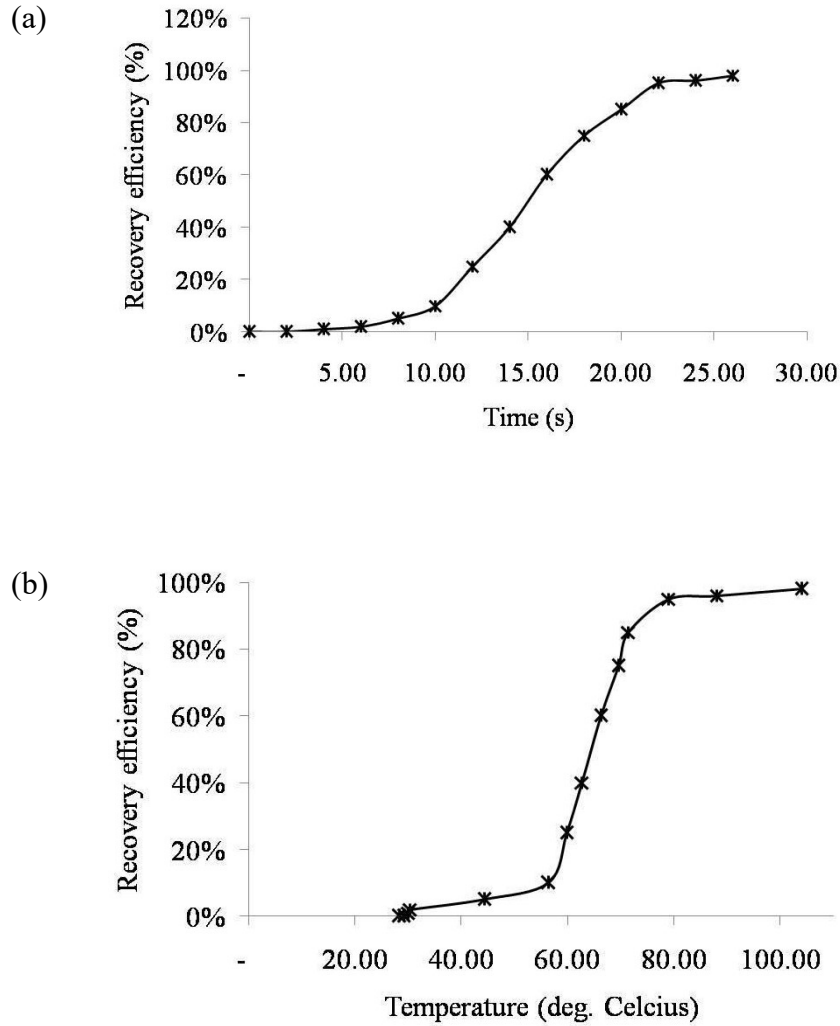
Figure 5.18 Relation between shape recovery, time and temperature for 25%CB in PU; (a) recovery efficiency-time plot; (b) recovery efficiency-sample temperature plot.

Shape fixity efficiency remained same for both thermal and electrical stimuli near 99%, while recovery efficiency was higher for electrical stimuli (98.2%) compared to the thermal stimuli (94%) as evident from Figure 5.17. Thermally activated SMP, got surface heated while the joule heating process volumetrically heated the material, thus resulted in better shape memory behavior. The recovery efficiency observed in this study is higher than the reported values from literature

for PU based SMPCs [Huang, 2010; Ahmad et al., 2012], which may be due to the use of a cross linked system, the conductivity of CB used and special design of PU system.

It can be observed that the recovery efficiency follows a sigmoid profile while plotted against time of heating for shape recovery (Figure 5.18(a)). This can be due to the spread of volumetric heating due to formation of multiple conducting networks of carbon particles inside the matrix as the temperature approaches T_g. The recovery efficiency at various time for electro-active SMP are measured by correlating with the angle of recovery corresponding to time. Referring to Figure 5.18(a), the time required to reach $T_g+20°$ C causes the worm to crawl parallel to the time axis and then rise sharply near 10 seconds. This is the point when the heating of the bulk occurs and shape memory is initiated. Figure 5.18(b) shows the efficiency values obtained while the sample temperature is varied. This shows significance of transition temperature in a shape memory process. The rate of shape recovery is found to be maximum between 60 °C and 80 °C, which is when the hard segments start to achieve mobility from the heat energy supplied by the passage of electricity. Thus, the plots can be a tool for the material scientists /designers for arriving at system designs considering different stages of recovery at different time /temperature.

The temperature generated inside the material due to the resistive heating effect of electric current passage (due to conductive fillers in the bulk), results in melting of the soft segments of the SMP. This facilitates the free movement of polymer chains thereby rearranging to its original configuration. A well accepted method of fold-deploy test was used to demonstrate the shape recovery and quantify the recovery efficiency for the nanocomposite. Shape recovery close to 100%, was observed for 25% weight fraction of CB in PU, which is higher than reported values from literature [Kulakov et al., 2016].
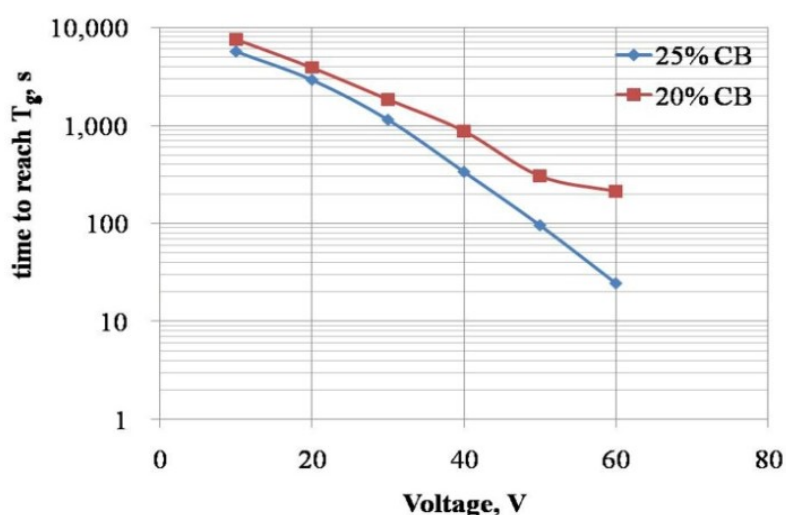
Figure 5.19 Comparison of time to achieve shape recovery for 20% and 25% CB filler

As the shape memory behaviour are dependent on transition temperature T_g, applied voltage, weight fraction of filler material, time of exposure to the heating, changes any of these parameters can result in tuneable property in the SMP. The tunable recovery speed (25 seconds for 60 volt and 25% CB weight fraction) based on voltage and volume fraction of fillers is an advantage for selecting materials specific applications.

Figure 5.19 depicts the difference in shape recovery time taken by nanocomposite with 20% and 25% filler. This reinforces the claim that the increased filler content caused possibility of more network formation resulting in better volumetric heating. It can be noted that an increase in voltage causes increased energy supply into the system which causes increased joule heating of system. It is observed that for lower filler contents (16%, 10% and 7%) above percolation threshold, the time taken to recover tend to orders of few hours. From an application point of view, the large recovery time makes the system insignificant and hence is not proceed further.

This increased efficiency displayed by 25% CB is attributed to uniform heat transfer in the system resulted from uniform distribution of conducting particles and due to the special formulation of PU matrix with controlled cross linking (by usage of optimal amount of tri-methylol propane as crosslinker). The trade-off in

cross-linking makes the synthesised system acquire properties of both thermoset and thermoplastic polymers. The high T_g high recovery efficient PU-CB shape memory nanocomposite synthesised can suit applications in aerospace deployment structures, elastic memory composites, medical applications like deployable stents, artificial muscle developments and in robotics for soft actuation techniques.

5.4.3 Thermodynamic relationship between voltage and time of actuation

It is known that passing electric current (I) through a resister (with resistance R) for a time duration t, generates heat energy (Joule's law) Q and is given by

$$Q = I^2Rt \qquad\qquad (5.5)$$

When the filler content increase beyond percolation threshold, multiple networks for electron passage are established. These parallel 3D networks formed due to uniformly distributed CB particles cause volumetric heating of the system. As the current 'I' continues for a time 't', the energy dissipation in the system due to resistance heating rises the system temperature to the transition temperature (T_g, *temperature at which the material becomes rubbery / elastic from a hard glassy state. For current polymer nanocomposite PU-CB system, the T_g has been found as 85°C, which is highest among the reported T_g for PU systems*) [Huang et al., 2012]. The energy gained by the system to change its temperature for ΔT can be quantified if a specimen of known mass 'm' and specific heat 'C' is used.

Hence,

$$Q = mC\Delta T \qquad\qquad (5.6)$$

The equations (5) and (6) being complimentary as energy supplied and heat generated in the system, equating them can give a relation to find time 't'. This explains how much time the voltage needs to be applied across the specimen for achieving T_g.
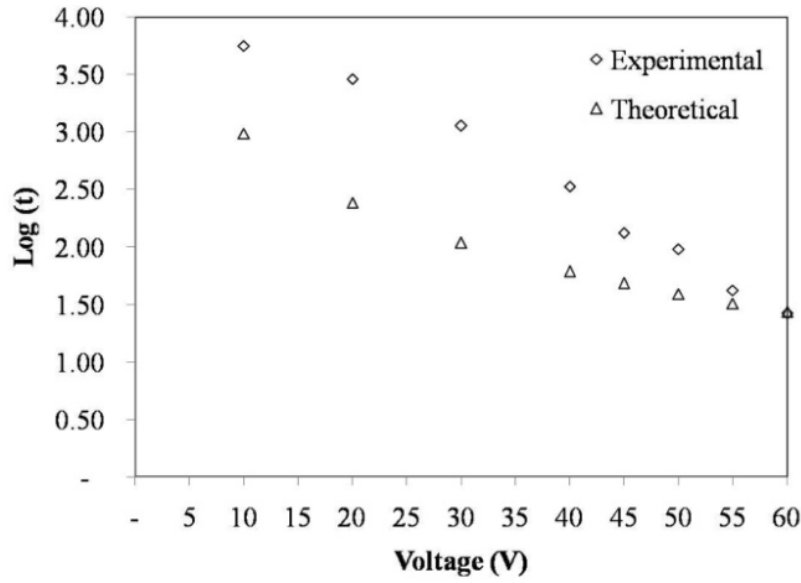
Figure 5.20 Time for reaching T_g (theoretical vs. experimental) for 25% CB filler

The time thus obtained (theoretical) is plotted against the actual observed time to reach T_g (experimental) while passing current through the system, as depicted in Figure 5.20.

A considerable gap exists between the theoretical and experimental value at small voltages, which is attributed to the heat dissipation to the surroundings at lower voltages (rate of energy supply < Energy dissipated). This is because of the low rate of heating at lower voltages due to less energy for electrons for crossing the tunneling barrier. As the voltage approaches 60 V, the heat loss due to convection / radiation from surface was constantly replenished by more and more electron movement and hence the experimental values merges towards high voltages. The actuation time and the available power supply for actuation are factors that influence the material usage in many applications. Hence an understanding of the relation between time to achieve transition temperature for each voltage application becomes critical from application point of view. The change is resulted from increased current for fixed resistance per increase of voltage that causes increased heating rate.

5.5 Summary

A Polyurethane nanocomposite system with carbon black possesing high T_g of 85°C (highest among reported so far for PU nanocomposite systems) and electro-active shape memory property was synthesised and characterised. The use of aliphatic isocyanate gave an intrinsic stability against UV radiations.

- The polymer microstructure, chemistry, hydrogen bonding, mechanical, thermal and electrical properties were studied.

- The electrical conductivity of the PU-CB system was modelled using non-linear programming and optimisation in visual C language.

- Experimentally, 6% by weight of carbon was observed as percolation concentration, which was found matching with the theoretical value of percolation threshold derived from the model (6.2% by weight of CB).

- The time required to achieve transition temperature for varying voltages were quantified, that can help in choice of power supply for specific applications in electro-activity.

- High shape recovery efficiency of 94% and 98% (for 25% CB loading) were observed for thermal and electro-actuation.

- For electro-active shape memory actuation, 60 volt power supply (for 25% CB filler) was applied which resulted in complete recovery in 25 seconds time.

II.Multi-walled carbon nanotube - Polyurethane SMP nanocomposites

To improve the efficiency of PU based SMM, which is triggered by thermal / electrical stimuli, it is inevitable for these fillers to possess good thermal or electrical conductivity. When dispersed uniformly in the matrix, it can lead to uniform heating of the system resulting in better actuation efficiencies due to the high electrical and thermal conductivities possessed by nanotubes. The measured electrical conductivity of metallic carbon nanotubes is in the order of 104 S/cm and the thermal conductivity at room temperature can be as high as 6600 W/mK [Andreas Thess et al., 1996; Savas Berber et al., 2000]. Therefore CNT becomes a potential candidate as filler for the PU to be actuated either by thermal or electrical stimuli. Polyurethane based nanocomposites with Multi-walled carbon nanotube were prepared as explained in chapter.4 using in-situ polymerization approach. The homogeneous dispersion of functionalized MWCNTs in PU matrix attributes for the properties observed in various characterization techniques. The Carbon nanotubes (CNT) type, method of synthesis, dimensionality and aspect ratio as well as polymer type and dispersion method are evaluated with respect to their impact on percolation threshold and shape memory effect. For avoiding the agglomeration (which has a negative impact on the properties of the nanocomposite) these nanotubes are subjected to functionalization process, where the CNTs are treated with carboxylic acid to introduce functional groups which repel the similar tubes causing proper dispersion in matrix. Use of carboxylic acid functionalised MWCNT and the filler alignment has got definite effect on the percolation conductivity of polymer nanocomposites as per studies of Quan et al., 2015.

Experimental and theoretical understanding of electrical percolation of Carbon nanotubes (MWCNT) in polyurethane nanocomposites was attempted via the work in this section. A comprehensive and systematic model of MWCNT-PU system was developed from trails of the CB-PU model developed earlier. The model also would help to predict the percolation threshold on providing necessary

inputs (dimensions of the nanotube, conductivity, tunneling barrier height, tunneling distance etc.) and thereby can avoid excessive iterations of experiments to arrive at the necessary conductivity for the SMM to be electrically active. The percolation predictions of the MWCNT-PU model developed were evaluated using experimental electrical characterizations. The prediction from the model for a specific MWCNT PU system has been evaluated experimentally, including detailed characterization. The percolation threshold determined from the model and the experiments have been compared and the deviations if any are explained. Since the interest of study was to evaluate the shape memory effect (SME) for which percolation threshold is of prime importance, the detailed study on the SME of the developed MWCNT PU system is also reported. MWCNTs were incorporated into a shape-memory polyurethane matrix by in situ polymerization, mixed through ultrasonic vibration and a relatively homogeneous distribution of the fillers was achieved, as explained in chapter 4. Chemical, microstructural, thermal and mechanical characterization established the superiority of the nanocomposite system (due to the combined properties of the filler and matrix). Shape memory effect of the nanocomposite was also evaluated for thermal and electrical activation stimuli. Relationships between the various parameters influencing the shape memory are studied in this attempt.

Functionalized pristine MWCNT PU nanocomposites were formulated and synthesized as explained in chapter.4. MWCNT filler was introduced in PU resin matrix in the weight fractions of 0.1%, 0.3%, 0.5%, 1.0%, 2.0%, 2.5%, 4.0%, 7.0% and 10.0% (by weight of solid content of the resin). The mixture, on ultra-sonication was solution cast in moulds of size 100 mm x 100 mm sheets of thickness 2.00 mm, which are black in colour.

5.6 Characterisation results

For the cured MWCNT PU nanocomposite sheets, samples as per requirement were sliced for various characterisations such as chemical, microscopic, spectroscopic, mechanical, thermal and electrical. The nanotube used for synthesis

was used pristine and hence to investigate the structure and chemical composition of the MWCNTs before use for nanocomposite synthesis need to be verified.

5.6.1 Chemistry, Hydrogen bonding and microstructure

The CNT used pristine in the synthesis is characterized for its IR spectrum response to ensure regarding the multi-walled cylindrical element (MWCNT). **Figure 5.21** depicts the FTIR spectrogram of the CNT.
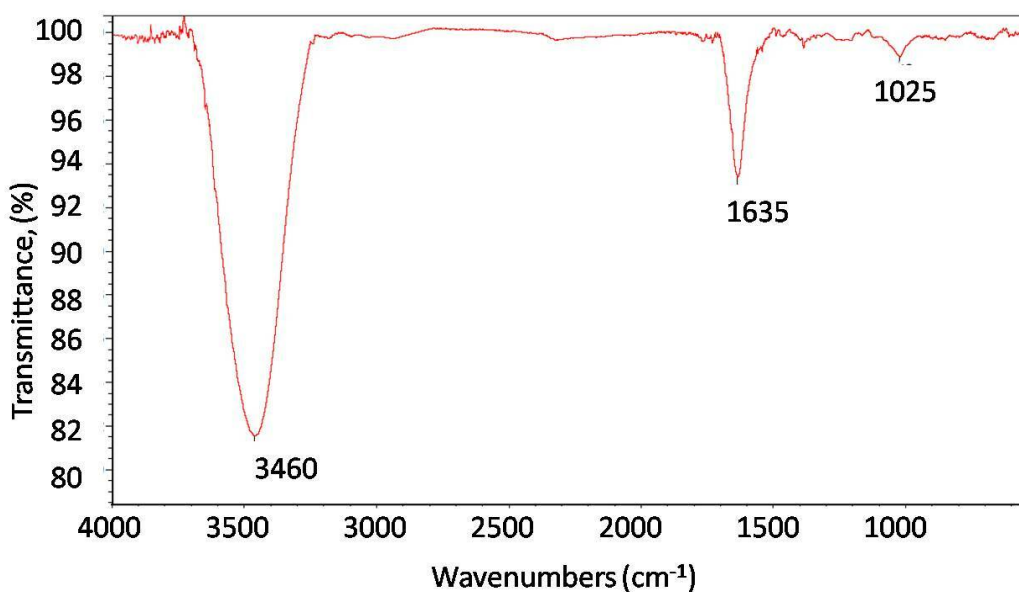
Figure 5.21 FTIR spectrogram of COOH-MWCNT used for synthesis of PU nanocomposite

The spectra depicted in Figure 5.21 indicate the presence of hydroxyl groups in MWCNTs indicated absorption bands around between 3200 cm^{-1} and 3600 cm^{-1} of the -OH stretching and the stretching at 1640 cm^{-1} correspond to the carboxylic (C=O) group attached to MWCNTs (fictionalization confirmation).

To understand the influence of the carbon fillers in the microstructure and basic shape memory property of the polyurethane system, a thorough study of the chemistry and hydrogen bonding by characterization is required. The enhancements of such properties are understood via the platform of analysis on results of microscopic and spectroscopic studies [Arun et al., 2019a].

A plot of the wavenumbers and infrared transmittance gives an idea regarding the influence of the filler content on the basic polyurethane linkages and the domains responsible for shape memory effect. **Figure 5.22** shows the typical FTIR plot for 0.3% weight fraction of MWCNT in PU resin.
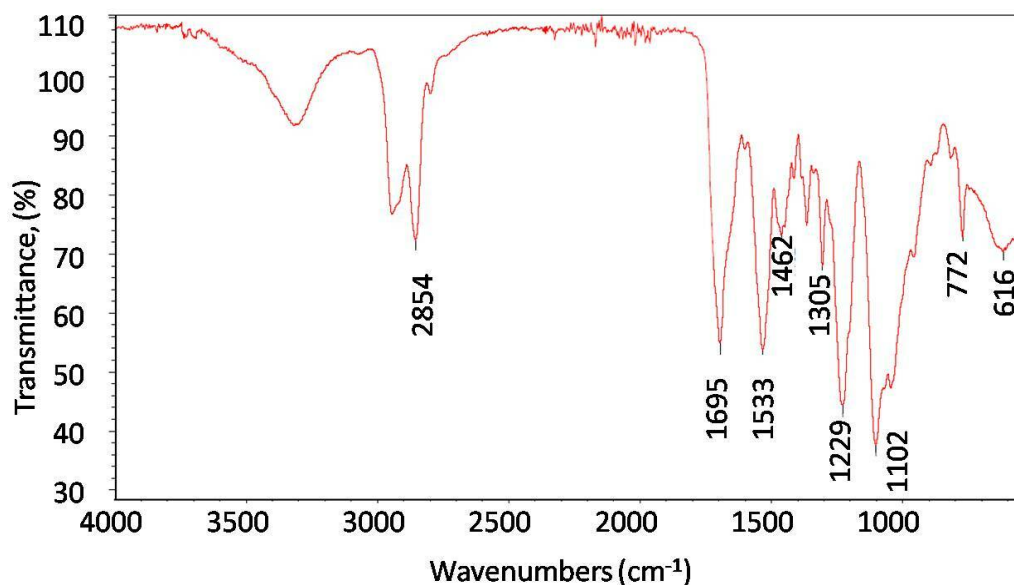
Figure 5.22 FTIR spectrogram 0.3% by weight of MWCNT in PU resin

Typical polyurethane linkages were observed in the FTIR spectrograms of nanocomposites with MWCNT in both fingerprint and functional regions. Due to the similar pattern of stretches, the representative spectrogram of 0.3% is considered for discussions. The stretch absorptions between 3200 and 3500cm^{-1} indicates the obvious primary and secondary amines in the form of N-H- bonds is confirmed. The significant backbone carbon and its hydrogen counterpart bond C-H stretching linkages are evident from the peaks between 2840 and 2950cm^{-1}. The peaks observed in the region between 1600 to 1700 cm^{-1} indicates the N-H bending, stretching of C=O and aromatic C=C bonds. Typical PU peaks absorptions between 1000 and 1520 cm^{-1} can be observed showing the C-H bending and C-N stretching. A considerable reduction in the transmittance intensity can be observed similar to that in case of CB PU nanocomposites as the carbon filler content increases. The absorption of the heat energy of IR radiations can be the attributed as reason for the reduction in transmittance of IT across the

material. This absorption of the IR causes the existence of overtones in higher carbon loaded specimen, which gets polarised and the energy level changes.
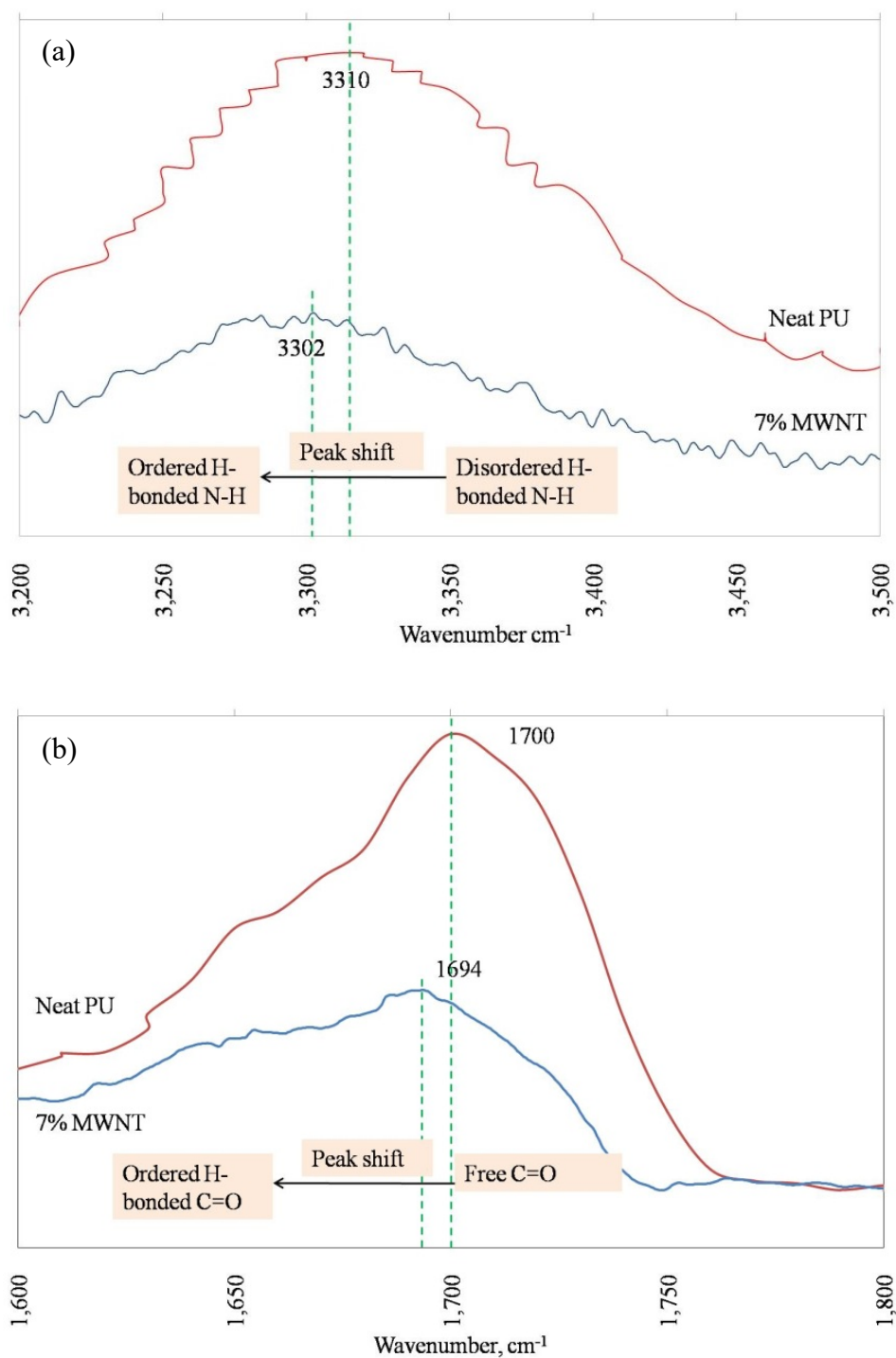
Figure 5.23 FTIR sprecta in (a) N-H- and (b) C=O stretching for neat PU and 7% MWCNT fillers in PU

The influence of the presence of fillers and the loading in the basic shape memory behaviour of PU are observed from the plots in Figure 5.23. The plot depicts the part of FTIR spectra for pure PU and 7% MWCNT (chosen for shape memory illustration test) between 3200 cm^{-1} and 3500 cm^{-1} to observe the N-H- and that between 1600 cm^{-1} to 1800 cm^{-1} for the C=O stretching [Arun et al., 2019a; Pangon et al., 2014].

Since the mixed soft & hard phase and the micro-phase separation are factors responsible for shape memory of a polymeric material, the nature of the local hydrogen bindings as detected at the N-H- and C=O region gives an indication of the behaviour of the polymer nanocomposite and its deviation from the base polymer. The disordered band – peak at 3310 cm^{-1} (as in Figure 5.23(a), at N-H- stretching arise from the soft phase and interfacial regions with mixed hard and soft phase. The ordered band – peak at 3302 cm^{-1}, arises from the N-H- strechings corresponding to the existence of the aligned urethane linkages. This confirms the enhanced shape memory behaviour due to the introduction of fillers causing an interface creation between hard and soft segments thus evident separation is depicted. The change in hydrogen bond is more evident at C=O region of the spectrogram. The free C=O band is shifted (1700 cm^{-1} to 1694 cm^{-1}) to an ordered H-bonding due to the addition of filler material. This may be due to the stiffening of the chain extender by the presence of the filler in the matrix.

Figure 5.24 depicts the UV spectrogram, where an obvious peak is observed at the lower wavelength region of the UV spectrum which shifts towards red region, with all the three MWCNT systems responding at nearly same wavelength with varying intensity. The peak intensity observed is due to the considerably same 'plasmon' resonances (interaction of free electrons of conductive material with polarised light causing oscillation) of the free-π electrons of the nanotube, at around 310 nm. The varying diameter distribution of MWCNT results in the shift of the right hand side of the peak towards higher wavelength / red shift [Graham A. Rance et al., 2010].
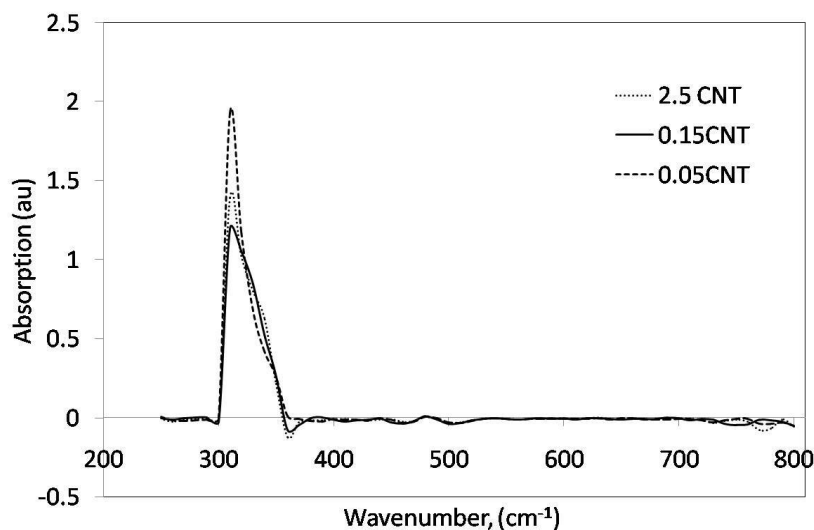
Figure 5.24 UV visible spectrogram for MWCNT in PU matrix for varying weight fractions

Thus it can be assumed that the sharpness of the peaks in case of 0.05% is due to relatively narrow particle size distribution, whereas the distribution range widens in case of 0.15% and 2.5% MWCNT. The presence of 'aliphatic' diisocyanate (IPDI) which are inactive towards UV radiations can also be assumed as a reason for the narrowness of the peak [Robert & William, 1983].

The typical UV spectrograms of both CB & MWCNT nanocomposites are compared in the Figure 5.25.
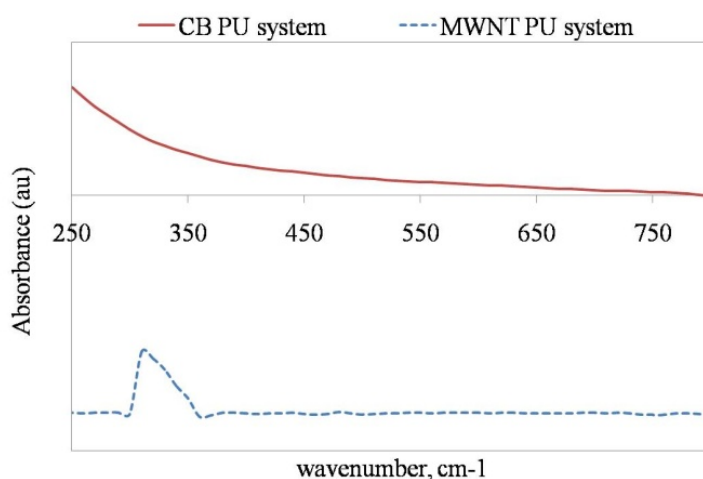
Figure 5.25 UV visible absorption spectrum of CB-PU and MWCNT-PU system

It can be observed that the CB PU nanocomposite is not having any significant peak whereas the representative MWCNT nanocomposite specimen shows a significant peak across 300 cm^{-1}. The presence of UV absorbing CB in the nanocomposite along with the aliphatic diisocyanate in the resin nullifies the effect of ultraviolet radiations in CB-PU system. The effect of aliphatic diisocyanate affects the broadness of peak in MWCNT-PU system still responding to UV radiations. Hence it can be inferred that the CB-PU system can resist the UV radiations while MWCNT-PU system is not suitable for space applications.
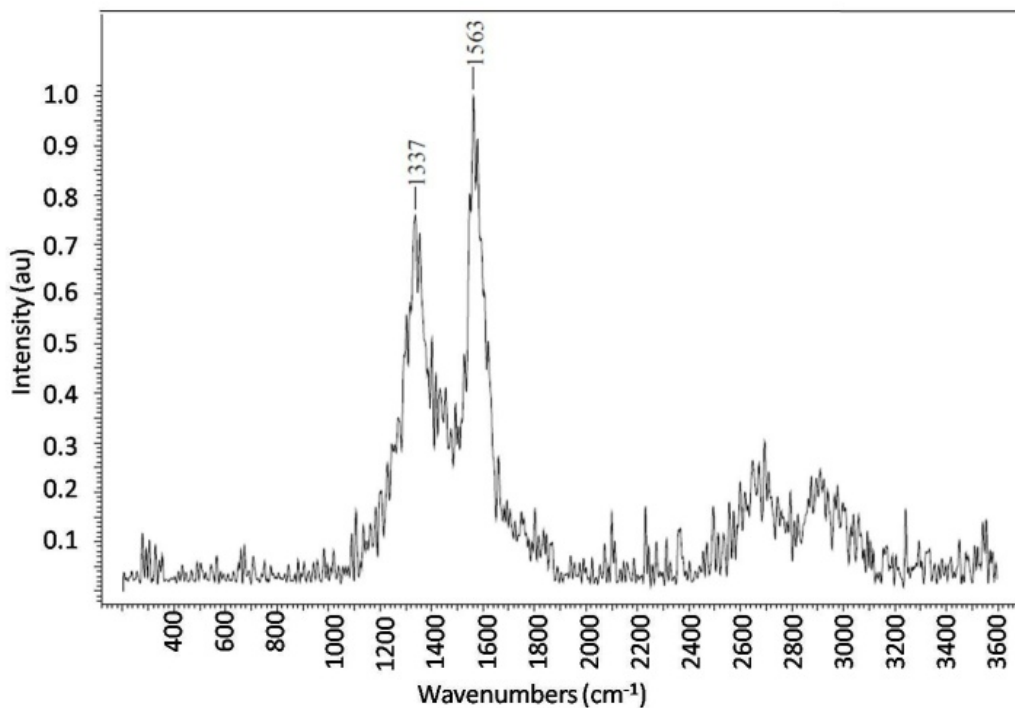
Figure 5.26 Raman spectrum of MWCNT indicating the D, G and the 2D band

For confirmation of nanotubes to be multi-walled, the Raman spectrum was used along with IR sectrum. The Raman spectrogram of the nanotubes used in this work is as depicted in Figure 5.26. The presence of the D, G and the 2D band at 1335 cm^{-1}, 1574 cm-1 and 2700 cm-1 clearly indicates the MWCNT signature [L. Bokobza & J. Zhang, 2012].

Scanning electron micrographs present an idea of the dispersion of the fillers in the matrix while observed in a cleaved surface. Figure 5.26 shows the SEM

images of 0.1%, 0.25%, 4.0% and 7.0% MWCNT fillers in PU matrix with 20,000X magnification.
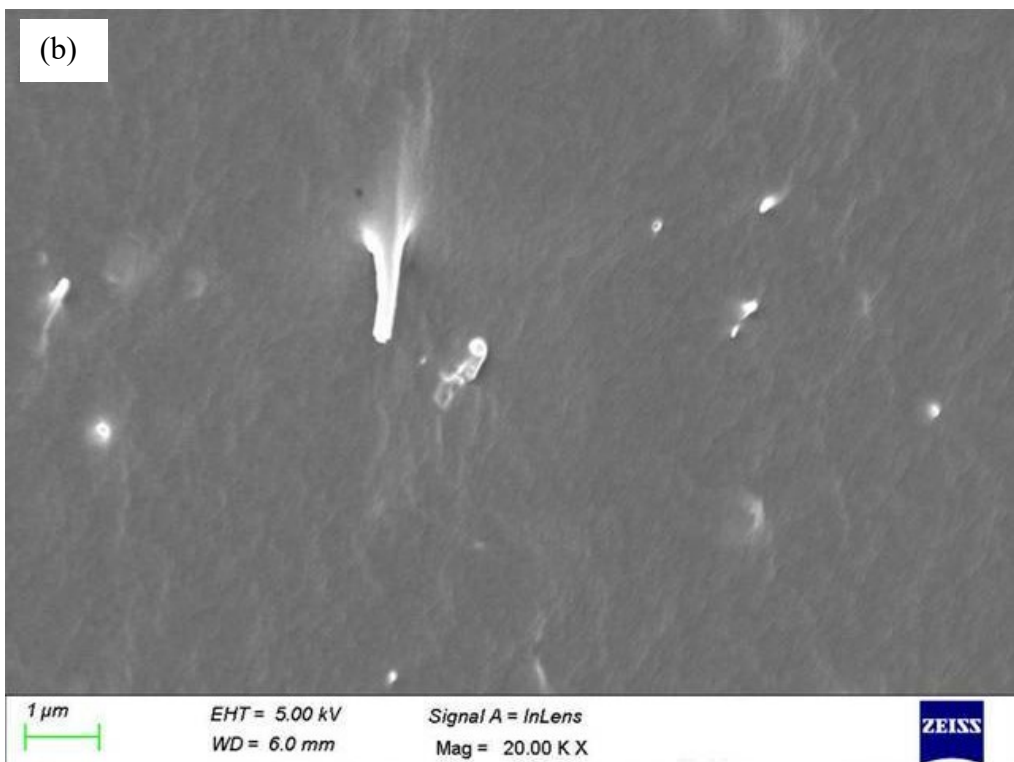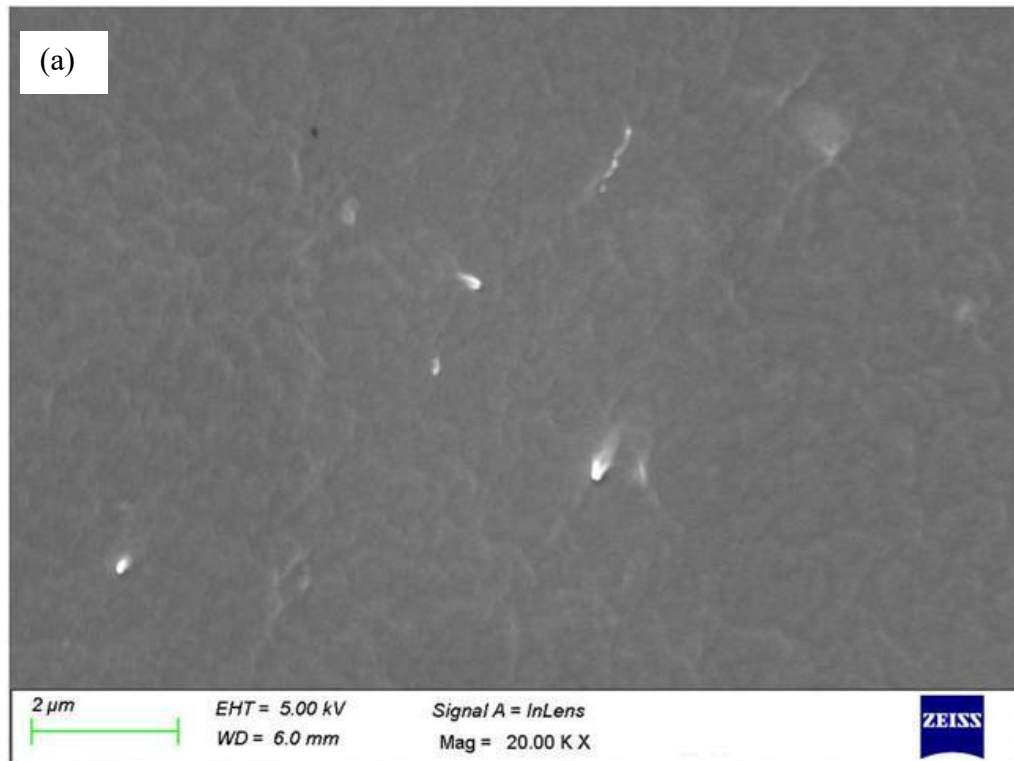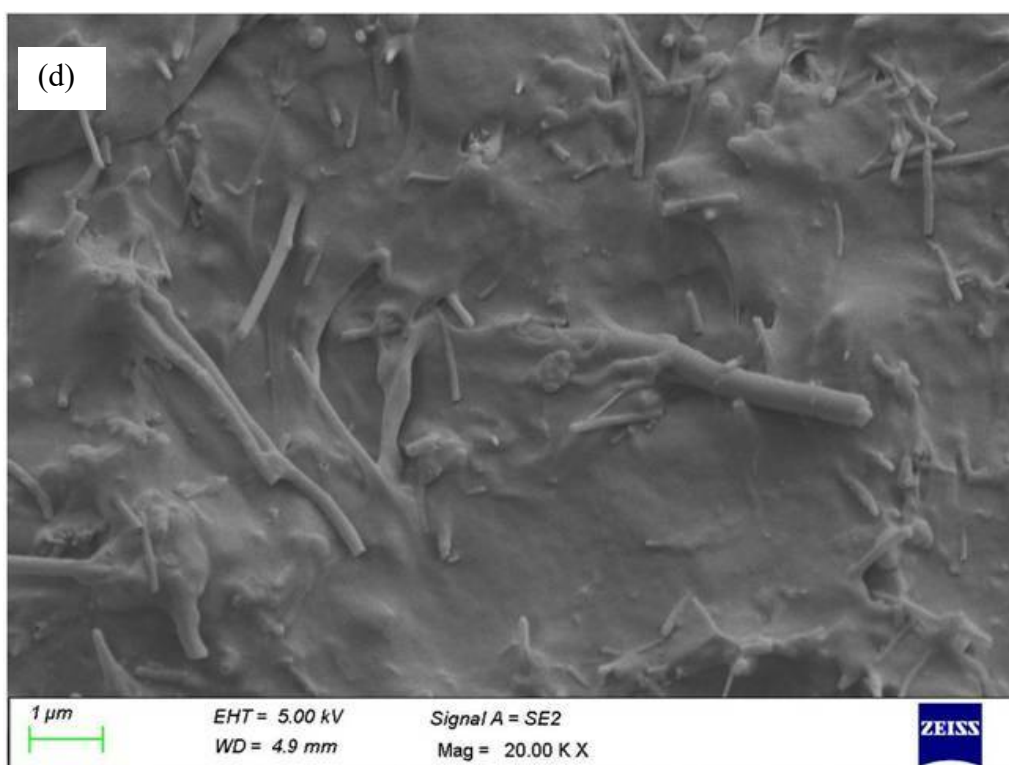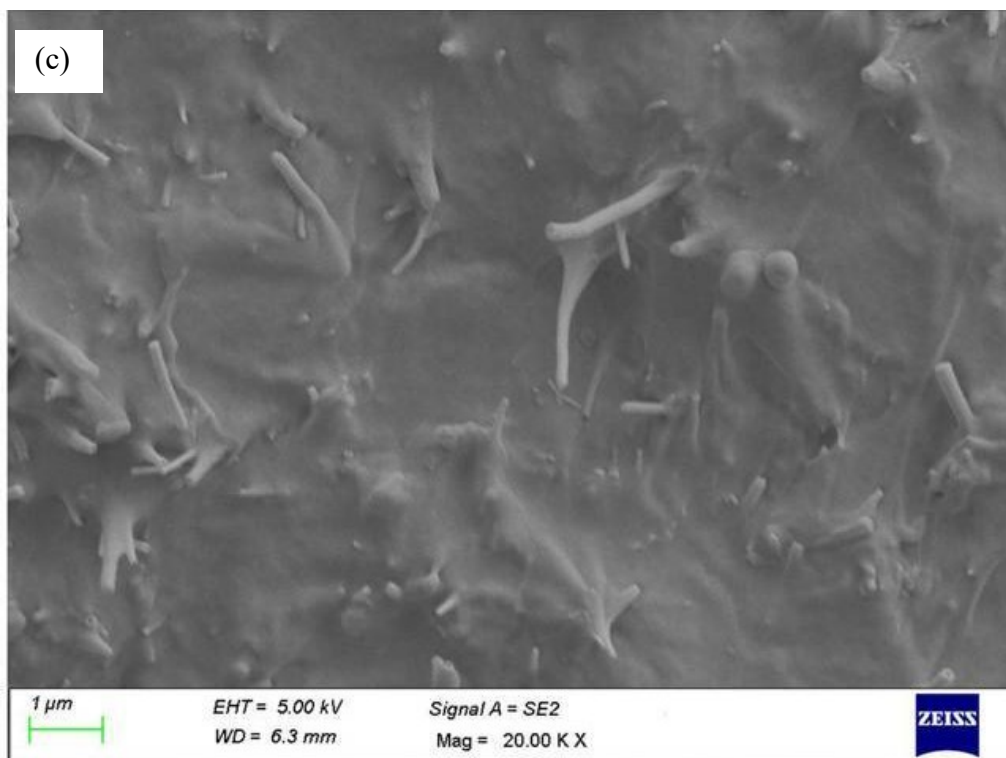
Figure 5.27 SEM micrographs for 0.1%, 0.25%, 4.0% and 7.0% MWCNT in PU resin

It can be seen that the density of nanotube increases from 0.1% to 0.25% (refer Figure 5.27(a) & (b)) and the closeness of fillers increase as the content increases.

At filler content of 4% and 7%, as in Figure 5.27(c) & (d) the contact of nanotubes resulting in a multiple continuous network is evident which pronounces the enhanced conductivity of the nanocomposite at these filler contents. The micrographs indicate effectiveness of ultra-sonication mixing process of the functionalised MWCNT, in preventing their agglomeration.

5.6.2 Thermal and mechanical properties

The TGA plot of the synthesised PU MWCNT composite is depicted in Figure 5.28(a), with the differential thermogram (differential temperature plotted against temperature - DTA). The TGA plot of PU MWCNT nanocomposite shows the material stability upto 300 °C, beyond which the covalent bonds are broken and volatile materials escape to leave a residue of nearly 5%. The enthalpy change observed at 328 °C and 417 °C shows the disintegration of the material by breaking of the covalent linkages between chains of PU as the carbon filler absorbs heat and acts as local heating elements causing internal heat sources.
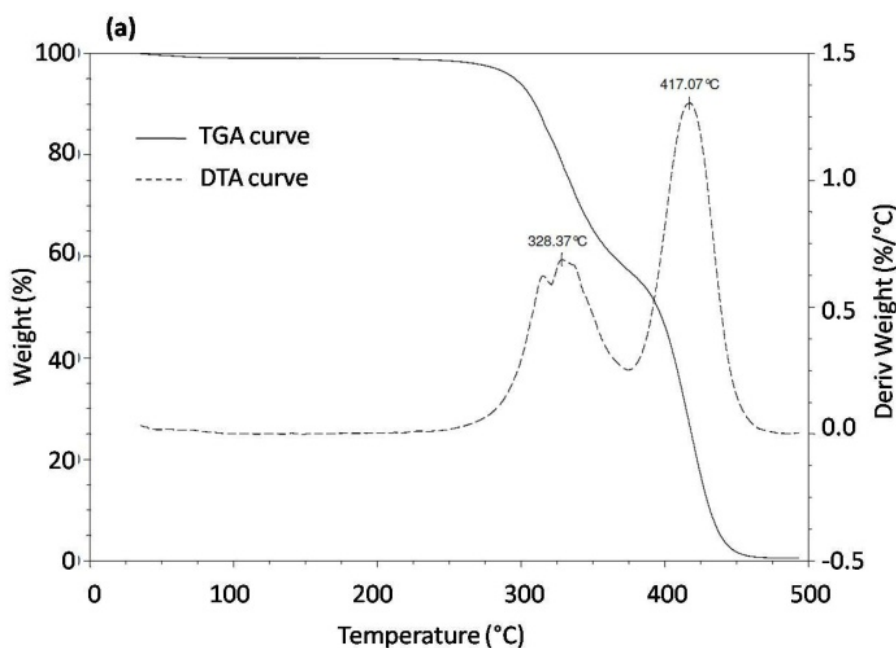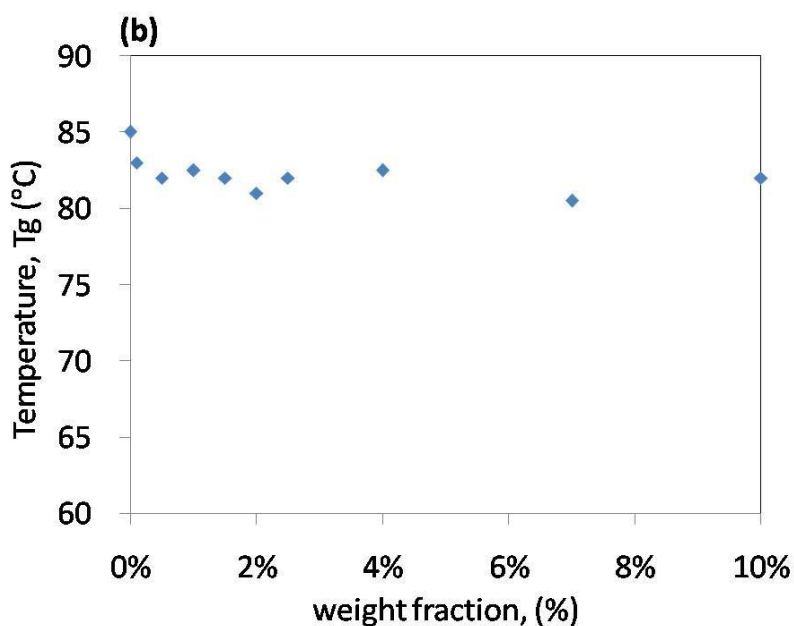
Figure 5.28(a) TGA curve showing the thermal stability of the material (1% MWCNT); (b) The T_g variation corresponding to varying MWCNT loading

The glass transition temperature is one of the significant parameter in case of a shape memory polymer nanocomposite for initiating the shape recovery. T_g of the synthesised nanocomposite was obtained for varying weight fractions of MWCNT from DSC analysis, which showed value around 81°C without any much major deviation with filler loading (refer Figure 5.28(b)). The T_g of the synthesised PU resin was 85 °C, which is attributed to the optimal crosslinked carbon chains and is the highest among the T_g reported, as established in another work by the authors [Arun et al., 2019a]. The minor variation in T_g due to the filler loading can be attributed to the heat absorption of the carbon nanotubes at lower content and increasing the overall thermal conductivity of the system thus reducing T_g [Anett Kiraly & Ferenc Ronkay, 2015]. On the other hand, the presence of nanotubes imparts in a larger interface area resulting in more rigidity of the composite [Ketan S. Khare & Rajesh Khare, 2013]. The degree of cure or presence of any traces of solvent in the system can account for the slight non linearity in variation of T_g with increasing filler content [A Allaoui & N. El Bounia, 2009].

The effect of addition of MWCNT in PU resin on the basic mechanical properties was evaluated by studying the modulus and elongation of the nanocomposites with varying filler content. Figure 5.29 depicts an increasing trend in the modulus

with respect to carbon loading and it is a reflection of the higher modulus possessed by the carbon nanotubes [Huang WM et al., 2012; Amal Esawi & Mahmoud Farag, 2007].
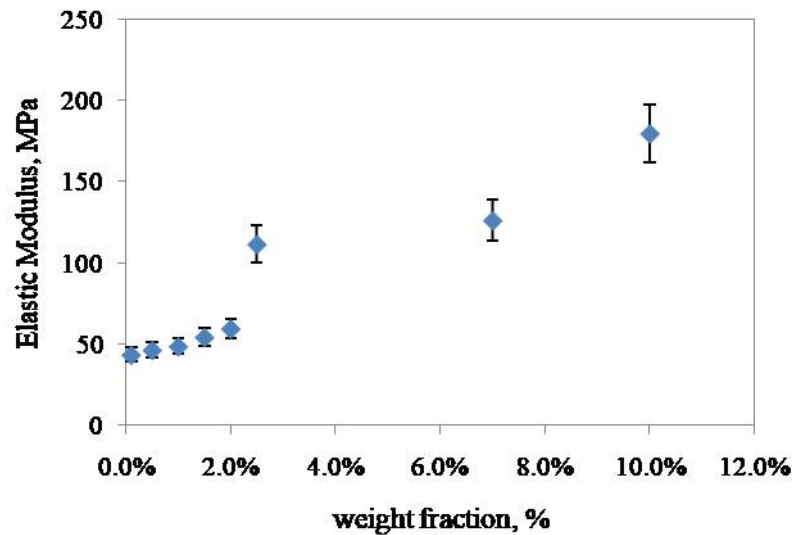
Figure 5.29 Elastic modulus for varying MWCNT loading

The increase in the modulus can also be attributed to the isotropic interfacial bond strength between the MWCNT and the resin which might be due to the large aspect ratios of nanotubes [Jonathan N. Coleman et al., 2006]. The nanocomposite at 2.5% MWCNT loading exhibited a 156% increase in the modulus (112 MPa) from that of 0.1% MWCNT weight fraction (44 MPa). It is observed that when the loading increased to 10% weight fraction, the modulus rose up to 313% (180 MPa) of that exhibited by 0.1% MWCNT. The covalent bond formation between the fucntionalised nanotube and the basic polyurethane linkages results in increased interfacial strength [Huang WM et al., 2012; N G. Sahoo et al., 2010; Hsu-Chiang Kuan et al., 2005]. Higher loadings of filler content resulted in increased interfacial strength leading to higher modulus and rigidity. Elongation of the nanocomposite varied between 600% and 300% due to the introduction of nanotube that resulted in higher rigidity of the matrix.

Comparing the effect of addition of CB and MWCNT to the PU matrix, both the fillers were found to increase in the elastic modulus of the respective systems, as evident from the Figure 5.30. The contribution of CB towards the mechanical

strength and modulus is lesser compared to that of MWCNT, due to the effect of geometry. The large aspect ratio and the higher modulus possessed by the MWCNT resulted in increased isotropic interfacial bond between the matrix and the filler (covalent bond formation between the MWCNT and the resin leads to increased interfacial strength) thus leading to high modulus of the system [Coleman et al., 2006; Huang et al., 2012].
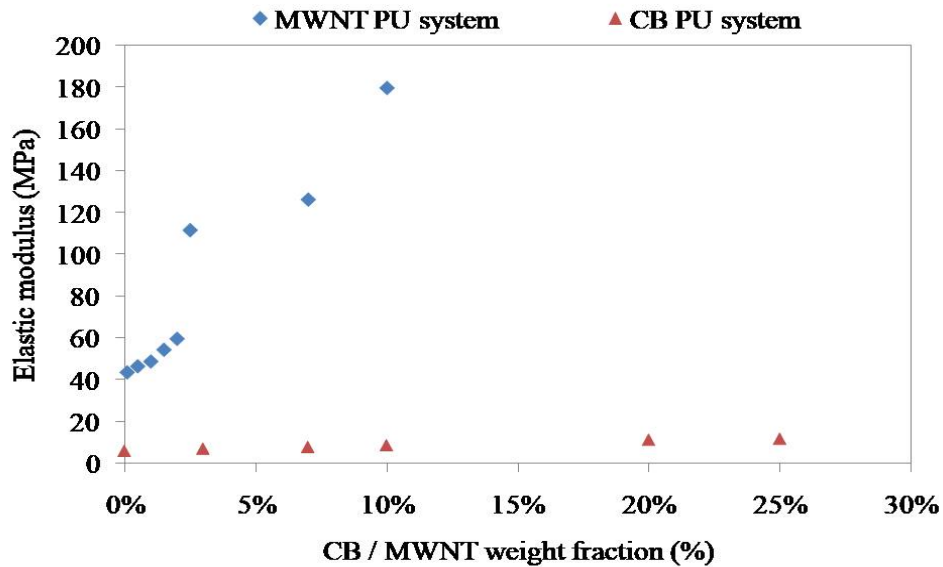
Figure 5.30. Variation of elastic modulus for varying CB & MWCNT loading

Fillers well dispersed in the matrix results uniform load distribution resulting in isotropic mechanical properties of the system. Bhattacharya, Mrinal, 2016 explains how the agglomeration of fillers results in reduction of mechanical strength or modulus of the system. As per his studies, the filler agglomerates act as stress concentration points inside the polymer matrix causing unequal load sharing resulting in failure.

5.6.3 Electrical resistivity

The resistivity of the material against MWCNT loading is depicted in Figure 5.31. It can be observed that the resistivity drops sharply between 0.1% and 0.3% of MWCNT loading, which can be attributed to the increased conductivity introduced by the nanotubes into the system. A sudden drop in the resistivity

values (observed around 0.25% weight fraction) denotes that the composite becomes electricity conducting.
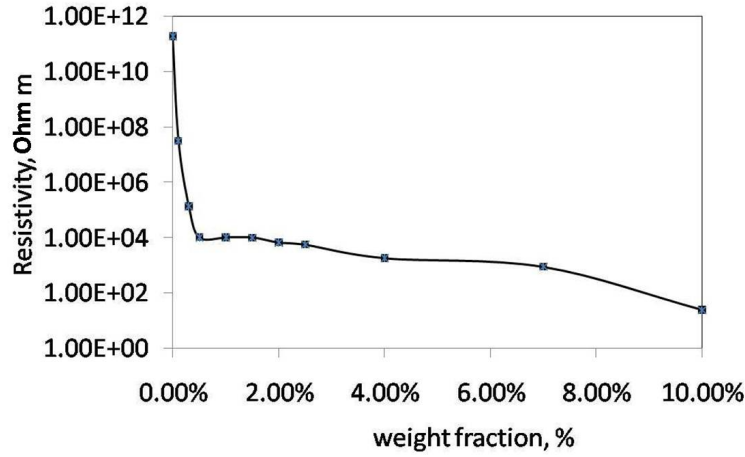
Figure 5.31 Electrical resistivity measured for weight fractions from 0% (pure PU) to 10% MWCNT

When the number of nanotubes increases there exist a probability for them to come in contact or remain closer so that the distance between the MWCNTs are lesser than the minimum tunnelling barrier. This causes a continuous path for the electrons to pass through the system making it conducting. The reduction in the resistivity is attributed to the increased contacts of MWCNT or the conducting networks formed between them. The same can be observed in the model where the particle closeness is evaluated for a percolation network [Xiaomei Z et al., 2011; Kirkpatrick Scott, 1973; Arun et al., 2019b].

5.7 Evaluation of the pseudorandom model and Monte Carlo simulations

The structural orientation model developed using the parameters of CB PU system was enhanced to the features of MWCNT system and is presented here to predict the percolation behavior of a MWCNT PU nanocomposite system.

The nanotubes of diameter 3 to 5 nm and aspect ratio ranging between 90 and 120 were introduced into the RCVE at pseudo random locations, by generating random numbers for position co-ordinates. The maximum and minimum number

of nanotubes (nanocylinders as per program) generated for diameter randomly between 3 nm to 5 nm and aspect ratio 90 to 120, considering the volume fraction 1-5% are as listed in Table 5.3.

Table 5.3 Number of CNTs possible per volume fraction (1% to 5%)

Volume fraction	No. of nanotubes
1%	849 - 5240
2%	1698 – 10479
3%	2546 – 15719
4%	3395 – 20959
5%	4244 - 26198

It is due to the wide range in nanotube counts, the same volume fraction can have the possibility of formations of conducting or non conducting network which are predicted by Monte Carlo simulations. The pseudo-random model is iterated by Monte Carlo method for various random positions and orientations of individual fillers and for varying filler loadings. The random positions as generated during Monte Carlo simulations ensures possibility of nanotubes coming closer to values less than the barrier distance or coming into contact with each other to form conducting networks that extends from one end to the other leading to electrical conduction [MSP Shafeer et al., 1998; , Akos A, 2012].

It is observed from the simulations that any content above 1% of MWCNT resulted in the formation of conducting networks and thus establishing electrical conductivity of the chosen system. In order to evaluate the percolation threshold, it was necessary to understand the system with volume fractions less than 1%. The

number of nanotubes for volume fractions varying from 0.1% to 0.9% in steps of 0.1 is shown in Table 5.4.

Table 5.4 Number of CNTs possible per volume fraction (0.1% to 0.9%)

Volume fraction	No. of nanotubes
0.1%	85 – 524
0.2%	170 – 1048
0.3%	255 – 1572
0.4%	340 – 2096
0.5%	424 – 2620
0.6%	509 – 3144
0.7%	594 – 3668
0.8%	679 – 4192
0.9%	764 – 4716

The method of Monte Carlo simulations were attempted for the volume fractions as shown in Table 5.4 and it revealed that the probability of conduction below 0.3% volume fraction was less than 50% and that beyond 0.4% volume fraction to be above 50%. Hence it was clear that the percolation threshold lies between 0.3% and 0.4% volume fraction. The model was configured for volume fractions between 0.31% and 0.39% volume fraction and the percolation threshold was

observed at 0.38%. Hence it can be inferred that CNTs between 1572 and 2096 numbers participated in conductive network formation during percolation.

Further computation can give better accuracy in the percolation concentration, but it is insignificant to arrive for such a system as the same needs to be experimentally verified for validation and is also a costly affair. Figure 5.32(a)-(d) shows the distribution of nanotubes in the RCVE for volume fractions of 0.02%, 0.1%, 0.3% and 0.5%.

(a)

(b)

(c)

(d)
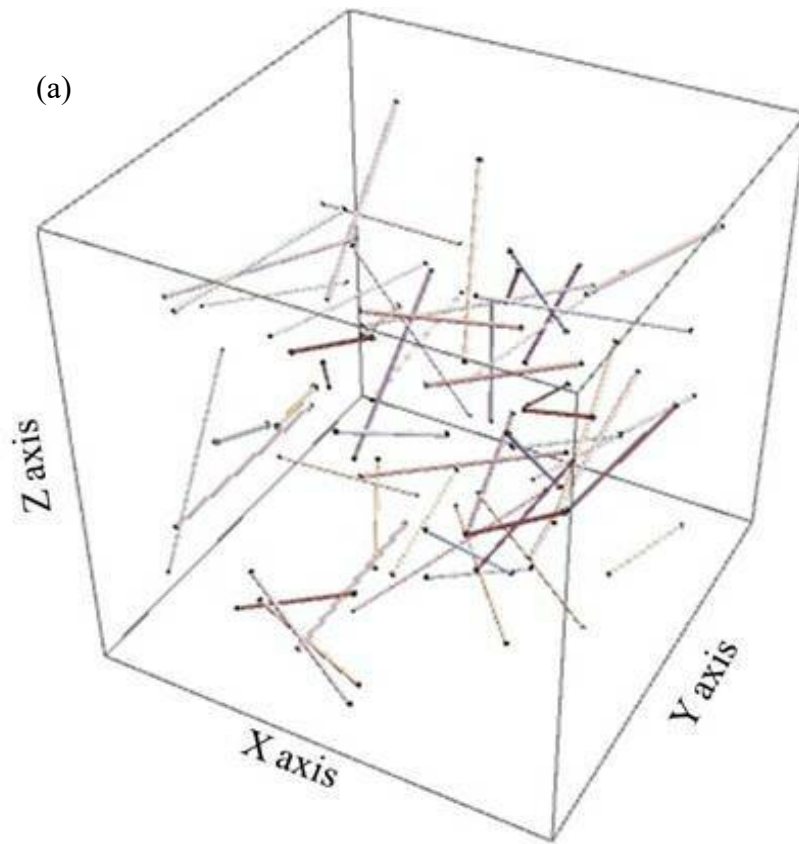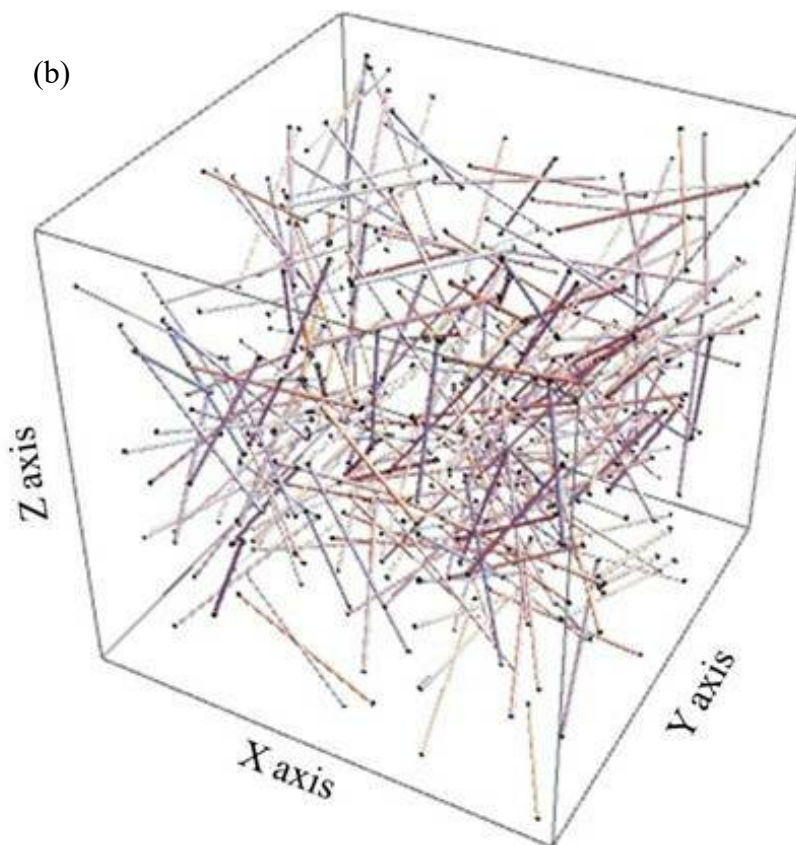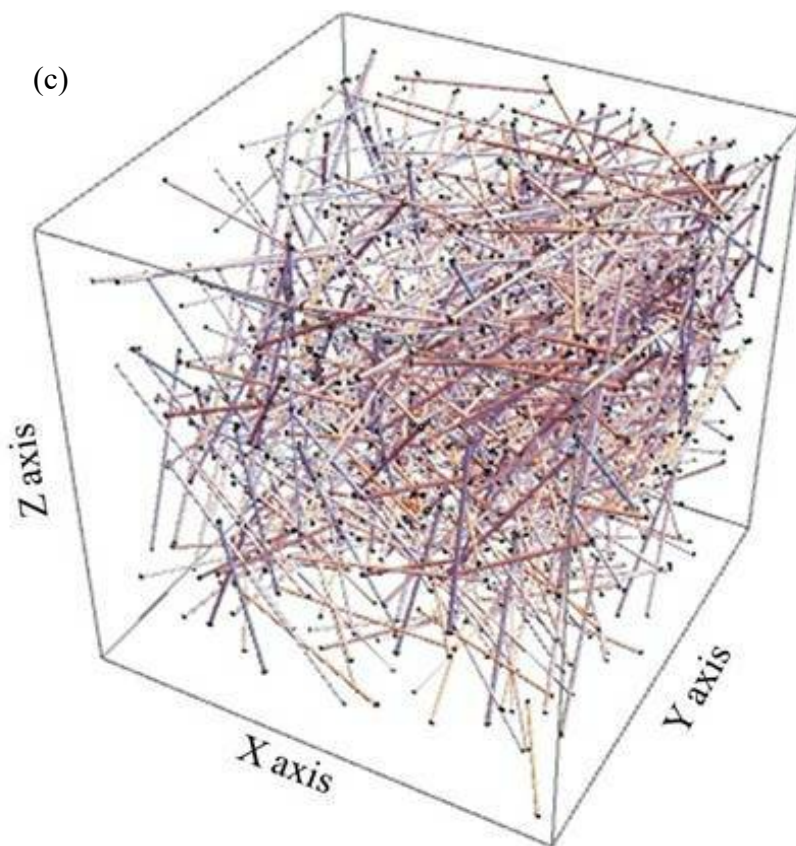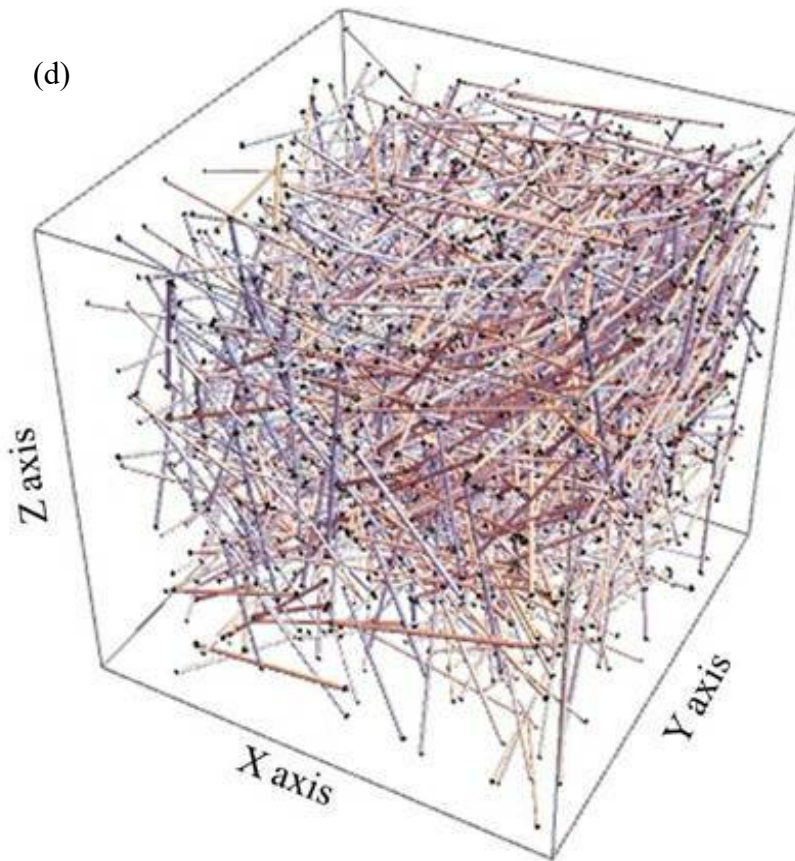
Figure 5.32 Visualisation of nanotube dispersions in the RCVE (generated in Wolfram Mathematica) at (a) 0.02% volume fraction, (b) 0.1% volume fraction, (c) 0.3% volume fraction and (d) 0.5% volume fraction (above percolation)

It can be observed from Figure 5.32 that the density of nanotube dispersion increases in the matrix as depicted in the visualisation. It is clear from the Figure 5.32(a) that, at 0.02% volume fraction 53 number of nanotube of different diameter, length, position and orientation exists which is not forming any continuous network. Figure 5.32(a) provides the visualisation for 0.1% volume fraction where exists 267 nanotubes which makes contacts with few nanotubes, yet there is no continuous network for a current conduction. From Figure 5.32(c), which depicts 0.3% volume fraction of nanotubes with 802 numbers of nanotubes, it can be inferred that even though the filler dispersion appears dense, there is no continuous network for electron path. For 0.5% volume fraction as shown in Figure 5.32(d), 1739 nanotubes are generated and it was found conducting with continuous network for conduction.
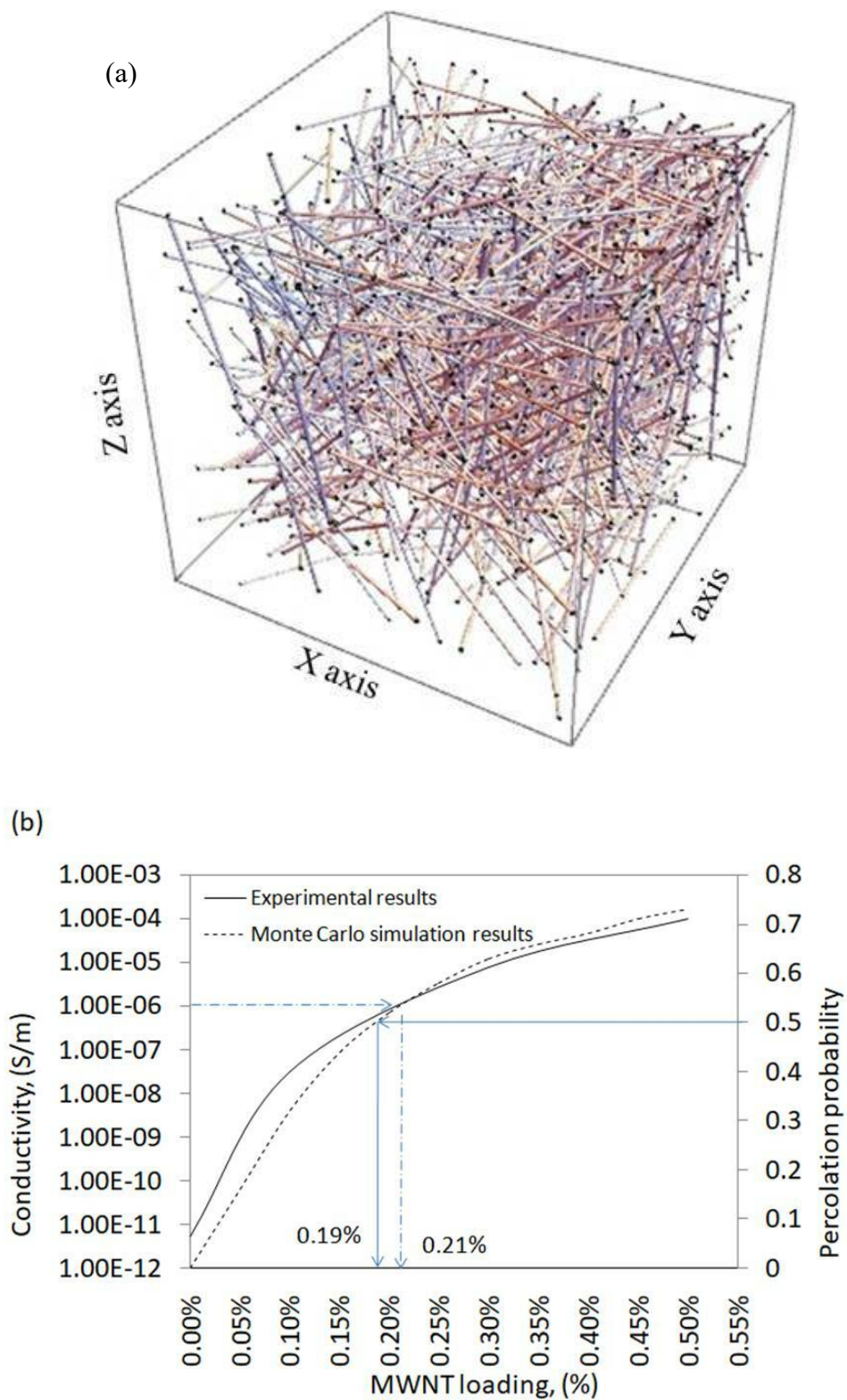
Figure 5.33 (a) Visualisation of the nanotube dispersed in the RCVE at percolation threshold (0.38% volume fraction); (b) MWCNT loading plotted against conductivity (log) and percolation probability

The Figure 5.33(a) shows the random dispersion of nanotubes in the RCVE at percolation of 0.38% volume fraction, for which experimental weight fraction equalent is 0.19% by weight of nanotubes. Figure 5.33(b) depicts the values of conductivity with respect to MWCNT loading as measured form the experiments and observed from the model.

As per the results of the Monte Carlo simulations, the nanotubes form continuous conductive networks resulting in continuous path for electrons between two terminals (refer Figure 5.33(a)). Corresponding plot of the probability of conduction (percolation probability) and weight fraction (half of volume fraction) of nanotubes indicates an increasing trend which approaches to maximum conduction probability of 1.0. The weight fraction corresponding to probability of 0.5 is assumed to be the percolation threshold in case of the pseudo random model, which is read as 0.19% weight fraction (0.38% volume fraction) in this case. Considering the experimental measurement, the conductivity increased exponentially with increase in MWCNT loading. The conductivity corresponding to the order of 10^{-6} S/m (midpoint of the curve) is considered as the percolation threshold, which is the minimum weight fraction at which the insulator becomes a conductor. From the plot of conductivity obtained from experiment against weight fraction, a percolation concentration / threshold of 0.21% weight of MWCNT can be observed [Arun et al., 2019b; MSP Shafeer et al., 1998].

The percolation thresholds obtained from experimental as well as model differs by mere 0.03% which is less than 10% deviation. Hence the model predictions can be considered matching with the experimental results thus validating the structural oriented pseudo random model for nanocomposite systems.

5.7.1.1 Electrical percolation

The values of the critical exponents 'k' (before percolation) and 'j' (after percolation) were obtained from the relationship between Log |p~pc| and Log σ, as depicted in Figure 5.34.
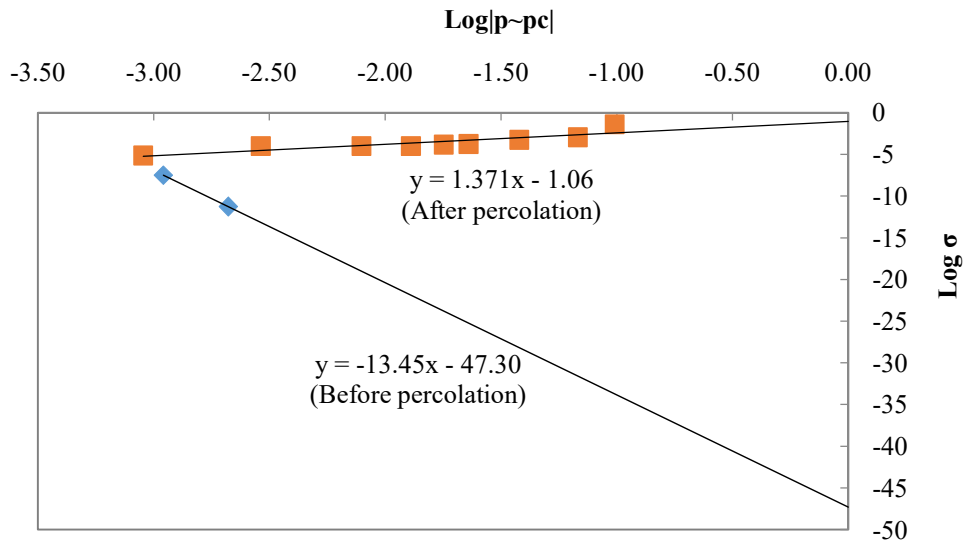
Figure 5.34 Plots of log σ vs. log (p ~ pc) based on classical percolation theory for the MWCNT nanocomposite

As the obtained electrical percolation from the experiment is 0.21% by weight of MWCNT, the critical exponents can be obtained from the slope of the lines connecting Log |p~pc| corresponding to Log σ. The '*k*' and '*j*' values obtained were -13.45 and 1.371 respectively. As observed in case of CB loading in PU resin, the 'k' value showed a higher magnitude compared to the published data. Since the inter-particle distance is reflected from the magnitude of exponents, it can be understood that the conduction below percolation is purely due to tunnelling. Due to the effect of the aspect ratio of the nanotubes, a sudden change in conductivity is resulted which causes the change in magnitude of 'k' to 'j' indicating contact conductivity from percolation threshold. The obtained 'j' value is less than 2.0, which shows an ordered network formation by contact of the nanotubes resulting in transformation of the insulating material to a conductor [Mdarhri et al., 2012].

5.7.1.2 Relationship of time and T_g

The time to achieve transition temperature corresponding to each voltage applied for 10% by weight of MWCNT in PU, are depicted in Figure 5.35.
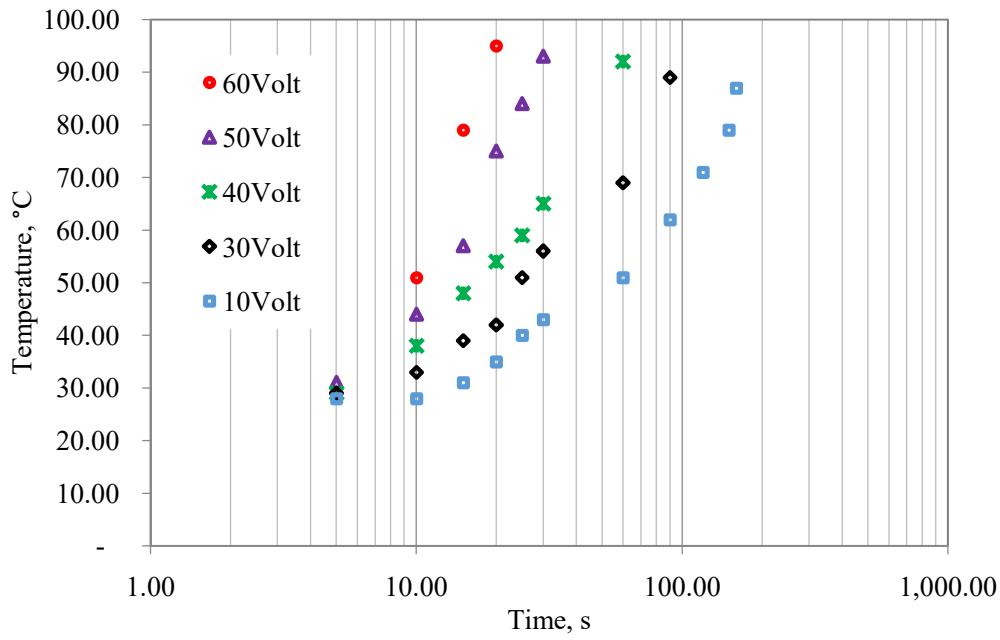
Figure 5.35 Variation in time to achieve transition with change in applied voltage (in 10% MWCNT nanocomposite)

It can be observed that the plot corresponding to 10V is represented by a rising parabola, which converges to a straight line while the voltage increases through 30V, 40V, 50V and 60V. The increased voltage provided reduces the energy barrier between the conductive fillers and this causes more electrons to jump across the tunneling barrier. This results in more and more network path formation with increased applied voltage for constant filler loadings [Kirkpatrick, 1973]. It can be found that the time to achieve T_g +20°C reduces from 108s to 19s while the voltage changes from 10V to 60V.

5.8 Shape memory effect in MWCNT PU nanocomposites

The shape memory effect was evaluated for thermal as well as electrical stimuli for which fold deploy test was employed. A sample of shape '**U**' was sliced from the thin sheet of the cured nanocomposite was considered for electrical actuation, whereas a rectangular strip was chosen for thermal stimuli response experiment of SME (as depicted in Figure 5.36(a)). MWCNT loading of 2.5%, 4.0%, 7.0% and 10.0% were attempted for demonstrating the SME in the system, while the time of

actuation was found to be in the order of hours in lower filler content (2.5%, 4.0% and 7.0%) which can be attributed to the number of networks that allow electric current resulting in heating of system. Hence it was decided to optimise the filler loading for SME based on time of actuation, maximum possible electrical conductivity and maximum filler loading possible and 10% MWCNT loading was chosen. The lower filler contents (above percolation threshold) can be useful for slower actuation demands such as timed deployment or synchronised actuations in aerospace systems, thereby giving an option to the designer to chose the material as per application.

The sample was trained to a temporary shape by constraining it to 'U' shape and heating up to T_g + 20°C. On cooling to the room temperature and removing the shape constrain, the 'U' shape was fixed.

5.8.1 Thermally activated SME

The shape fixity efficiency was arrived from the angle between the two parallel legs on training by thermal stimuli. After cooling the sample to room temperature, further application of heat by external heater shall facilitate the recovery of original shape, as depicted in Figure 5.36(b). Thermally active shape recovery was achieved in 21 seconds with average (for 10 cycles) shape fixity and recovery efficiency as 91.61% and 95.06% respectively [Huang WM, 2010; Ahmad M et al., 2012].

5.8.2 Electro-active SME

With the basic character of PU to recover the original shape from a temporarily trained shape, the induced conductivity enhances the material to be activated by electric current. On training to temporary shape by electrical stimuli, the angle formed by the two parallel legs of 'U' are measured to arrive at the shape fixity efficiency. The sample is then connected to the power source and a voltage of 60V was applied and the corresponding recovery efficiencies were noted for 10 numbers of cycles. The electro-active shape recovery is depicted in Figure 5.36(c), which shows that the material recovers its original shape by 19 seconds.

This is considerably faster compared to the recovery speeds reported for MWCNT SMPCs. The shape fixity and recovery efficiency for electrical actuation are found as 97.11% and 98.60% respectively [Arun et al., 2019a].
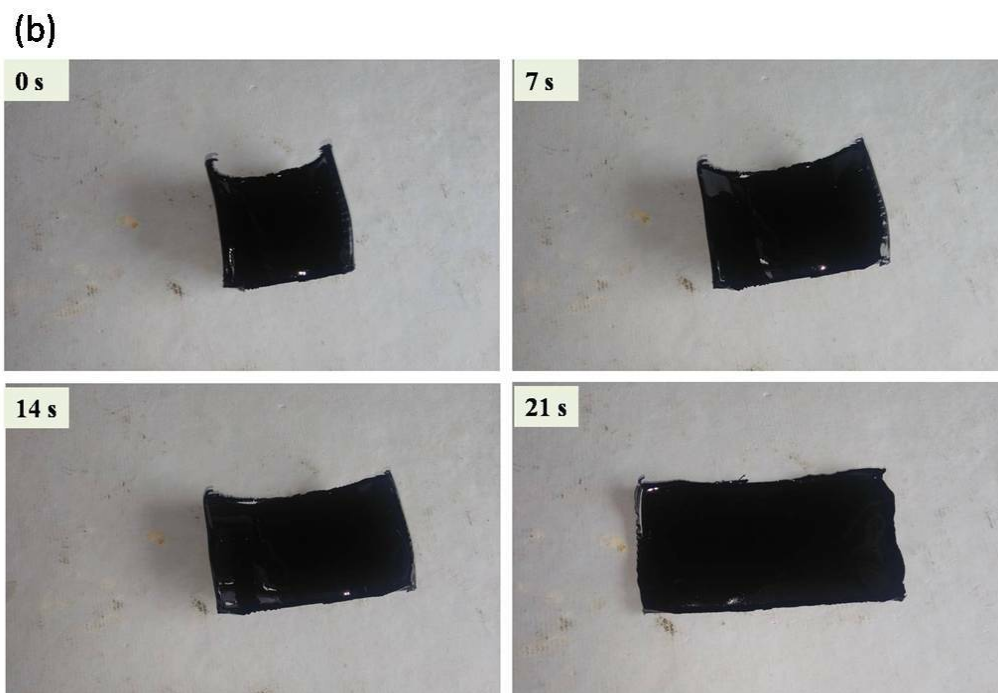
(c)
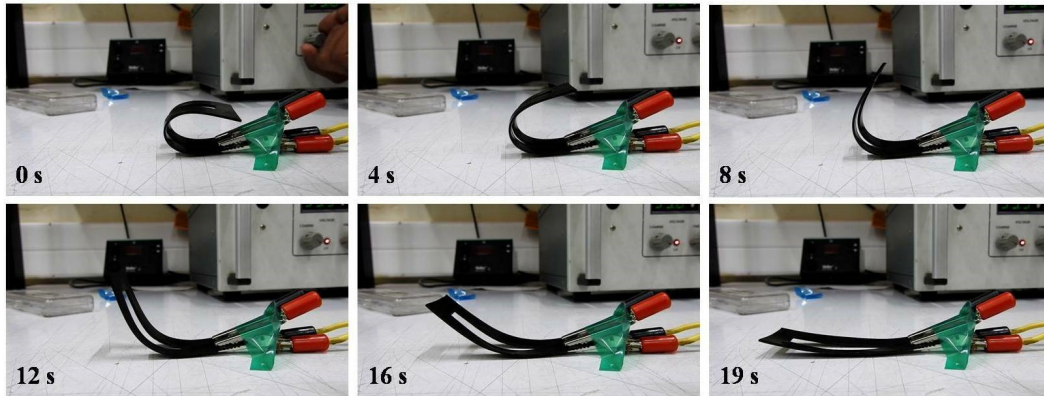
Figure 5.36 (a) Sample used for shape memory demonstration using thermal and electrical stimuli; (b) thermally active SME by fold-deploy test, recovering original shape in 21 s; (c) electro-active SME by fold-deploy test, recovering original shape in 19 s.

SME with thermal stimuli (external heater application) showed lesser fixity and recovery efficiency compared to the electrical stimuli. This is due to the difference in heating the system where thermal stimuli induces surface heating which will be subjected to convection heat loss to the surroundings, thus resulting in lower rate of heating. Whereas in electro-actuation, the nanocomposite is heated volumetrically by joule heating and thus the heat loss to surroundings is compensated. Thus the electro-active system recovers faster with better efficiency than thermal actuation. Figure 5.37(a) and (b) depicts the comparison of shape fixity and recovery efficiency for thermal and electrical actuation.
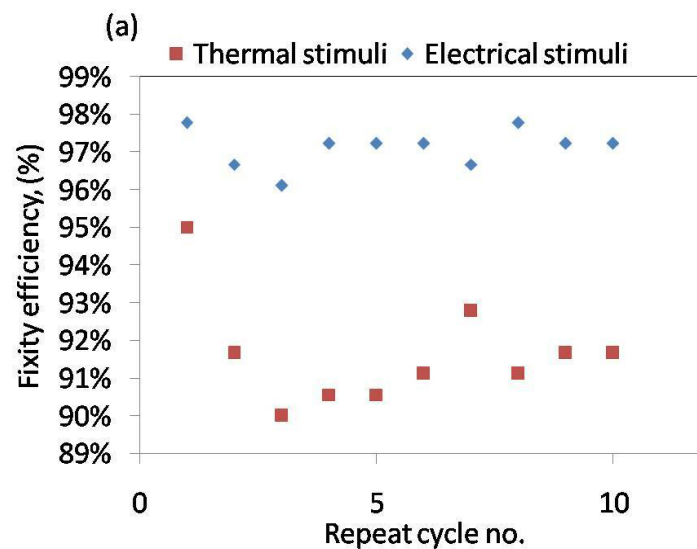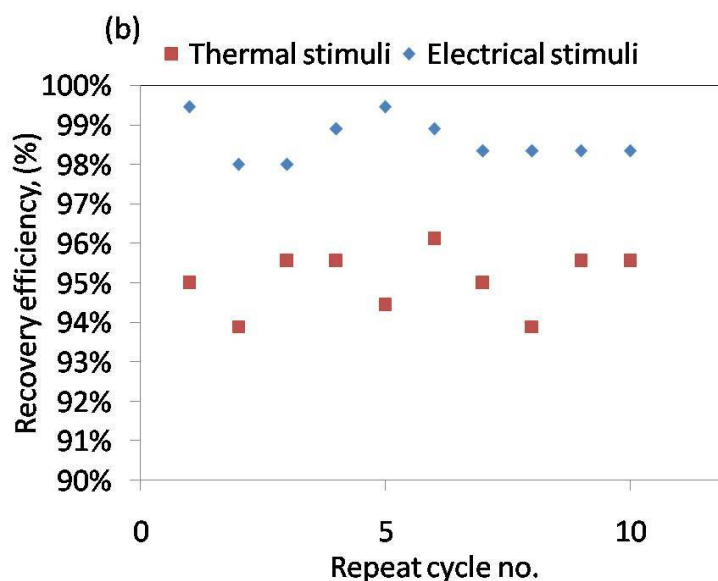
Figure 5.37 (a) Shape fixity efficiency of thermal and electrical actuation; (b) Shape recovery efficiency of thermal and electrical actuation

The relationship of temperature and recovery efficiency was measured by non-contact thermometer during shape recovery by both thermal and electrical stimuli and depicted in Figure 5.38 (a). It can be observed that the temperature of the system during both the stimuli application follows linear pattern, which attributes to the fairly uniform distribution of the fillers by means of ultra-sonication that heats the material evenly during application of temperature. Figure 5.38 (b) shows the relationship of time against the recovery efficiency for thermal and electrical stimuli. The plot follows a sigmoidal shape in case of electrical actuation, whereas the thermal stimulated shape memory shows a linear increase beyond 5 s. The sigmoidal shape can be explained as the conduction that occurs through the multiple branched networks inside the nanocomposites (causing volumetric heating) by either tunnelling or contact of MWCNT reinforcement. The slow start upto 5 s and then the linear increase of thermal actuation is due to the heat absorption by the uniformly distributed MWCNT fillers which acts as local heaters thus raising the inner temperature facilitating mobility of hard segments of the PU nanocomposite [Huang WM et a., 2012, Arun et al., 2019a].
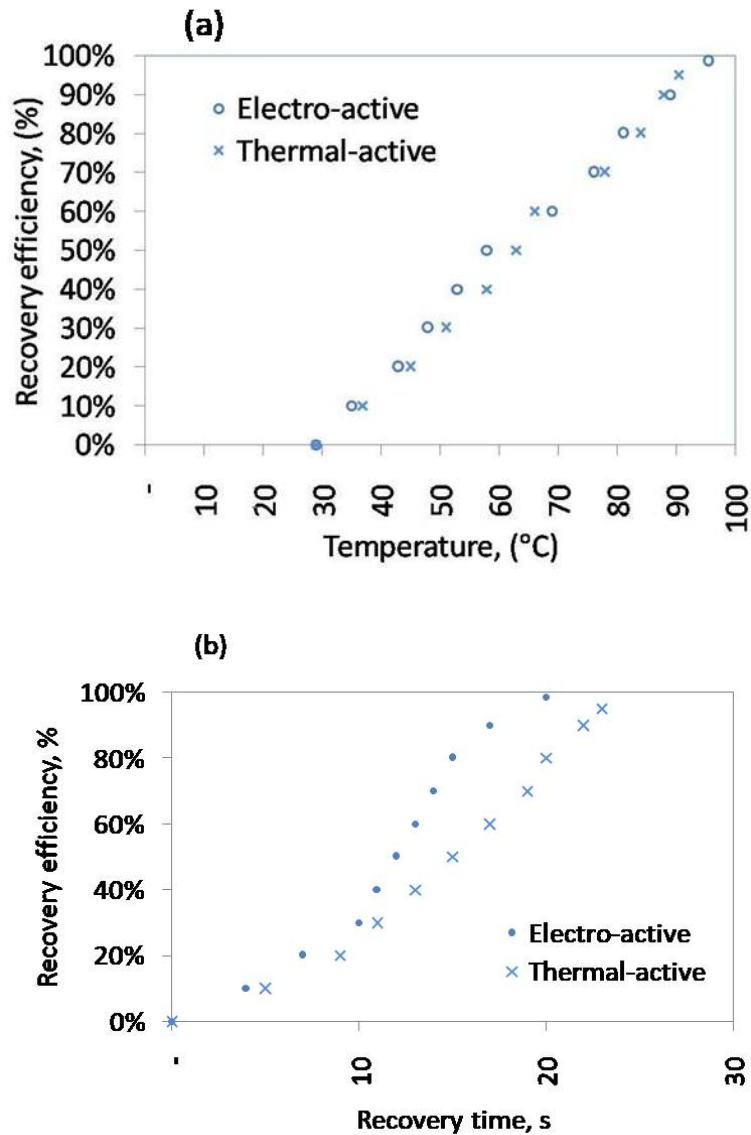
Figure 5.38 (a) Relationship between temperature and shape recovery efficiency for thermal and electrical actuation; (d) Relationship between shape recovery efficiency and recovery time for thermal and electrical actuation

5.9 Summary

A comprehensive model based on structural orientation was developed in visual C platform, which can predict the conductivity of nanocomposites with known filler characteristics. The model visualizes cylindrical nanotubes dispersed in a representative volume at random positions, and orientations for various filler contents. The possibility of formation of continuous conductive networks was

verified for filler contents between 0.1% and 10% and simulated for various positioning of the nanotubes using Monte Carlo methods.

- The percolation threshold was obtained to be 0.38% by volume of nanotubes, which is equivalent to 0.19% by weight of MWCNT.
- The synthesized PU MWCNT nanocomposite system showed a percolation threshold of 0.21% by weight of MWCNT.
- The developed PU MWCNT nanocomposite was evaluated for its shape memory ability by thermal and electrical stimuli. Recovery efficiencies of 95.06% and 98.60% respectively for thermal and electrical actuation was obtained, which are highest among the reported data.
- The shape recovery was obtained in 21s and 19s for thermal and electrical actuation respectively.

III. Synergistic studies on Carbon black – MWCNT hybrid PU SMP nanocomposite

Carbon based fillers such as graphite nanoplatelets, exfoliated clay, carbon black (CB), carbon nanotubes (CNT), carbon nano fibers (CNF), graphene etc., are considered as potential candidates for synthesis of electrically conductive nanocomposites [Han, Z. & Fina, A, 2011; Ma, Peng Cheng et al., 2009]. Studies have proven that though the conventional conducting fillers like CB or CNF possess the percolation threshold values as high as 6% - 10% for it to be electrically conductive and for it to have good shape memory ability, larger filler content of 15%-20% is required which results in the degradation of mechanical properties [Arun et al., 2019b; Ma, Peng Cheng et al., 2009]. Nano fillers like CNTs, graphene, exfoliated clay etc., as replacement to conventional fillers have proven to be effective, as they possess lower value of percolation thresholds for nanocomposites with better electrical and mechanical properties [Jang, S. & Yin, H, 2016; Qi, Xiaodong et al., 2016; Ajayan, Pulickel M et al., 2000].This advantage is attributed to the better conductivity and high aspect ratios of these fillers compared to the conventional reinforcements. The high cost and the associated difficulties with the dispersion of CNTs and graphene led to studies on combining the fillers to form hybrid heterogeneous nanocomposite systems [Ma, Peng Cheng et al., 2009; Liu, Yanju et al., 2014, 2008; Xue, Deqing et al., 2016; Huang, W. M et al., 2010]

Due to the low cost and abundant availability of CB, it is one of the most preferred reinforcement filler for synthesizing conductive polymer nanocomposites. However, the reported percolation threshold of CB filled polymer composites is relatively large compared to the fillers with higher aspect ratios [Leng J S et al., 2008; Lan Xin et al., 2008; Ding, Z, 2012]. Thus, CNTs having very high aspect ratios and low percolation threshold values can be a potential replacement of conventional CB fillers in a hybrid system [Martin CA et al., 2004; Yoshino K et al., 1999; Bauhover & Kovacs, 2009].

Studies pertaining to the synergy between multiple fillers on hybrid system focus on one of the properties such as electrical conductivity, mechanical property and transition temperature only [Backes E H et al., 2018; Ismail, H et al., 2011; Bhattacharya, M, 2016; Zha, Ruhua et al., 2017; Song, S, 2018; Yan, N et al., 2009; Safdari, M & Al-Haik, 2012, A Noll et al., 2013]. The co-existence of the fillers for network formation attributes for the electrical conductivity of the hybrid systems. Studies of Schartel, Bernhard et al., 2015 [Schartel, B et al., 2015] and Ma, Peng Cheng et al., 2007 reports that the ternary composites (two fillers and matrix) with MWCNT and CB as fillers in epoxy resin matrix have shown electrical property similar to the binary MWCNT composites (one filler and matrix). The synergistic effect was found to improve the electrical behavior, while the rheological properties were getting affected compared to the binary system. Dorigato, Andrea et al., 2018 have studied about polybutylene terephthalate (PBT) filled with CB and CNT at different relative ratios, and found that the synergistic effect of both nanofillers with even dispersion in the matrix resulted in achieving rapid surface heating through Joule effect even at lower voltages. Kumar, S et al, 2010 and Ma, Peng Cheng et al., 2009 studied regarding the synergistic effects for mixed CB and MWCNTs and observed that the aspect ratios, geometric shapes and surface preparations does influence the electrical and mechanical properties. The study reported that the properties of the hybrid system are found to be in an intermediate state between binary those containing CB and MWCNT alone on the macroscopic scale. **Figure 5.39** (a), (b) and (c) shows the illustration of dispersed fillers in binary nanocomposites with CB, CNT and hybrid ternary CB& CNT as fillers.

The individual probable network formations are also depicted for each case, where Figure 5.39(c) indicates the possible synergy between both the fillers forming continuous networks in the system.
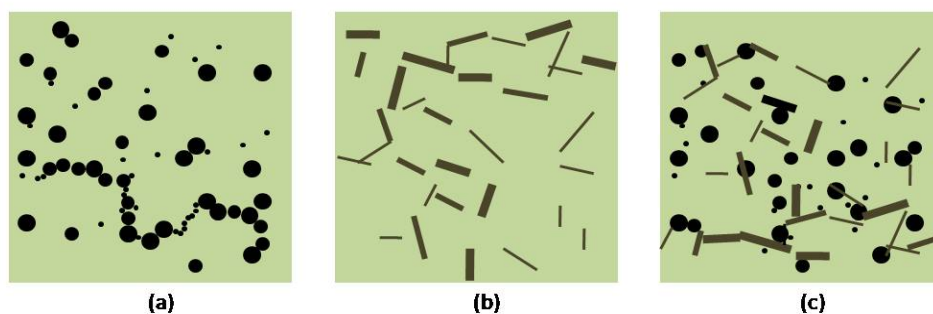
Figure 5.39 Depiction of CB, CNT and hybrid nanocomposites with filler dispersions; (a)CB as filler forming networks; (b) CNT as filler forming networks; (c) Synergy of CB and CNT forming networks

Most of the studies have concentrated on the effect on electrical and mechanical properties due to the synergy between the fillers. An evaluation of the individual filler contributions towards a combination would help to arrive at optimal filler content for specific applications. Electrical conductivity, uniform dispersion of fillers in the matrix for rapid Joule heating, mechanical strength and elongation are significant properties for a shape memory material (SMM). A balance on such properties by varying the multiple fillers can result in a superior material for shape memory applications.

It is understood that the factors such as geometry / shape, surface preparations, presence of solvent traces after curing, dispersion / mixing methodology adopted, sequence of mixing, time of mixing, dimension of fillers, viscosity of the resin, inter-filler interaction, density difference, conductivity difference, strength and difference in elastic behaviour can affect the hybrid composite properties. Authors, though this paper, investigate regarding the synergistic effect of above mentioned factors, between CB and MWCNT in Polyurethane (PU) matrix. A consideration on the individual contribution of the fillers towards the property of nanocomposite is a unique feature of this work. PU being a popular material for shape memory application having inherent shape memory behaviour (due to the presence of multiple phases in the polymer domain), was chosen as the matrix for synthesising the hybrid nanocomposite system. Different weight fractions of CB and MWCNT were combined to form ternary hybrid systems and the characterizations of each system were studied to understand the effect of varying

content of the fillers. The results of the hybrid system were compared with that of binary nanocomposites of individual fillers to evaluate the influence of CB and MWCNT on the synthesis, mechanical & electrical properties and shape memory effect. The influence of CB against ultraviolet protection of the hybrid system was also verified to cater for space applications.

Super conductive CB, (99% pure, Alfa Aesar) with average particle diameter of 240nm and spherical in geometry was one of the filler in the ternary hybrid system. Acid functionalized MWCNTs (99.99% pure, Chemapol industries) with diameter ranging between 3 to 5 nm with aspect ratio between 90 and 120 were added as second filler to prepare the conducting heterogeneous nanocomposite. The spherical and tubular geometry of CB and MWCNT would present interesting synergistic results in hybrid nanocomposite properties. For the material to exhibit good Shape Memory Effect (SME), the bulk of the composite is required to be heated up to the transition temperature (T_g). Electro-active shape memory is influenced by the electrical conductivity of the material resulting in joule heating, whereas the thermal conductivity of the nanocomposite governs the thermally-stimulated SME.

Since conductivity corresponding to electrical percolation threshold demarcates the material between insulator and conductor, the combinations of CB and MWCNT were so chosen that the weight fractions of individual fillers are below the reported percolation threshold values [Han, Z & Fina, A, 2010; Song, W. S, 2016]. This helps to prepare hybrid systems with lower filler loadings having better properties compared to binary composites.

1%, 3% and 5% weight content of CB were chosen corresponding to which MWCNT were added in weight fractions 0.05%, 0.1%, 0.15%, 0.2% and 0.25%. The fillers were added to the resin and subjected to 30 minutes of ultra-sonication for dispersion, which was chosen over mechanical mixing to prevent damage of the MWCNT while mixing [Han, Z & Fina, A, 2010]. The resin-filler mixture was cast to thin sheets with PU solvent and cured in room temperature for 240 hours for complete solvent evaporation. Solvent based system was chosen to have control over the viscosity of the resin matrix during synthesis and casting.

Subsequently, the specimen was de-moulded and post curing at 150 °C for 10 hours for complete solvent removal.

5.10 Characterization results

5.10.1 Chemistry and microstructure

Basic PU linkages were observed in the functional and fingerprint regions of the FTIR spectrogram (refer Figure 5.40) and the same profile was observed for all the filler combinations. This specifies that the increased filler loading has little effect of IR absorption and was reflected in the spectrum. Representative FTIR spectrum of combination 5% CB and 0.25% MWCNT is depicted in Figure 5.40.

The overtones around $3600 cm^{-1}$ denote the presence of non-bonded OH stretch (alcohol in the basic PU). The stretch absorptions around $3300 cm^{-1}$ indicate the primary and secondary amines (N-H- bonds) and O-H stretchings. The significant backbone carbon and its hydrogen counterpart bond, C-H stretching linkages are evident from the peaks between 2840 and $2950 cm^{-1}$.
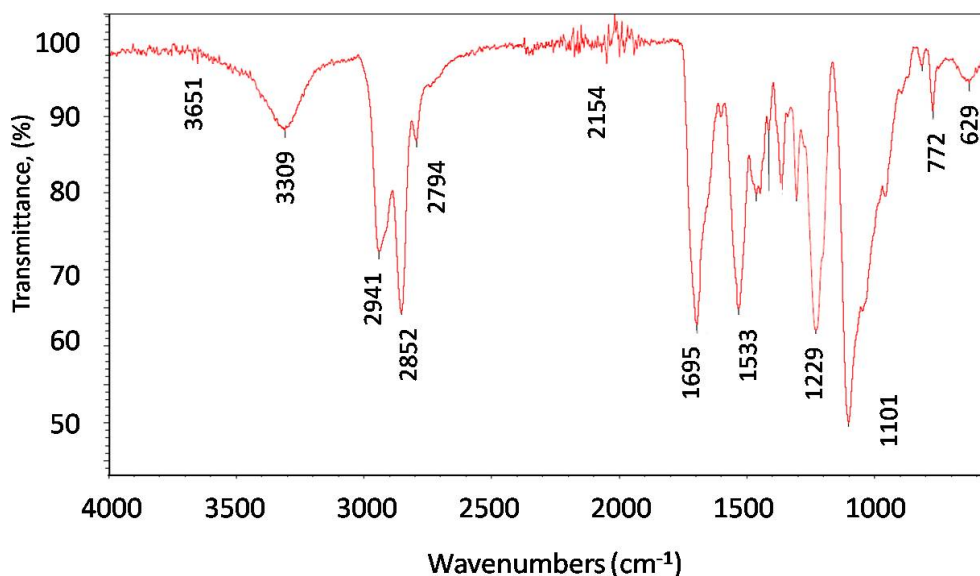
Figure 5.40 ATR-FTIR spectra of 5% CB and 0.25% MWCNT in PU

The overtones at $2000 cm^{-1}$ are indicative of the radiation absorption by the fillers, which is having meager intensity. The peaks observed in the region between 1600

to 1700 cm^{-1} indicates the N-H bending, stretching of C=O and aromatic C=C bonds. Typical PU peaks absorptions between 1000 and 1530 cm^{-1} can be observed showing the C-H bending, C-N stretching and the aromatic ring stretching. The peaks around 629 - 800 cm^{-1} are indicative of the aromatic C-H out of the plane bending, which is typical to the PU linkage signatures.

No specific peak of absorbance was observed for the hybrid nanocomposites while exposing it to UV radiations, as depicted in Figure 5.41.
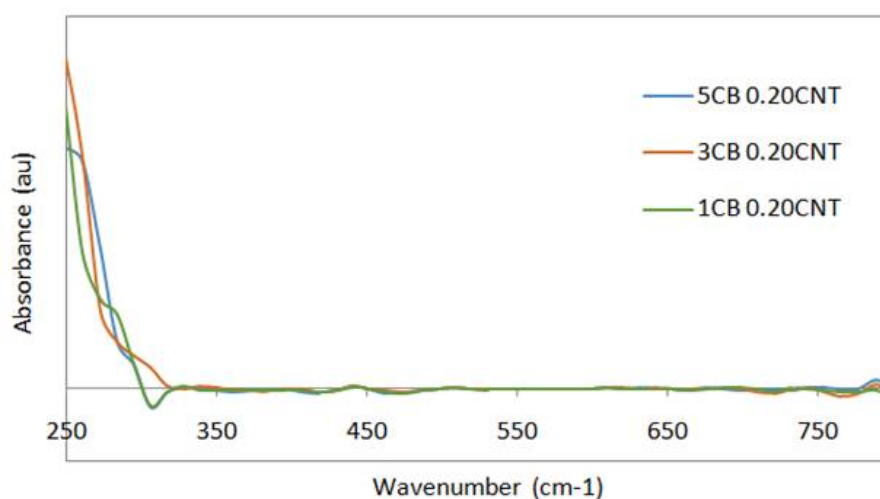
Figure 5.41 UV visible spectrogram for CB - CNT in PU matrix for varying weight fractions

The stability of PU CB nanocomposite against UV radiations were reported elsewhere by the authors [Arun et al., 2019a]. This was explained as the result of two factors of which one is the stability induced by presence of 'saturated cyclic and aliphatic polyisocyanates' IPDI [Robert. A.O & William T S, 1983]. The second factor is attributed to the presence of the CB as filler material that is a proven UV stabiliser for polymers [Arun et al., 2019a, George W, 2015]. Hence the hybrid nanocomposite prepared was found to be resistant to UV radiations, attributed to the contribution of CB in the system in addition to the aliphatic component of PU. Since MWCNT are UV active, considerable peaks can be observed in UV characterizations of nanotubes composites [Song, W. S, 2016]. The response towards UV enables the polymer nanocomposites with MWCNT fillers to be UV curable. As observed from Figure 5.41, the presence of CB and

the UV resistant PU resin will dominate over the UV active MWCNT in the hybrid ternary system resulting in absence of any peak in UV spectrogram.

c — 1 µm — EHT = 2.00 kV — WD = 6.6 mm — Signal A = SE2 — Mag = 4.50 K X — Date :27 Mar 2019 — Time :10:48:25 — ZEISS

d — 1 µm — EHT = 2.00 kV — WD = 6.6 mm — Signal A = SE2 — Mag = 4.50 K X — Date :27 Mar 2019 — Time :10:48:57 — ZEISS
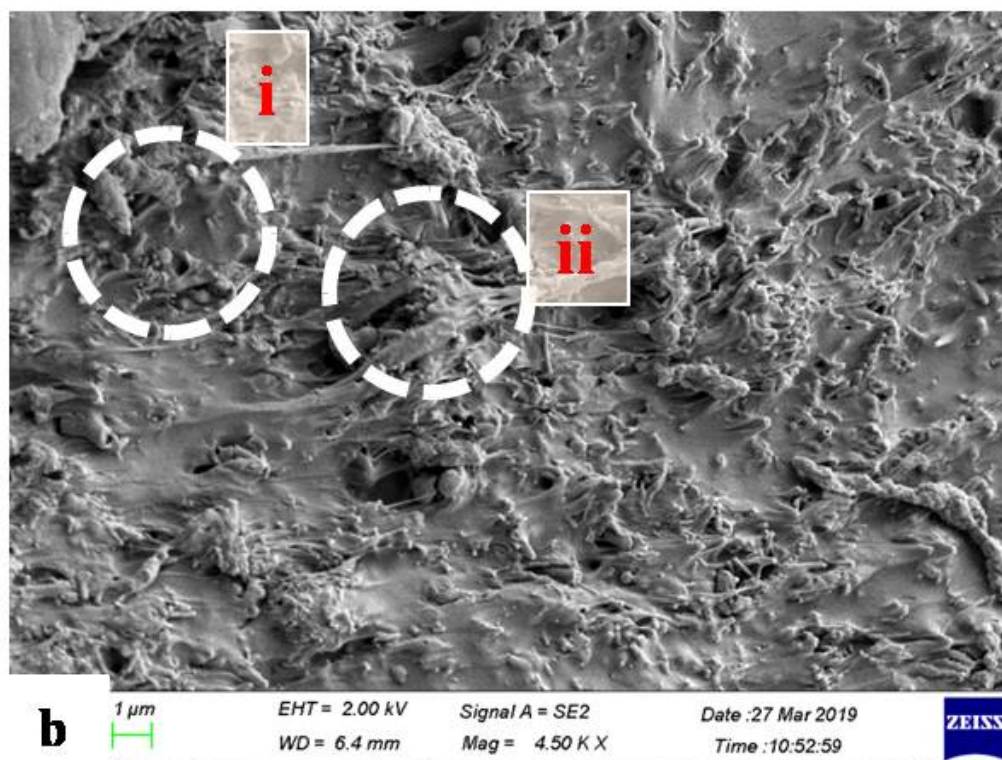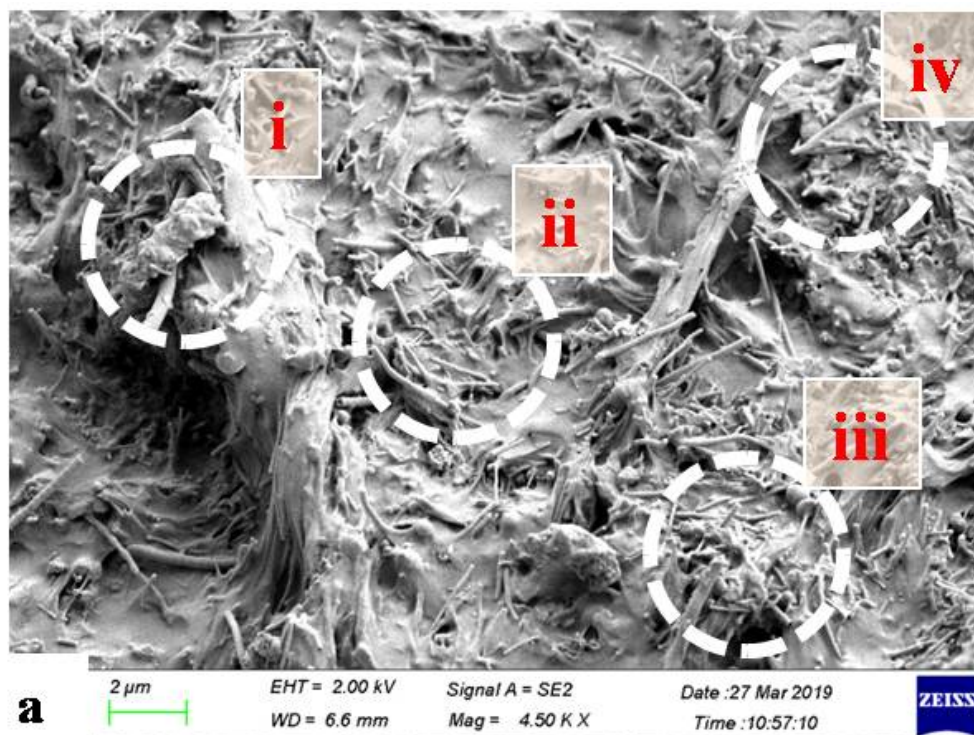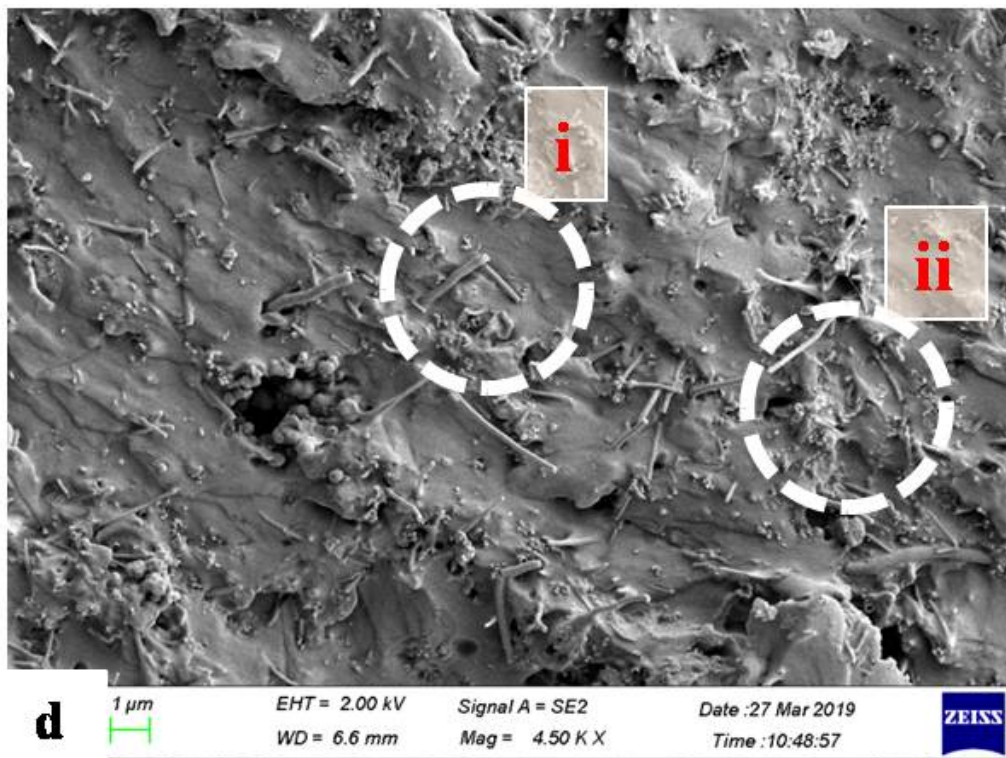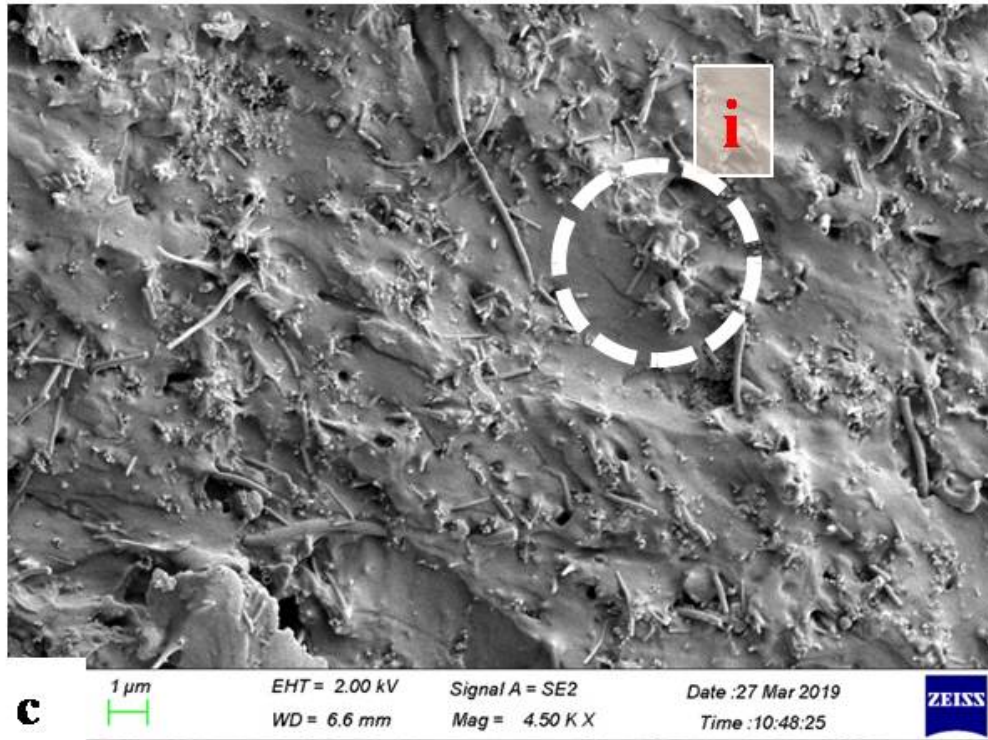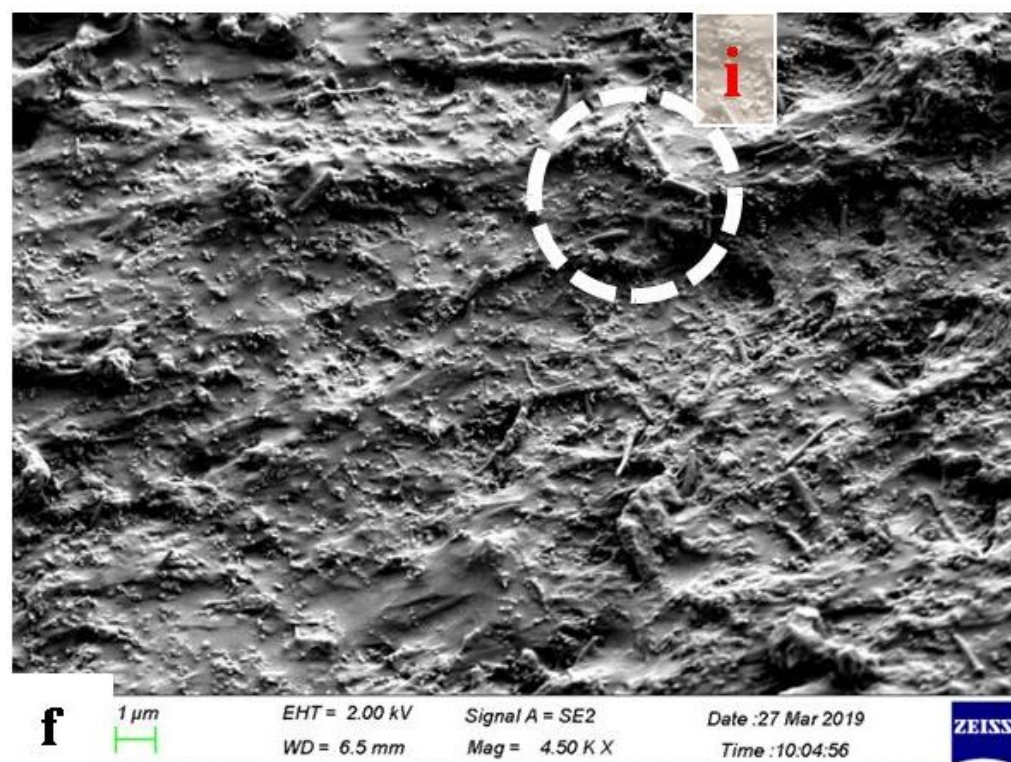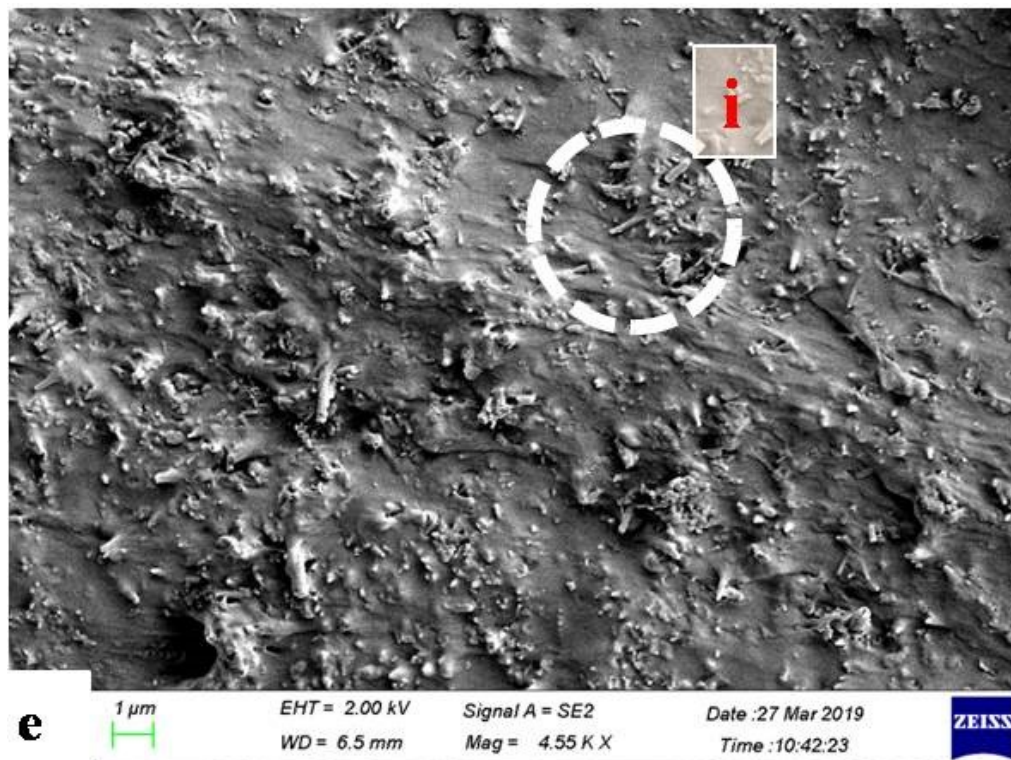
Figure 5.42 SEM micrographs showing varying CB – MWCNT loading; (a) 5% CB / 0.25% MWCNT; (b) 5% CB / 0.15% MWCNT; (c) 3% CB / 0.25% MWCNT; (d) 3% CB / 0.15% MWCNT; (e) 1% CB / 0.25% MWCNT; (f) 1% CB / 0.15% MWCNT

The hybrid nanocomposite was analysed for its microstructure and the dispersion of the fillers using scanning electron microscopy (as depicted in Figure 5.42 (a) to (f). The population density of the CB and MWCNT increased with filler loading, which can be observed from the SEM images.

SEM images give a clear picture regarding the dispersion, interaction of fillers & matrix and the possibility of contact or closeness of particles in the matrix. Figure 5.42(a) & (b) shows micrographs of 5% CB loading with MWCNT content of 0.25% & 0.15% from which it can be observed that the considerably high nanotubes content with CB led to agglomeration despite MWCNT being functionalized. The highlighted area representing 'i' in Figure 5.42(a) and 'ii' in Figure 5.42(b), shows the agglomeration of the CB and MWCNT fillers, hence negating the functionalisation effect of MWCNT. The highlighted regions 'ii', 'iii' and 'iv' of Figure 5.42(a) and 'i' in Figure 5.42(b) shows the closeness of CB & MWCNT resulting in continuous filler networks in the matrix. At higher CB loading of 5%, the functionalization advantage of MWCNT was found to be nullified and the effect of agglomeration was observed in the composite. As we move across the Figure 5.42(b) to (f), it can be observed that the agglomeration tendency was reduced with reduction in CB content. Figure 5.42(c) & (d) depicts micrographs of 3% CB loading with 0.25% & 0.15% MWCNT loading, where the filler dispersion were found uniform in the cross section. Reduction in CB from 5% to 3% shows results in fairly uniform dispersion of MWCNT as the effect of functionalisation is evident at lower CB loading. The regions representing 'i' in Figure 5.42(c), 'i' & 'ii' in Figure 5.42(d) shows the uniform dispersion of the fillers in the ternary system. Figure 5.42(e) & (f) shows 1% CB loading and 0.25% & 1.5% MWCNT loading, where the fillers were found well separated and no agglomeration was observed. The contact of MWCNT forming conductive networks is indicated with areas showing 'i' in both Figure 5.42(e) and (f). It can be inferred that there exists positive and negative synergy while mixing MWCNT and CB in a polymer matrix. From Figure 5.42(a) and (b), it can be understood that there exists a CB loading beyond which it affects the functionalization of the MWCNT resulting in agglomeration. Hence higher CB loading above 5% is found

ineffective towards uniform dispersion in a ternary hybrid system with functionalized MWCNT.

5.10.2 Thermal and mechanical

The T_g of the hybrid system for various filler loadings was obtained from the DSC analysis and was found to vary marginally with addition of MWCNT for matrix with CB(as depicted in Figure 5.43).
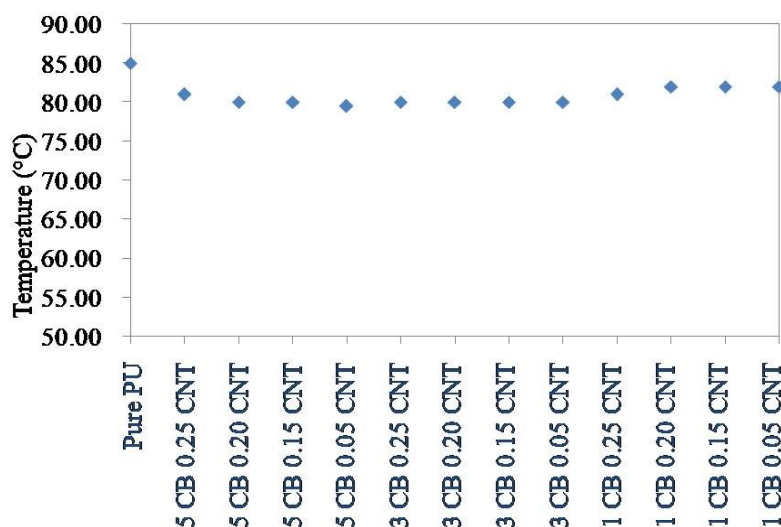
Figure 5.43 Glass transition temperature distributions of hybrid nanocomposites with varying CB and MWCNT loading

The basic PU resin was found to show high T_g of 85 °C as reported elsewhere by the authors [Arun et al., 2019a]. It is observed that at higher CB loading (at 5% CB), the T_g remains around 79.5°C which increases to 80°C while the CB loading reduces to 3% and subsequently to 82°C for 1% CB loading. MWCNT was found to have little effect on T_g of the system as the absorbed heat is transmitted to a larger area by the MWCNT having high aspect ratio inside the matrix. The nanotubes hinder the polymer chain movements at elevated temperature resulting in retaining the rigidity of the system and hence T_g is not reduced by its presence. The effect of CB as mentioned above can be interpreted as due to the plasticizing effect which facilitates chain movement at elevated temperature. The CB spherical fillers forms concentrated heat source by absorbing the heat provided to reach T_g.

This heat is transferred to the interface and thereby to the matrix by CB, resulting in reaching T_g of the material earlier [Arun et al., 2019a].

Hence, addition of CB to a MWCNT PU system forming a ternary hybrid composite was observed to affect the T_g by reducing it with increased CB loading. A positive synergy exists when both the fillers result in an enhancement in properties, whereas negative synergy denotes the degradation of the properties.

An increasing trend is observed in the elastic modulus of the hybrid nanocomposites with increasing CB and MWCNT loading. Figure 5.44 depicts the variation in modulus values for various CB and MWCNT loading.
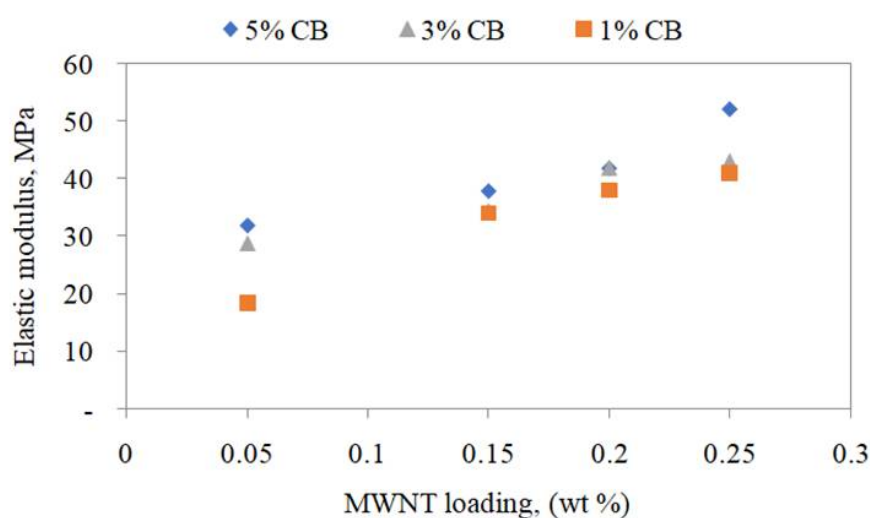
Figure 5.44 Change in elastic modulus with varying CB / MWCNT loading

It can be understood that the filler geometry, aspect ratio and the functionalisation of the fillers influence the bond strength and hence elastic modulus of a hybrid system. The carbon atoms in the carboxylic acid functional group of MWCNT forms covalent bonds with the PU resin linkages resulting in better mechanical modulus [Song, S. H, 2018]. Similarly, the near spherical CB in nano-scale resulted in larger surface to volume ratio leading to increased surface energy. This caused better interfacial adhesion in the particulate-filled system, thus resulting in increased elastic modulus.

From Figure 5.44, it can be observed that the modulus value increased with increase in CB loading for a constant MWCNT content. The increased CB loading resulted in larger surface energy leading to enhanced interfacial adhesion of CB to the matrix and thus contributing towards the increase of modulus values. Similar rate of increase in modulus was observed per CB loading while MWCNT was increased from 0.05% to 0.25% by weight. The modulus varied between 31MPa to 52MPa for 5% CB with increasing MWCNT loading. For 3% CB loading, modulus value ranged between 29MPa to 43MPa and for 1% CB loading, elastic modulus varied between 19MPa to 40MPa for increasing MWCNT content.

The hybrid system showed elongation upto 400% (3% CB, 0.25% MWCNT), which lies between the elongation reported for individual CB and MWCNT systems [Arun et al., 2019a, Huang, W. M et al., 2010]. The percentage elongation showed a reducing trend with increased filler loading, whereas 3% CB content and 0.25% MWCNT showed highest value among the combinations, which defines the trade-off between the CB and MWCNT content towards contribution to maximum strain to failure. The high specific surface area due the spherical geometry of CB system and the interfacial bonds attributes to the contribution of CB towards elongation of the hybrid system [Huang, W. M et al., 2010].

5.10.3 Electrical conductivity

The hybrid nanocomposite showed increasing electrical conductivity with increased MWCNT content per CB weight fraction. The conductivities varied from the order of 10^{-12} to 10^{-5} S/m, with 5% CB – 0.25% MWCNT combination showing highest conductivity. The process of electrical conductivity in a nanocomposite is explained by means of electron hopping or quantum tunnelling and by contact of fillers. The latter phenomenon is observed while the conducting fillers are separated by a minimum distance called tunnelling distance / barrier distance and the contact of fillers causes electron to move across the low resistance path causing electric current flow. The tunnelling distance depends on the resin and the filler conductivity, which is approximately 1 to 1.2 nm for PU

CB / MWCNT system [Arun et al., 2019b, Song, W. S, 2016; Sun, X. & Song, M, 2009]. Hence fillers coming closer than 1.2 nm form a continuous path for the electron resulting in conductive nanocomposites. Increased CB and MWCNT filler loading results in possibility of denser matrix with these fillers dispersed closer resulting in increased probability of conductive network formations. Figure 5.45 depicts the change in electrical conductivity for various combinations of CB and MWCNT systems.
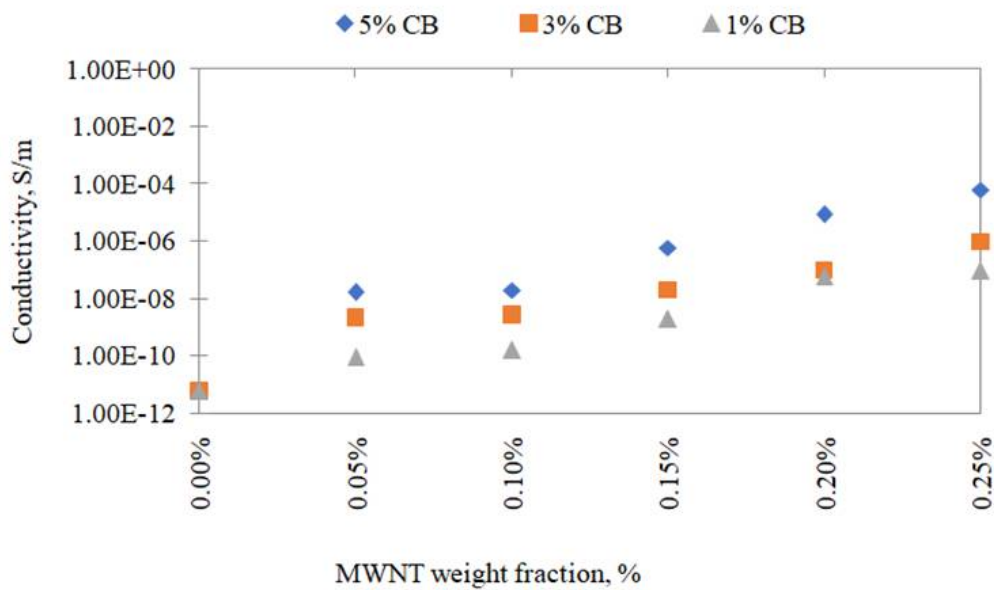
Figure 5.45 Electrical conductivity of nanocomposites as a function of the filler content

Compared to the observed conductivity of binary CB nanocomposite system at 1%, 3% and 5% loading, the combination conductivity values are higher as the MWCNT enhances the overall composite conductivity [Arun et al., 2019a]. From Figure 5.45, it can be observed that the conductivity of the system changes by an order of 2 with 2% increase in CB content (from 1% to 3% to 5%) for constant MWCNT loading. This signifies the formation of multiple filler networks causing rapid increase of filler content. The average conductivity of PU nanocomposite corresponding to 3% and 5% CB loadings in a binary system as per a previous work by the authors are 9.4×10^{-11} S/m and 1.3×10^{-9} S/m. Compared to these values, the conductivity of the hybrid system for 3% and 5% (refer Figure 5.45) varies from 10^{-9} to 10^{-6} S/m and 10^{-8} to 10^{-4} S/m respectively. The contribution of

MWCNT resulted in the large improvement of conductivity, by connecting the CB particles for electron paths in the hybrid system, as observed from the SEM images where the CB and MWCNT in contact. The synthesized hybrid system with combinations 5% CB – 0.15% MWCNT, 5% CB – 0.2% MWCNT, 5% CB – 0.25% MWCNT and 3% CB-0.25% MWCNT shows conductivity value above 10^{-6} S/m, which is the border line between insulators and conductors [Edwin Kashy et al., 2019]. The minimum filler content at which the composite changes from an insulator to conductor is referred as percolation threshold and the corresponding value for the synthesized dual filler hybrid nanocomposite system is 5% CB – 0.15% MWCNT. Thus the synthesized material becomes superior to the binary nanocomposites where the reported percolation thresholds are high [Arun et al., 2019a, Huang, W. M et al., 2010].

5.10.3.1 Relationship of time and T_g

Figure 5.46 depicts the relationship between the time to reach T_g+20°C and the temperature change with respect to the varied voltage for 5% CB – 0.25% MWCNT hybrid system.
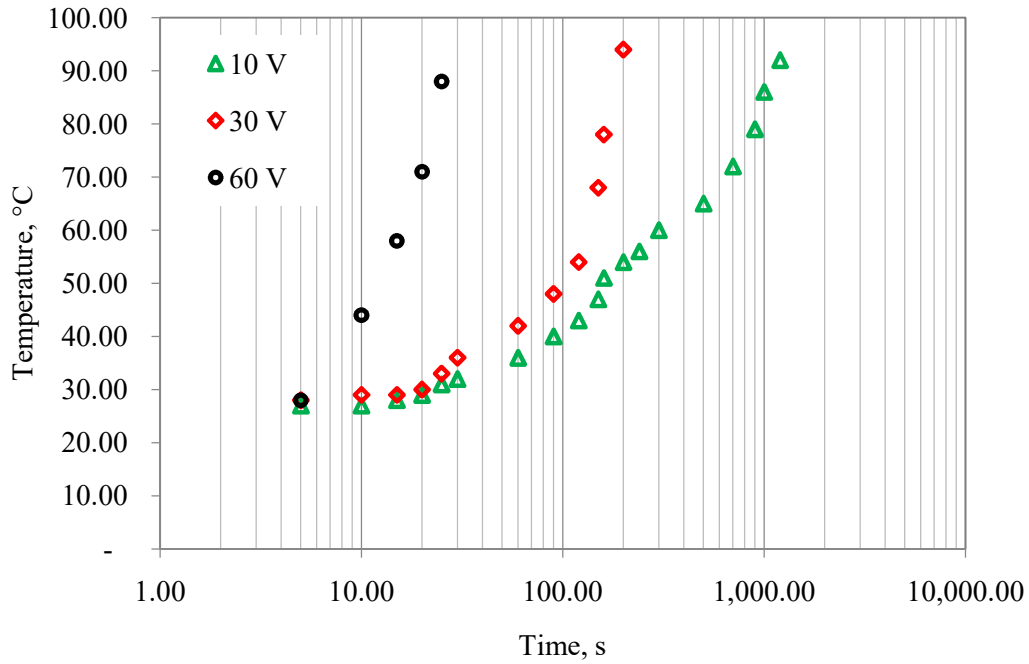
Figure 5.46 Variation in time to achieve transition with change in applied voltage (5% CB - 0.25% MWCNT)

The nanocomposite system gets heated up by joule heating while applying different voltage. For 10V, the plot shows a vertical-axis parabolic profile; whereas the plot gets linear as the applied voltage increases through 30V to 60V (refer Figure 5.46). Similar to the previous two systems, the increased energy supplied has facilitated the multiple network paths causing increased rate of heating.

5.11 Shape memory effect

Fold deploy test was employed for evaluating the Shape Memory Effect (SME) in a hybrid nanocomposite and to understand the synergistic contribution of individual fillers. The SME was evaluated for both thermal as well as electrical stimuli. From the synthesized hybrid system the sample with filler content 5% CB and 0.25% MWCNT was found optimal for SME demonstration. Since the maximum electrical conductivity was observed for 5% CB and 0.25% MWCNT combination, the same was chosen for SME demonstration.
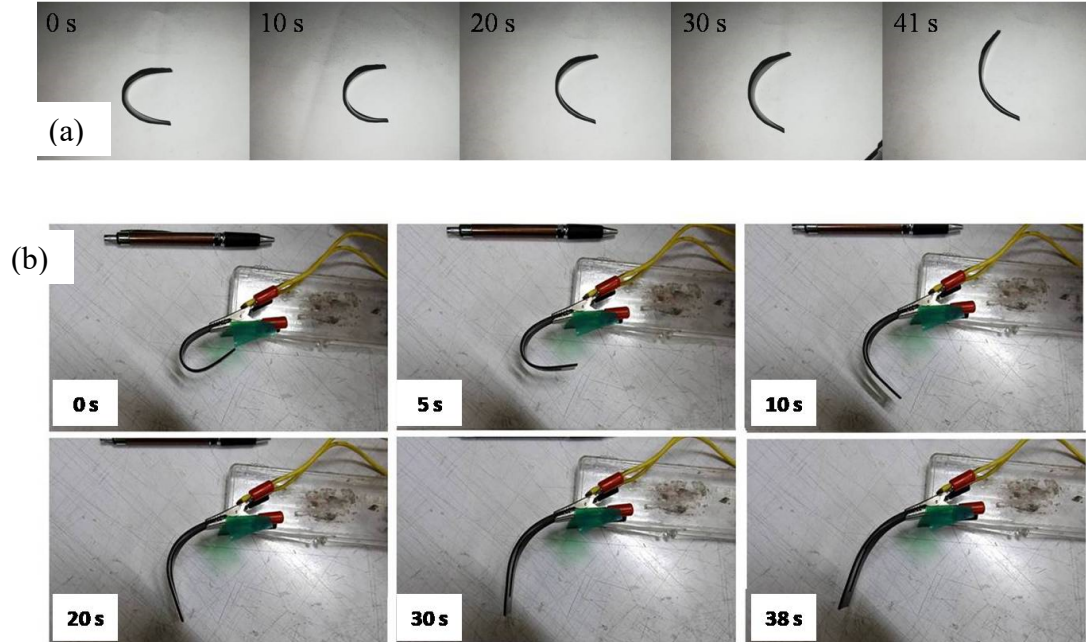
Figure 5.47 Shape memory demonstration using thermal and electrical stimuli; (b) thermally active SME recovering the original shape in 41 s; (c) electrically active SME recovering the original shape in 38 s

The sample was sliced to shape 'U' from cured hybrid nanocomposite and was used for electrical actuation. A thin rectangular strip of the sample was sliced for evaluation of SME by thermal stimulation. Figure 5.47 depicts both thermally and electrically stimulated shape memory effects. The shape memory is a property associated with the hard and soft domains of the PU resin which gets activated by heat. The fillers introduced in the resin matrix can facilitate heating of the polymer matrix by means of increasing the thermal or electrical conductivity. At lower filler content, the rate of heating of the system is slower and hence the efficiency and recovery speed will be lesser compared to higher filler contents. It was observed that lower filler loading were found to take longer duration (in the order of hours) which is attributed to the lower number of conductive networks formed in the matrix [Arun et al., 2018].

For shape memory evaluation, the sample was trained to a temporary shape 'U' after heating up to T_g + 20°C with suitable constraint. For thermal actuation, external heaters were used to achieve the T_g + 20°C whereas a DC power supply of 60V was connected to the specimen for electrical actuation. On training to the temporary shape, the sample is cooled to room temperature. The angle of shape fixity was measured against the original shape and was recorded for 10 discrete cycles.

5.11.1 Thermally activated SME

The sample which was trained to temporary shape (U shape as in Figure 5.47(a)) and cooled was then subjected to external heating by blow heater, to a temperature T_g + 20°C. Across the T_g, the material gets softened and the shape recovery was initiated and the original shape regained. On complete recovery, the final recovered angles as well as the duration of recovery were recorded and the efficiency of recovery was estimated from the angle of recovery for the 10 cycles [Arun et al., 2019a; 2019b; Fonseca, M. A et al., 2013]. Figure 5.48(a) shows a typical thermal actuation cycle of the hybrid system, where the 'U' shape gets transformed to original straight configuration on heating. The average shape recovery time for the 10 cycles was observed as 41 seconds with the average

shape fixity and recovery efficiency of 89.60% and 80.10% respectively. An individual CB system with 25% filler loading was used for shape memory evaluation by the authors in another work [Arun et al., 2019a]. The observed fixity and recovery efficiency was 99% and 94% for thermal stimuli and the complete recovery was observed in 50 seconds [Arun et al., 2019a]. Hence the hybrid system with 5% CB and 0.25% MWCNT was superior comparing the duration of shape recovery observed from 25% CB alone in PU system. It can be observed that the CB content came down to $1/5^{th}$ (5% from 25%) of the binary system by addition of MWCNT in the system, and thus featuring the contribution of MWCNT in the hybrid system.

5.11.2 Electrically activated SME

For electro-actuation, the sample was connected to 60V DC power supply and the recovered angles for each cycle were observed for 10 discrete trials. The virtual conductive networks formed by the fillers inside the matrix allow electron passage and results in joule heating of the system (refer Figure 5.48(b)) and when the system reaches the T_g of the material, initiates shape recovery due to the property of PU. The inclusion of CB and MWCNT fillers increased the electrical conductivity of the hybrid nanocomposite and the original shape was recovered in 38 seconds (average of 10 discrete cycles). The shape fixity and recovery efficiencies were recorded as 91.20% and 84.30% respectively for electro-actuation of the synthesized hybrid system with 5% CB and 0.25% MWCNT.

The binary system with 20% CB in PU matrix have shown a recovery time of 116 seconds by passing 60V DC [Arun et al., 2019b], whereas the hybrid ternary system synthesised has recovered the original shape in 38 seconds. The large aspect ratio of MWCNT is assumed to have formed bridges between the CB in the matrix forming continuous networks in the system (refer to Figure 5.39 (c), where the possible network formation is illustrated). Hence, a $1/4^{th}$ CB loading provide faster shape recovery in case of hybrid system while comparing with binary system of CB in PU. The recovery duration was also observed to be 38 s which is $1/3^{rd}$ of that of the binary system.

The significance of the hybrid nanocomposite system (CB-MWCNT-PU) over the binary system with CB-PU is depicted in Figure 5.48(a) & (b).
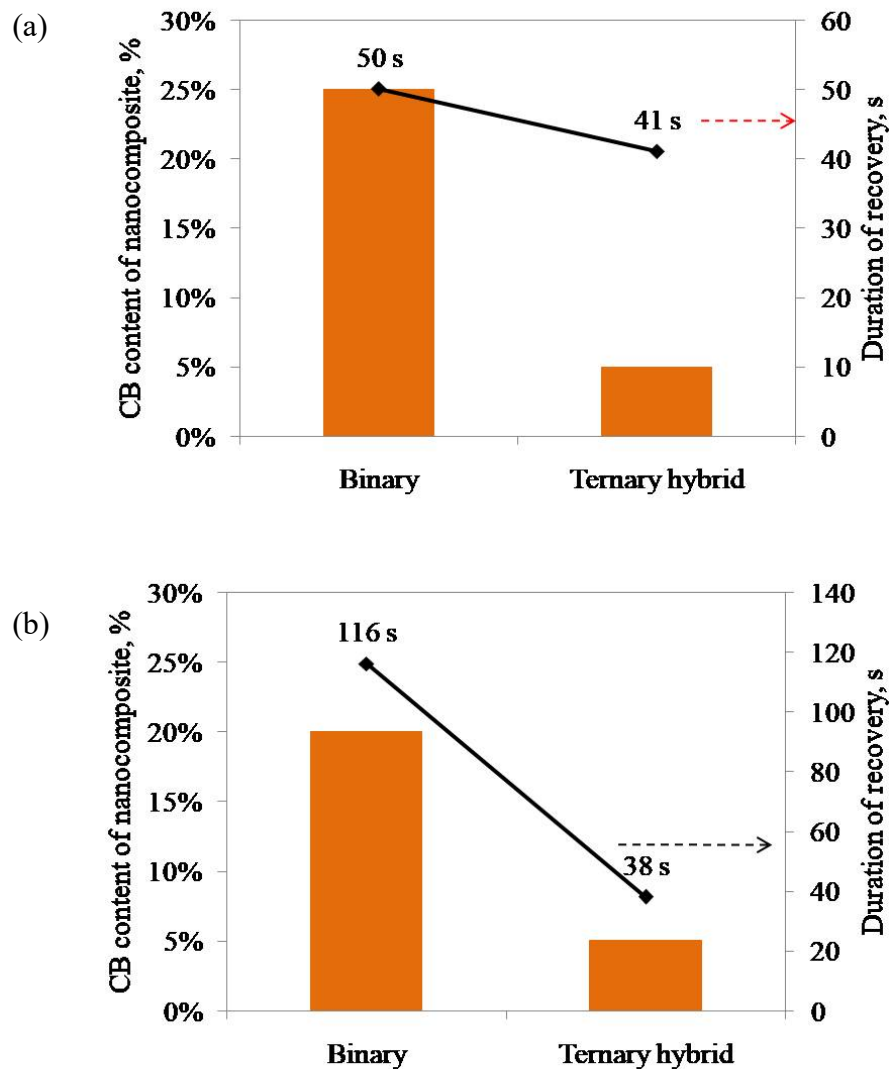
Figure 5.48 Advantage of hybrid nanocomposite system over the binary systems depicted in terms of CB loading for different stimuli; (a) Thermally activated SME – 25%CB (binary), 5%CB/0.25%CNT (hybrid); (b)Thermally activated SME – 20%CB (binary), 5%CB/0.25%CNT (hybrid)

The possible reduction in CB content for fixed MWCNT can be due to the high aspect ratio of nanotubes which while randomly distributed in the matrix form connections between the CB spherical particles and causing current conduction. The huge reduction in recovery time from 116 s to 38 s shows the formation of multiple three dimensional networks between CB and MWCNT fillers in the PU matrix.

5.12 Summary

A hybrid heterogeneous nanocomposite with varying content of CB and MWCNT was synthesized from high T_g PU resin matrix.

- Due to the presence of CB along with the basic resin property, the synthesized hybrid nanocomposite was found resistant to UV radiations.
- SEM micrographs revealed that at higher CB loading, the functionalisation of MWCNT was not found effective and agglomeration was observed.
- The T_g was found reducing at higher CB loading due to the plasticizing effect of the spherical geometry and the effect of CB acting as local heat source.
- Mechanical strength was found increasing with increased filler loading.
- The hybrid system showed increased electrical conductivity with increased MWCNT content per CB weight fraction.
- A percolation threshold value for the current CB-MWCNT combinations was obtained as with 5%CB/0.15% MWCNT, which is lower than the reported values for individual binary systems.
- The thermally activated shape memory recovery was achieved in 41 seconds (at 1/5th of the duration reported for 25%CB content in binary systems).
- For electrical stimuli, the original shape was recovered in 38 seconds for the current study against 116 seconds for 20% CB as reported.

CHAPTER.6

SUMMARY AND CONCLUSIONS

Materials those alter their behavior physically or morphologically on sensing any external stimuli such as electricity, magnetism, heat, moisture etc., have been on the research table since time immemorial. When the said alteration corresponds to memorizing the original shape of the material or structure, such materials assume the name shape memory materials. This thesis work tried to focus on the electrical stimuli response of shape memory materials, by synthesizing polymeric shape memory nanocomposites that are electro-active. Review of the relevant literature in the area helped to establish the requirement of such an investigation. A coherent narration of the details of raw materials that have gone into realization of the nanocomposite, the methods employed, characterization techniques, results and discussions are sequentially put forth in the chapters subsequent to the literature survey. A comprehensive attempt has been made to accomplish the listed objectives of the work with theoretical and substantial experimental validation. A concise summary of the significant contributions of the thesis along with the scope for future explorations based on the work are presented in this chapter.

6.1 Summary

An electrically conductive polyurethane shape memory composite using Carbon Black, Multi-Walled carbon NanoTubes and a combination of both in varying proportion was synthesized. A theoretical model to predict the electrical percolation threshold for the systems, based on geometric-statistical approach has been devised and evaluated based on the experimental outcomes. The combination of multiple fillers behaves different from that of individual filler system, and hence a synergy study was done with CB and MWCNT mixed in varying contents in polyurethane resin and the properties were evaluated. Shape

memory behaviors of the three systems were evaluated by electrical and thermal actuation, for evaluating the recovery speed, efficiency of shape fixity and recovery.

6.1.1 CB - PU SMP nanocomposite

The synthesized Polyurethane resin exhibited high glass transition temperature of 85°C compared to the published data which is attributed to the cross-linking adopted and the use of low molecular weight polyols. The use of aliphatic isocyanate gave an intrinsic stability against UV radiations for the resin which was further enhanced in the nanocomposite while CB was added as reinforcement filler. The usage of CB as filler enhances the stability against UV radiations by absorbing them and dissipating as heat energy, without affecting the material basic properties. The CB content was varied from 0% to 40% and was characterized for optimizing the filler for electro-active SME demonstration. The polymer microstructure, chemistry, hydrogen bonding, mechanical, thermal and electrical behaviours were studied for the CB polyurethane nanocomposite system.

A percolation threshold of 6% by weight of carbon was observed experimentally. The electrical conductivity of the PU-CB system was modelled using non-linear programming and optimisation in visual C language. A cubical volume element with CB spherical particles was dispersed in it for varying content and the possibility of the current conduction was evaluated for each case. Monte Carlo simulation method was adopted to understand the percolation behaviour of the system. Percolation probability of 0.5 was observed corresponding to 6.2% weight fraction of CB in PU matrix, as per the Monte Carlo simulation results. Hence the generated computer model was validated thus establishing a prediction tool for spherical nanofiller reinforced nanocomposites.

On passage of electricity, the nanocomposites with filler loading more than percolation threshold formed continuous networks, which facilitated joule heating of the system. The time required to achieve transition temperature of 85°C for varying voltages were quantified, that can help in choice of power supply for

specific applications in electro-activity. Thermal-active (by means of blow heaters) and Electro-active (by connecting to 60V power supply) shape memory behaviour was evaluated for 25% CB loading and the recovery time was found to be 50s and 26s respectively. High shape recovery efficiency of 94% and 98% were observed for thermal and electro-actuation for the system. The uniform volumetric heating resulted from joule heating of the system, with well dispersed filler was understood as the reason for improved efficiency in electro-active SMPC.

6.1.2 MWCNT - PU SMP nanocomposites

A comprehensive model based on structural orientation was developed for MWCNT PU nanocomposite system in visual C platform, which can predict the conductivity of nanocomposites with known filler characteristics. The model visualizes cylindrical nanotubes dispersed in a representative volume at random positions, and orientations for various filler contents. The possibility of formation of continuous conductive networks was verified for filler contents between 0.1% and 10% and simulated for various positioning of the nanotubes using Monte Carlo methods. The percolation threshold was obtained to be 0.38% by volume of nanotubes, which is equivalent to 0.19% by weight of MWCNT.

This percolation threshold value was verified by developing a PU MWCNT nanocomposite system with high T_g PU resin. The synthesized PU MWCNT nanocomposite was characterized for chemical, morphological studies and mechanical, thermal and electrical properties. The electrical conductivity measured for varying filler loading showed that 0.21% by weight of MWCNT correspond to the percolation threshold of the system. The close match of the percolation threshold between the model and the experiment established the reliability of the model.

This model can thus be a generalized tool for any polymer nanocomposite systems with nanotube fillers. The percolation threshold reported in this work is lowest among the data reported so far, which is advantageous as it enhances the nanocomposite properties with lesser amount of MWCNT. The developed PU

MWCNT nanocomposite was evaluated for its shape memory ability by thermal and electrical stimuli. Recovery efficiencies of 95.06% and 98.60% respectively for thermal and electrical actuation was obtained, which are highest among the reported data. 21s and 19s were the duration observed respectively for the thermal and electrically stimulated shape memory nanocomposites.

6.1.3 Synergistic studies on CB – MWCNT hybrid PU SMP nanocomposite

A hybrid heterogeneous nanocomposite with varying content of CB and MWCNT was synthesized from high T_g PU resin matrix. Due to the presence of CB along with the basic resin property, the synthesized hybrid nanocomposite was found resistant to UV radiations thus making it suitable for space applications. SEM micrographs revealed that at higher CB loading, the functionalisation of MWCNT was not found effective and agglomeration was observed. This depicts the existence of an optimal CB content (5% by weight) beyond which the uniform dispersion is affected. The T_g was found reducing at higher CB loading due to the plasticizing effect of the spherical geometry and the effect of CB acting as local heat source. Mechanical strength was found increasing with increased filler loading, which showed a positive synergy between CB and MWCNT towards the elastic modulus of the nanocomposite. The hybrid system showed increased electrical conductivity with increased MWCNT content per CB weight fraction. A percolation threshold value for the current CB-MWCNT combinations was obtained as with 5%CB/0.15% MWCNT, which is lower than the reported values for individual binary systems. SME was evaluated for both thermal and electrical stimuli individually and the recovery duration and efficiencies were recorded. The thermally activated shape memory recovery was achieved in 41 seconds (at $1/5^{th}$ of the duration reported for 25%CB content in binary systems). The shape fixity and recovery efficiency observed for thermally active SMPC were 89.60% and 80.10% respectively. For electrical stimuli, the original shape was recovered in 38 seconds for the current study against 116 seconds for 20% CB as reported. The corresponding shape fixity and recovery efficiencies of the synthesized hybrid system were observed to be as 91.20% and 84.30% respectively. The study has

explored the synergy of multi filler nanocomposite hybrid system and has compared the properties with binary systems and presents a combination of CB and MWCNT with better properties than binary nanocomposites.

A consolidated depiction of the summary of the work is shown in Figure 6.1
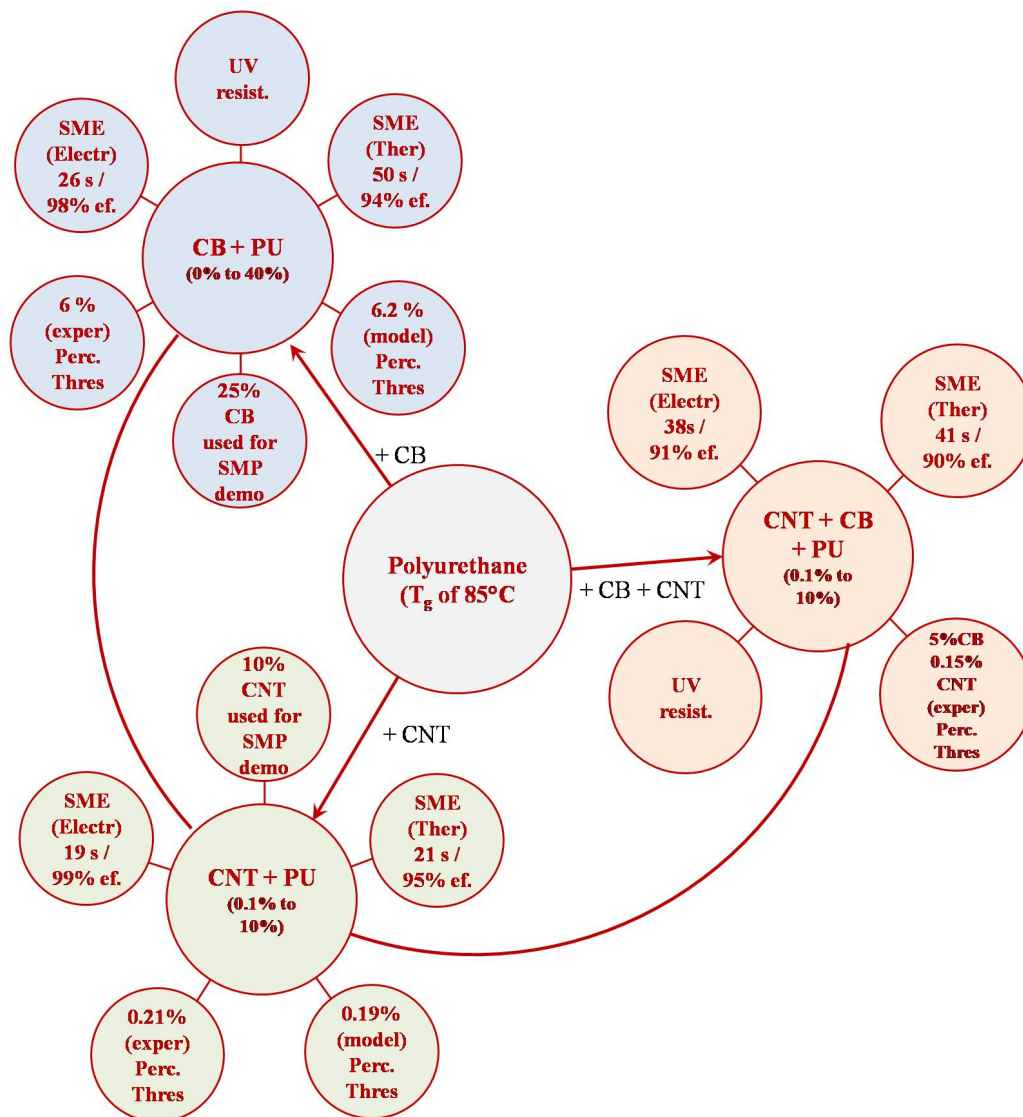
Figure 6.1 Spider diagram depicting the summary of the work

6.2 Significant contribution of the work

- A high glass transition PU shape memory polymer resin was synthesized with T_g of 85°C, which is highest among the reported, and was characterized for other basic properties

- The resin possesses the ability to resist harmful UV radiations, due to the presence of aliphatic diisocyanates in PU. Addition of CB as reinforcement fillers add to this ability by protecting the system from UV radiations, thereby making it qualify for space grade applications.

- CB PU, MWCNT PU and CB-MWCNT PU based nanocomposite systems were developed characterized for its chemical, physical and morphological features

- A generalized reliable structural model for understanding and predicting percolation in nanocomposite systems was developed and established

- The synergistic combination studies of CB and MWCNT proved to be advantageous in terms of joule heating and faster recovery compared to the binary systems.

- Electro-active shape memory was evaluated and established for CB, MWCNT and combination of CB & MWCNT systems with PU matrix.

- Highest recovery efficiency and fastest among the recovery speed for PU based shape memory systems were observed while comparing with the reported data.

6.3 Scope for future work

Enough scope is available in both experimental and modeling of nanocomposites with this work as basis. The possibilities of future explorations with this work as a platform are discussed in this section.

- Antenna structures, reflectors and flexible solar substrates can be realized in proto-scale to study the scale effect of the recovery of shape memory system developed in this work.

- The model developed in this work can be extended to 2-D systems like graphene oxide papers as reinforcements in polymer matrices.

- A modeling approach with nano fillers having shapes other than those discussed in this work will be a novel attempt towards geometric-statistical modeling concepts.

- A consideration towards the thermodynamic aspects of heat transfer inside the system between the filler and matrix can give an insight on the micro-aspects of joule heating phenomena inside a shape memory nanocomposite system.

- The interface between filler and matrix plays a major role in electrical current conduction, which can be studied for different geometry of fillers.

- Modeling of multi-filler systems with different geometry and contents can be useful in predicting the electrical properties of such systems.

- Since usage of isocyanates is not safe for materials in direct contact with human body, non-isocyanate polyurethane shape memory studies can be a unique attempt.

6.4 Closure

The comprehension of this investigation provides the liberty to the researchers and designers to choose an alternate simplified system away from the conventional actuation mechanisms. An understanding of the conductivity phenomenon in nanocomposites helps to deduce different combinations of the fillers and to arrive at the optimal composition theoretically prior to synthesis. The reliable model established for tubular and spherical geometry nanofillers can be used for predicting the electrical percolation threshold of nano-systems, which can help to narrow the band of experimental trials. The synergistic approach opens up the horizons for combining the advantages of individual nanofillers to create novel materials with superior properties.

Reference

1. AAllaoui and N El,Bounia. 2009. How carbon nanotubes affect the cure kinetics and glass transition temperature of their epoxy composites?.eXPRESS Polymer Letters.; **3(9)**: 588-594

2. AczelAkos. Modelling of an electroactivepolymer actuator. 2012. Procedia Engineering;**48**:1-9

3. Aguilar J O. Bautista-Quijano J R. Avilés F. 2010. Influence of carbon nanotube clustering on the electrical conductivity of polymer composite films, Express Polymer Letters, **4(5):** 292-299

4. Ahir, S. V., Huang, Y. Y., Terentjev, E. M., 2008. Polymers with aligned carbon nanotubes: Active composite materials, Polymer, **49(18):** 3841-3854

5. Ahmad M, Xu B, Purnawali H, et al., 2012. High performance shape memory polyurethane synthesized with high molecular weight polyol as the soft segment. ApplSci;**2**:535–548

6. Ajayan, Pulickel M. Schadler, Linda S. Giannaris, Cindy. et al., 2000. Single-Walled Carbon Nanotube - Polymer Composites : Strength and Weakness. *Adv. Mater. Res.***12**, 750–753.

7. Ajayan, Pulickel M. Tour, James M, 2007. Nanotube composites, Nature, **447(28)**:1066-1068

8. Akos A. 2012. Modelling of an electroactive polymer actuator. ProcediaEng;**48**:1–9

9. Alan, Lai. Zehui, Du. Chee, Lip, Gan. et al., 2013. Shape Memory and Superelastic Ceramics at Small Scales, American Association for the Advancement of Science (AAAS), Science 341, no. **6153**: 1505–1508.

10. AmalEsawi and Mahmoud Farag, 2007. Carbon nanotube reinforced composites: Potential and current challenges. Materials & Design; **28**: 2394-2401

11. Amirhossein, Biabangard. Oskouyi. Pierre Mertiny. 2011. Monte Carlo model for the study of percolation thresholds in composites filled with circular conductive nano-disks. Procedia Engineering; **10**: 403–408

12. Amy M Marconnet.Namiko Yamamoto. Matthew A Panzer et al., 2011. Thermal Conduction in Aligned Carbon Nanotube- Polymer Nanocomposites with High Packing Density, American Chemical Society Nano **5(6)**: 4818–4825

13. Andreas Thess, Roland Lee, Pavel Nikolae et al., 1996. Crystalline Ropes of Metallic Carbon Nanotubes. Science; **273 (5274)**: 483-487

14. AnettKiraly, FerencRonkay.2015. Temperature dependence of electrical properties in conductive polymer composites. Polymer Testing; **43**: 154-162.

15. Arnold Steven M. 2012. Materials selection for aerospace, Introduction to Aerospace Materials: NASA/TM-2012-217411, **E-18042,** NASA Glenn Research Center; Cleveland, OH, United States

16. Asiri, A. M. 2016. Nanocomposites and Importance of Nanofiller in Nanocomposites. *Dev. Prospect. Appl. Nanosci. Nanotechnol.* 157–179

17. Backes, E. H., Passador, F. R., Leopold, C., et al., 2018.. Electrical, thermal and thermo-mechanical properties of epoxy/multi-wall carbon nanotubes/mineral fillers nanocomposites. *J. Compos. Mater.* **52**, 3209–3217

18. Balasubramanian M. 2014.Composite materials and processing. Boca Raton: CRC Press;. **ISBN: 9781439879351**

19. Balberg I 2002. A comprehensive picture of the electrical phenomena in carbon black – polymer composites. Carbon **40**: 139–143

20. Behl, M. and Lendlein, 2007. A. Shape-memory polymers are an emerging class of active polymers that. Mater. Today **10**, 20–28

21. Behl, Marc. Lendlein, Andreas., 2007. Shape-memory polymers, Materials Today, **10(4)**: 20-28

22. Belashi Azita 2011, PhD thesis, Theses and Dissertations. 525. The University of Toledo

23. Bertei, Antonio. Choi, H.-W, J.G. Pharoah et al., 2012. Percolating behavior of sintered random packings of spheres. Powder Technology, **231**: 44–53

24. Bhattacharya, M. 2016. Polymer nanocomposites-A comparison between carbon nanotubes, graphene, and clay as nanofillers. Materials (Basel). **9**, 1–35

25. Biabangard, Oskouyi, Amirhossein, Sundararaj, Uttandaraman and Mertiny, Pierre. 2014. Tunneling Conductivity and Piezoresistivity of Composites Containing Randomly Dispersed Conductive Nano-Platelets. Materials **7**: 2501-2521

26. Biju, R., C. P. Reghunadhan Nair, 2013. Synthesis and characterization of shape memory epoxy-anhydride system, Journal of Polymer Research, **20(2)**: 82p

27. C.C. Wang, W.M. Huang, Z. Ding, Y. Zhao, H. Purnawali., 2012. Cooling-/water-responsive shape memory hybrids, Composites Science and Technology **72:** 1178–1182

28. Cai, Wen-Zhong. Tu, Shan-Tung and Gong, Jian-Ming. 2006. A Physically Based Percolation Model of the Effective Electrical Conductivity of Particle Filled Composites. Journal of Composite Materials, 40/23: 2131-2142

29. Cao Qing, Song Yihu, Tan Yeqiang et al. 2010. Characterization of carbon black-filled immiscible polypropylene/polystyrene blends. CARBON **48**: 4268–4275

30. Chaterji, Somali. Kwon, Keun. Park, Kinam., 2005. Smart Polymeric Gels: Redefining the Limits of Biomedical Devices, Biophysical Chemistry, **257(5)**: 2432-2437

31. Chawla, K, Krishnan, 2014. Composite materials: Science and Engineering, Springer international edition **ISBN: 9781441931245**

32. Chen Wei, Tao Xiaoming and Liu Yuyang. 2006. Carbon nanotube-reinforced polyurethane composite fibers, Composite science and technology.**66**:3029-3034

33. Chiang, Tsung-Han and F, Wager, John. 2018. Electronic Conduction Mechanisms in Insulators. IEEE transactions on electron devices **65(1)**:223-230

34. D. He, N.N. Ekere and L.Cai 1999. Computer simulation of random packing of unequal particles. Physical review E, Vol. **60 (6)**:7098-7104

35. Dale, M, Pitt. James, P, Dunne and Edward, V, White., 2015. A Wind Tunnel Test of the Full scale Boeing Multi-Functional Aircraft Inlet, Multifunctional Structures / Integration of Sensors and Antennas, Meeting Proceedings **RTO-MP-AVT-141, 16**:1 – 16

36. Davidson, Jacob D. Goulbourne, N. C., 2015. Microscopic mechanisms of the shape memory effect in crosslinked polymers, Smart Materials and Structures, **24(5)**: 055014 -27

37. Deng, Zexing. Guo, Yi. Zhao, Xin. Li et al., 2016. Stretchable degradable and electroactive shape memory copolymers with tunable recovery temperature enhance myogenic differentiation, Acta Biomaterilia **46**: 234-244

38. DI, Arun, KS Kumar Santhosh, Satheesh Kumar B, et al., 2019. High glass-transition polyurethane-carbon black electro-active shape memory nanocomposite for aerospace systems. Mater Sci Technol.;**35(5)**:596-605

39. DI, Arun, P Chakravarthy, R Arockiakumar, et al. 2018. Shape memory materials. Boca Raton: CRC Press;. **ISBN: 9780815359692**

40. DI, Arun, P Chakravarthy, S B Girish et al., 2019.Experimental and Monte Carlo simulation studies on percolation behaviour of shape memory polyurethane carbon black nanocomposite. Smart Materials and Structures.; **28(5):** 055010-055021

41. Ding, Zhen., 2012. Shape Memory Hybrids: Mechanism and Design for Tailored Properties, (Post graduate thesis work), School of Mechanical and Aerospace Engineering Nanyang Technological University

42. Dorigato, A., Brugnara, M. & Pegoretti, A. 2018. Synergistic effects of carbon black and carbon nanotubes on the electrical resistivity of poly(butylene-terephthalate) nanocomposites. *Adv. Polym. Technol.* **37**, 1744–1754.

43. Du, Fei Peng. Ye, En Zhou. Yang, Wen. et al., 2015. Electroactive shape memory polymer based on optimized multi-walled carbon nanotubes/polyvinyl alcohol nanocomposites, Composites Part B: Engineering, **68**: 170-175

44. Du, H Y. Liu, L W. Chen, F L. et al., 2014. Design and manufacturing smart mandrels using shape memory polymer, Proceedings of International Conference on Computational Methods, **5**: 1-8

45. Dyana Merline, J. Reghunadhan Nair, C P., 2012. Carbon / epoxy resin based elastic memory composites, Eurasian Chemico-Technological Journal, **14(3):** 227-232

46. Edwin Kashy, Eustace E. Suckling et al., 2019. Electricity. Encyclopaedia Britannica, inc. https://www.britannica.com/science/electricity/Conductors-insulators-and-semiconductors. Access Date: April 28, 2019

47. Fallis, A.G., 2013. Applications of shape memory alloys in space engineering past and future, Journal of Chemical Information and Modeling, **59(9)**: 1689-1699

48. Fang, Guangqiang. Peng, Fujun; Wenxiao Lee. 2010. Shape Memory Polymer Composite and its Applications in Deployable Space Truss Structures, Materials and Structures Symposium (C2), **5:** 6718p

49. Feller, J.-F. Electrically Conductive Nanocomposites: Chapter: 6. in Comprehensive Composite Materials II (ed. T. Peijs; E. T. Thostenson; C. H. Zweben; P. Beaumont) 2, 248–314 (Elsevier, 2018). **ISBN: 9780081005330**

50. Feng Chuang and Jiang Liying 2013. Micromechanics modeling of the electrical conductivity of carbon nanotube (CNT)– polymer nanocomposites. Composites: part A. **47**: 143-149

51. Flory, P. J., and Rehner, J., Jr., 1943. Statistical Mechanics of Crosslinked Polymer Networks, J. Chem. Phys., 11, 512p

52. Friedrich, Klaus and Breuer, Ulf. 2015. Multifunctionality of Polymer Composites. Elsevier. **ISBN: 9780323264341**

53. Fonseca, M. A. Abreu, B. Gonçalves, F. A M M et al., 2013. Shape memory polyurethanes reinforced with carbon nanotubes. Compos. Struct. **99**, 105–111

54. G, T, Nolan and P, E, Kavanagh. 1992. Computer simulation of random packing of hard spheres. Powder technology; **72**: 149-155

55. Gall, K., 2002. Shape memory polymer nanocomposites, Acta Materialia, **50(20)**: 5115-5126

56. Garrett JT, Runt J, Lin JS. 2000. Microphase Separation of Segmented Poly(urethane urea) Block Copolymers, Macromolecules. **33(17)**:6353-6359

57. George W. 2015. Handbook of UV degradation and stabilization. Canada: ChemTec Publishing. **ISBN 9781895198867, 1895198860**

58. Gopal, N., Chae, Y., Jin, H. & Cho, J. W. 2007. Science and Influence of carbon nanotubes and polypyrrole on the thermal , mechanical and electroactive shape-memory properties of

polyurethane nanocomposites. **67**, 1920–1929

59. Graham A. Rance, Dan H. Marsh, Robin Nicholas, et al. 2010. UV–vis absorption spectroscopy of carbon nanotubes: Relationship between the π-electron plasmon and nanotube diameter. Chemical Physics Letters, **493**: 19-23.

60. Gross, Korey Edward., 2008. Mechanical Characterization of Shape Memory Polymers to Assess Candidacy as Morphing Aircraft Skin (Post graduate thesis work), University of Pittsburgh, Pennsylvania

61. Gu Shuying, Yan Beibei, Liu Lingling et al. 2013. Carbon nanotube-polyurethane shape memory nanocomposites with low trigger temperature, European polymer journal, **49**:3867-3877

62. Gunes IS. 2009. Analysis of shape memory properties of polyurethane nanocomposites PhD thesis, The University of Akron Ohio USA

63. H Lu, Y Yao, L Lin. 2013. Carbon-based reinforcement in shape-memory polymer composite for electrical actuation. Pigment Resin Technol, **43(1)**: 26–34

64. Hager, Martin D. Bode, Stefan. Weber, Christine. Schubert, Ulrich S., 2015. Shape memory polymers: Past, present and future developments, Progress in Polymer Science, **49**: 3-33

65. Han, Z. and Fina, A. 2011Thermal conductivity of carbon nanotubes and their polymer nanocomposites: A review. *Prog. Polym. Sci.* **36**, 914–944

66. Hartl, D J. Lagoudas, D C., 2007. Aerospace alications of shape memory alloys, Journal of Aerospace Engineering, **221(April)**: 535-552

67. Hayashi, Shunichi. Drive, Grove. Industry, Mitsubishi Heavy., 2003. Applications of cold hibernated elastic memory (CHEM) structures, Proceedings of SPIE - The International Society for Optical Engineering., (**August**): 5056

68. He Yong, Zhang Xiniya, Runt James. 2012. The role of diisocyanate structure on microphase separation of solution polymerized polyureas, Polymer, **55**: 906-913

69. Hiroshi, Aida. Koji, Nishida. Itaru, Awane., 1979. The Glass Transition Temperatures of Copolymers of N-Alkyl Substituted Maleimide and Methylacrylate, Memoirs of the Faculty of Engineering Fukui University, **27(1)** :49-62

70. Hsu-Chiang Kuan, Chen-Chi M. Ma, Wei-Ping Chang et al. 2005. Synthesis, thermal, mechanical and rheological properties of multiwall carbon nanotube/waterborne polyurethane nanocomposite. Composites Science and Technology, **65**: 1703–1710

71. Hu Jinlian, Zhu Yong, Huang Huahua et al., 2012. Recent advances in shape-memory polymers: Structure, mechanism, functionality, modeling and applications, Progress in Polymer Science, **37(12)**:1720-1763

72. Hu, Ning. Masuda, Zen. Fukunaga and Hisao. 2007. Prediction of electrical conductivity of pplymer filled by carbon nanotubes. Proceedings of 16th International conference on composite materials, Kyoto Japan. **FrGM1-03**

73. Huang W, M, Yang B, Yong FQ. 2012. Polyurethane shape memory polymers. Boca Raton: CRC press;. **ISBN: 9781138075009**

74. Huang W, M,. Y, Zhao. C, C, Wang. Z, et al., 2012. Thermo / chemo-responsive shape memory effect in polymers: A sketch of working mechanisms, fundamentals and optimization, Journal of Polymer Research, **19(9)**: 952-986

75. Huang W, M. 2010. Thermo-Moisture Responsive Polyurethane Shape Memory Polymer for Biomedical Devices. The Open Medical Devices Journal. **2**:11-19

76. Huang, W. M. Ding, Z. Wang, C. C. Wei, et al., 2010. Shape memory materials, Materials Today, **13(7-8)**: 54-61 **ISBN: 9781138075009**

77. Huang. W, M., 2013. Shape Memory Polymers (SMPs) – Current Research and Future Applications, AZO Materials: 1-7

78. Huang.W, M. C.L. Song,Y.Q. Fu,C.C. Wang,Y. 2013. Shaping tissue with shape memory materials, Advanced Drug Delivery Reviews, **65(4)**: 515-535

79. Icardi, U. Ferrero, L., 2009. Preliminary study of an adaptive wing with shape memory alloy torsion actuators, Materials and Design, **30(10)**: 4200-4210

80. Ismail, H., Ramly, A. F. and Othman, N. 2011. The effect of carbon black/multiwall carbon nanotube hybrid fillers on the properties of natural rubber nanocomposites. *Polym. - Plast. Technol. Eng.* **50**, 660–666.

81. J, L, Finney. 1976. Fine structure in randomly packed, dense clusters of hard spheres. Materials Science and Engineering **23 (2–3)**: 199–205

82. Jang, S.H and Yin, H. 2016. Characterization and modeling of the effective electrical conductivity of a carbon nanotube / polymer composite containing chain-structured ferromagnetic particles. Journal of composite materials. **51(2)**: 171-178

83. Jason M. Keith, Julia King and, Rodwick L. Barton. 2006. Electrical conductivity modeling of carbon-filled liquid-crystalline polymer composites. Journal of Applied Polymer Science, **102**: 3293 - 3300.

84. Javid, S. Vatankhah, M., 2016. Fundamental investigation on the mechanisms of shape memory polymer reversibility, International Journal of Chemical Studies, **4(4)**: 43-45

85. Jiang, Qian. Wang, Xin. Zhu, Yuntian. Hui, David. Qiu, Yiping., 2014. Mechanical, electrical and thermal properties of aligned carbon nanotube/polyimide composites, Composites Part B: Engineering, 56: 408-412

86. Jonathan N. Coleman, Umar Khana, Werner J.Blaua et al. 2006. Small but strong: A

review of the mechanical properties of carbon nanotube–polymer composites. Carbon, 44(9): 1624-1652

87. Jung, Y. C., Yoo, H. J., Kim, Y. A., et al., 2010. Electroactive shape memory performance of polyurethane composite having homogeneously dispersed and covalently crosslinked carbon nanotubes. Carbon N. Y. 48, 1598–1603.

88. K S. Santhosh Kumar, Biju, R. Reghunadhan Nair, C P., 2013. Progress in shape memory epoxy resins, Reactive and Functional Polymers, 73(2): 421-430

89. K. Fan, W. M. Huang, C. C. Wang, Z et al., 2011. Water-responsive shape memory hybrid: Design concept and demonstration, eXPRESS Polymer Letters 5(5) :409–416.

90. Kaplanoglu, Erkan., 2012. Design of Shape Memory Alloy-Based and Tendon-Driven Actuated Fingers Towards a Hybrid Anthropomorphic Prosthetic Hand, International Journal of Advanced Robotic Systems, INTECH, 9(77) :1-6

91. Keith Jason M, A. King Julia and L. Barton Rodwick. 2006. Electrical conductivity modeling of carbon-filled liquid-crystalline polymer composites. Journal of Applied Polymer Science. **102**: 3293–3300

92. Ketan S. Khare and Rajesh Khare. 2013. Effect of Carbon nanotube dispersion on glass transition in cross-linked epoxy carbon nanotube nanocomposites: role of interfacial interactions. J. Phys. Chem. B.; 117: 7444-7454.

93. Kim Byung Kyu, Lee Sang Yup and Xu Mao. 1996. Polyurethanes having shape memory effects, Polymer, 37: 5781-5793

94. Kim, J.B., Lee, S.K., & Kim, C.G. 2009, proceedings of ICCM17, Edinburgh, UK:1-11

95. Kirkpatrick Scott. 1973. Percolation and conduction, Reviews of modern physics, 45(4):574-588

96. Kong, Deyan. Xiao, Xinli., 2016. High Cycle-life Shape Memory Polymer at High Temperature, Scientific Reports-Nature Publishing Group **92** :1-10

97. Konstantin, Sobolev and Adil, Amirjanov. 2007. The simulation of particulate materials packing using a particle suspension model. Advanced Powder Technol; **18(3)**: 261–271

98. Kremer F, Ezquerra T A, Mohammadi M et al. 1988. Solid State Communications **66(2)**: 153-157

99. Kuksenok, Olga. Balazs, Anna C. Liu, Y. Harris, V. Nan. et al., 2016. Stimuli-responsive behavior of composites integrating thermo-responsive gels with photo-responsive fibers, Materials Horizons, **3(1)**: 53-62

100. Kulakov Vladimir, Aniskevich Andrey, Ivanov Sergey et al. 2016. Effective electrical conductivity of carbon nanotube–epoxy nanocomposites, Journal of composite materials.1-10

101. Kumar, S. Sun, L. L. Caceres, S. et al. 2010. Dynamic synergy of graphitic nanoplatelets and multi-walled carbon nanotubes in polyetherimide nanocomposites. Nanotechnology 21

102. Kyeong Su and Kim Byung Kyu. 2013. Synthesis and properties of shape memory graphene oxide/polyurethane chemical hybrids, Wiley online library, -Sept:1-6

103. L. Barton Carter Rodwick 2008, PhD thesis, Michigan Technological University

104. L, Barton, Rodwick. M, Keith, Jason, A, King, Julia. 2007. Electrical conductivity model evaluation of carbon fiber filled liquid crystal polymer composites. Journal of Applied Polymer Science. **106**: 2456–2462

105. L. Bokobza, J. Zhang. 2012. Raman spectroscopic characterization of multiwall carbon nanotubes and of composites. eXPRESS Polymer Letters. **6(7)**: 601–608

106. L.F. Liu, Z.P. Zhang, A.B. Yu 1999. Dynamic simulation of the centripetal packing of mono-sized spheres Physica A: Statistical Mechanics and its Applications; **268**: 433–453

107. Lan, Xin. Leng, Jin Song. Liu, Yan Ju. et al., 2008. Investigate of Electrical Conductivity of Shape-Memory Polymer Filled with Carbon Black, Advanced Materials Research, **47-50**: 714-717

108. Lan, Xin. Zhang, Ruirui. Liu, Yanju.et al., 2011. Fiber Reinforced Shape-Memory Polymer Composite and Its Application in Deployable Hinge in Space, Proceedings of 52nd AIAA/ASME/ASCE/AHS/ASC Structures, Structural Dynamics and Materials Conference, Denver, Colorado: 1-10

109. Lau, Kin-Tak. Hui, David., 2002. Effectiveness of using carbon nanotubes as nanoreinforcements for advanced composite structures, Carbon, **40(9)**: 1605-1606

110. Leng J S, Huang WM, Lan X *et al*. 2008. Significantly reducing electrical resistivity by forming conductive Ni chains in a polyurethane shape memory polymer/carbon black composite, Appl Phys Lett **92**:204101.

111. Leng Jinsong, Lu Haibao, Du Shanyi 2008, Proceedings of 49th AIAA/ASME/ASCE/AHS/ASC Structures, structural dynamics and material conference Schaumburg. **April**:2203

112. Leng, J. S. Lan, X. Liu, Y. J. Du, S. Y. Huang, W. M. Liu, N. Phee, S. J. Yuan, Q., 2008. Electrical conductivity of thermoresponsive shape-memory polymer with embedded micron sized Ni powder chains, Applied Physics Letters, **92(1)**: 9-11

113. Leng, Jinsong. Lan, Xin. Liu, Yanju. Du, Shanyi., 2011. Shape-memory polymers and their composites: Stimulus methods and applications, Progress in Materials Science, **56(7)**: 1077-1135

114. Leng, Jinsong. Lu, Haibao. Du, Shanyi., 2008. Conductive Shape Memory Polymer Composite Technology and Its applications in aerospace, proceedings of 49th

AIAA/ASME/ASCE/AHS/ASC Structures, structural dynamics, and materials conference; 16th AIAA/ASME/AHS adaptive structures conference, Schaumburg, Illinois, April: 1-8

115. Leng, Jinsong. Lu, Haibao. Liu, Yanju. Huang, Wei Min. Du, Shanyi., 2009. Shape-Memory Polymers—A Class of Novel Smart Materials, MRS Bulletin, **34(11)**: 848-855

116. Leng, Jinsong. Ye, Lin., 2009. Smart Materials and Nanocomposites - Bring Composites to the Future, Composites Science and Technology, **69(13)**: 2033

117. Lester B. Vernon, Beaver, and Harold M. Vernon,.1941. Process of Manufacturing Articles of Thermoplastic Synthetic Resins, United States Patent **2,234,993**, Cl 18-55

118. Li, Yuanqing., Samad, Y. A., Polychronopoulou, K., *et al.* 2014. Highly Electrically Conductive Nanocomposites Based on PolymerInfused Graphene Sponges. *Sci. Rep.* **4**, 1–6

119. Lin, John., 2006. Shape Memory Rigidizable Inflatable (RI) Structures for Large Space Systems Applications, Proceedings of 47th AIAA/ASME/ASCE/AHS/ASC Structures, Structural Dynamics, and Materials Conference, Newport, Rhode Island, **May**: 1-11

120. Lindsay D. Norman, Edwin E. Maust Jr., 1971), Computer simulation of particulate systems, bulletin **no. 658**, Bureau of mines, US dept. of the interior. 35-46

121. Liu, C. Qin, H. Mather, P. T., 2007. Review of progress in shape-memory polymers, Journal of Materials Chemistry, **17 (16)**: 1543-1558

122. Liu, Yanju. Du, Haiyang. Liu, Liwu et al., 2014. Shape memory polymers and their composites in aerospace applications: a review. *Smart Mater. Struct.* **23**, 023001

123. Liu, Yanju. Lv, Haibao. Lan, Xin. Leng, Jinsong. Du, Shanyi., 2009. Review of electro-active shape-memory polymer composite, Composites Science and Technology, **69(13)**: 2064-2068

124. Liu, Yanju. Wang, Xiaohua. Lan, Xin. Lv, Haibao. *et al.,* 2008Shape memory polymer composite and its application in deployable hinge for space structure. *Proc. SPIE 2008; Sensors Smart Struct. Technol. Civil, Mech. Aerosp. Syst.* **6932**, 693210–693218

125. Lohar, G. S. & Jogi, B. F. 2018. Influence of Carbon Black (CB) on Mechanical Behaviour and Microscopic Analysis of Poly-propylene (PP)/ Acrylonitrile-butadiene- styrene (ABS) Nanocomposites. Procedia Manuf. **20:** 85–90

126. Lu, Haibao. Huang, W, M. Liang, Fei et al., 2013. Nanoscale design of nanosized particles in shape-memory polymer nanocomposites driven by electricity, Materials, **6(9)**: 3742-3754

127. Lu, Haibao. Liang, Fei. Yao, Yongtao. et al., 2014. Self-assembled multi-layered carbon nanofiber nanopaper for significantly improving electrical actuation of shape memory polymer nanocomposite, Composites Part B: Engineering, **59**: 191-195

128. Luo, Hongsheng. Li, Zhiwei. Yi, Guobin. et al., 2014. Multi-stimuli responsive carbon

nanotube-shape memory polymeric composites, Materials Letters, **137**: 385-388

129. Luo, Hongyan. Liao, Yanjin. Abel, Eric. et al., 2010. Hysteresis behavious and modeling of SMA actuators, Shape Memory Alloys: 61-80

130. Luo, Xiaofan. Mather, Patrick T., 2010. Conductive shape memory nanocomposites for high speed electrical actuation, Soft Matter, **6(10)**: 2146

131. Luo, Xiaofan. Mather, Patrick T., 2013. Design strategies for shape memory polymers., Current Opinion in Chemical Engineering, **2(1)**: 103-111

132. Luo, Xiaofan. Mather, Patrick T., 2013. Shape Memory Assisted Self-Healing Coating, ACS Macro letters: **2**, 152−156

133. Lux, F. 1993. Review Models proposed to explain the electrical conductivity of mixtures made of conductive and insulating materials. Journal of Materials Science. **28**: 285-301

134. M. J. D. Powell 1994, Advances in Optimization and Numerical Analysis, eds. S. Gomez and J.-P. Hennart (Kluwer Academic: Dordrecht): 51-67

135. Ma lan, Zhao Jun, Wang Xiaoyan et al. 2015. Effects of carbon black nanoparticles on two-way reversible shape memory in crosslinked polyethylene. Polymer. **56**:490-497

136. Ma, Peng Cheng. Liu, Ming Yang. Zhang, Hao. et al. 2009. Enhanced electrical conductivity of nanocomposites containing hybrid fillers of carbon nanotubes and carbon black. ACS Appl. Mater. Interfaces **1**, 1090–1096

137. Ma, Peng Cheng. Zhang, Hao. Wang, Sheng Qi. et al. 2007. Electrical conducting behavior of hybrid nanocomposites containing carbon nanotubes and carbon black. EMAP 2007 - Int. Conf. Electron. Mater. Packag. 2–5

138. Maitland, D. J, 2014. Carbon fillers for actuation of electroactive thermoset shape memory polyurethane composites by resistive heating, Ph.D. thesis, Texas A&M University,

139. Marc,Bosiers. Dierk,Scheinert. Jeroen. Hendriks. et al., 2016. Results from the Tack Optimized Balloon Angioplasty (TOBA) study demonstrate the benefits of minimal metal implants for dissection repair after angioplasty, Journal of Vascular Surgery, **64- 5**: 1552

140. Martin CA, Sandler JKW, Shaffer MSP et al. 2004. Formation of percolating networks in multi-walled carbon nanotube epoxy composites. Compos Sci Technol.; **64(15)**:1236-2309

141. Mather, Patrick T. Luo, Xiaofan. Rousseau, Ingrid A., 2009. Shape Memory Polymer Research, Annual Review of Materials Research, **39(Nov)**: 445-471

142. Mdarhri A, Brosseau C, Zaghrioui M et al. 2012, Journal of applied physics **112**: 034118

143. Meng Harper and Li Guoqiang. 2013.. A review of stimuli-responsive shape memory poly composites. Polymer. **54**:2199-2221

144. Meng, Q., Hu, J. & Zhu, Y. 2007. Shape-Memory Polyurethane / Multiwalled Carbon Nanotube Fibers. Applied polymer science. **106(2)**: 837-848

145. Merline, J, Dyana. Reghunadhan, Nair, C, P. Ninan, K, N. 2008. Synthesis, Characterization, Curing and Shape Memory Properties of Epoxy-Polyether System, Journal of Macromolecular Science, Part A - Pure and Applied Chemistry, **45(4)**: 312-322

146. Merzouki Abdelhafid and Haddaoui Naceredine 2012, International Scholarly Research Network Polymer Science **ID 493065**: 1-7

147. Mhand Hifi and Rym M'Hallah 2009, Advances in Operations Research Volume, Article **ID 150624**, 22

148. Michaud, V., 2004. Can shape memory alloy composites be smart? Scripta Materialia, **50(2)**: 249-253

149. Mohd Jani, Jaronie. Leary, Martin. Subic, Aleksandar. Gibson, et al., 2014. A review of shape memory alloy research, applications and opportunities, Materials and Design, **56**: 1078-1113

150. Mohr, R. Kratz, K. Weigel, T. Lucka-Gabor. et al., 2006. Initiation of shape-memory effect by inductive heating of magnetic nanoparticles in thermoplastic polymers, Proceedings of the National Academy of Sciences of the United States of America, **103(10)**: 3540-3545

151. MSP, Shafeer. X, Fan and A,H, Windle. 1998. Dispersion and packing of carbon nanotubes. Carbon. **36(11)**: 1603–1612

152. Müller, K. Kerstin Bugnicourt, Elodie Latorre et al. 2017. Review on the Processing and Properties of Polymer Nanocomposites and Nanocoatings and Their Applications in the Packaging, Automotive and Solar Energy Fields. Nanomaterials **7**, 74

153. N G. Sahoo, S. Rana, J.W. Cho, et al. 2010. Polymer Nanocomposites Based on Functionalized Carbon Nanotubes. Progress in Polymer Science.**35**: 837-867

154. Nielsen E Lawrence and Landel F Robert. 1994. Mechanical properties of polymers and composites, CRC press, Boca Raton **ISBN: 9780824789640**

155. Noll. Andreas, Friedrich. Klaus, Burkhart. Thomas, et al. 2013. Effective multifunctionality of poly(p-phenylene sulfide) nanocomposites filled with different amounts of carbon nanotubes, graphite, and short carbon fibers. Polymer Composites. **34(9)**: 1405-1412

156. Oliver K. Johnson, Daniel Seegmiller, David T. Fullwood et al. 2011. Characterization of electrical properties of polymers for conductive nano-composites. SAMPE: **Acc. No: ADA578048.**

157. Ortín, Jordi. Delaey, Lucas, 2002. Hysteresis in shape-memory alloys, International Journal of Non-Linear Mechanics: **37(8)** 1275-1281

158. Otsuka, K. Wayman,C, M; 1999. *Shape Memory Materials*: Cambridge University Press. **ISBN: 9780521663847**

159. Pangon Autchara, Dillon Gregory P, Runt James. 2014. Influence of mixed soft segments on microphase separation of polyurea elastomers, Polymer.**55**:1837-1844

160. Park JinHo, Dao Dung Trung, Lee Hyung-il et al. 2015. Properties of graphene/ shape memory thermoplastic polyurethane composites actuating by various methods Materials. **7**:1520-1538

161. Park, Joung Man. Kim, Sung Ju. Jang, Jung Hoon. et al., 2008. Actuation of electrochemical, electro-magnetic, and electro active actuators for carbon nanofiber and Ni nanowire reinforced polymer composites, Composites Part B: Engineering, **39(7-8):** 1161-1169

162. Patricio. E. Reyes-Morel, Jyh-Shiarn. Cherng, I-Wei. Chen,. 1988. Transformation Plasticity of CeO2-Stabilized Tetragonal Zirconia Polycrystals: II, Pseudoelasticity and Shape Memory Effect, Journal of the American Ceramic Society 71(8): 648-57

163. Piasecki, R. 2003. Effective conductivity in a lattice model for binary disordered media with complex distributions of grain sizes. Physica Status Solidi (b) **236**: 625-633

164. Pilate, Florence. Toncheva, Antoniya. Dubois, Philippe. Raquez, et al.,, 2016. Shape-memory polymers for multiple applications in the materials world, European Polymer Journal, **80**: 268-294

165. Pitt, Dale M. Dunne, James P. White, Edward V., 2002. SAMPSON smart inlet design overview and wind tunnel test: II. Wind tunnel test, Proceedings of the SPIE, 4698: 24-36

166. Progelhof RC, Jim Throne, RR Ruetsch. 1976. Methods for Predicting the Thermal Conductivity of Composite Systems: A Review. Polymer Engineering & Science.; **16**: 615 – 625

167. Qi, Xiaodong. Dong, Peng. Liu, Zhenwei. et al. 2016. Selective localization of multi-walled carbon nanotubes in bi-component biodegradable polyester blend for rapid electroactive shape memory performance. Compos. Sci. Technol. **125**, 38–46

168. Qing, Q Ni. Ohki, Takeru. Ohsako, Norihito. Iwamoto, Masaharu., 2013. Thermo-mechanical Behavior of Smart Composites with Shape Memory Polymer, proceedings of International Conference on Composite Materials- Smart Materials & Structures, Beijing, China: ID-1332

169. Quackenbush, Todd R. Carpenter, Bernie F. Boschitsch, Alexander H. Danilov, Pavel V., 2008. Development and test of an HTSMA supersonic inlet ramp actuator, Proceedings of SPIE - The International Society for Optical Engineering, 69300: 11p

170. Quan Qian, Xizhong An, Haiyang Zhao, et al. 2018. Numerical investigations on random close packings of cylindrical particles with different aspect ratios. Powder Technology.; **343**: 79-86.

171. Quan, Du. Hai, Xu., 2015. Shape Memory Alloy in Various Aviation Field, Procedia Engineering, **99**: 1241-1246

172. R Arockiakumar. Takahashi M. Takahashi S. et al., 2013. Materials Science & Engineering A Microstructure , mechanical and shape memory properties of Ti – 55Pd – 5 x (x ¼ Zr , Hf , V , Nb) alloys, Materials Science & Engineering A **585**:86–93

173. R Arockiakumar. Takahashi M. Takahashi S. et al., 2014. X-ray diffraction studies on Ti-Pd shape memory alloys, Materials Science Forum **783-786**: 2517-2522

174. R. Hernandez Yenny, Gryson Alex, M. Blighe Fiona et al., 2008. Comparison of carbon nanotubes and nanodisks as percolative fillers in electrically conductive composites. Scripta Materialia **58**: 69–72

175. Radzuan, Nabilah, Afiqah, Mohd. Sulong, Abu, Baker. Sahari, Jaafar. 2017. A review of electrical conductivity models for conductive polymer composite. International journal of hydrogen energy **42**:9262-9273

176. Ragin Ramdas, M. Santhosh Kumar, K. S. Reghunadhan Nair, C. P., 2015. Synthesis, structure and tunable shape memory properties of polytriazoles: dual-trigger temperature and repeatable shape recovery, Journal of Materials Chemistry A, **3(21)**: 11596-11606

177. Raja, M., Ryu, S. H. and Shanmugharaj, A. M. 2013. Thermal, mechanical and electroactive shape memory properties of polyurethane (PU)/poly (lactic acid) (PLA)/CNT nanocomposites. Eur. Polym. J. **49**, 3492–3500

178. Ralls, Kenneth, M. Courtney, Thomas, H. Wulff, John., 1976. *Introduction to Material Science and Engineering*: Wiley & Sons. **ISBN: 9780471706656**

179. Ratna, Debdatta. Karger-Kocsis, J., 2008. Recent advances in shape memory polymers and composites: A review, Journal of Materials Science, **43(1)**: 254-269

180. Razavi R, Zare Y. 2017. A two-step model for the tunneling conductivity of polymer carbon nanotube nanocomposites assuming the conduction of interphase regions. RSC Advances; **7**: 50225–50233

181. Remi, Jullien. Andre, Pavlovitch and Paul, Meakin. 1992. Random packings of spheres built with sequential models J. Phys. A: Math. Gen; **25**: 4103-4113

182. Robert. A.O & William. T S. 1983. High solids internally U.V stabilized melamine cured urethane paint. United States Patent: **4387194**.

183. Safdari, M. & Al-Haik, M. 2012. Electrical conductivity of synergistically hybridized nanocomposites based on graphite nanoplatelets and carbon nanotubes. *Nanotechnology* **23**.

184. Santo, Loredana. Quadrini, Fabrizio. Accettura, Antonio. et al., 2014. Shape memory composites for self-deployable structures in aerospace applications, Procedia Engineering,

88: 42-47

185. Sattar Rabia, Kumar Ayesha, Siddiq Muhammed. 2015. Thermal, mechanical and electrical studies of shape memory polyurethane/polyaniline blends, Chinese Journal of polymer science. **33(9)**:1313-1324

186. Savas Berber, Young-Kyun Kwon and David Tománek. Unusually High Thermal Conductivity of Carbon Nanotubes. Physical review letters. 2000; **84(20)**: 4613-41616

187. Scalet, G. Auricchio, F. Bonetti, E. Castellani, L. Ferri, D. Pachera. et al., 2015. An experimental, theoretical and numerical investigation of shape memory polymers, International Journal of Plasticity. **67**: 127-147

188. Schartel, B., Dittrich, B., Wartig, K. et al., 2006. The influence of layered, spherical, and tubular carbon nanomaterials' concentration on the flame retardancy of polypropylene. *Polym. Compos.* 1230–1241

189. Seidel, Gary, D and Lagoudas, Dimitris, C 2009. A Micromechanics Model for the Electrical Conductivity of Nanotube-Polymer Nanocomposites. Journal of composite materials. **43(9)**: 917-941

190. Shi, Ying. Yoonessi, Mitra. Weiss, R. A., 2013. High Temperature Shape Memory Polymers, Macromolecules; **46(10)**: 4160-4167

191. Shi, Ying., 2013. High temperature shape memory polymers & ionomer modified asphalts (PhD thesis), University of Akron, Ohio

192. Simmons John G, 1963. Generalized Formula for the Electric Tunnel Effect between Similar Electrodes Separated by a Thin Insulating Film Journal of applied physics. **34**: 1793-1802

193. Skylar Tibbits, 2014. 4D Printing: Multi Material Shape Change, John Wiley & Sons Ltd, **84(1)**: 116–121

194. Sokolowski, Witold M., 2004. Cold Hibernated Elastic Memory self-deployable and rigidizable structure and method therefore, United States Patent US 006702976 B2, **2(12)**: 2-4

195. Song, S. H. 2018. The Effect of Clay/Multiwall Carbon Nanotube Hybrid Fillers on the Properties of Elastomer Nanocomposites. Int. J. Polym. Sci. 1–8

196. Song, W. S. 2016. Percolation, Electrical Conductivity and EMI Shield Analysis of CNT Composites Percolation , Electrical Conductivity , and EMI Shield Analysis of CNT Composites. 1–42

197. Soto Matias, Esteva Milton, Martínez-Romero Oscar et al., 2015. Modeling Percolation in Polymer Nanocomposites by Stochastic Microstructuring. Materials **8**: 6697–6718

198. Stoyan Y., Yaskov G. (2008) Packing Identical Spheres into a Rectangular Parallelepiped.

In: Bortfeldt A., Homberger J., Kopfer H., Pankratz G., Strangmeier R. (eds) Intelligent Decision Support. Gabler. **ISBN: 9783834909305**

199. Sun, L. Huang, W M. Ding, Z. Zhao. et al., 2012. Stimulus-responsive shape memory materials: A review, Materials and Design, **33(1)**: 577-640

200. Sun, X. & Song, M. 2009. Highly Conductive Carbon Nanotube / Polymer Nanocomposites Achievable ?. 155–161

201. Sung-Hwan Jang and Huiming Yin. 2015. Effective electrical conductivity of carbon nanotube-polymer composites : a simplified model and its validation. Mater. Res. Express. **2**: 045602-045613

202. Sunitha, K. Santhosh Kumar, K S. Mathew, Dona. et al., 2013. Shape Memory Polymers (SMPs) derived from phenolic cross-linked epoxy resin via click chemistry, Materials Letters, **99**: 101-104

203. SV Ahir, YY Huang, EM Terentjev. 2008. Polymers with aligned carbon nanotubes: Active composite materials. Polymer (Guildf). **49(18)**: 3841–3854

204. Taha, O M A. Bahrom, M B. Taha, O Y. et al., 2015. Experimental Study on Two Way Shape Memory Effect Training Procedure for Nitinol Shape Memory Alloy, ARPN Journal of Engineering and Applied Sciences, **10(17)**: 7847-7851

205. Taherian. Reza, Hadianfard. Mohammad. Jaffar, Golikand, Ahmad, Nozad. 2012. A new equation for predicting electrical conductivity of carbon-filled polymer composites used for bipolar plates of fuel cells. Journal of Applied polymer science **128(3)**: 1497-1509

206. Tong, T H., 2007. Maleimide based high temperature shape memory polymers, United States Patent US 007276195 B1, **1(12)**

207. Uchino, Kenji., 2016. Antiferroelectric Shape Memory Ceramics, Actuators **5(11)**:1-23

208. Van Humbeeck, Jan., 1999. Non-medical applications of shape memory alloys, Materials Science and Engineering: A, **273-275**: 134-148

209. Varga, Matija. Tröster, Gerhard., 2014. Designing an interface between the textile and electronics using e-textile composites, Proceedings of the 2014 ACM International Symposium on Wearable Computers Adjunct Program (ISWC '14) Seattle, WA USA: 255-260

210. Vernon, Lb. Vernon, Hm., 1941.Producing molded articles such as dentures from thermoplastic synthetic resins, United States Patent US **2234993 2**: 18-55

211. Vijay, K, Varadan. K, J, Vinoy. S, Gopalakrishnan., 2006. Smart material systems and mems- design and development methodologies, John Wiley & Sons. **ISBN: 9780470093610**

212. Volk, Brent., 2005. Characterization of Shape Memory Polymers Research and Technology

Directorate, Research and Technology Directorate: 1-11

213. Wadood, A. Takahashi, M. Takahashi, S. et al., 2012. High-Temperature Mechanical and Shape Memory Properties of TiPt-Zr and TiPt-Ru Alloys, Materials Science & Engineering A, 2012 MSA29380

214. Wang, Wenxin. Liu, Dongyan. Liu, Yanju. et al., 2015. Electrical actuation properties of reduced graphene oxide paper/epoxy-based shape memory composites., Composites Science and Technology, **106**: 20-24

215. Wang, Xuan Lun. Oh, Il Kwon. Kim, Jin Bong., 2009. Enhanced electromechanical performance of carbon nanofiber reinforced sulfonated poly(styrene-b-[ethylene/butylene]-b-styrene) actuator., Composites Science and Technology, **69(13)**: 2098-2101

216. Wei, Z G. Sandstrom, R. Miyazaki, S., 1998. Shape-memory materials and hybrid composites for smart systems - Part I Shape-memory materials, Journal of Materials Science, **33(15)**: 3743-3762

217. Wei, Z G. Tang, C Y. Lee, W B., 1997. Design and fabrication of intelligent composites based on shape memory alloys, Journal of Materials Processing Technology, **69(1-3)**: 68-74

218. Winzek, Bernhard. Schmitz, Sam. Rumpf, Holger. et al., 2004. Recent developments in shape memory thin film technology, Materials Science and Engineering A, **378(1-2 SPEC. ISS.)**: 40-46

219. Wolfgang Bauhover & Josef Z. Kovacs. 2009. A review and analysis of electrical percolation in carbon nanotube polymer composites. Compos Sci Technol.**69**: 1486-1498

220. Wu. Guozhang, Asai. Shigeo, Zhang. Cheng et al. 2000. A delay of percolation time in carbon-black-filled conductive polymer composites. Journal of applied physics **88(3)**: 1480-1487

221. Wu, Xuelian. Huang, W.M. Zhao, Yong. et al., 2013. Mechanisms of the shape memory effect in polymeric materials, Polymers, **5(4)**: 1169-1202

222. X Zeng, X Xu, P M Shenai, et al. 2011. Characteristics of the electrical percolation in carbon nanotubes / polymer nanocomposites. The Journal of Physical Chemistry C. **115 (44)**, 21685-21690

223. Xiao, Xinli. Kong, Deyan, 2016. High Cycle-life Shape Memory Polymer at High Temperature, Scientific Reports Nature Publishing Group, **Sep 33610** :1-10

224. Xiao, Xinli. Kong, Deyan. Qiu, Xueying. et al., 2015. Shape-Memory Polymers with Adjustable High Glass Transition Temperatures, Macromolecules, **48(11)**: 3582-3589

225. Xiao, Xinli. Qiu, Xueying. Kong, Deyan. et al., 2016. Optically transparent high temperature shape memory polymers, Soft Matter, **12(11)**: 2894-2900

226. Xiaomei Z, Xu X, Shenai PM, et al. 2011 Characteristics of the electrical percolation in carbon nanotubes/polymer nanocomposites (PhD thesis). School of Materials sci- ence and Engineering NTU

227. Xie, F. Huang, L. Leng, J. Liu, Y., 2016. Thermoset shape memory polymers and their composites, Journal of Intelligent Material Systems and Structures, **27(18)**: 2433-2455

228. Xie, Fang. Huang, Longnan. Liu, Yanju. Leng, Jinsong., 2014. Synthesis and characterization of high temperature cyanate-based shape memory polymers with functional polybutadiene/acrylonitrile, Polymer, **55(23)**: 5873-5879

229. Xie, Tao., 2011. Recent advances in polymer shape memory, Polymer, **52(22):** 4985-5000

230. Xin Lan, Jinsong Leng , Yanju Liu. et al., 2008. Investigate of Electrical Conductivity of Shape-Memory Polymer Filled with Carbon Black. Materials, C. **50**: 714–717

231. Xu, Jianwen. Song, Jie., 2011. Thermal Responsive Shape Memory Polymers for Biomedical Applications, Biomedical Engineering – Frontiers and Challenges, 125-142

232. Xue, Deqing. Yuan, Ruihao. Zhou, Yumei. et al., 2016.Design of high temperature Ti-Pd-Cr shape memory alloys with small thermal hysteresis. Sci. Rep. **6**, 28244

233. Xuelian, Wu. Huang, W,M. Yong, Zhao. et al., 2013. Mechanisms of the Shape Memory Effect in Polymeric Materials, polymers. **5**: 1169-1202

234. Y, G, Stoyan and G, N, Yaskov. 1998. Mathematical Model and Solution Method of Optimization Problem of Placement of Rectangles and Circles Taking into Account Special Constraints. Intl. Trans. in Op. Res. **5(1)**: 45-57

235. Yamabe-mitarai, Y. Arockiakumar, R. Wadood, A. et al., 2015. Ti (Pt , Pd , Au) based high temperature shape memory alloys, Materials Today: Proceedings **2S**; 517 –522

236. Yan, N., Wu, J. K., Zhan, Y. H. et al., 2009. Carbon nanotubes/carbon black synergistic reinforced natural rubber composites. Plast. Rubber Compos. **38**, 290–296

237. Yan, Zhao. Yuexin, Duan. Lu, Yuan. Fengxia, Guan., 2009. The dispersion of SWCNTs treated by dispersing agents in glass fiber reinforced polymer composites, Composites Science and Technology, **69(13)**: 2115-2118

238. Yang Bin and Huang Wei Min. 2005. Water-driven programmable polyurethane shape memory polymer: Demonstration and mechanism. Applied physics letters. **85(11)**:114105

239. Yang Bin, Huang Wei Min, Li¸Chuan et al. 2005. Effects of moisture on the glass transition temperature of polyurethane shape memory polymer filled with nano-carbon powder, European polymer journal. **41(5)**:1123-1128

240. Yang, Dazhi., 2000. Shape memory alloy and smart hybrid composites — advanced materials for the 21st Century, Materials & Design, **21(6)**: 503-505

241. Yang, Wen Guang. Lu, Haibao. Huang, W, M. et al., 2014. Advanced shape memory

technology to reshape product design, manufacturing and recycling, Polymers, **6(8)**: 2287-2308

242. Yin, Weilong. Fu, Tao. Jingcang, Liu. Leng, Jinsong. 2009. Structural shape sensing for variable camber wing using FBG sensors, Proceedings of SPIE - The International Society for Optical Engineering, **7292(March)**: 1-11

243. Yong H, Xiniya Z, James R. 2012. The role of diisocyanate structure on microphase separation of solution polymerized polyureas. Polymer (Guildf). **55**:906–913

244. Yoshino K, Kajii H, Araki H et al. 1999. Electrical and optical properties of conducting polymer-fullerene and conducting polymer-nanotube composites. Full Sci Technol.**7(4)**: 695-711

245. Z.P Zhang, L.F Liu, Y.D. Yuan and A.B. Yu 2001. A simulation study of the effects of dynamic variables on the packing of spheres. Powder Technology **116**: 23–32

246. Zeng Xiaomei, Xiafeng Xu, Prathamesh M Shenai et al. 2011. Characteristics of the electrical percolation in carbon nanotubes/polymer nanocomposites, PhD thesis. School of Materials science and Engineering NTU

247. Zha, Ruhua. Chen, Ming. Shi, Tuo. et al. 2017. Double dimensionally ordered nanostructures: Toward a multifunctional reinforcing nanohybrid for epoxy resin. RSC Adv**. 7**, 1177–1190

248. Zhang H, Wang H, Zhong W, et al. 2009. A novel type of shape memory polymer blend and the shape memory mechanism. Polymer (Guildf). **50(6)**:1596–1601

249. Zhang Heng, Wang Haitao, Zhong Wei et al. 2009. A novel type of shape memory polymer blend and the shape memory mechanism, Polymer. **50(6)**:1596-1601

250. Zhang Rui, Dowden Alice, Deng Hua et al. 2009. Conductive network formation in the melt of carbon nanotube/thermoplastic polyurethane composite, Composite science and technology. **69**:1499-1504

251. Zhang, Dawei. Liu, Yanju. Leng, Jinsong., 2008. Infrared Laser-Activated Shape Memory Actuators, Earth & amp; Space 40988: 1-7

252. Zhang, Fenghua. Zhang, Zhichun. Zhou, Tianyang. et al., 2015. Shape Memory Polymer Nanofibers and Their Composites: Electrospinning, Structure, Performance, and Applications, Frontiers in Materials, **2(Oct)**: 1-10

253. Zhang, Heng. Wang, Haitao. Zhong, Wei. Du, Qiangguo., 2009. A novel type of shape memory polymer blend and the shape memory mechanism, Polymer, **50(6)**: 1596-1601

254. Zhang, Lingyan. Wan, Chaoying. Zhang, Yong., 2009. Morphology and electrical properties of polyamide 6/polypropylene/multi-walled carbon nanotubes composites, Composites Science and Technology. **69(13)**: 2212-2217

Publications from the thesis

Refereed Journal

1. D. I. Arun, K. S. Santhosh Kumar, B. Satheesh Kumar, P. Chakravarthy, Mathew Dona & B. Santhosh (2019) High glass-transition polyurethane-carbon black electro-active shape memory nanocomposite for aerospace systems, Materials Science and Technology, 35(5):596-605; DOI: 10.1080/02670836.2019.1575054

2. DI Arun, P Chakravarthy, BS Girish, K. S. Santhosh Kumar, B. Santhosh. (2019) Experimental and Monte Carlo simulation studies on percolation behaviour of shape memory polyurethane carbon black nanocomposite, Smart Materials and Structures, *Smart Mater. Struct.* 28 055010; DOI: 10.1088/1361-665X/ab083b

3. DI Arun, R, Kumar Arun. P Chakravarthy. BS Girish. KS Santhosh Kumar, B. Santhosh. (2019), Structural-Modeling and Experimental Validation of Percolation Threshold for Nanotube-Polyurethane Shape Memory System, Materials Science and Technology, DOI: 10.1080/02670836.2019.1661660

4. DI Arun, P Chakravarthy, KS Santhosh Kumar. B. Santhosh. (2019) Synergy studies on polyurethane-carbon black-multi walled carbon nanotube based heterogeneous electro-active shape memory nanocomposite system, Bulletin of Material Science, Springer (Under review)

Conference papers

5. DI Arun, KS Santhosh Kumar, P Chakravarthy, B Santhosh. (2019) Comparative study on electro-active shape memory Polyurethane nanocomposites with Carbon black and Multi-walled carbon nano tube fillers, Proceedings of International Conference in Advanced Materials 2019 (June 12-14), Nirmalagiri College Kannur Kerala India, ISBN: 978-81-931227-4-7, p.61 (accepted for publication in AIP Proceedings)

Books

6. DI Arun, P Chakravarthy, R Arockiakumar, Santhosh B (2018) Shape memory materials, CRC Press, Boca Raton ISBN: 9780815359692

Doctoral committee members

1. **Dr. Manoj Nair T** (Chairman)
   Associate Professor & Head, Department of Aerospace Engineering
   Indian Institute of Space science and Technology, Valiyamala, Kerala India

2. **Dr. Balasubramanian M** (External expert)
   Professor, Department of Materials and Metuallurgy
   Indian Institute of Technology Madras, Tamil Nadu India

3. **Dr. Chakravarthy P** (Convener, Supervisor)
   Associate Professor, Department of Aerospace Engineering
   Indian Institute of Space science and Technology, Valiyamala, Kerala India

4. **Dr. Santhosh B** (Supervisor)
   Group Director, Carbon Carbon Development Group
   Composite Entity, Vikram Sarabhai Space Centre, Kerala India

5. **Dr. Biju Das** (Member)
   Associate Professor, Department of Aerospace Engineering
   Indian Institute of Space science and Technology, Valiyamala, Kerala India

6. **Dr. Sreejalekshmi G** (Member)
   Associate Professor, Department of Chemistry
   Indian Institute of Space science and Technology, Valiyamala, Kerala India

7. **Dr. Sasikumar P** (Member)
   Scientist / Engineer – SG, Quality Division for Composites,
   Structural Reliability Entity, Vikram Sarabhai Space Centre, Kerala India

Biodata

ARUN.D.I

Scientist / Engineer, Composite Pressurised System Group,

Composite Materials and Structural Entity,

Vikram Sarabhai Space Centre ISRO Thiruvananthapuram, Kerala

arunisro12@gmail.com, +91 9495277367, +91 8921097891

Date of Birth: 02nd August 1986

EDUCATION SUMMARY

PhD in Aerospace Engineering	*2016-till date*
Indian Institute of Space Science and Technology, Trivandrum	
M. Tech in Construction Technology & Management	**2008-2010**
Indian Institute of Technology, Delhi	
CGPA	8.2
B. Tech in Civil Engineering	**2004-2008**
University of Kerala; College of Engineering, Trivandrum	
CGPA	7.7

WORK EXPERIENCE

Vikram Sarabhai Space Centre, Thiruvananthapuram	*2014 – present*

- Scientist / Engineer– Composite Pressure Systems Group, Composite Entity

ISRO Satellite Centre, Bangalore	*2012 – 2014*

- Engineer SC – Satellite Integration and Testing Establishment

Larsen & Toubro Construction - Infrastructure, Chennai	*2010 – 2012*

- Assistant Manager – Planning : *Kattupalli Shipyard cum Port Project*